Behaviour of Retrofitted Masonry Shear Walls Subjected to Cyclic Loading

Zur Erlangung des akademischen Grades eines

DOKTOR-INGENIEURS

von der Fakultät für

Bauingenieur-, Geo- und Umweltwissenschaften
der Universität Fridericiana zu Karlsruhe (TH)

genehmigte

DISSERTATION

von

M.Sc.Ing. Abdelkhalek Saber Omar Mohamed

Aus Ägypten

Tag der mündlichen Prüfung:	26. Novemer 2004
Hauptreferent:	Prof. Dr. -Ing. L. Stempniewski
Korreferent:	Prof. Dipl.-Ing. Matthias Pfeifer

Karlsruhe 2004

Abstract

The recent earthquake in different countries of the world, such as those in Iran (2003), Algeria (2003), India (2001), Turkey (1999) and Vrancea (1997) have shown, particularly masonry walls were damaged. Thus, masonry walls are the most vulnerable elements of buildings when subjected to earthquake loading. Therefore, it is necessary to find practical solutions by study the behaviour of these walls, first without and then with retrofitting under monotonic and/or cyclic seismic loading.

For this study, an experimental program has been conducted using the pseudo-dynamic experimental set-up that was designed at the Institute of Reinforced Concrete Structures, at the University of Karlsruhe, Germany. Its purpose was to analyse the behaviour of masonry walls first without and then with retrofitting.

The present study had two stages; The first stage aimed to study the behaviour of masonry walls experimentally and numerically. The numerical study was conducted by developing a suitable constitutive model; While the second stage concerned with the experimental and numerical investigating of the strengthening and repairing of the masonry walls structures, using glass fibre reinforced polymers (GFRP), that are epoxy-bonded to the exterior surfaces of the walls. The numerical investigation was accomplished by developing anchorage strength bond model to study the effect of such GFRP on masonry.

Both models were programmed and incorporated into a three-dimensional finite element code: Abaqus 6.4 [1] and they have been verified and validated with experimental results.

In the first stage, a three-dimensional non-linear finite element model, based on two-parameter damage coefficients has been developed to

study the behaviour of masonry walls numerically. This model, which is based on the continuum damage theory, takes into account for different behaviours in tension and compression. Such an approach, revealed to be valuable in understanding the global behaviour of masonry structures, in particular, the numerical results are in close agreement with experimental data.

The masonry was treated as a homogenized material, for which the material properties were obtained by a homogenisation technique. The damage theory proved to be a good choice to exploit in this area of structural mechanics, due especially to its efficiency combined with simplicity.

The numerical implementations performed gave a good description of the failure process as well as accurate prediction of the behaviour of masonry structures.

The numerical results have shown that the shear strength and the shear behaviour are much influenced when loading the wall in addition to the shear force with vertical load.

In the second stage of the work, the aim of the developed bond strength model was to study the behaviour of the strengthened and/or repaired masonry walls structures when using GFRP as a retrofitting material.

The comparisons of the numerical results from both models with the experimental results have shown, generally, close agreement.

By retrofitting the pre-damaged wall with GFRP-laminates, its initial shear stiffness could be restored, the ductility raised and the carrying capacity increased by 60%. The results have shown that this kind of retrofitting is effective in improving the shear capacity and ductility of masonry walls and will be a reliable method in increasing the structural reliability of un-reinforced masonry buildings.

To my father & mother;

To my brothers & sisters;

To my wife & children

Preface

Praise be to ALLAH with the blessings of whom the good deeds are fulfilled

The present dissertation was developed during my work as doctoral candidate and scholarship holder at the Institute of Reinforced Concrete Structures, at the University of Karlsruhe, Germany.

I would like to express my special thank and appreciation to Professor Stempniewski (Chairman of the Institute) for the encouragement and supervising for many years.

I thank also heartily Professor Eibl for his advices and suggestions during this work.

I thank also Professor Pfeifer (Chairman of the Institute of Load-Bearing Constructions, at the University of Karlsruhe) for undertook the co-examiner.

My thanks are to all colleagues of the Institute for their useful and meaningful discussions.

I thank also the Egyptian Government for the financial support through a scholarship to make my doctor degree in Germany.

At last but not the least, I thank my father, my mother, my brothers, and my sisters for every thing they did, and still doing for me. I am also thankful to my wife for her unwavering patience, understanding and encouragement and to: may sons, Mohamed and Youssef; to my daughter, Iman, for keeping me accompanied during the accomplishment of this dissertation. I thank also my wife's mother for her constant support and encouragement.

Karlsruhe, in November 2004

Abdelkhalek Saber Omar Mohamed

List of Contents

1 Introduction 1
1.1 General Remarks 1
1.2 Fibre Reinforced Polymers (FRPs) 4
1.3 Objectives and Scope 5
1.4 Contents of the Dissertation 6
2 Theoretical Background 9
2.1 Seismological Background 9
2.2 Codes and Instructions for Masonry in Seismic Areas. 12
2.2.1 Geometric Requirements for Shear Walls 13
2.2.2 Buildings Natural Period 14
2.2.3 Seismic Actions on the Buildings using the Response Spectra Method 15
2.3 Determination of Seismic Structural Response using Time-History Method 18
2.4 Choice of the Finite Element 19
2.5 Masonry Characteristics 20
2.5.1 Masonry Components 20
2.5.2 Material Properties of Masonry 21
2.5.3 Masonry Properties 21
2.5.4 Masonry subjected to In-Plane Shear 28
2.5.5 Failure Criteria 34
2.6 Material Behaviour under Cyclic Loading 44
2.7 Damage Theory Background 46
2.7.1 Basic Assumptions 48
2.7.2 Strain-Based Formulation 49
2.7.3 Stress-Based Formulation 51
2.7.4 Concepts of the Continuum Damage Mechanics 53
2.8 Proposed Masonry Models 54
3 Developed Constitutive Law for the Analysis of Masonry 59
3.1 Introduction 59
3.2 Constitutive Model for the Analysis of Masonry 62
3.2.1 Scalar Damage Model 63
3.2.2 Homogenisation 65
3.2.3 Numerical Analysis 69

3.3 Experimental Results of a Wall made from Autoclaved Aerated Concrete (AAC) Blocks _____ 82
3.4 Comparison between the Experimental and Calculation Results of the wall made from Autoclaved Areated Concrete (AAC) Blocks 87
4 Anchorage Strength Model for Fibre Reinforced Polymers (FRP) bonded to Masonry 93
4.1 Fibre Reinforced Polymers (FRP) Properties _____ 93
4.1.1 Basic Properties of the Composite Materials 94
4.1.2 Resin Systems 95
4.1.3 Properties of Fibres and other Engineering Materials 98
4.1.4 Fibre Laminates Types 99
4.1.5 Laminate Mechanical Properties 101
4.2 Anchorage Strength Models for FRP and Steel Plates bonded to Concrete Blocks _____ 102
4.2.1 Failure Modes 103
4.2.2 Existing Shear Anchorage Strength Models 106
4.2.3 Empirical Models 106
4.2.4 Fracture Mechanics-Based Models 107
4.2.5 Design Proposals 110
4.3 Comparison with Experimental _____ 113
4.4 New Model by J.F. Chen _____ 115
4.4.1 Stress in Bonded Plate 119
4.5 Constitutive Model for the Analysis of Retrofitting of Masonry _____ 121
4.5.1 Introduction 121
4.5.2 Anchorage Strength Model for Glass Fiber Reinforced Polymers (GFRP) bonded to Masonry 122
4.6 Experiments to determine the Performance of the Glass Fibre Reinforced Polymers (GFRP) on the Autoclaved Aerated Concrete (AAC) Blocks _____ 125
4.7 Experimental Results of Pre-Damaged-Retrofitted Wall of Section (3.3) with the Glass Fibre Reinforced Polymers (GFRP)-Sheets _____ 128
4.7.1 Numerical Results 133
5 Summary, Conclusions and Recommendations 141
5.1 Summary _____ 142
5.2 Conclusions _____ 143

5.3 Recommendations for Future Work _____144
Kurzfassung.....145
List of References 151
Appendices 171
Appendix A: Orthotropic Material Properties of Masonry_____171
Appendix B: Structural Relationship of Masonry Constituent Materials_
_____175

1 Introduction

1.1 General Remarks

Masonry is a traditional building material, which is widely used throughout the world in the construction industry.
Since the dawn of history, the major advantage of using masonry has been the widespread geographical availability of its raw material. This factor holds true even today, as many developing countries find masonry to be the most economical building material. In the recent years the application of masonry as a major load bearing material has increased rapidly, perhaps partly due to the recognition of problems associated with concrete structures and to its high aesthetic appeal.
There is also evidence of its increasing use in sports centres, industrial and commercial buildings, bridge abutments and diaphragm and retaining walls.

Masonry represents a structural material of growing importance in civil engineering and, more specifically, in earthquake engineering. The main reasons for this are: the present trend toward preservation and restoration of existing, often ancient structures and the increasing economical competitiveness of masonry construction in many areas including seismic areas, compared to reinforced concrete or steel buildings.

Masonry structures, although used for centuries, still represent a challenge to structural analysis due to their complicated, multi-faceted mechanical behaviour. Masonry has a number of serious drawbacks when it comes to earthquake resistance. It is naturally brittle, because of large mass, it has high inertial response to earthquake. Its quality of construction is difficult to control and less research has been done, regarding its seismic behaviour.

The response of masonry to cyclic loading exhibits a very notable degradation of stiffness and, eventually, also of compressive strength (softening).

Mechanically, masonry can be regard as a heterogeneous periodic material (composite), which consists of mortar as a matrix, of brick as reinforcing (short fibres) and from some standpoints (interface) as a third phase. Such interpretation leads to the use of homogenisation methods.

In general, un-reinforced masonry (URM) walls have a poor performance record even in moderate earthquakes. Their behaviour is usually brittle with little or no ductility and structural and non-structural elements suffer various types of damage ranging from invisible cracking to crushing and, eventually, disintegration. This behaviour is due to the rapid degradation of stiffness, strength and energy dissipation, which results from the brittle sudden damage of the masonry wall. This constitutes a major source of hazard during seismic events and can create a major seismic performance problem facing earthquake engineering today.

Figure 1.1 illustrates the collapse of URM walls due to in-plane and out-of-plane loads after the 2003-Algeria earthquake.

Figure 1.1: Failure of URM walls (Algeria 2003): a) In-plane Failure, b) Out-of-plane Failure, c) Combined Failure

Convential retrofitting techniques can be classified into two categories: damage repair and strength of the structure. The techniques used to repair damage in the form of cracks are:

- Filling the cracks and voids by injecting epoxy or grout
- Using brick or metallic elements to stitch the large cracks and the weak areas.

The available procedures for strengthening or stiffening of the masonry are:

- Steel plates or angles as external reinforcement
- Using post-tensioning for the Existing structures
- The hollow masonry units are injected using non-shrink Portland cement t or epoxy grout
- Coating of the surface with reinforced cement paste or shot crete

These methods, however have been proven to be impractical for the most part, as they add considerable mass to the structure and are labour intensive, both of which resulting in higher costs.
To avoid these problems, a new trend in repair and strengthening of structures is the use of fibre-reinforced polymers (FRPs).

1.2 Fibre Reinforced Polymers (FRPs)

The fibre reinforced materials have the form of composite, which are made of at least two elements working together to produce a material, which has a different properties than that of its individual elements. In practice, most composite materials consist of a matrix as the bulk material and some kind of reinforcement, usually in the form of a fibre to increase the strength and stiffness of the matrix. The function of the matrix is to bind the fibres together and allows the load transfer evenly between the fibres. It also protects the fibres from the environment and bonds them to the surface, transferring the load from the structure into the fibres.

In addition to lower installation costs, the use of fibre reinforced polymer (FRP) composites possess some advantages compared to other retrofitting techniques [212]. For example: the disturbance of the occupants of the facility is minimal, there is no loss of valuable space and, generally, the installation is fast and easy. In addition, from the structural point of view, the dynamic properties of the structure remain unchanging because there is no addition of weight and stiffness. Any alteration to these properties would lead to an increase in seismic forces. These composite materials are lightweight, thinner and have ten times the strength of steel. They are also non-corrosive, durable, allow for a degree of design flexibility and have low-creep and elongation. Several types of FRP materials have increasingly been used for repair and retrofit of concrete and masonry structures in the recent years, in different forms, such as glass fibre reinforced polymers (GFRP), carbon fibre reinforced polymer (CFRP) and armid fibre reinforced polymers (AFRP). The ease of installation of FRP composite on both the exterior and interior of masonry makes this strengthening technique attractive.
The two most common fibres used are E-Glass and carbon fibre. Epoxy has been found to be the best resin.

Due to its economical balance of cost and strength properties, the predominant fibre for civil engineering application is the glass fibre. Therefore, it has been used for the retrofitting purpose in this work.

1.3 Objectives and Scope

The growing importance of masonry as a structural engineering material in the field of civil engineering necessitates the study of its behaviour, especially in earthquake areas, where masonry has an increasing economical competitiveness over reinforced concrete and steel structures.

The poor performance of the masonry even, in moderate earthquakes, because of brittle failure and no ductility of its components, showed that a retrofitting technique is required in order to improve these mechanical properties.

The first aim of this work is to develop a three-dimensional non-linear finite element model based on the continuum damage theory using a two parameters damage model. Here, masonry is treated as a composite material, with masonry units and mortar joints forming its constituents.
A homogenisation technique is introduced to obtain the average mechanical response of masonry. The properties of the equivalent orthotropic material are used to formulate the system stiffness matrix in the finite element analysis.

The second aim is to develop an anchorage strength bond model for FRP bonded to the masonry to show the effect of retrofitting on the masonry using these new materials in order to improve the mechanical properties of masonry, such as ductility and shear behaviour for these structures as well as to eliminate brittle failure mode.

1.4 Contents of the Dissertation

The dissertation is composed of five chapters.

Chapter one introduces general remarks on the problem and the objectives of the work.

Chapter two introduces the seismological background. The different norms and instructions used for masonry, with their requirements for masonry in seismic areas, are also here implemented. The masonry behaviour under tension, compression and in-plane loadings and its failure criteria are also introduced in this chapter. The chapter also contains the damage theory formulations.

Chapter three presents the constitutive damage model developed in this work to study the behaviour of masonry structures basing on the continuum damage theory. Calculation examples using the developed model, compared with the experimental results from the literature are also introduced in this chapter . A comparison is made between the numerical results, using the developed model, and the experimental results, obtained at the Institute of Reinforced Concrete Structures, at the University of Karlsruhe, Germany, on autoclaved aerated concrete (AAC) blocks masonry wall is also here included.

Chapter four includes a review of the theory of the composites and the properties of the different materials used in the construction of the laminate. The different anchorage strength models for FRPs bonded to masonry and/or concrete are also introduced in this chapter. The bond model of the FRPs developed in this work to study the behaviour of masonry when being retrofitted with FRPs is also here implemented. A comparison of the numerical results from the developed bond model with the experimental results of AAC-masonry wall retrofitted with GFRP-sheets obtained at the Institute of Reinforced Concrete Structures, at the University of Karlsruhe, Germany, is also presented in this chapter.

Chapter five summarizes the conclusions from the present work and gives recommendations for the future research in the areas of masonry analysis and repair and strengthening of masonry with FRPs materials.

2 Theoretical Background

In this chapter, the general formulations and assumptions used in the analysis of masonry walls under consideration are presented.
In the first part of this chapter, a seismic background is introduced. Then, the different norms and instructions for masonry in seismic areas are presented. Afterwards, the masonry characteristics and different failure criteria are provided. Then, the theory of continuum damage mechanics, which provides a rigorous framework in developing the constitutive relationships for the materials, is presented. At the end, a representation of the different proposed models for masonry are implemented.

2.1 Seismological Background

The earthquake is the shaking of the ground caused by the sudden rupture of rock formations with corresponding high-energy release. An earthquake [138] may also stem from volcanic activity or from the collapse of subterranean (natural or man-made) cavities.
The released energy propagates in the form of seismic waves extending out in all directions, eventually reaching the ground surface.

The magnitude of the fractured area or rupture zone may be tens or even hundreds of Km long and tens of Km wide. The rock material strength and the relative displacement or, offset, at the fault are the most important physical parameters determining the destructiveness of an earthquake.

The earthquake reaches the ground surface in the form of seismic waves. There are two types of seismic waves:

- P (primary, longitudinal, push-pull, irrotational) waves are the fastest waves propagating from the rupture or focal zone, followed by,
- S (secondary, transverse, shear, rotational) waves.

The seismographs of the earthquake stations draw the earthquake waves. These graphs (seismograms) are the background for seismic-research.

The most important terms characterising the position of the focal zone relative to earth-surface are summarized in Figure 2.1.

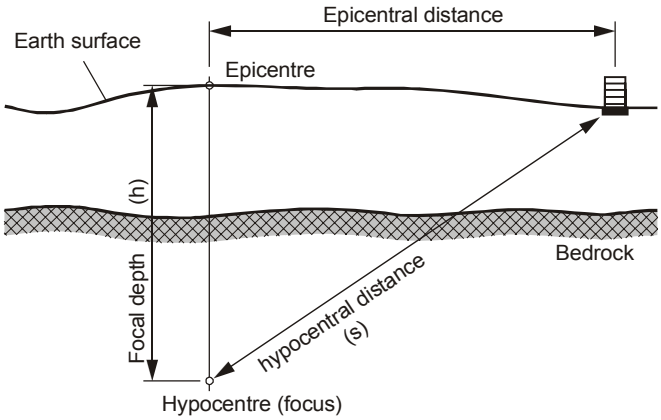

Figure 2.1: Focal zone related terms

The point inside the ground from which the earthquake waves originate is called the hypocentre (focus) of the earthquake.
On the ground surface directly above the hypocentre lays the epicentre. The distance between the epicentre and the reference point (e.g. building site) is called the epicentral distance.
The distance between the epicentre and the hypocentre is called focal depth (h), and the distance between the hypocentre (focus) and the building site is called hypocentral distance (s). The focal depth (h) for most earthquakes is up to 60 Km. For h〉300 Km the earthquakes are unimportant from the structural engineering viewpoint, while for h=10 Km, the earthquake can cause very heavily damage.

The seismographs register the acceleration time-history in two horizontal (NS and EW) and vertical directions. The translation components (displacements) can be determined by the integration of the velocity and acceleration time-history.

The magnitude of an earthquake is determined from the maximum seismic registration and gives a measurement of the energy released by the earthquake from the hypocentre. Thus, this measurement is independent of the observer's location.

Earthquake having a magnitude of less than 5 are not expected to cause structural damage, whereas, magnitudes greater than 5 can produce potentially damaging ground motions. The magnitude itself of an earthquake is not sufficient to indicate whether structural damage can be expected. The severity of the ground motions observed at any point is called the earthquake intensity. This measures the effects of the ground motions on the natural and man-made objects. In the United States, the standard measure of intensity is the modified Mercalli (MM) scale. In Europe, the Medvedev-Sponheuer-Karnik (MSK) scale is used. Both are 12-point scales ranging from I=1 (not felt by anyone) to I=12 (total destruction).

Table 2.1.presents a simplified version of the MSK scale.

Intensity	Characteristics
1	Only registered by instruments
2	Noticed by very few persons
3	Noticed by some persons
4	Noticed by many; rattling of window panes and crockery
5	Suspended objects swing; sleeping persons are awoken
6	Slight damage in buildings, some barely visible plaster cracks
7	Noticeable plaster cracks, cracks in masonry walls and chimneys
8	Large masonry cracks, collapse in cornices and mouldings
9	Collapse of walls and roofs of some buildings, some ground sliding
10	Several buildings collapse, ground fissures of up to 1m width
11	Many fissures and landslides
12	Marked landscape changes

Table 2.1: Simplified MSK scale according to DIN 4149 part 1 [57]

2.2 Codes and Instructions for Masonry in Seismic Areas.

The seismic codes are necessary for engineers and other practitioners either in design or construction of the buildings.

Euro Code 8 (EC8) [50,51,52,64] representing a new generation of structural design codes in Europe, defines requirements for the design of buildings against earthquake action.
For reinforced concrete structures, steel and timber, the seismic code regulations can be implemented with less problems than for masonry structures, since un-reinforced masonry (URM) cannot make use of a large reduction of accelerations response resulting from ductile earthquake response, especially when perforated bricks are used with regard to thermal insulation as desirable in such countries of Europe.
In drafts of ENV 1998-1, a rather than low ductility, behaviour factor of $q = 1.5$ is recommended for URM in order to reduce the design response acceleration in comparison to the linear elastic values.

In EC8, stated that for masonry Euro Code 6 (EC6) ([47,48,147,49]) regulations are also applied in connection with EC8.
In the seismic earthquake areas, for design, construction and analysis of buildings, the regulation of DIN 4149 [57] are also applied.
The earthquake loads according to EC8 regulations are bigger than those to DIN 4149.
The shear-capacity using regulations of DIN-1053 [46] suitable values leads to reducing the big loads according to EC6.

It is necessary to mention here the International Association of Earthquake Engineering (IAEE) [87,88], which have the publications: Earthquake Engineering & Structural dynamics and regulations for seismic design [58]. The informations about seismic design criterion, seismic zones and seismic loads are included In these regulations. Included also, are the earthquake design codes and regulations for 41 countries of the world. Newly included is EC8 and ISO 3010.

The international recommendation for design and construction of un-reinforced and reinforced masonry structures (CIB) [36] are used as the basis for the preparation of chapter 6 of part 1.3 of the EC8.
Since the Second World War, the development of the major masonry Standards in Britain, Switzerland, the united states and Yugoslavia has progressed from static analysis techniques to the start of the inclusion of modern dynamic analysis tools [151].

2.2.1 Geometric Requirements for Shear Walls

The geometric requirement for shear walls according to PrEN 1998-1-draft 2000 [177] are presented in Table 2.2

Masonry Type	$t(mm)$	h_{ef}/t	h/l
Un-reinforced, with natural stone units	≥ 400	≤ 9	≤ 2
Un-reinforced, manufactured stone units	≥ 300	≤ 12	≤ 2
Un-reinforced, manufactured stone units in zones of low seismicity	≥ 175	≤ 15	≤ 2.5
Confined masonry	≥ 240	≤ 15	≤ 3
Reinforced masonry	≥ 240	≤ 15	No restriction

Table 2.2: Geometric requirements for shear walls According to PrEN 1998-1-draft 2000 [177]

with

t = thickness of the wall

h_{ef} = effective height of wall according to clause 4.4.4 of part 1-1 of EC6

l = length of the wall

h = greater clear height of the openings adjacent to wall

Seismic zones with a design ground acceleration not greater than $0.1g$ are classified as low seismicity zones.

2.2.2 Buildings Natural Period

According to EDIN 4149:2002-10 [57], the value of the natural period for buildings with heights up to $80\,m$ may be calculated from the relationship

$$T = c_t \cdot H^{3/4} \tag{2.1}$$

with

T = fundamental period of buildings in s

H = height of building in m

c_t = 0.05 for masonry

c_t = 0.075 for reinforced concrete

The relation between the fundamental period of a building and its height according to EDIN 4149:2002-10 [57] is shown in Figure 2.2 for masonry and concrete.

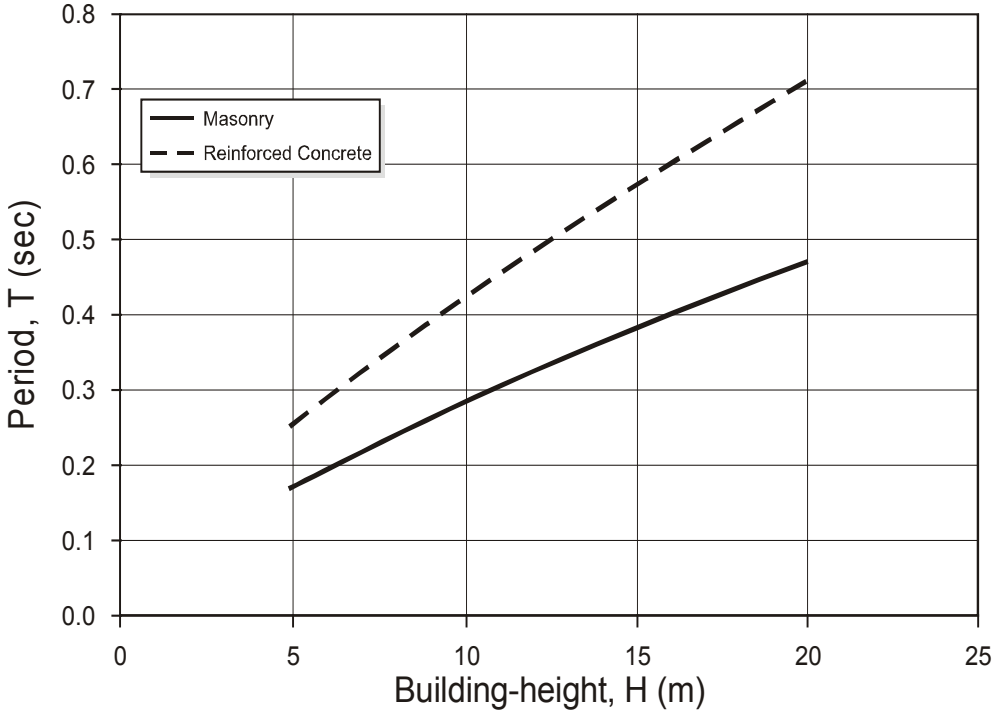

Figure 2.2: The relationship between the building height and its period according to EDIN: 2002-10 [57]

2.2.3 Seismic Actions on the Buildings using the Response Spectra Method

Many methods have been developed in order to determine the response of structures to ground motion shaking caused by an earthquake. These methods vary in their accuracy and cost.
The three methods used are: the response spectra method, the equivalent static load method and the time-history method.
The response spectrum method provides a convenient means to summarize the peak response of all possible linear single degree of freedom (SDF) systems to a particular component of ground motion. A plot of the peak value of a response quantity as a function of the natural vibration period, T_n, of the system, or related parameter such as circular frequency ω_n or cyclic frequency f_n is called the response spectrum of that quantity. Each such plot is for SDF systems having a fixed damping ratio ζ, and several such plots for different values of ζ are included to cover the range of damping values encountered in actual structures.

The representation of seismic action on the buildings by using the response spectra method is used in most countries today. By this method, the earthquake effect on the building can be described using elastic ground acceleration response spectra (elastic response spectra).
To take into account the dissipation energy from earthquake by hysteric energy–dissipation in plastic deformation, the response spectra is reduced by using a factor (q), leads to the design response spectra.
By using the design response spectra, the non-linear behaviour is taken into account without its high computational cost. This procedure has the the disadvantage of this procedure that only the maximum internal forces and displacement can be calculated but not their values related to their time history.
For URM, q equals to 1.5.
The elastic response spectra diagram is shown in Figure 2.3.

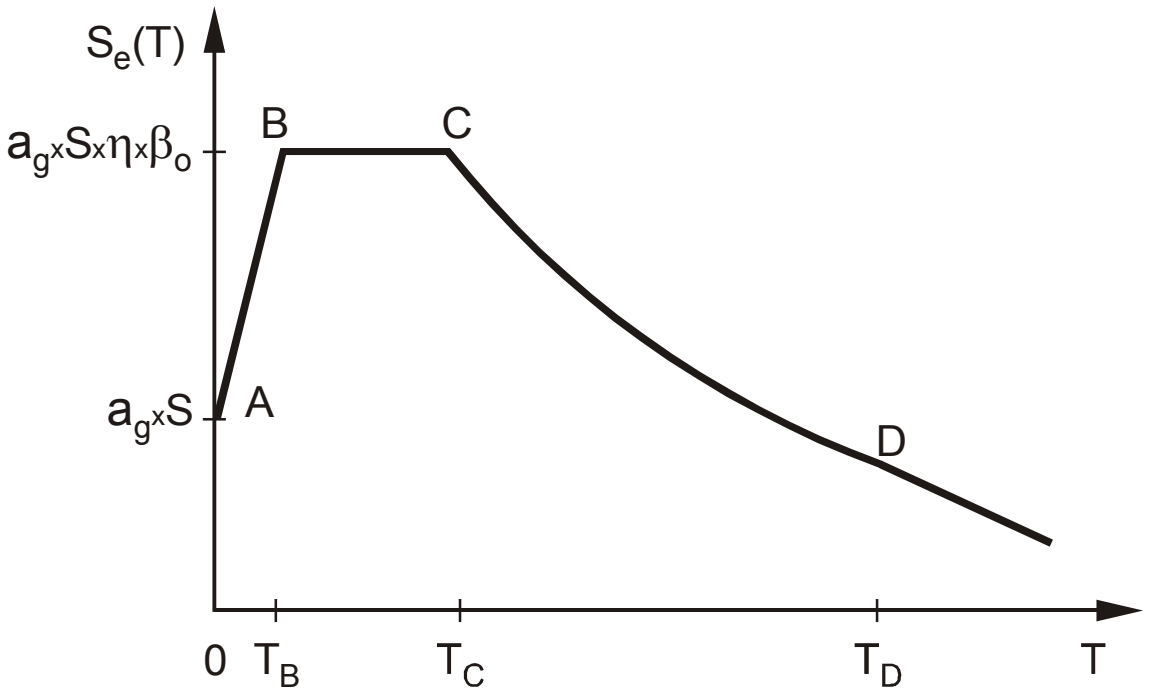

Figure 2.3: Elastic response spectra, according to EC8 [177]

For

$$
\begin{aligned}
0 \le T \le T_B \rightarrow \quad & S_e(T) = a_g.S\left(1+\frac{T}{T_B}\left(\eta.2.5-1\right)\right) \\
T_B \le T \le T_C \rightarrow \quad & S_e(T) = a_g.S.\eta.2.5 \\
T_C \le T \le T_D \rightarrow \quad & S_e(T) = a_g.S.\eta.2.5\left(\frac{T_C}{T}\right) \\
T_D \le T \le 4s \rightarrow \quad & S_e(T) = a_g.S.\eta.2.5\left(\frac{T_C T_D}{T^2}\right)
\end{aligned}
\qquad (2.2)
$$

Where

$S_e(T)$ = ordinate of the elastic response spectra

T = vibration period of a linear single degree of freedom system

a_g = design ground acceleration for the reference return period

T_B, T_C = limits of the constants spectral acceleration branch

T_D = value defining the beginning of the constant displacement response range of the spectra

S = soil parameter [177]

η = damping correction factor with reference value $\eta = 1.0$ for 5% viscous damping

β_0 = amplification factor of the acceleration spectra, for 5% viscous damping, $\beta_0 = 2.5$ [177]

The values of the parameters T_B, T_C, T_D and S are in [177] depending on the subsoil class.
The seismic effect on the buildings may also be represented in terms of ground acceleration time-history and related quantities (velocity and displacement).
The minimum duration T_s of the stationary part of the accelerograms for epi-central areas should be equal to $10\ s$.

The equivalent horizontal force for earthquake action on the building construction is calculated as

$$F_E = S_d \cdot W \tag{2.3}$$

with

W = the construction weight
S_d = the maximum value of the design acceleration spectra

$$S_d = \frac{\alpha \times S \times 2.5}{q}$$

q = behaviour factor $= 1.5$ for un-reinforced masonry
α = $\frac{a_g}{g}$, where, $g = 9.81 m/s^2$

This is the simplest method to determine the structural response to earthquakes. By this method only linear calculations (elastic material behaviour are performed). The determined base shear is then distributed onto each story of the building according to its stiffness using some simple law and the subsequent static computation of displacement and internal forces yields the informations required for designing or checking.

The horizontal force to the single stories $\mathrm{F_i}$ is then given by

$$F_i = F_E \frac{W_i h_i}{\sum_{i=1}^{n} W_i h_i} \tag{2.4}$$

(2.4) shows the distribution law given in EC8 for the base shear,
where

F_i = the equivalent static force in the i^{th} story

h_i = the height of the single story in respect to the base of the building

W_i = the weight of the single story

2.3 Determination of Seismic Structural Response using Time-History Method

In this method, direct dynamic calculations, usually non-linear (non-elastic material behaviour) are performed. The accelerograms are used as input. The following system of the differential equations is to be solved

$$[M]\left\{\ddot{u}(t)\right\} + \{F_D(t)\} + \{F_R(t)\} = -[M]\{r\}\ddot{u}_g(t) \tag{2.5}$$

where

$[M]$ = the diagonal mass matrix

$\{r\}$ = the unit vector

$\{F_D(t)\}$ = the vector of the damping force

$\{F_R(t)\}$ = the vector of the reaction forces

$\left\{\ddot{u}(t)\right\}$ = the vector of the system accelerations

$\left\{\ddot{u}_g(t)\right\}$ = the vector of the ground acceleration

To integrate (2.5), there are two different methods:

- Modal analysis (modal superposition), used only for linear system
- Direct integration for linear and non-linear systems

- **In Modal Analysis,** the differential equation (2.5) is uncoupled and the solution for every eigenvector is not dependent on the others. The total solution is determined by linear superposition.

- **In Direct Integration,** a direct integration technique in time domain is employed for (2.5). In this method, various accelerograms with different characteristics are employed.

2.4 Choice of the Finite Element

In this work, the masonry layers are modelled using three dimensional, 8-noded continuum elements as shown in Figure. 2.4.

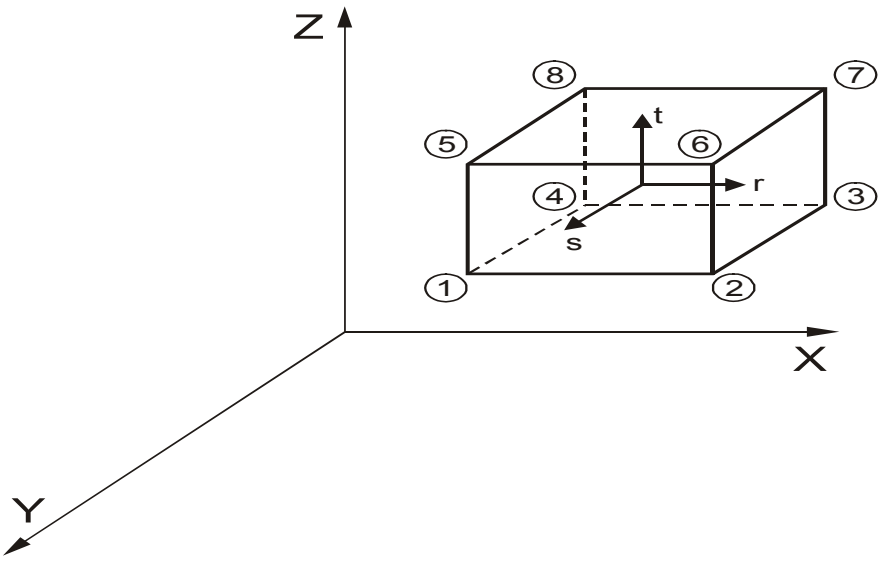

Figure 2.4: Three-dimensional, 8-noded continuum element

The choice of the order of numerical integration is important in practice., firstly, because the cost of analysis increases when a higher order integration is employed and secondly, because by using a different integration order, the results can be affected greatly. These considerations are important in three-dimensional analysis. Therefore, the proper application of Gauss quadrature (see Figure 2.5) requires that certain choices be made such as: which element to select and what kind and order of numerical integration to use.

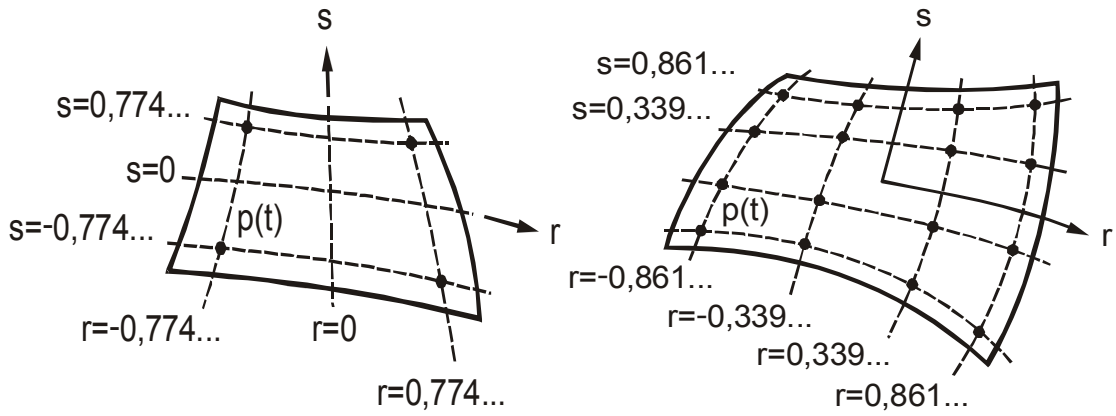

Figure 2.5: Gauss numerical integrations over rectangular domains

In this work, the BFGS-algorithm [225] is used to update and preserve matrix symmetry and positive definiteness. Two criteria must be achieved to accomplish the convergence in the i^{th} iteration-step. These are:

1. $\Psi_i / f < 5.0E-3.0$ where f is the applied force on the structure.
2. $\delta a_i / a_{i+1} < 1.0E-3.0$ where a is the vector of degree of freedoms.

2.5 Masonry Characteristics

2.5.1 Masonry Components

Masonry consists of two main components: brick and mortar. Bricks are often rectangular in shape, although other esoteric forms can be custom-made to serve an ornamental purpose. Brick units can be solid or hollow. Masonry units can be made of clay, concrete, calcium silicate (or sand lime), stone and glass. The most commonly available units are bricks and blocks made from clay, concrete and calcium silicate.

Mortar, which is the second component of masonry, consists of a mixture of cement, sand and lime. In addition to the sealing function to fill the irregularities between masonry units, mortar acts as a bonding agent between masonry units to help in resisting seismic and wind action. The use of cement provides mortar with the required strength, whereas, the

addition of lime to cement improves workability, water retentivity and bonding characteristics of mortar.

2.5.2 Material Properties of Masonry

Brick and block masonry units are usually used to construct walls and piers, which are designed to resist vertical compressive loads. As a result, the uni-axial compressive strength of masonry is usually the predominant factor in designing load-bearing walls. However, brick walls are also subjected to a large magnitude of horizontal shear forces and lateral pressure, perpendicular to the wall-plane caused by seismic, wind and lateral earth pressure. These in-plane and out-of-plane lateral forces may control the design of masonry walls. Thus, an understanding of the behaviour of masonry walls under the combined action of normal and shear loads is imperative to the successful design of masonry structures, as well as for the repair and/or strengthening existing structures.

The compressive strength of masonry is substantially lower than the compressive strength of bricks or block units from which the wall is made. On the other hand, the compressive strength of mortar cubes is lower than the compressive loads which the mortar in the horizontal and vertical joints are capable to withstand due to the restraining conditions on their lateral strains arising, from a biaxial or tri-axial state of stress.

An understanding of the behaviour of masonry walls under the combined action of shear and normal loading is essential for the analysis of masonry walls subjected to seismic loadings. Extensive research and experimental work have focused on the investigation of shear behaviour of masonry walls.

2.5.3 Masonry Properties

2.5.3.1 Masonry subjected to Uni-Axial Compression Strength

D'Ayala [40] introduced the following equation to compute the masonry compressive strength from those of masonry units and mortar as

$$\sigma_{cw} = 0.538.\sigma_{cm} + 0.241.\sigma_{cb} \tag{2.6}$$

or as normalized equation to take into account the high sensibility of the masonry strength to the mortar height, the above equation can be written as

$$\frac{f_{cw}}{h_w} = 0.0216.\left(\frac{f_{cb}}{h_b} + \frac{f_{cm}}{h_m}\right) \tag{2.7}$$

with

σ_{cw} = the masonry compressive strength

σ_{cm} = the mortar compressive strength

σ_{cb} = the brick compressive strength

h_w = the masonry wall height

h_m = the mortar height

h_b = the masonry unit height

According to Binda [15], σ_{cw} can be calculated as

$$\sigma_{cw} = \frac{f_{bt,fl}}{v_b + \dfrac{m \cdot v_m - v_b}{1 + m \cdot r}} \tag{2.8}$$

where

$f_{bt,fl}$ = flexural tensile strength of the bricks

v_b, v_m = the lateral deformability coefficients (Poisson's ratio) for brick and mortar, respectively

$m = \dfrac{E_b}{E_m}$

$r =$ = the ratio between brick and mortar thickness

A significant deviation from linearity in the stress-strain relationship can only be observed for values of stresses higher than $0.75\sigma_{cw}$ [15].

Mehlmann [137] stated a relationship to calculate the compressive strength of masonry wall, σ_{cw}, from the mean values for unit and mortar compressive strength as

$$\sigma_{cw} = 0.83 \cdot \sigma_{cb,m}{}^{0.66} \cdot \sigma_{cm,m}{}^{0.18} \qquad (2.9)$$

with

$\sigma_{cb,m}$ = mean unit compressive strength

$\sigma_{cm,m}$ = mean mortar compressive strength

According to EC6 [146], the characteristic compressive strength for un-reinforced masonry using normal mortar is calculated from the relationship

$$f_k = k \cdot \sigma_{cb}^{0.65} \cdot \sigma_{cm}^{0.25} \qquad N/mm^2 \qquad (2.10)$$

with

σ_{cb} = the compressive strength of the masonry units in loading direction according EC6 [146], clause 3.1.2.1 in N/mm^2

k = a factor takes the values $0.4 - 0.6$

For perforated masonry units

$$f_k = f_k \times 0.5 \qquad (2.11)$$

The characteristic compressive strength of masonry walls made from autoclaved aerated concrete or calcium silicate blocks using thin-mortar is calculated from

$$f_k = 0.8 \cdot \sigma_{cb}^{0.85} \qquad (2.12)$$

It can also be calculated from equation (2.10) with $k = 0.5 - 0.7$

The compressive strength of masonry walls using light mortar is calculated from

$$f_k = k \cdot \sigma_{cb}^{0.65} \qquad N/mm^2; \qquad (2.13)$$

$$\sigma_{cb} \le 15 \qquad N/mm^2;$$

$$k = 0.55 - 0.8$$

According to DIN 1053-1[46], the characteristic compressive strength is calculated as

$$f_k = \sigma_0 / 0.35 \qquad (2.14)$$

(σ_0 Values are in DIN 1053-1)

Powell/Hodgkinson [175] introduced a stress-strain relationship for different types of masonry units, which is shown in Figure 2.6.

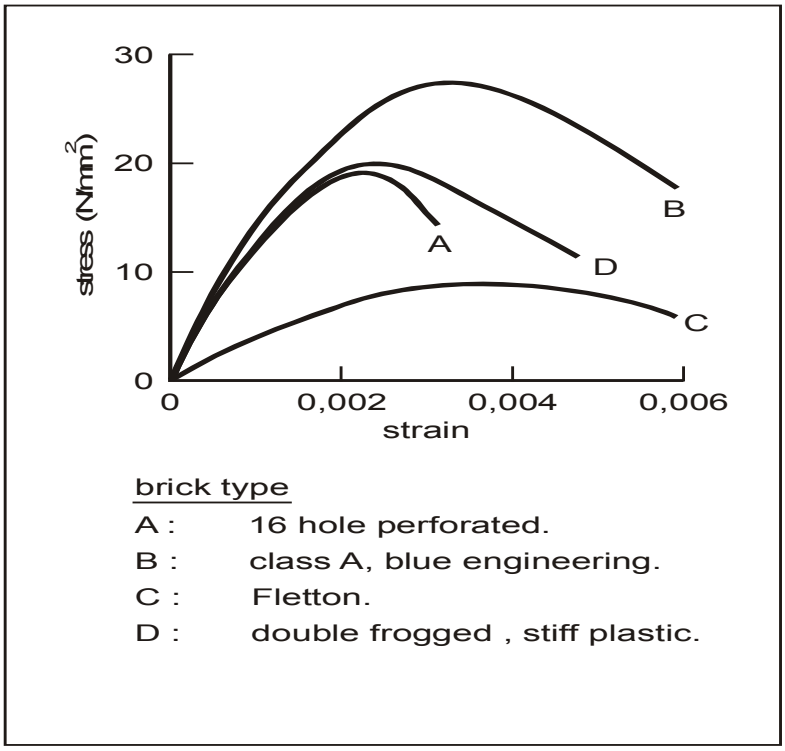

Figure 2.6: Typical stress-strain diagram of masonry, according to Powell and Hodgkinson [175]

2.5.3.2 Tension Strength of Masonry

The tension strength of masonry compared to its compression strength is very small.
The transfer of forces through the vertical joints is neglected [188] as shown in Figure 2.7.
The failure shape depends on the whether the loading is perpendicular or parallel to the direction of bed mortar joints. The unit tensile strength or unit/mortar shear strength governs the failure.

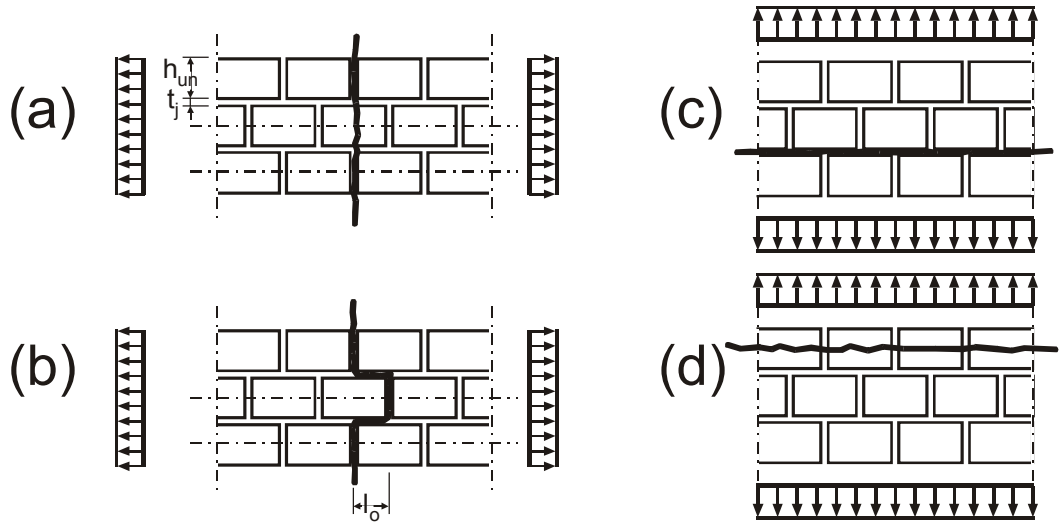

Figure 2.7: Modes of failure of masonry under tensile stress, according to Schubert [188]

- Tension Normal to the Bed Joint

The cracks are either along the bed joint or in the units parallel to the unit length. Thus, the governing values are the unit tensile strength in the direction of unit height or the adhesive shear strength between the unit and the bed joint mortar, (see Figures 2.7(c),(d)).
The masonry tension strength is determined from the following relationships [188]

$$f_{t,ma} = f_{th,b}$$
$$f_{t,ma} = f_{ta} \qquad (2.15)$$

- Tension Parallel to the Bed Joint

There are two possible failure cases can be occurred in this case depending on whether the unit tensile strength or the unit/mortar shear strength governs. The cracks can be formed either in both the mortar and the units or in the mortar.

- Case 1: The Cracks are in the Mortar Joints and Units (see Figure 2.7(a)).

This case happens when there is high unit/mortar shear strength and the masonry units are of poor quality and/or there is a high compressive strength normal to the bed joint.
To determine the tension strength for masonry in this case, the following equations can be used

$$f_{t,ma} \cdot (h_{un} + t_j) = f_{t,un} \cdot h_{un/2}$$
$$f_{t,ma} = 0.5 \cdot f_{t,un} \cdot \frac{1}{1 + t_j / h_{un}} \qquad (2.16)$$

- Case 2: The Cracks are in the Mortar only (see Figure 2.7(b)).

This case happens when there is a high unit tensile strength and the mortar tensile strength is small and/or the compressive strength normal to the bed joints is small. The masonry tensile strength is calculated as

$$f_{t,ma} \cdot (h_{un} + t_j) = f_{sh} \cdot l_0$$
$$f_{t,ma} = (f_{sh0} + \mu \cdot \sigma_n) \frac{l_0}{1 + t_j / h_{un}} \qquad (2.17)$$

where

$f_{t,un}$ = unit tensile strength in the direction of the unit length
t_j = height (thickness) of the bed joint
h_{un} = unit height
f_{sh0} = cohesion between unit and bed mortar joint
l_0 = overlap length
μ = coefficient of friction
σ_n = acting compression strength perpends to the bed mortar joints

The adhesive shear strength of the interface between unit and bed mortar joints (f_{sh0}) are for normal and lightweight mortar ranges from $0.05 \; to \; 0.8 \; N/mm^2$. For calcium silicate and aerated concrete units these values are distinctly lower (mostly lower than $0.3 \; N/mm^2$) compared to clay bricks and lightweight concrete units (mostly exceeding $0.4 \; N/mm^2$).

For thin layer mortar (f_{sh0}) they are greater than $0.5\,N/mm^2$. In general in most cases, the values are ranging between $0.5\ and\ 1.0\,N/mm^2$ [188].

To determine the unit tensile strength, Marzahn [129] introduced the following relationships

$$f_{bt,ax} = 0.26.f_{b,cyl}^{\ 0.67} \tag{2.18}$$

$$f_{bt,ax} = 0.72.f_{bt,sp} \tag{2.19}$$

$$f_{bt,ax} = 0.5.f_{bt,fl} \tag{2.20}$$

where

$f_{bt,ax}$ = the axial tensile strength of bricks

$f_{bt,sp}$ = the splitting tensile strength of bricks

$f_{bt,fl}$ = the flexural tensile strength of bricks

The tensile strength of the solid units in the direction of unit-length and in the direction of unit-height is equal, because there are no test results for the tensile strength in the direction of the unit-height.

2.5.3.3 Elasticity (Young's) Modulus

Binda [15] stated a relationship for the elasticity modulus of the masonry expressed as a function of the components-moduli as

$$E = E_b \frac{1+r}{r + E_b / E_m} \tag{2.21}$$

where

r = the ratio between the unit height and mortar thickness

E_b, E_m = the modulus of elasticity for unit and mortar, respectively

According to EC6 [146], the elasticity modulus, E is calculated as

$$E = 1000 \cdot f_k \tag{2.22}$$

and the shear modulus is given by $G = 0.4E$

Sihna [200] introduced the following equation to determine the elasticity modulus as

$$E = 1180\left(f_c\right)^{0.83} \qquad MPa \qquad (2.23)$$

Ganz [69] presented the following values for the Elasticity modulus, E and shear modulus, G, for masonry. These values are presented in Table 2.3 depending on the brick type

Brick type	E	G/E
Clay	$1000 \cdot \sigma_{cw}$	0.20
Calcium Silicate	$1000 \cdot \sigma_{cw}$	0.45
Concrete	$1200 \cdot \sigma_{cw}$	0.35

Table 2.3: Masonry Elastic and shear Moduli, according to Ganz [69]

2.5.4 Masonry subjected to In-Plane Shear

Many authors have investigated the behaviour of masonry under in-plane shear and, at the same time, with vertical loads. Examples of the arrangements of these experiments used previousely are given in Figure 2.8. Lourenco [112] reported that, depending on the nature of the test, crack pattern and failure of the URM shear walls depend on the combination of the applied loads (ratio of the racking to the compressive loads, R/C), wall geometry and properties of the constituents' materials.

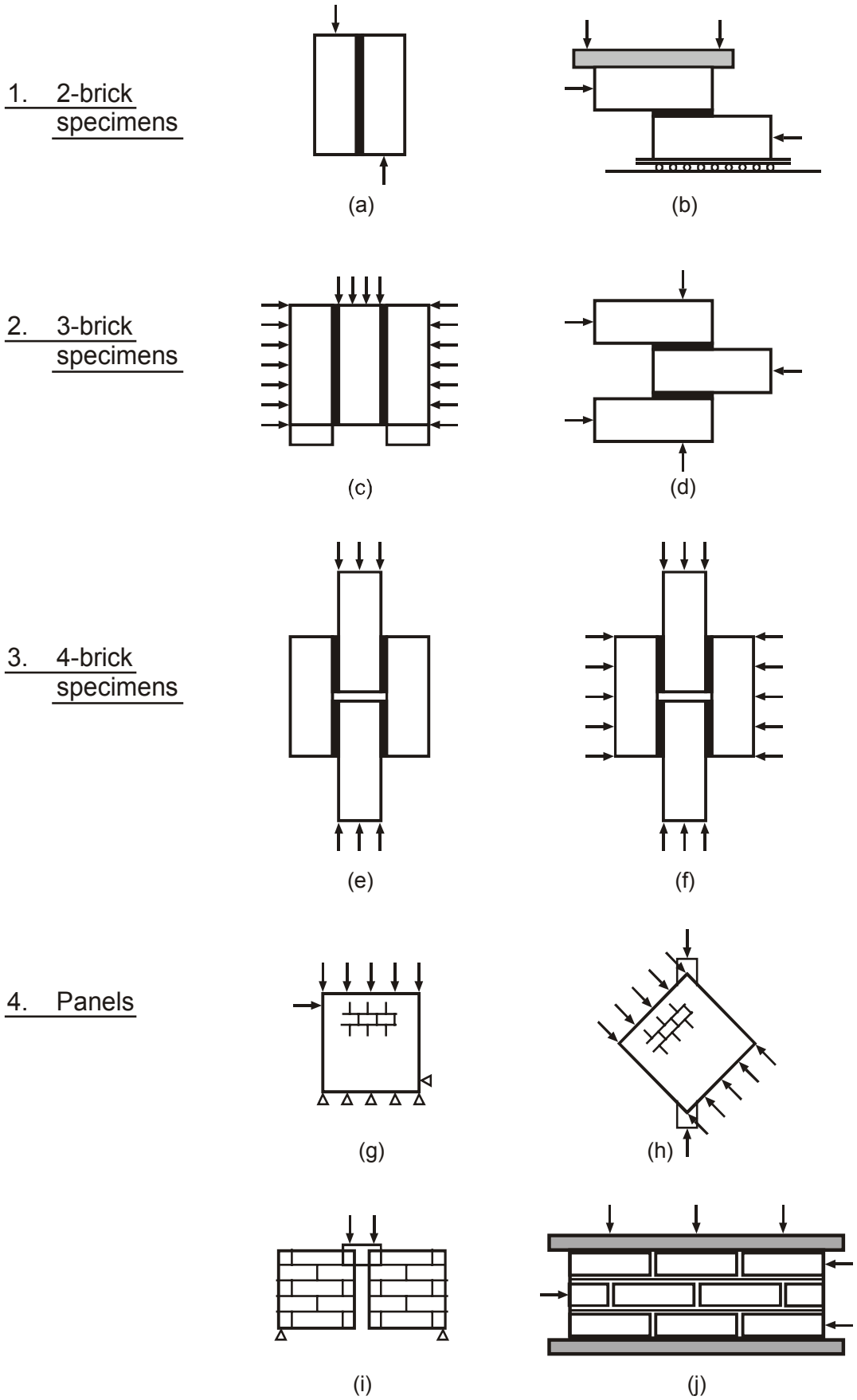

Figure 2.8: Test arrangements for biaxial loadings of masonry, according to Brain [20]

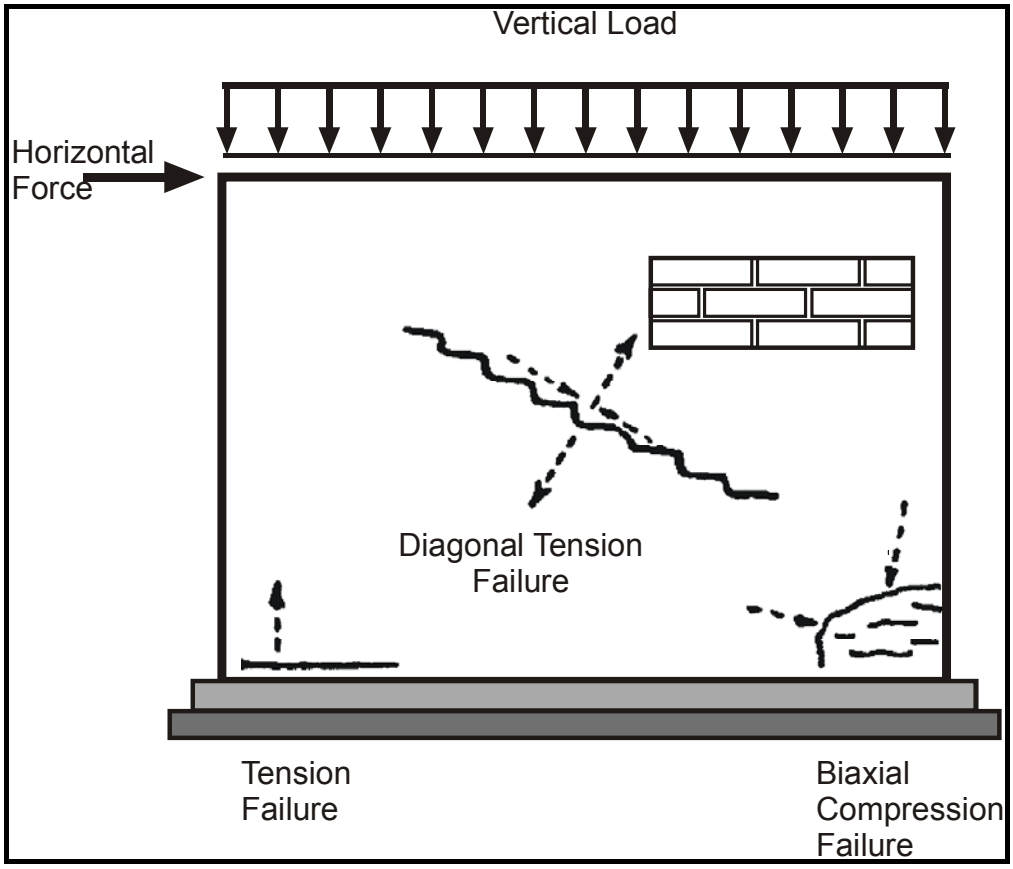

Figure 2.9: Modes of failure of shear wall, according to [168]

After Page [168] the potential regions of local failure are shown in Figure 2.9. Toe failure occurs by crushing under biaxial compression stress. Failure usually occurs by splitting and spalling normal to the plane of the wall. This failure occurs mostly when the height to length ratio of the wall is relatively high.

Failure at the heel occurs when vertical loads are low in relation to the racking load. This results in the development of the tensile stresses normal to the bed joint with a consequent horizontal crack.

Failure in the centre of the plane is commonly described as ‘’shear failure’’ and is typified by a diagonal crack. Failure actually occurs in the bed and header joints under a combination of principal tensile and compressive stresses, with subsequent sliding occurring along the joints.

By changing the shear load-directions; the cross-cracks pattern is formed, which is very typical for earthquake damage for masonry walls.

The shear failure occurs when the ratio of wall's height to its length, is small. When the vertical load is small and the mortar joints are weak, the cracks are forming in the head and bed joints, leading to the stepwise crack pattern. This can be caused by either exceeding the bond and shear friction resistance or the mortar tensile strength. This cracks form is ductile, because, the wall after the first crack can withstand more vertical loads gradually until the wall is damage. In cyclic loading, the wall exhibits large deformation with constant strength as shown in Figure 2.10. The vertical load transfers through the horizontal joints, even when width of the cracks becomes very large. Wall failure occurs after numerous runs caused by both the excessive opening of the cracks and local failure of the units in the lower corners.

When the vertical load is high and the masonry units have small tension strength, the cracks running suddenly in the units. This kind of failure is brittle failure with small energy dissipation and high stiffness degrading.

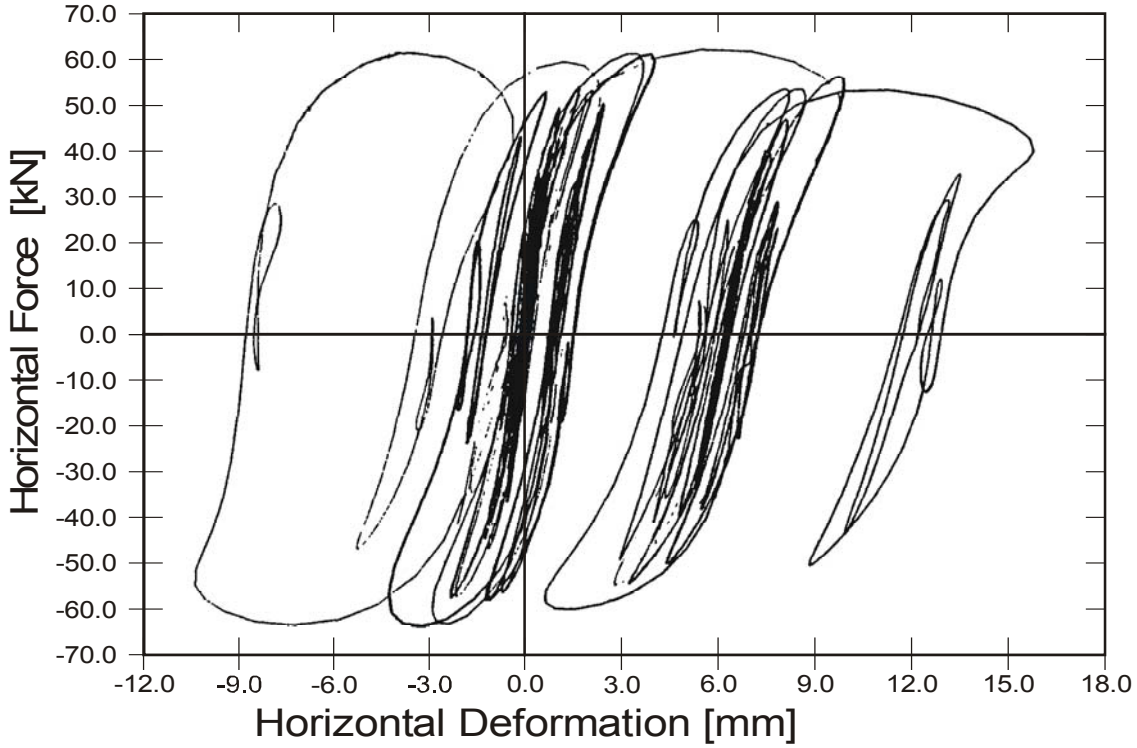

Figure 2.10: Horizontal force versus horizontal deformation in case of mortar-failure, with vertical load: 1 *MPa* , according to [125]

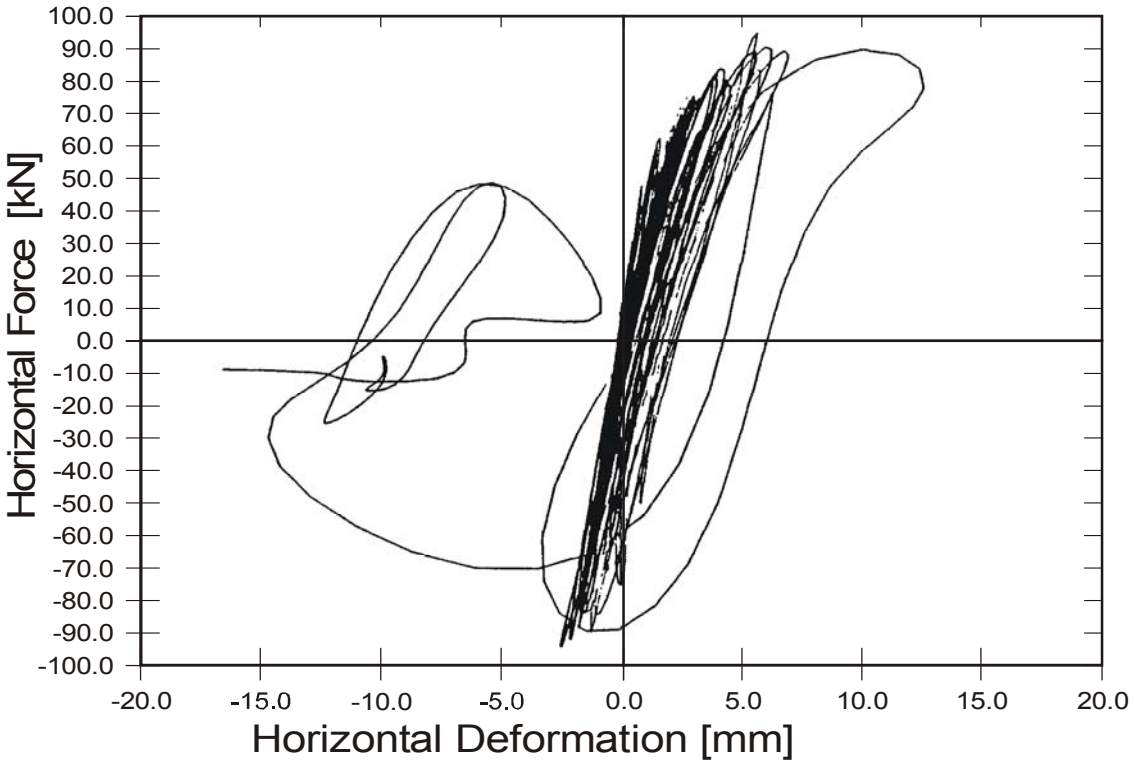

Figure 2.11: Horizontal force versus horizontal deformation in case of mortar-units-failure, with vertical load: 1.5 *MPa* , according to [125]

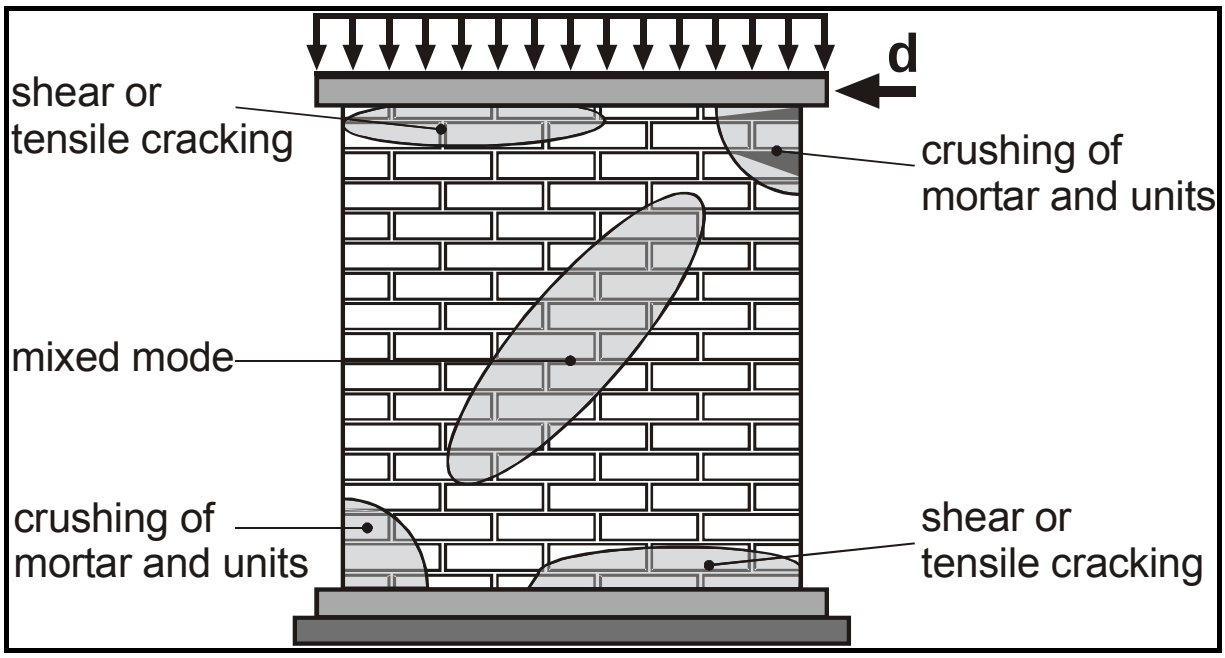

Figure 2.12: Modes of failure for shear walls without openings [112]

The individual partial areas slide off on these cracks showing sudden collapse (see Figure 2.11 for cyclic loading.)

The above explanation is approved by the experiments conducted by Lourrenco [112]. For shear wall, the arrangements and crack patterns from these tests are shown in Figure 2.12. Lourenco [112] observed that the first crack occurred near the heel of the wall, followed (depending on ratio of R/C) by the mixed mode crack and finally by the crushing of the compressed toe of the shear wall.

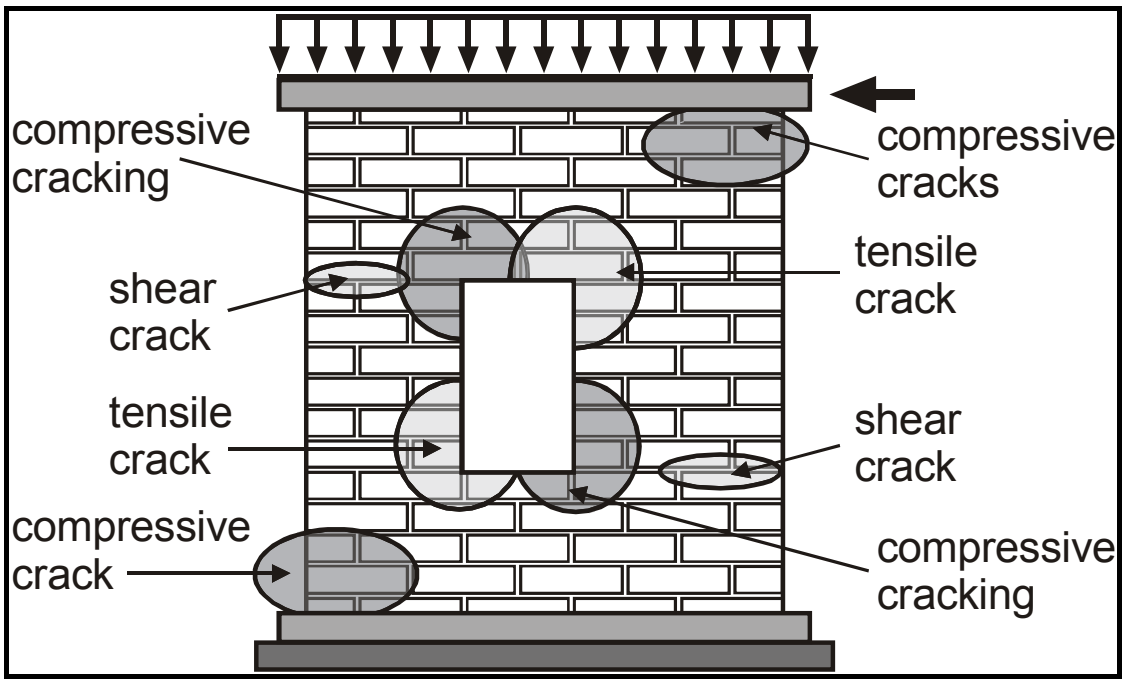

Figure 2.13: Modes of failure for shear walls with opening [112]

Figure 2.13 shows the failure mechanism for shear walls with openings[112]. In this case, the observed possible crack pattern was as follows: firstly diagonal cracks arise from the possible four locations from the four corners of the opening; then followed by tensile cracks arised from the outer side of the two piers around the opening; and finally, compressive cracks appeared.

The magnitude and inclination of the principal tensile stress is influenced primarily by the ratio of vertical load to the horizontal racking load. The shear strength of the wall increases significantly with the increasing amount of vertical load.

Walls subjected to seismic loading progressively degrade due to repeated load reversal. All or some of the above failures occur at the

locations appropriate to the direction of loading. In most cases, under cyclic loading, it is reported in ([224,95,89,2]), that a wall rocks on its base as uplift occurs at the appropriate end of the wall. This may corresponds with gradual shedding of bricks from the tension end and/or local crushing in the compression region of the wall.

2.5.5 Failure Criteria

Mann [125] reported that the shear failure theory developed for static loading can also, in principal, be applied on seismic loading ([121] to [124]).

The basis of the shear theory [125] is the assumption that no shear forces can be transferred in the vertical joints, as shown in Figure 2.14. These joints have no axial pressure; they are subjected to shrinkage of the mortar, and are often poorly constructed. Mann [125] gave three possible failure, as shown in Figure 2.15. They are explained as follows:

1. In the region (a), the failure occurs in the bed joint and is characterised as a stepped crack for small values of normal stress, σ_n and a minimum effective friction.
2. In the region (b), the failure occurs in the units, as the existing friction is enough to resist the shear force.
3. In the region (c), compression failure occurs for large values of the normal stress, σ_n with the limiting value β_R for $\tau = 0$.

The dashed line in the $\tau - \sigma$ diagram (Figure 2.15) represents a curve path, which is in accordance with Mohr's enveloping curve for homogeneous material.

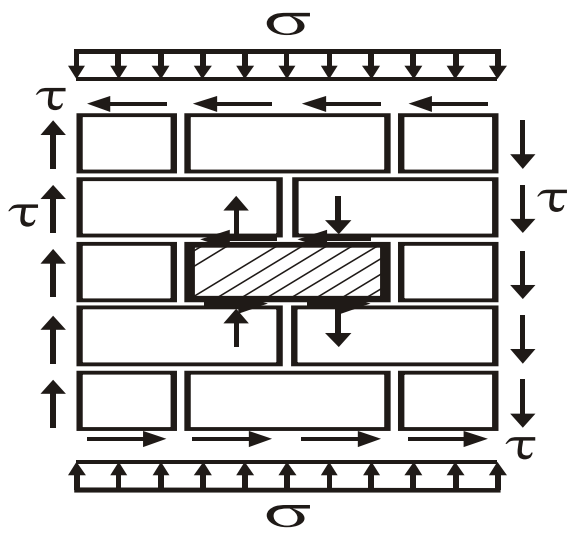

Figure 2.14: Stress state of the shear wall, according to Mann [125]

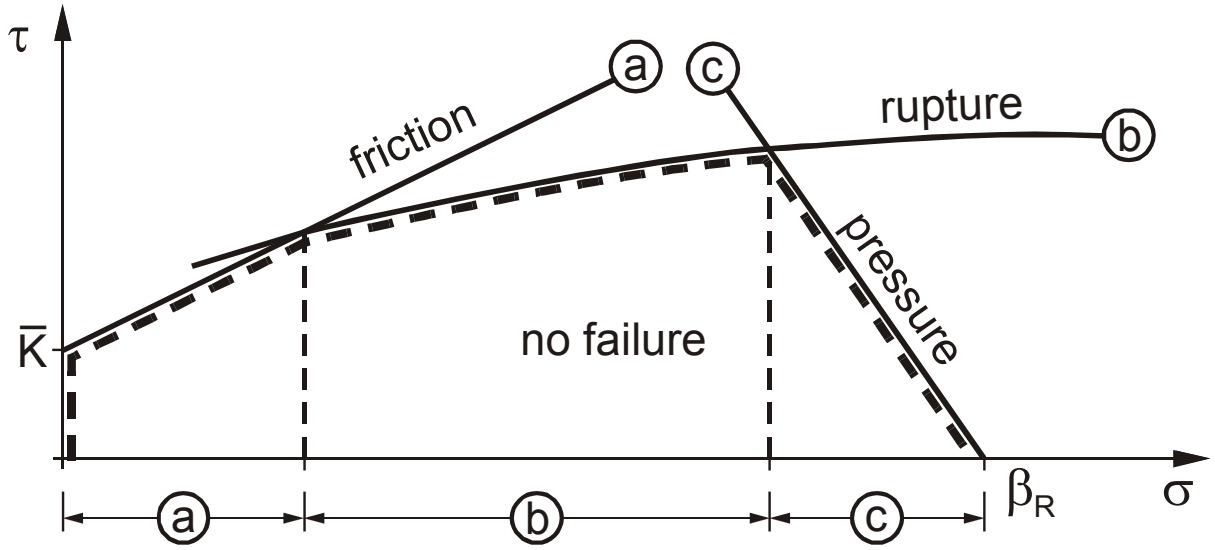

Figure 2.15: $\tau - \sigma$ failure surface, according to Mann [125]

All enveloped τ / σ values are safe. All non-enclosed τ / σ values would fail.

With small σ the failure is occurred by joint failure, with large σ caused by unit rupture and with very large σ values caused by compressive failure.

The behaviour of the masonry walls at failure under shear stresses and compression stresses can be expressed by a simplified relationship which takes the form of a Coloumb criterion [168], as

$$\tau = \tau_0 + \mu\sigma_n \qquad (2.24)$$

where

τ = shear strength at pre-compression

τ_0 = shear strength at zero pre-compression (cohesion between bed-mortar joints and the masonry units)

μ = an apparent friction coefficient

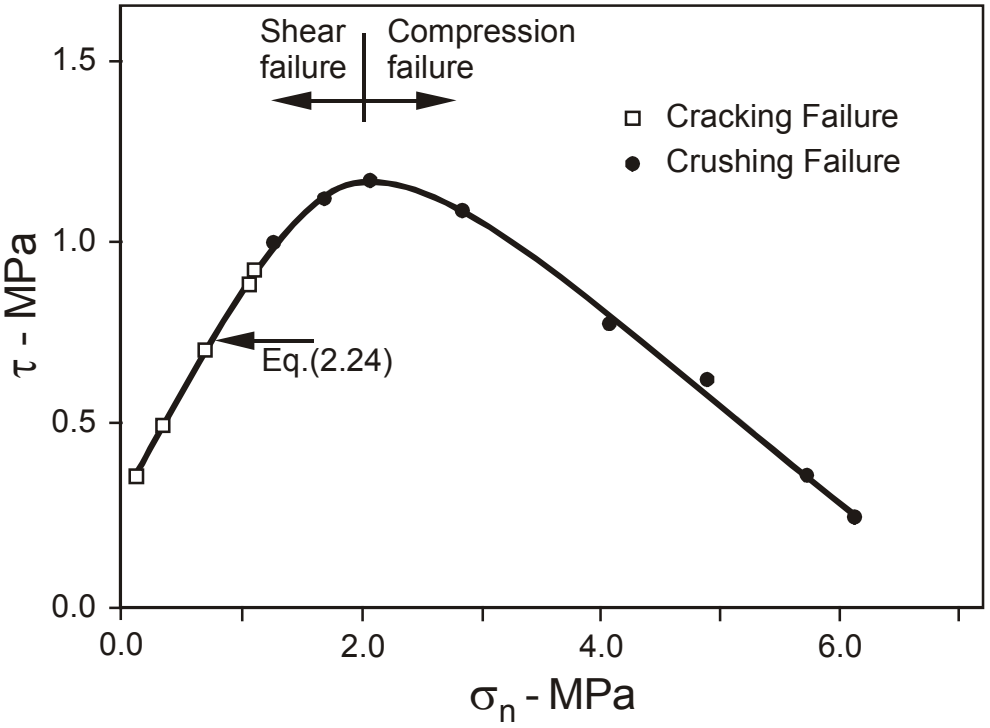

Figure 2.16: $\tau - \sigma$ failure surface, according to Page [163]

It necessary to mention that Page [163] reported that the Mohr-Coulomb-criteria are true for small values of the normal compressive strength, $\sigma_n \leq 2\,MPa$. Because, when $\sigma_n > 2\,MPa$, i.e., when the vertical normal force is high in relation to the racking force, a crushing failure may occur in the region of the toe of the wall. In this case, equation (2.24) does not apply as straight line, and check of the compressive capacity should be made as shown in Figure 2.16.

Mirabella [139] stated that the cohesion, $\tau_0 = 0.23$ and the friction coefficient, $\mu = 0.57$ (equivalent to friction angle of 30^0). The shear strength can be taken to be equal $5-10\,\%$ of compressive strength of the masonry.

According to the EC6 [146], the characteristics shear strength for un-reinforced masonry, f_{vk}, can be calculated as

$$f_{vk} = f_{vko} + 0.4.\sigma_d \tag{2.25}$$

where

f_{vk0} $= 0.1 - 0.3 \quad N/mm^2$

σ_d $=$ the design compressive strength normal to the shear load-direction, calculated from EC6 [46]

The characteristic shear strength, f_{vk} is replaced by the shear-capacity according to DIN 1053-1

$$f_{vk} = \gamma \cdot \tau \le \beta_{RHS} + \bar{\mu} \cdot \sigma_n \qquad \textit{shear failure} \tag{2.26}$$

and if

$$f_{vk} \le 0.45 \cdot \beta_{RZ} \sqrt{1 + \frac{\sigma_n}{\beta_{RZ}}} \quad \textit{masonry unit tension failure} \tag{2.27}$$

where

β_{RHS} $=$ computed value of the reduced surface shear stress according to DIN 1053-1 [46]

β_{RZ} $=$ masonry unit tension strength

σ_n $=$ normal stress to bed-joint

The factor of safety for masonry-mechanical properties in the load-carrying capacity analysis for earthquake, $\gamma_M = 1.2$.

Ganz and Thurlimannn [71] and Mojsilovic [142] extended the Page's work [166] on the static properties of solid clay masonry tested, at the limits of failure, to include extruded masonry. They established the failure surface for masonry under in-plane, quasi-static loading. This type of analysis has been included in the modern codes of practice to provide a sound rational approach to methods of static analysis.

For URM with no tension, the failure criteria after Mojsilovic [142] is shown in Figure 2.17. The in-plane stress components, $\sigma_x, \sigma_y, and\ \tau_{xy}$ are shown in Figure 2.17(a). The failure surface consists of 6 parts with the following failure conditions

$$\tau_{xy}^2 - \sigma_x \sigma_y \leq 0 \tag{2.28}$$

and the compressive strength limits are described as

$$\tau_{xy}^2 - (\sigma_x + f_x)(\sigma_y + f_y) \leq 0 \tag{2.29}$$

the sliding failure of the masonry units is described as

$$\tau_{xy}^2 + \sigma_y (\sigma_y + f_y) \leq 0 \tag{2.30}$$

the no tension criteria and the sliding criteria in the bed joints are described as

$$\tau_{xy}^2 + \sigma_x \left[\sigma_x + 2c \tan\left(\frac{\pi}{4} + \frac{\varphi}{2} \right) \right] \leq 0 \tag{2.31}$$

and

$$\tau_{xy}^2 - (c - \sigma_x \tan\varphi)^2 \leq 0 \tag{2.32}$$

respectively. Finally, Mojsilovic [142] considered the potential slip lines aligned with the head joints criterion as

$$\tau_{xy}^2 - \left(\frac{c_b}{2} - \sigma_y \tan\varphi_b \right)^2 \leq 0 \tag{2.33}$$

where

c_b and φ_b denote the cohesion and the angle of internal friction of the block material, respectively

$f_x, f_y =$ uni-axial compressive strengths of masonry perpendicular and parallel to the bed joints

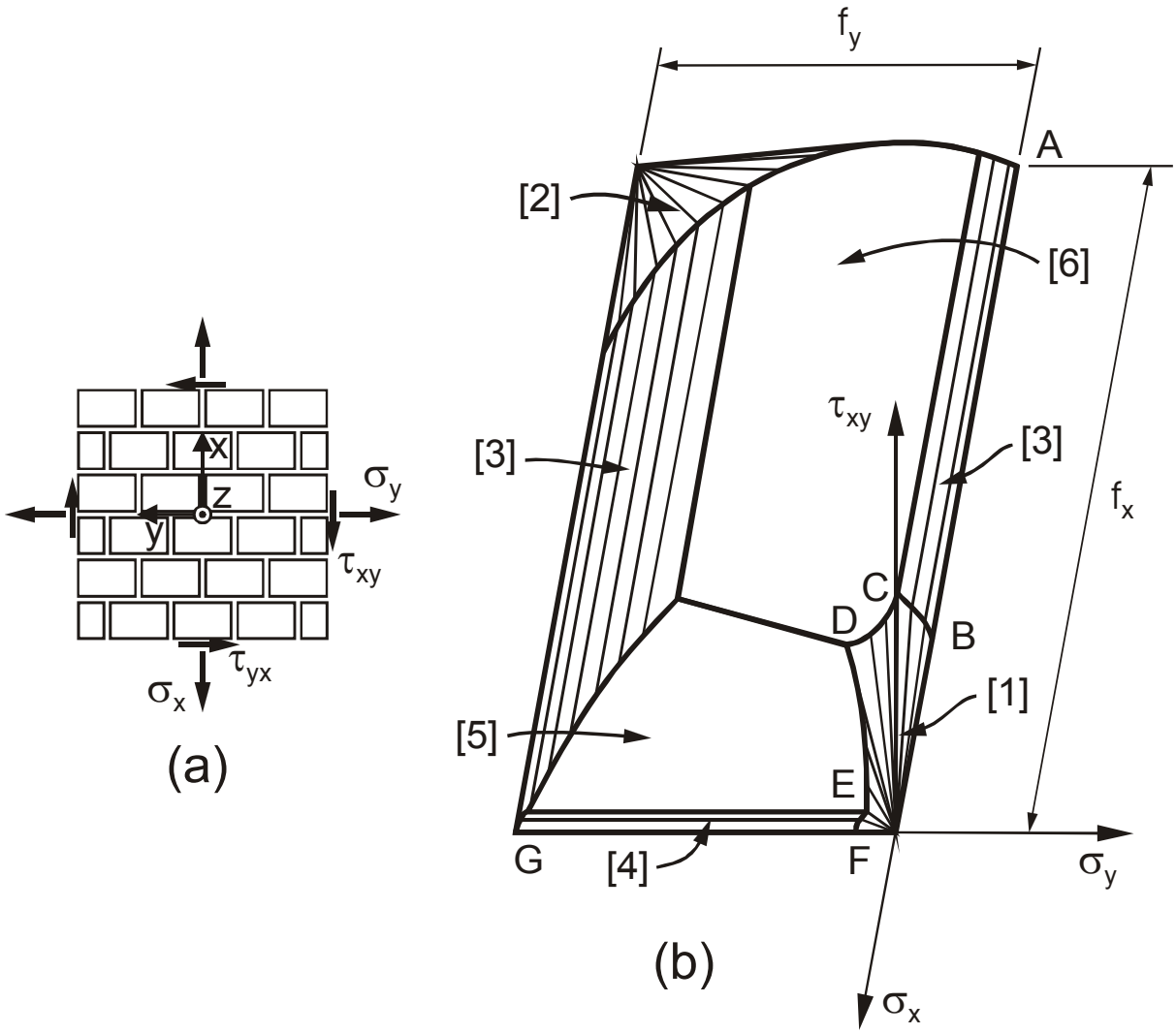

Figure 2.17: Failure criteria for masonry without tension (Material parameters: $c = f_y/25.$; $c_b = f_y/4.$; $\tan\varphi = 3/4$; $\tan\varphi_b = 3/4$), according to Mojsilovic [142]

The strength of masonry subjected to biaxial stress depends not only on the magnitude and sense of the principal stresses $\sigma_1 and \sigma_2$ but also on their inclination θ to the bed and header joints, which acts as plane of weakness.

In general, a three-dimensional failure surface is required to define the failure of a shear wall (Page et al. [155,119,162,[167,163,156,160,159, 157]).This failure surface is a function of the principal stresses, σ_1,σ_2 and the joint inclination angle, θ. Then, there are a failure surfaces for the compression-compression, tension-compression and tension-tension zones.

- Compression-compression zone.

Figure 2.18 shows the modes of failure of brickwork under compressive loads, after Page [162]. For the uni-axial compressive loading, the failure occurred by cracking and sliding in the joint or in a combination mechanism which involves both bricks and joints, depending on the orientation of the joints to the applied load.

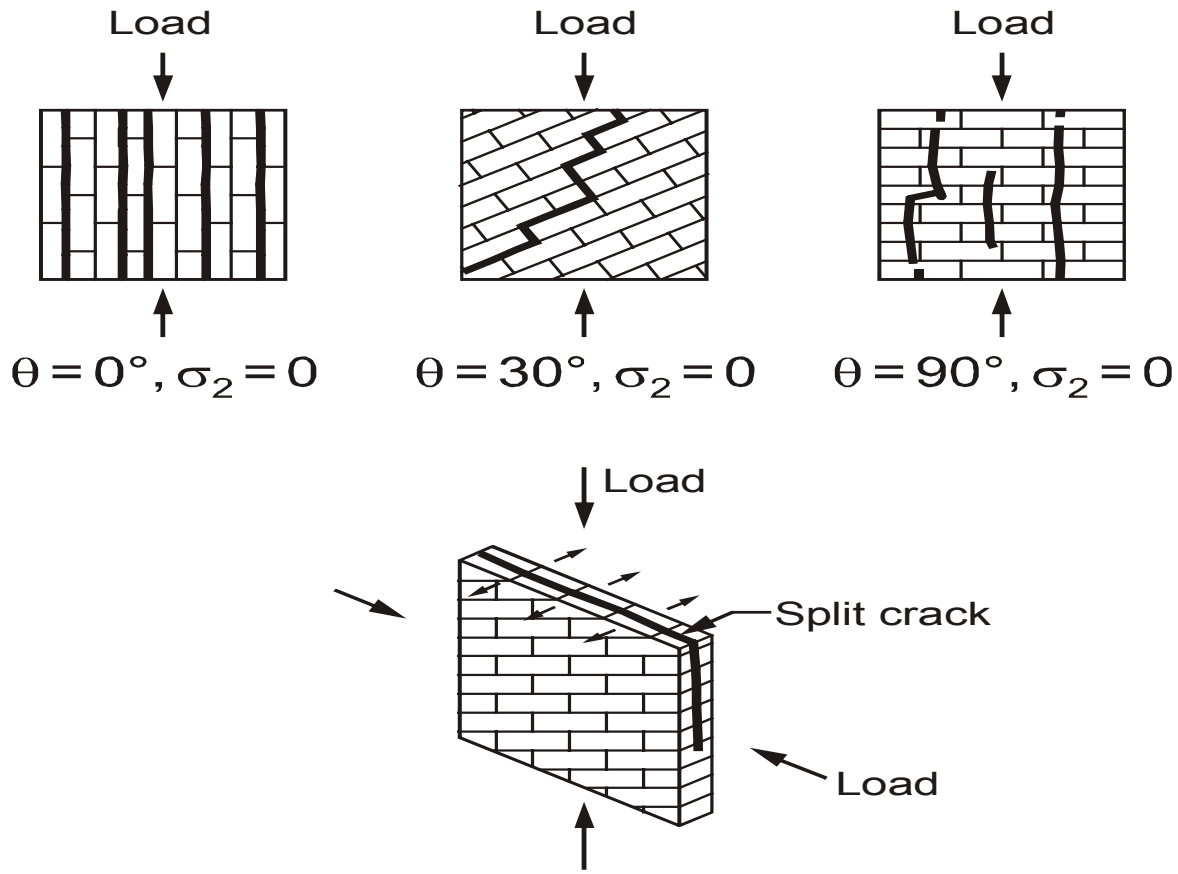

Figure 2.18: Failure modes for uni-axial and biaxial compression tests on brickwork according to Page [162]

The bed joint orientation plays no role in case of biaxial compression, where the splitting failure occurred in a plane parallel to the free surface of the specimen regardless the mortar inclination angle.
The relationship between vertical compressive stress, σ_1 and horizontal stress, σ_2 for different values for the bed-joint inclination angle, is shown in Figure 2.19.

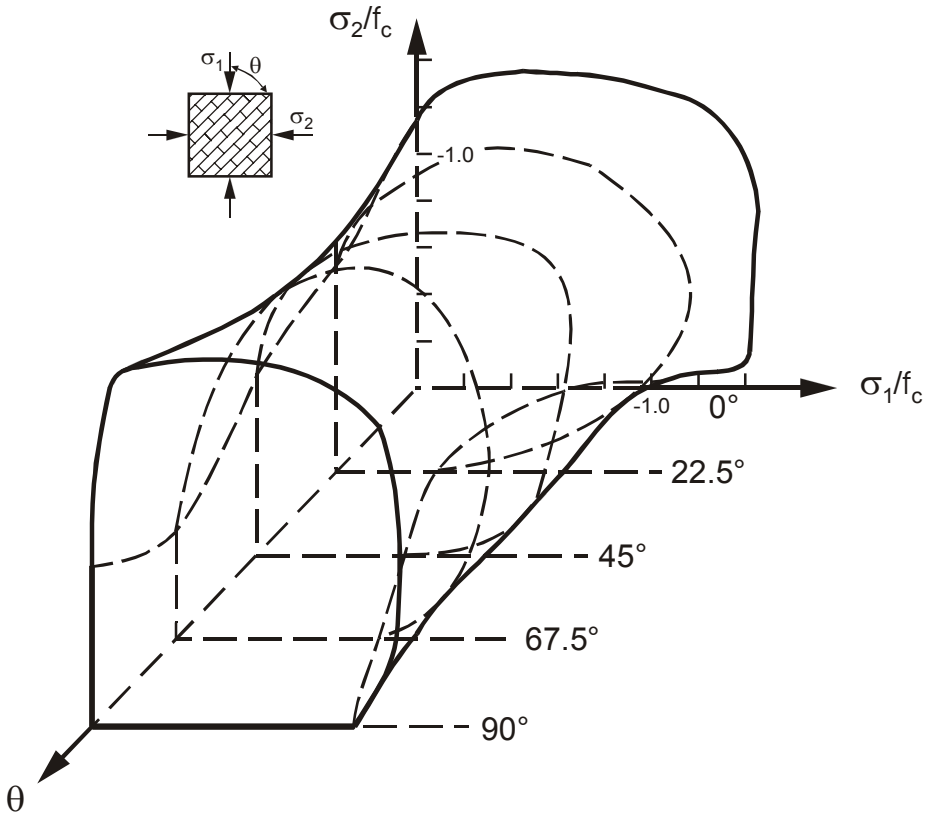

Figure 2.19: Failure surface of brickwork loaded in biaxial compression, according to Page [162]

- Tension-Tension Zone

Due to the complexity of performing tension-tension tests on masonry assemblage as well as the difficulties of applying tensile loads to a material with an inherently low tensile strength, Page [161] used an iterative finite element program to obtain the tension-tension failure surface shown in Figure 2.20 for different values of bed inclination angle. The failure surface in this case depends on the relation between the shear and tensile strength of the assemblage and a function of the principal stress ratio and bed inclination angle.
All failure in this zone propagates along the joint. Final failure occurs when a sufficient number of joints have failed to allow collapse of the wall.

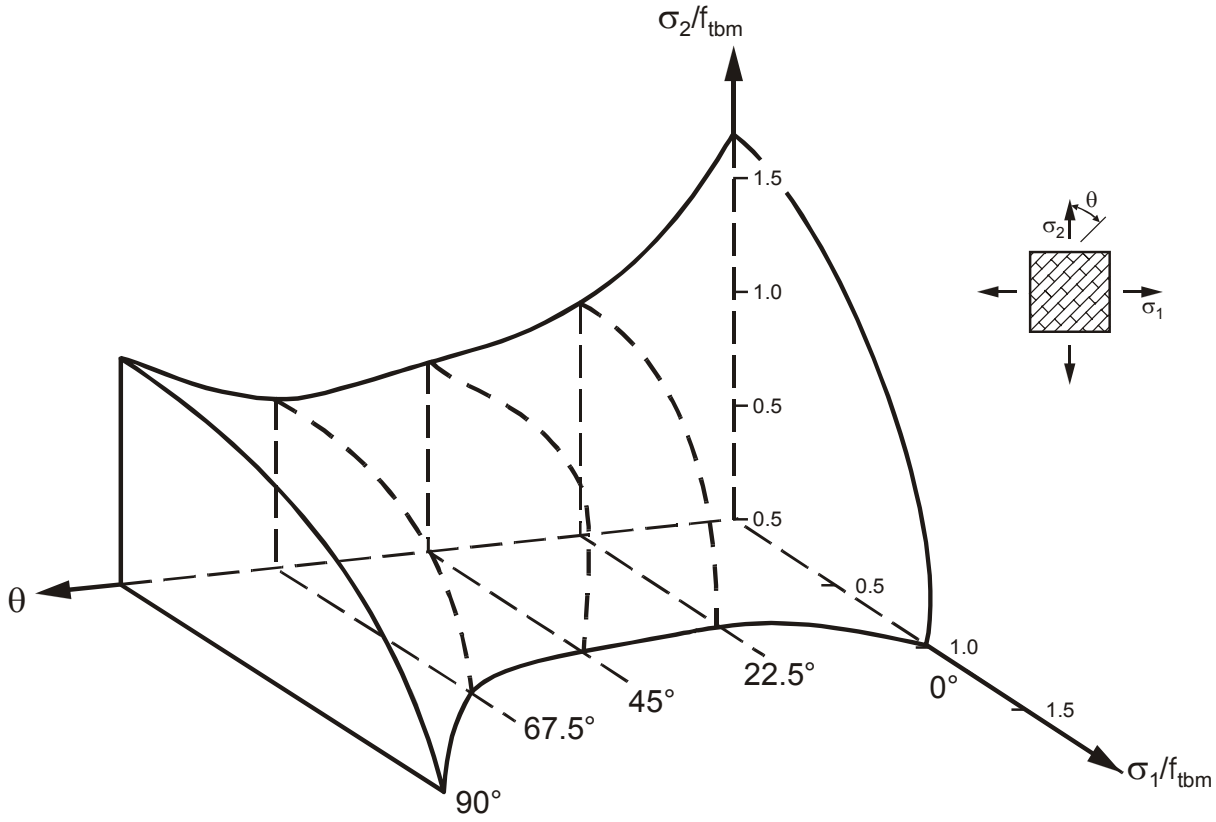

Figure 2.20: Failure surface of brickwork loaded in biaxial tension, according to Page [161]

- Tension-Compression Zone

The possible failure modes are shown in Figure 2.21. These are joint failure, combined brick-joint failure and brickwork compression failure in a plane normal to the wall-plane depending on the mortar inclination and σ_1, σ_2 relationship.

The failure surface for this case is presented in Figure 2.22.

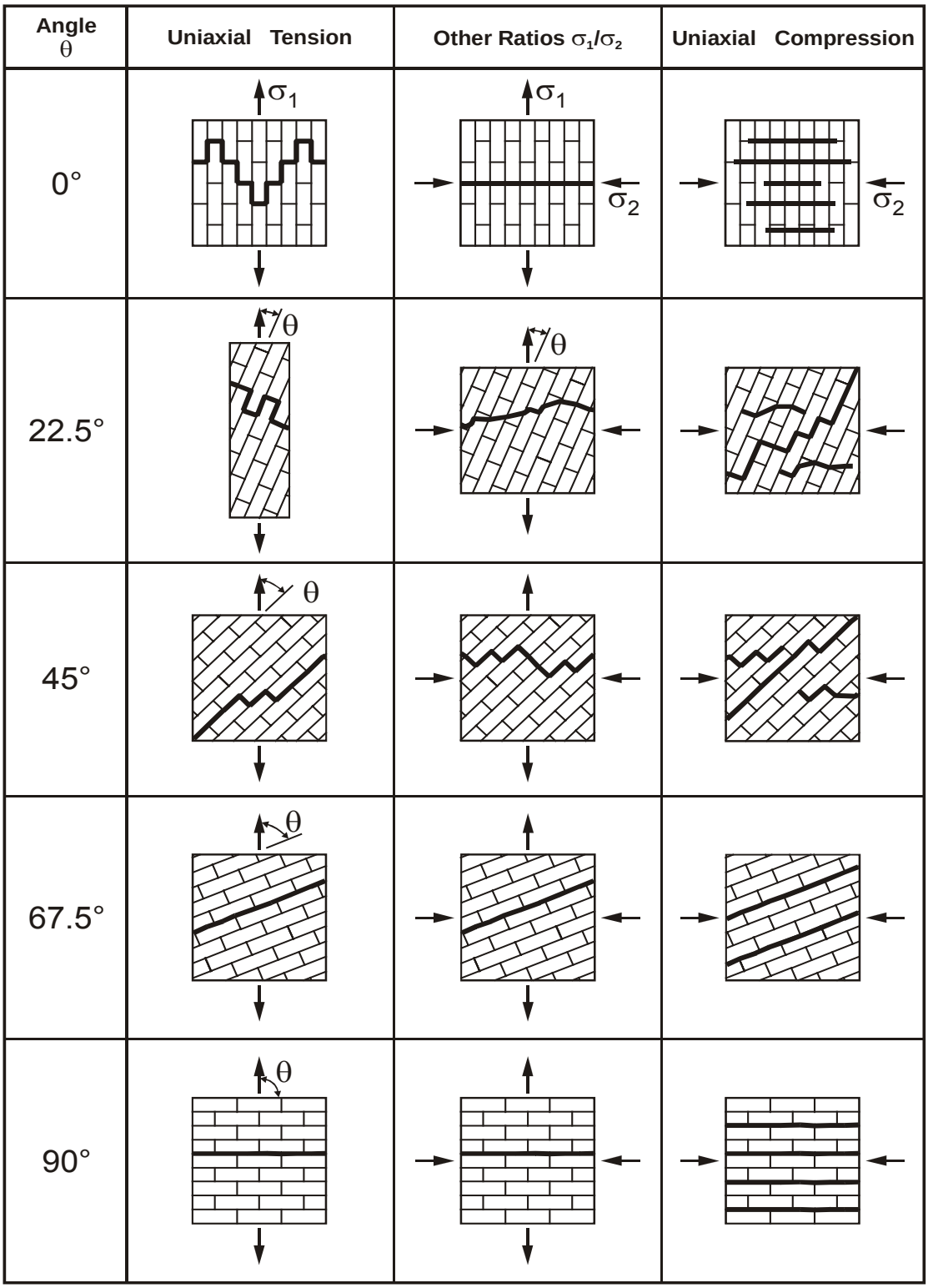

Figure 2.21: Biaxial tension-compression failure modes, according to Page [162]

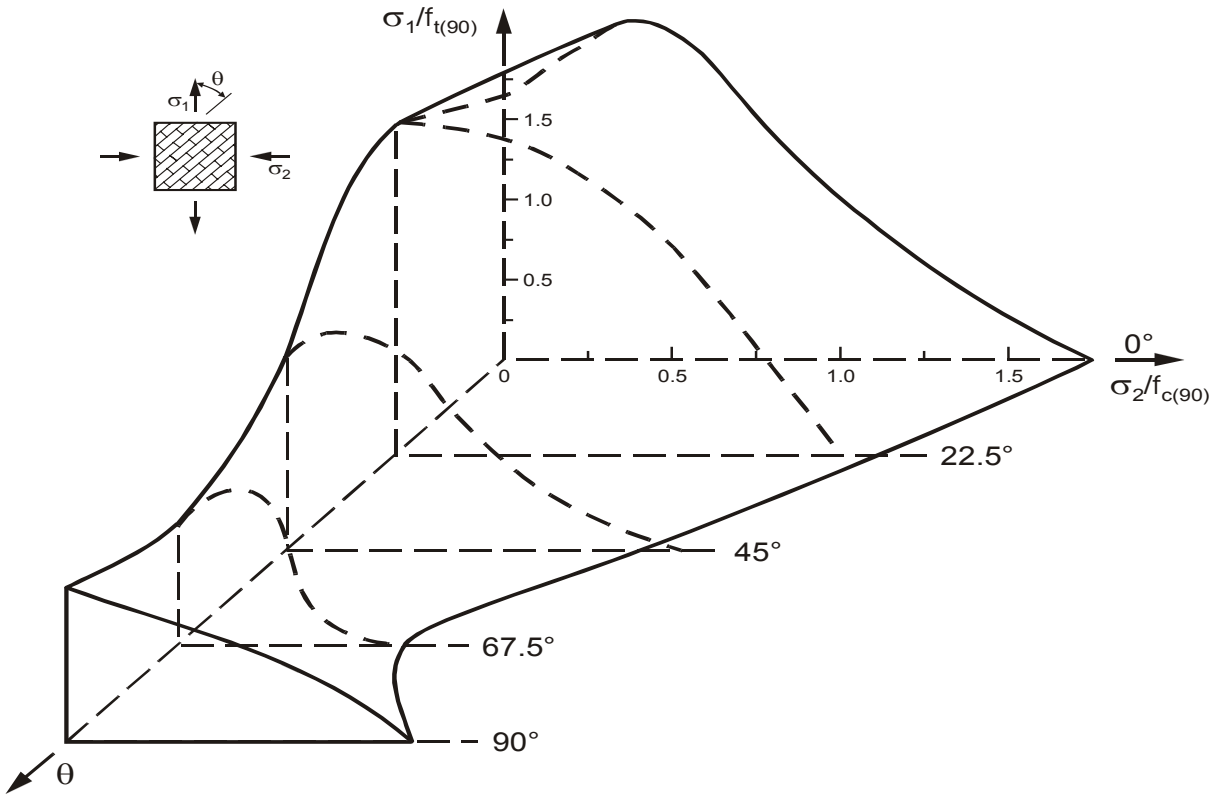

Figure 2.22: Failure surface of brick masonry in the tension-compression range, according to Page [162]

2.6 Material Behaviour under Cyclic Loading

The typical material behaviours under cyclic loading are shown in Figure 2.23. There are three different types of behaviour as:

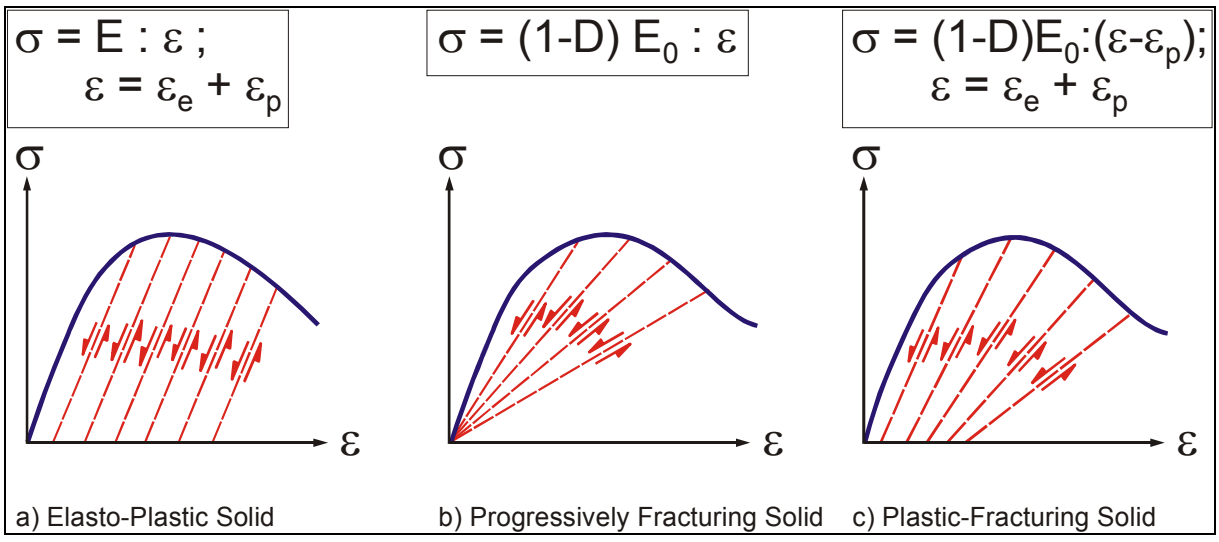

Figure 2.23: Typical material behaviours

- ***Elasto-Palstic Behaviour***

The elato-plastic behaviour is shown in Figure 2.23(a), for which the irreversible or plastic strain is observed upon unloading, but the unloading-reloading lines always follow straight lines that are parallel to the initial tangent of the stress-strain curve.
In other words, the stiffness of elastic unloading-reloading does not change with plastic deformation material. Non-linearity is due to the existence of plastic strains. This type of material behaviour can be generally described by the theory of plasticity.

- **Progressively Fracturing Behaviour**

Figure 2.23(b) shows the typical elastic behaviour, where, upon unloading, the material retains to its free state of stress-strain without any occurrence of plastic deformation. However, the slope of the unloading-reloading line decreases with increasing the straining. Material non-linearity is due to stiffness degradation. This behaviour can be studied by the continuum damage theory. It is also used in the formulation of the three-dimensional damage model which is developed in this work for masonry using an effective strain value for the strain values in the x, y and z directions.

- **Plastic-Fracturing Behaviour**

This behaviour is shown in Figure 2.23(c) and it is a combination of the above mentioned two behaviours. This behaviour can be studied by the damage theory combined with the plasticity theory.

The response of brickwork to cyclic loading exhibits a very notable degradation of stiffness and also,eventually, of compressive strength (softening). These phenomena, occurring in many other materials, are the central and expanding domain of continuum damage mechanics (see e.g. [102, 105,127, 133,135 ,180]).

The natural period of a building typically increases during a strong earthquake [176], indicating that the damage of the structure has caused a loss of stiffness.
The damage evolution law is so formulated that the damage coefficient, D, may never decrease [119].

2.7 Damage Theory Background

The damage of materials is the progressive physical process by which they break. The mechanics of damage, is the study, through mechanical variables, of the mechanisms involved in this deterioration when the materials are subjected to loading. At the micro-scale level, this is the accumulation of micro-stresses in the neighbourhood of defects or interfaces and the breaking of bonds, which both damage the material. At the meso-scale level of the representative volume element this is the growth and the coalescence of micro-cracks or micro-voids which together initiate one crack. At the macro-scale level, this is the growth of that crack. The first two stages may be studied by means of the damage variables of the mechanics of continuous media defined at the meso-scale level. The third stage is usually studied using fracture mechanics with variables defined at the macro scale level.

When studying engineering materials such as metals and alloys, polymers and composites, ceramics, rocks, concrete, and wood, it is very surprising to see how such materials, which have different physical structures, are similar in their qualitative mechanical behaviour. All show elastic behaviour, yielding, some form of plastic or irreversible strain, anisotropy induced by strain, cyclic hysteretic loops, damage by monotonic loading or by fatigue, and crack growth under static or dynamic loads. This means that the common meso-scopic properties can be explained by a few energy mechanisms that are similar for all these materials. This is the main reason that it is possible to explain material behaviour successfully with the mechanics of continuous media and the thermodynamics of irreversible processes, which model the materials without detailed reference to the complexity of their physical microstructures.

All engineering materials have a composite character in that, on a microscopic scale, they consist of a fine dispersion of one phase in another. But for simplicity, in considering the elastic properties of materials, this microscopic scale is ignored. Thus, the two terms that describe the engineering materials are the homogeneity and the isotropy; This means that the properties at a point in the material are constants in all directions (isotropic) and they are independent of position in the material (homogenous).

In this section, the general formulations and assumptions used in the analysis of masonry walls under monotonic and/or cyclic loading under consideration are presented. These formulations are based on the continuum damage theory.
These general formulations are valid for the masonry walls under both monotonic and/or cyclic loading by using a two-parameters, scalar, damage model, based on the finite-elements method by considering the masonry as an orthotropic after the homogenisation technique.
Models for elastic degradation and damage based on loading surfaces are becoming popular and widely used for constitutive modelling of engineering materials such as concrete, masonry, rock, ceramics, etc. A number of formulations have been proposed in recent years [24],[26]. These include how to formulate general isotropic as well as anisotropic degradation in a standard unified way.

Here, masonry is treated as a composite material, with masonry units and mortar joints forming its constituents. Each constituent is assumed to behave as an isotropic, linear elastic-brittle material. After the homogenisation technique, masonry is considered as an orthotropic material.

Continuum damage mechanics is a constitutive theory that describes the progressive loss of material integrity due to the propagation and coalescence of micro cracks, micro voids, and similar defects. These changes in the microstructure lead to a degradation of the material stiffness observed on the macro-scale.

The theory of continuum damage mechanics (CDM) provides a rigorous framework to develop constitutive relationships for such materials.
This theory was first proposed by Kachanov [91] to describe creep rupture in metals. It was later extended and applied to static rupture, fatigue and creep of materials. In the late 1970's, it was found that CDM could accurately model strain-softening behaviour.
This theory is further developed to describe the isotropic or orthotropic behaviour of concrete ([55], [56], [97], [106], [153]). Further applications of this theory are still under active development.

The continuum damage approach as a non-local concept eliminates problems of spurious mesh sensitivity and incorrect convergence. It ensures that refinements of finite element mesh cannot lead to spurious localization of strain, damage and energy dissipation into strain-softening zone of vanishing volume.
Bazant [10] presented two arguments showed that the continuum damage procedure is a non-local. The first argument that the damage is a non-local variable that is a function of the average (non-local) strain from a certain neighbourhood of the given point rather than a function of the continuum stress at that point and can never decrease. The second argument, is the crack interaction, that one crack may amplify the stress intensity of an adjacent crack.

2.7.1 Basic Assumptions

The general assumptions used to state type of damage are summarized as follows:

1. The current state of the micro structural arrangement governs the material response.
2. A finite set of internal variables, termed ``damage variables`` describes the current state of microstructural arrangement. A scalar or tensorial quantity is used to measure the damage. Scalar measurement is used because of its simplicity.

2.7.2 Strain-Based Formulation

- **Free Energy Potential**

When the progressively fracturing solid is subjected to static loading and isothermal conditions, the potential of the free energy ψ can be expressed as a scalar-valued function of the strain tensor ε_{ij} and damage variable D as follows

$$\psi = \psi(\varepsilon_{ij}, D) \tag{2.34}$$

The construction of this function is required to study the influence of damage on the elastic properties of the material.
The damage variable is scalar for the case of isotropic damage, where the form of the function $\psi(\varepsilon_{ij}, D)$ is described as

$$\psi = \frac{1}{2}(1-D)C_{ijkl}\varepsilon_{ij}\varepsilon_{kl} \tag{2.35}$$

where
C_{ijkl} =the initial elastic modules tensor of the undamaged material
It can be seen that for $D = 0, \quad \psi(\varepsilon_{ij}, 0)$ represents the strain energy of the undamaged material.

2.7.2.1 Clausius-Duham Inequality

The constitutive relationships (relationships between stress and strain) may not be set arbitrarily; They have to obey certain rules. These rules are based on the principles of thermodynamics.

The first principle of thermodynamics constitutes the law of conservation of energy, by stating that: ``The total time rate of change in energy (kinetic and internal) balances the total supply of energy through external forces and heat.´´

The second principle of thermodynamics is the introduction of the entropy, η to describe the thermal state of a solid. Entropy is a scalar variable that expresses the variation of energy associated with the variation of temperature. The production of entropy, $\dot{\eta}$, for an isothermal or pure mechanical process, is defined as

$$\dot{\eta} = \sigma_{ij}\dot{\varepsilon}_{ij} - \dot{\psi} \tag{2.36}$$

The second principle of thermodynamics postulates that: ``The total time rate of change in entropy must be positive.´´ Thus

$$\dot{\eta} = \sigma_{ij}\dot{\varepsilon}_{ij} - \dot{\psi} \geq 0 \tag{2.37}$$

This expression embodies both the first and second principle of thermodynamics and is called the **Clausius-Duham inequality.** Processes satisfying the Clausius-Duham inequality are said to be thermodynamically admissible.

By taking the derivative of (2.34) with respect to the time and then substituting the results into (2.37), we obtain

$$\sigma_{ij}\dot{\varepsilon}_{ij} - \frac{\partial \psi}{\partial \varepsilon_{ij}}\dot{\varepsilon}_{ij} - \frac{\partial \psi}{\partial D}\dot{D} \geq 0 \tag{2.38}$$

In order that the inequality hold for all values of $\dot{\varepsilon}_{ij}$, it is required that

$$\sigma_{ij} - \frac{\partial \psi}{\partial \varepsilon_{ij}} = 0 \quad or \quad \sigma_{ij} = \frac{\partial \psi}{\partial \varepsilon_{ij}} \tag{2.39}$$

and

$$-\frac{\partial \psi}{\partial D}\dot{D} \geq 0 \tag{2.40}$$

The derivation leading to (2.39) and (2.40) by exploiting the Clausius-Duham inequality is often referred to as the Colemen method [34].

The total stress-strain relationship is represented by (2.39), while (2.40) represents the rate of energy dissipation in a damage process.

The thermodynamic force or termed damage force, Y, conjugate to the damage variable D, is represented as

$$Y = \frac{\partial \psi}{\partial D} \tag{2.41}$$

and the damage variable $\dot{D}$ is termed as the thermodynamic flux or dissipative flux. Therefore, the Clausius-Duham inequality can always, therefore, be written in the form of a scalar product of the vector of the thermodynamic force and the vector of the thermodynamic flux.

2.7.2.2 Stress-Strain Relationships

If the free energy ψ expression is given, the total stress-strain relationship can be determined by (2.40). From (2.40), the incremental form of stress-strain relationship can be derived as

$$d\sigma_{ij} = \frac{\partial^2 \psi}{\partial \varepsilon_{ij} \partial \varepsilon_{kl}} d\varepsilon_{kl} + \frac{\partial^2 \psi}{\partial \varepsilon_{ij} \partial D} dD \tag{2.42}$$

2.7.3 Stress-Based Formulation

The stress-based formulation [197] is built around the assumption of a complementary free energy potential in the form

$$\Phi = \Phi (\sigma_{ij}, D) \tag{2.43}$$

in which σ_{ij} is the stress tensor, D is the damage variable.

If D is a scalar, then Φ can be further written as

$$\Phi = \frac{1}{2(1-D)} D_{ijkl} \sigma_{ij} \sigma_{kl} \tag{2.44}$$

in which D_{ijkl} is the tensor of initial compliance, expressed in terms of Young's modulus, E and Poisson's ratio, ν for isotropic material.
When $D = 0$, $\Phi(\sigma_{ij}, 0)$ represents the complementary energy of undamaged material. In the case of isothermal, the Clausius-Duham inequality is expressed in terms of the complementary free energy in the following form

$$\dot{\Phi} = \dot{\sigma}ij\varepsilon_{ij} \geq 0 \tag{2.45}$$

for any admissible process. By Differentiation of (2.43), and substitution of the result into (2.45) then

$$\varepsilon_{ij} = \frac{\delta\Phi}{\delta\sigma_{ij}} \tag{2.46}$$

with a dissipative inequality

$$\frac{\partial\Phi}{\partial D}\dot{D} \geq 0 \tag{2.47}$$

and the thermal dynamic force Y is expressed as

$$Y = \frac{\delta\Phi}{\delta D} \tag{2.48}$$

For the isotropic damage case, it follows that from (2.44)

$$Y = \frac{1}{(1-D)^2} D_{ijkl}\sigma_{ij}\sigma_{kl} \tag{2.49}$$

By differentiation of (2.46) the damage evolution law for the damage rate dD or $\dot{D}$ is obtained as

$$d\varepsilon_{ij} = \frac{\delta^2\Phi}{\delta\sigma_{ij}\delta\sigma kl} d\sigma_{kl} + \frac{\delta^2\Phi}{\delta\sigma_{ij}\delta D} dD \tag{2.50}$$

2.7.4 Concepts of the Continuum Damage Mechanics

The theory of linear elasticity assumes that Hooke's law is valid and that the material returns to its starting condition when the applied loads are removed. This assumption works for many design cases but not for masonry buildings subjected to earthquake loading. These types of buildings degrade; the shear walls fail and the buildings collapse under some seismic loads [151,194].
The development and usage of the continuum damage mechanics theory is described by Krajcinovic [99].

One of the failure modes for masonry is the de-bonding of the interface between the mortar and the masonry unit. This is a common failure mode in poorer quality masonry. The method outlined in Lemaitre [107] estimates the damage parameters for this failure mode.
The theory of damage mechanics is predicted on the assumption that the intrinsic elastic constants are invariant properties, measured using tensile rather than compression tests. The elastic stiffness constants are the upper bound for the stiffness functions (see Krajcinovic [99]). The stiffness then is noted to change as the material fails or degrades. This degradation is quantified using the damage parameter, D.
The scalar representation of the damage parameter is

$$D = \frac{E - \overline{E}}{E} \tag{2.51}$$

or alternatively

$$D = 1 - \frac{\overline{E}}{E} \qquad 0 \le D \le 1.0 \tag{2.52}$$

The damage parameter, D, is zero at the commencement of the experiment and its value is given by the change in the effective stiffness, $\overline{E}$, relative to Young's modulus, E. The theoretical maximum value for D is one; however; a critical value of 0.5 is generally reached at the point of fracture [151].

2.8 Proposed Masonry Models

The constitutive models for masonry are generally divided into two categories, namely; micro- and macro-modelling.

In the micro-modelling of the masonry, masonry bricks and mortar joints are separately discretized, thus allowing the adoption of suitable constitutive laws for each component. This approach can be highly accurate and can give good insight into micro-stresses in masonry. The main disadvantage of the micro-models is the large computational effort they require (i.e., large number of degrees of freedom of the numerical model) which limit their applicability to the analysis of small details of structures and the failure criteria is relatively difficult due to the complexity of the interaction between mortar and masonry units. Another disadvantage of such micro-modelling is that due to the shortage of the experimental results, the simulation of loading and reloading is more complex.

In fact, the constitutive behaviour of masonry is orthotropic due to the geometrical arrangement of its constituents, (i.e., units and mortar), even if the properties of each component are usually isotropic.
Several homogenisation techniques to obtain macro-constitutive law starting from the micro constitutive laws of the constituents have been developed.

The other effective and practical constitutive formulations for the modelling of masonry are the macro-models. The computational advantage of these macro-models is based on the fact that in finite element approach the mesh discretization does not have to accurately describe the internal structure of masonry and macro-elements, having dimensions significantly greater than that of the single brick units, can be defined. Macro-modelling does not need a large amount of input data which refer to material characteristics of the constituents and their junctions. It does not produce a large number of elements (CPU-time), as it is needed for micro-modelling and large structures can be modelled without costly experiments. Another advantage of macro-modelling is

that the failure surface often has an easy shape. Also, the loading and reloading of the material can be considered.

The constitutive model developed in this work is based on the macro-modelling approach.

The definitive work of Lourenco [112] provides a starting point for considering the development of masonry models. He looked to masonry as composed of a series of discrete blocks separated by mortar elements.
Page [166] in his original work on the failure surface for solid clay masonry has modelled these mortar elements separately.
Masiani [130] treated masonry as a structured continuum.
The use of the structured continuum from the work of Page [166] to that of Masiani [130] demonstrates that a discrete structured continuum is an acceptable representation of masonry. The difficulty with discrete models has always been the computational expense of these types of models. This, generally, requires some form of homogenisation of the model.
A numerical analysis of structural masonry subjected to a uniform, in-plane tensile stress/strain field, is investigated employing various homogenisation techniques are applied by Lee [102].
Pande [57] and Zhao [223] reported that the orthotropic material properties of the orthotropic-homogenised masonry are function of:

1. Dimensions of the brick
2. Young's modulus and Poisson's ratio of the brick
3. Young's modulus and Poisson's ratio of the mortar
4. The thickness of the mortar joint

The structural matrices S_b, S_{bj}, S_{hj}, which relate the stresses in the homogenised material to the stresses in the brick, the bed-joint and the head-joint, respectively are functions of

i. Geometry of brick/mortar
ii. Material properties of brick/mortar

Nichols and Totoev [150] used an elastic analysis of a structured continuum for two buildings with one degree of homogenisation. They eliminated the header joints to attain computational efficiency.

Page's work [166] was on the static properties of solid clay masonry tested at the limits of failure.

Ganz and Thurlimannn [71] extended this research to include extruded masonry. They established the failure surface for masonry under in-plane quasi-static loading. This type of analysis has been included in the modern codes of practice to provide a sound rational approach to static analysis methods.

The Slovenian Team's work [208] since the mid-sixties was on the dynamic analysis of masonry.

Page [155] developed a finite element model for masonry with mortar ``links.´´

Ali and Page [4] performed an extensive finite element model for masonry subjected to concentrated loads. To establish the material properties that were appropriate for their model, they tested the material in the laboratory.

Pande [172] utilized an equivalent elastic modulus for brick masonry.

Pande [171] evaluated the analytical formula proposed by the European code to determine the compressive strength of masonry.

Lourenco and Rots [110] have identified the need to establish mechanical models, they obtained experimental data for masonry with a part of their work to obtain a mathematical model for masonry. Their model allows for the damage accumulation in the material and change in effective stiffness properties with time.

Papa [174] has proposed a uni-lateral damage model for masonry deriving from the extension of a damage model, originally developed for isotropic material, to the orthotropic case.

Nichols [151] studied the progressive degradation of masonry shear walls subjected to harmonic loading. He assumed a linear damage function in the form of

$$D = 0.0018\,\varepsilon \tag{2.53}$$

His calculated results for the damage parameter are shown in Figure 2.24, where he measured the strain as $\mu\varepsilon$.

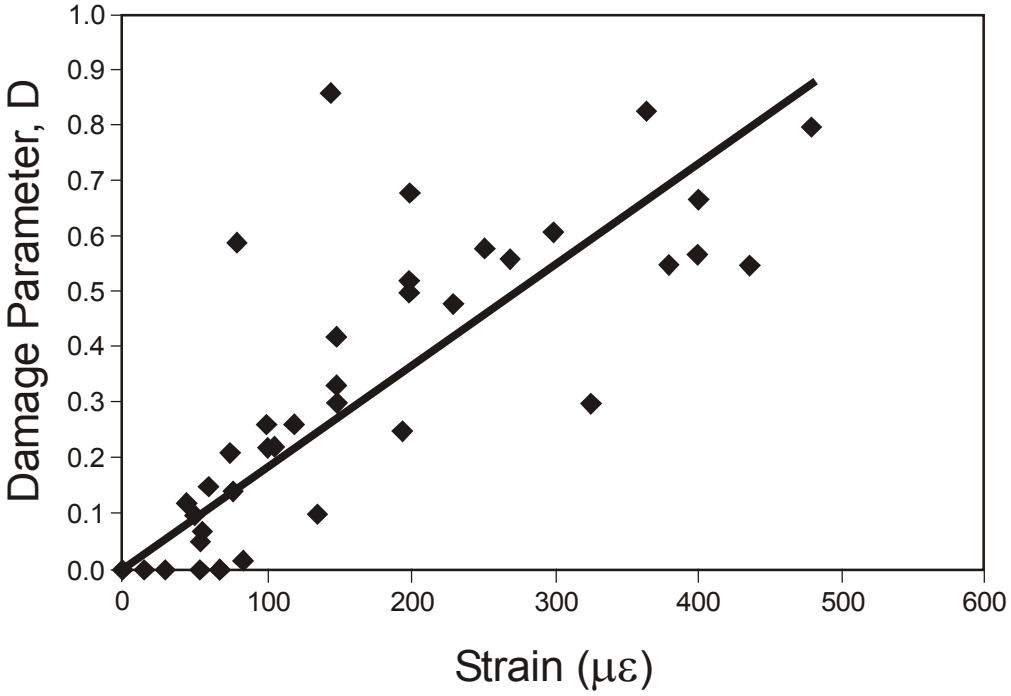

Figure 2.24: Damage parameter versus strain[150]

Berto [12] developed a damage model which can deal only with plane stress situation, its formulation is as follows

$$\begin{pmatrix} \sigma_x \\ \sigma_y \\ \sigma_z \end{pmatrix} = (I - D) \begin{pmatrix} \overline{\sigma_x} \\ \overline{\sigma_y} \\ \overline{\sigma_z} \end{pmatrix} \tag{2.54}$$

where
$I =$ the third ordered identity matrix

$$\overline{\sigma} = E : \varepsilon \tag{2.55}$$

and D is the 3×3 damage matrix.

Figures 2.25 and 2.26 show the response of masonry in terms of stress-strain in uni-axial tension and compression, respectively. As can be observed that the damage models are able to reproduce the softening behaviour in tension as well as the hardening and softening behaviour in

compression and the irreversible strain evolution in cyclic behaviour can also be well captured [12].
Strain softening is a well-known phenomenon associated with brittle materials such as concrete and masonry.

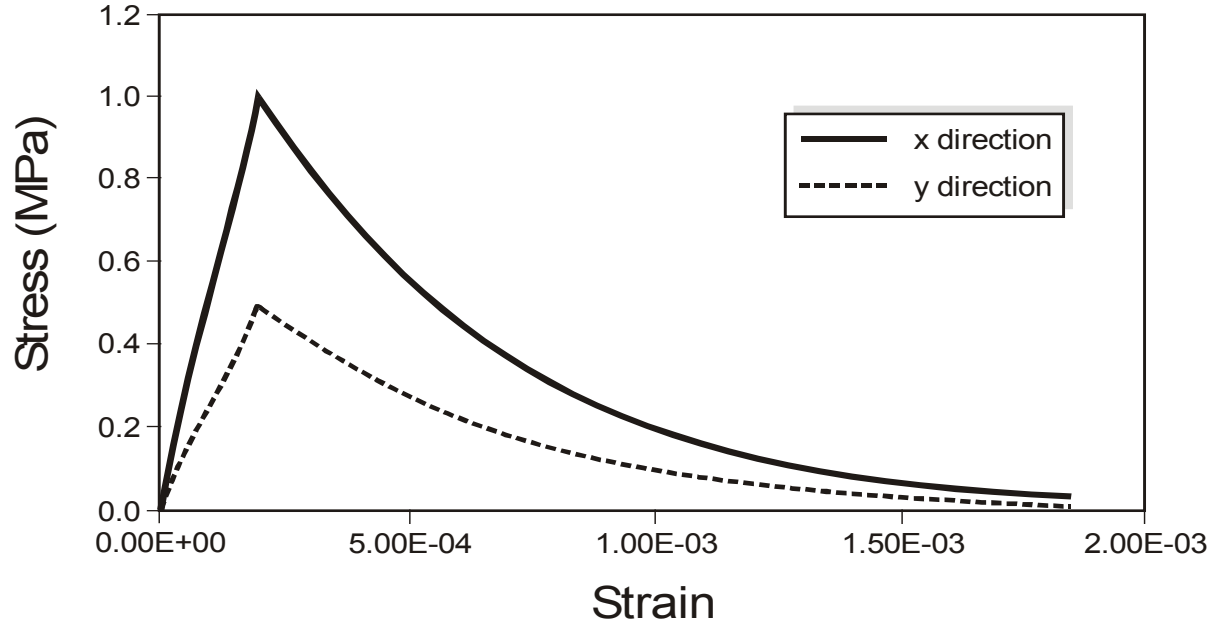

Figure 2.25: Typical stress-strain curves of masonry in uni-axial tension along the two material axes, according to Berto [12]

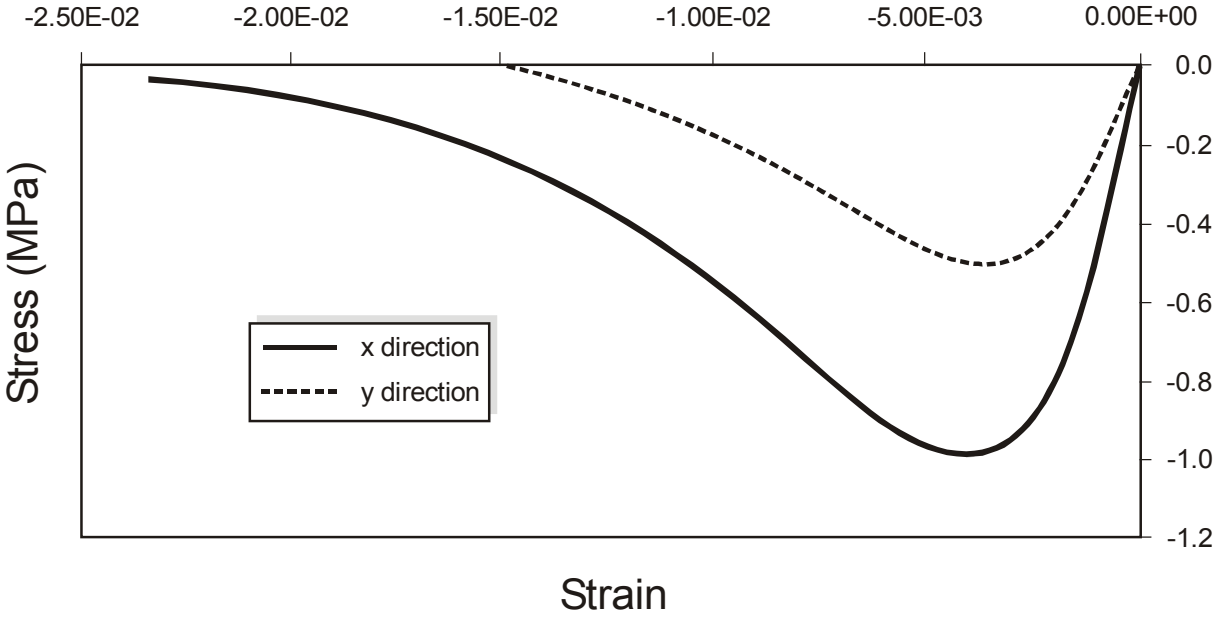

Figure 2.26: Typical stress-strain curves of masonry in uni-axial compression along the two material axes, according to Berto [12]

3 Developed Constitutive Law for the Analysis of Masonry

3.1 Introduction

The modelling of masonry is a highly uncertain and frustrating task for many reasons. These are primarily the uncertainty associated with adding material properties, different failure modes, along with the interaction between the in-plane and out-of-plane behaviour, as well as the complicated anisotropic nature of masonry, due to shear-compression interaction, along the weak mortar joint planes. The effect of reversing cyclic in-plane forces, the incomplete knowledge of the behaviour of quasi-brittle materials and the lack of conclusive experimental and analytical results to substantiate a reliable design procedure for these types of structures, further complicates rational analysis.

One major problem for the analysis of masonry structures using numerical tools is the need of homogenisation due to the high computational costs associated with the direct simulation of the components when the analysis concerns real dimensions structures.
The finite element analysis of masonry is especially difficult as the analysis of masonry structures requires consideration of the complex nature of brittle fracturing materials as well as the effects of jointing and the way in which the joints, as planes of weakness, change the composite response to load.

Masonry has a number of serious drawbacks for earthquake resistance; because of its large mass, it has high inertial response to earthquake; its quality of construction is difficult to control; and less research has been done regarding its seismic response behaviour.
Failure is governed by diagonal cracking, ductility is lower and when high vertical loads are applied, the behaviour is brittle.

Shear walls are those that resist forces in their own plane. The degradation of the shear walls reduces their stiffness and affects their ability to withstand additional cyclic loading.

Masonry walls exhibit a non-linear response to applied loads as a result of the non-linear behaviour of both their constituents, namely the mortar and masonry units. In addition to this, non-linear behaviour results from the interaction of the two materials, which have different physical properties. Due to its lower stiffness, the mortar experiences larger lateral strain than the masonry units. The stiffer masonry units, producing a lateral compression in the mortar joint, resist the lateral mortar strain. By restraining the mortar, preventing its lateral expansion, a tension force is induced on the masonry unit. This lateral tension in the masonry unit explains the classical masonry assembly compression failure mode, which is vertical splitting of the masonry units.
Therefore, axial compression loading typically result in failure due to tension stresses normal to the applied load, whereas shear loads on masonry assemblies induce diagonal tension [109].

It is now widely recognized that masonry walls, used for cladding and/or partition in buildings, significantly alter their seismic response and their effect in changing the stiffness, the ultimate lateral load capacity as well as the ductility supply of the building system should be accounted for in the analysis and design.

A specific finite element macro-model based on the continuum damage theory has been developed for the analysis of the URM walls under monotonic and/or seismic cyclic loading after the homogenisation technique.
Another damage model, developed to study the effect of the strengthening and repair of the URM walls using GFRP is presented in the following chapter.

Most of the existing studies on masonry behaviour, are based on the following methods:

- Classical approach, i.e., limit analysis, and
- Numerical modelling, often based on the finite element method

In the framework of numerical modelling, two main approaches can be used in the analysis of masonry behaviour: the micro-modelling of single

components (e.g., units and mortar) or the macro-modelling of the masonry as a composite material [114].
Moreover, an adequate computational model should include the fundamental mechanisms that characterize the masonry behaviour at failure, i.e.,

- Sliding along a bed or head joint at low values of normal stresses;
- Cracking of the masonry units (bricks, blocks, ect...) under direct tension;
- Diagonal tensile cracking of masonry units at values of normal stress sufficient to develop frictional behaviour in the joints; and
- Spilting of units as a result of mortar dilatancy at high values of normal stress

Recently, many computational studies of actual masonry structures are based on macro-modelling approaches, in which attempts are made to incorporate most of the phenomena described above within a continuum description (see [111]). In the context of macro-modelling approach the usual numerical modelling strategies can be adopted, such as the classical plasticity theory, damage theory approach, ect.

In this study, the damage theory model has been adopted. It has been revealed to be a good choice to exploit in this area of structural mechanics (see [38]), due especially to its efficiency combined with simplicity.
Two of the main problems of such an approach are the definition of the damage evolution curve and the introduction of the orthotropy, which is typical of the masonry structure in the model.
The former can be overcome by identifying the mechanical properties of masonry from the behaviour of its constitutive materials (brick and mortar) through a homogenisation technique and/or by calibrating such values via a micro-modelling approach in such a way that each element contains only one material. The introduction of the orthotropy in the model, within the framework of the damage approach, requires taking into account both the orthotropy due to the geometry of units and mortar, and the orthoropy due to the damaging process. This is a very complex

issue and, until now, only a few models have been developed according to such requirements (see [185]).

The aim of this work is to analyze the response of masonry walls under monotonic loading and/or cyclic loading, by using a two-parameters, scalar, isotropic, damage model, based on the finite-elements method and the continuum damage theory by considering the masonry as orthotropic after the homogenisation technique as well as analysing the effect of retrofitting and repair on the masonry wall using GFRP laminates.
For the analysis of these masonry walls being investigated, the following assumptions have been considered:

1. Masonry units are isotropic, linear elastic, brittle materials. It is generally known that masonry units, and particularly those produced by the extrusion process, may not be isotropic. However, if the anisotropic characteristics of the units are known, it is possible to take this into account in the mathematical framework presented herein
2. Mortar is assumed to be isotropic, linear elastic
3. There is no slippage between the masonry units and the mortar joints (bed joints and perpend joint)
4. It is assumed that the perpend joints are continuous. This assumption may appear unrealistic but it has been shown, by Liang [108] that, it does not affect the stresses in the constituents to any appreciable degree

3.2 Constitutive Model for the Analysis of Masonry

A three-dimensional analysis of masonry walls subjected to cyclic shear is considered.
For this, an 8-noded solid element together with orthotropic material properties, derived from the strain energy of the composite material is used throughout.
Here, masonry is treated as a composite material, with masonry units and mortar joints forming its constituents. Each constituent is assumed to behave as isotropic, linear elastic, brittle material.

Two-stages homogenisation technique is introduced to obtain the average mechanical response of masonry. The equivalent orthotropic material properties are used to formulate the system stiffness matrix in the finite element analysis.
To describe the behaviour of the material components a model, which based on the continuum damage theory is proposed.
This model, based on the introduction of two damage variables, describes the behaviour of brittle materials subjected to cyclic loads.
The numerical implementations performed gave an accurate description of the failure process as well as an accurate prediction of the behaviour of masonry structures.
The damage laws take into account for the different behaviours in tension and compression. They have been validated with reference to available experimental data.
Numerical results have shown that shear strength and shear behaviour of the wall are much influenced by loading the wall in addition to the shear force with vertical load. An explanation of the developed model for masonry is presented in the subsequent sections that follow:

3.2.1 Scalar Damage Model

Such an approach originally was developed for concrete [132], and reveals to be valuable in understanding the global behaviour of masonry structures as well.
In this model, the material is supposed to behave elastically and to remain isotropic. The initial stiffness matrix of the material E_0, and, the damage factor D. Assuming a Cartesian system of co-ordinates as shown in Figure 3.2,

the stress-strain relationship is

$$\sigma = \left(1 - D\right) E_0 \varepsilon \tag{3.1}$$

where

σ = the non-linear stress tensor

ε = the elastic strain

It is assumed that extensions are responsible for crack propagation. The loading surface that used is inspired from the St.Venant's equation of maximum principal strain as

$$f\left(\varepsilon,E,K_0\right)=\left(\tilde{\varepsilon}\right)-K\left(D\right) \tag{3.2}$$

with $\left(\tilde{\varepsilon}\right)$= the equivalent strain and is given by

$$\left(\tilde{\varepsilon}\right)=\sqrt{\sum_{i=1}^{3}\left(\langle\varepsilon_i\rangle_+\right)^2};\ \ \left(\langle x\rangle_+\right)=\frac{|x|+x}{2};\ \ \varepsilon_i \tag{3.3}$$

are the principal strains and $E=\left(1-D\right)E_0$

The hardening-softening Parameter $K\left(D\right)$ takes the highest value of the equivalent strain $\left(\tilde{\varepsilon}\right)$ ever reached by the material at the considered point to retain the previous loading history. Initially $K\left(D\right)$ is the threshold K_0 under which the material does not damage.

The response in tension or compression is described by the following laws coupling two types of damage D_t and D_c [133], corresponding respectively to damage measured in uni-axial tension and compression.
The general form of the evolution law of damage is represented by (3.5). This evolution law is given by two functions F_t and F_c in (3.5). The total damage D is the weighted sum of D_t and. D_c. In (3.7) the weights α_t, α_c are functions of the strain state.

$$D=\alpha_t\times D_t+\alpha_C\times D_C;\quad D_t=F_t(\tilde{\varepsilon})\ and\ D_C=F_C(\tilde{\varepsilon}) \tag{3.4}$$

with

$$F_i(\tilde{\varepsilon})=1-\frac{\left(1-A_i\right)K_0}{\tilde{\varepsilon}}-\frac{A_i}{e^{\left(B_i(\tilde{\varepsilon}-K_0)\right)}};\ \ i=t,c \tag{3.5}$$

the tensors ε_t and ε_c in which only the positive and negative principal stresses appear, respectively, and are defined as

$$\varepsilon_t = E^{-1} : \sigma_t \quad ; \quad \varepsilon_c = E^{-1} : \sigma_c \tag{3.6}$$

The weight α_t and α_c are defined by the following expression [132]

$$\alpha_t = \sum_{i=1}^{3} H_i \frac{\varepsilon_{ti}\left(\varepsilon_{ci} + \varepsilon_{ti}\right)}{(\tilde{\varepsilon})^2} ; \alpha_c = \sum_{i=1}^{3} H_i \frac{\varepsilon_{ci}\left(\varepsilon_{ci} + \varepsilon_{ti}\right)}{(\tilde{\varepsilon})^2} \tag{3.7}$$

and

$H_i = 1$ *if* $\varepsilon_i = \varepsilon_{ci} + \varepsilon_{ti} \geq 0$ *otherwise,* $H_i = 0$

The material parameters $K_0, A_t, B_t, A_c, and\ B_c$ in the evolution laws are identified independently from compression tests on cylinder, and bending on the sign of the principal stresses, α_t and α_c are the coefficients defining the contribution of each type of damage for general loading. From (3.7) it can be verified that in uni-axial tension $\alpha_t = 1; \alpha_c = 0; D = D_t$ and vice versa in compression. It is assumed that the material fails when the damage reaches a value D_{cr} given by

$$D_{cr} = \alpha_t \times D_{tcr} + \alpha_c \times D_{ccr} \tag{3.8}$$

where the critical values of the damage parameters D_{tcr} and D_{ccr} are the values of the damage for which the strain in uni-axial tension and compression is 1.5 times the strain corresponding to the peak stress. This assumption arises from the consideration that the experimental results of tension and compression tests on brittle materials show that the failure occurs when the maximum strain is 1.5 times the strain corresponding to the maximum stress.

3.2.2 Homogenisation

The substitution of masonry by homogenized (fictious) material with orthotropic material properties (3.9) is named ‘’homogenisation’’. The homogenized properties are given in analytical form based on the equivalence of the strain energies of the homogenized material to that of the constituents.

Masonry can be represented by a system, vertically layered constituted by the horizontal mortar bed joints and the horizontal staked brick-head mortar joint system (see Figure.3.1).

The homogenisation technique is important for the analysis of masonry structures with numerical tools due to the high computational costs associated with a direct simulation of the components.

The orthotropic material properties proposed by Pande [170] are used to model the masonry walls in the sense of an equivalent material. The basic assumptions made to drive the equivalent material are:

1. brick and mortar are perfectly bonded;
2. Perpend mortar joints are continuous

The second assumption is necessary in the homogenisation procedure. With reference to Figure.3.1, the homogenisation process consists of determining the elastic properties of the horizontal staked brick-head mortar joint system, Figure.3.1(a) and, successively, the elastic properties of the vertical layered system (see Figure.3.1(c)) constituted of this homogenized material and of the mortar bed joint, Figure.3.1(b).

The derivations of the equivalent orthotropic material matrix $\left[\overline{C}\right]$ elements are included in appendix A, These elements are functions in $(E_b, u_b, G_b, G_{hj}, G_{bj}, E_{hj}, E_{bj}, u_{hj}, u_{bj}, l_b, h_b, t_{hj}, t_{bj})$,

where:

$E_b, E_{hj}, E_{bj}, G_b, G_{hj}, G_{bj}$ = the elastic damaged modules of brick, head mortar joint and bed mortar joint, respectively

u_b, u_{hj}, u_{bj} = Poisson's ratios for the masonry units and mortar, respectively

l_b, h_b = the length and height of the brick unit, respectively

t_{hj}, t_{bj} = the thickness of the head and bead mortar joint,respectively

$$\overline{\varepsilon} = \left[\overline{C}\right]\overline{\sigma} \tag{3.9a}$$

$$\left[\bar{C}\right] = \begin{bmatrix} \frac{1}{\bar{E}_x} & -\frac{\bar{u}_{xy}}{\bar{E}_x} & -\frac{\bar{u}_{xz}}{\bar{E}_x} & 0 & 0 & 0 \\ -\frac{\bar{u}_{yx}}{\bar{E}_y} & \frac{1}{\bar{E}_y} & -\frac{\bar{u}_{yz}}{\bar{E}_y} & 0 & 0 & 0 \\ -\frac{\bar{u}_{zx}}{\bar{E}_z} & -\frac{\bar{u}_{zy}}{\bar{E}_z} & \frac{1}{\bar{E}_z} & 0 & 0 & 0 \\ 0 & 0 & 0 & \frac{1}{\bar{G}_{xy}} & 0 & 0 \\ 0 & 0 & 0 & 0 & \frac{1}{\bar{G}_{yz}} & 0 \\ 0 & 0 & 0 & 0 & 0 & \frac{1}{\bar{G}_{xz}} \end{bmatrix} \qquad (3.9b)$$

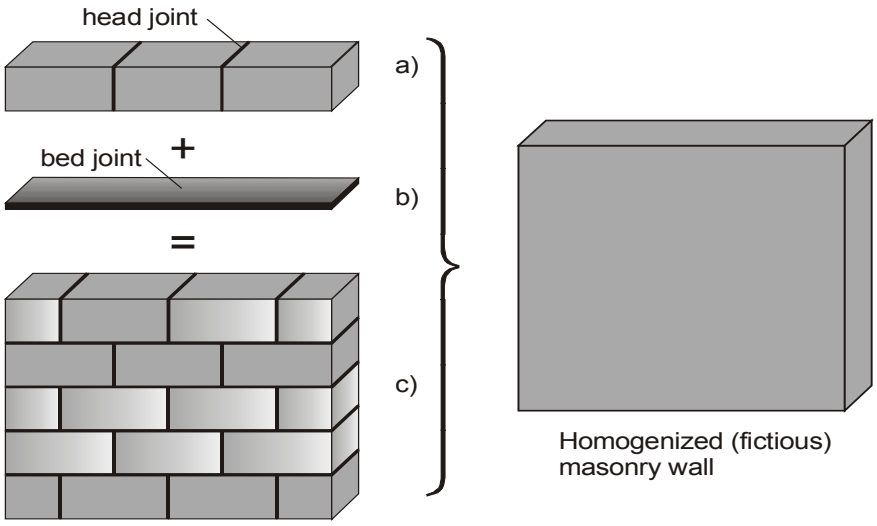

Figure 3.1: Brick mortar system with two sets joints

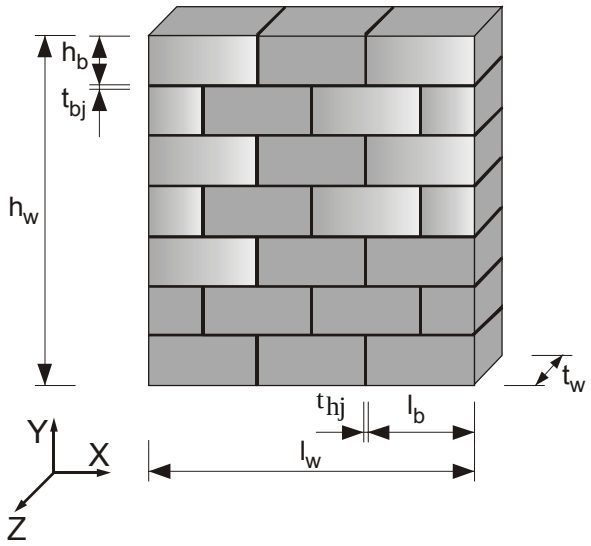

Figure 3.2: Masonry wall numerically investigated

The equivalent orthotropic material properties defined above are used to formulate the system stiffness matrix in the finite element analysis. With this stiffness matrix, a damage model based on the continuum damage theory is presented. This damage model is implemented in the finite element program, Abaqus6.4 [1]. The stresses/strains in the constituent materials can be evaluated through the structural relationships, i.e.

$$\sigma_b = \left[S_b\right]\bar{\sigma};\ \beta_{hj} = \left[S_{hj}\right]\bar{\sigma};\ \beta_{bj} = \left[S_{bj}\right]\bar{\sigma} \tag{3.10}$$

where, subscripts $b, hj, and\ bj$ represent brick, bed mortar joint and perpend mortar joint, respectively.

Explicit expressions for the elements of the above structural matrices are given in [170] and they are implemented in appendices A and B. These are functions of:

- Dimensions of the masonry units
- Elastic parameters (Young's , shear modules and Poisson's ratio) of masonry units
- Elastic parameters (Young's shear modules and Poisson's ratio) of mortar
- Thickness of mortar joints

3.2.3 Numerical Analysis

After the implementation of the masonry material law in the finite element program, Abaqus6.4 [1], the numerical analysis is carried out.
The masonry is considered as an equivalent homogenous orthotropic material after the homogenisation process. The analysis is performed in three-dimensions.

In Figure 3.2, the masonry wall, numerically investigated, is reported. The masonry wall units have a $400mm$ length, a $250mm$ width and a $200mm$ height.
The thickness of head and bed mortar joints is $10mm$. The wall is loaded with different loading histories. Young's modules of the mortar and bricks are $21700MPa$ and $9700MPa$, respectively. The masonry wall dimensions are $770mm$ in length, $830mm$ in height and $120mm$ in thickness.

In Figures 3.3 and 3.4, the uni-axial stress-strain curve in compression and tension for the masonry wall,respectively. Here, the masonry wall fails when the strain in uni-axial tension and compression is 1.5 times the strain corresponding to the peak stress. This assumption arises from the consideration that the experimental results of tension and compression tests on brittle materials show that failure occurs when the maximum strain is about 1.5 times the strain corresponding to the maximum stress. These Figures show that the damage model is able to reproduce the softening behaviour in tension as well as the hardening and softening in compression. The damage versus the strain is also shown in Figure (3.3), where the wall failed at 70% damage.

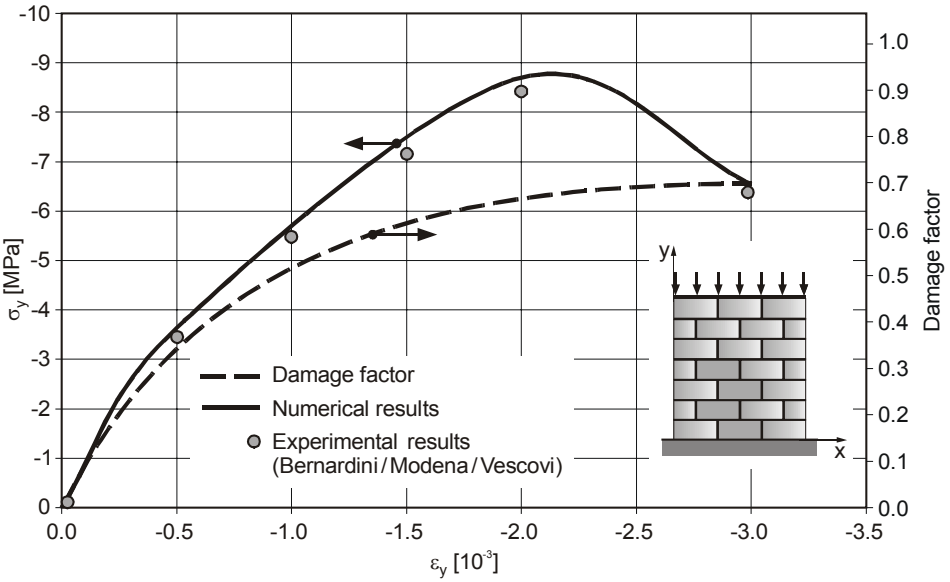

Figure 3.3: Stress-strain and damage factor-strain relationships of the masonry wall under uni-axial compression

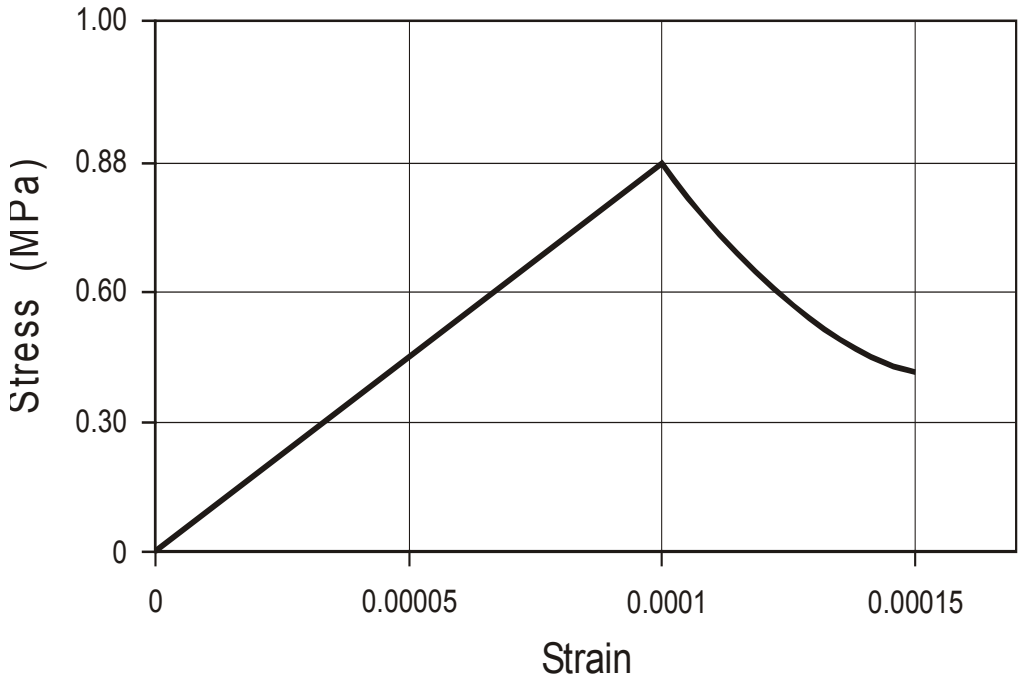

Figure 3.4: Stress-strain relationship of the masonry wall under uni-axial tension

- **Development of Masonry Failure Surface**

As is shown in chapter two, the failure surface is necessary to determine the onset of failure within masonry and its nature after reaching the elastic limit. Figure 3.5 shows the failure surface from the analysis in the four zones, i.e., compression-compression, tension-tension and tension-compression zones, compared with the results from Huges [86]. It is seen that the failure surface of the masonry is not isotropic like that of

the concrete, because masonry is an orthotropic material having one strong axis and one weak. Therefore, the failure surface has differing uni-axial tensile and compressive strengths in both x and y directions. Although the general shape of the curves is similar, the failure curve of the present study lies inside the other two. This due mainly due the differences in the strength as well as the assumption, in the developed model, that the masonry fails when reaching a critical damage value, D_{cr}, which corresponds to strain of 1.5 of the strain corresponding to the maximum stress.

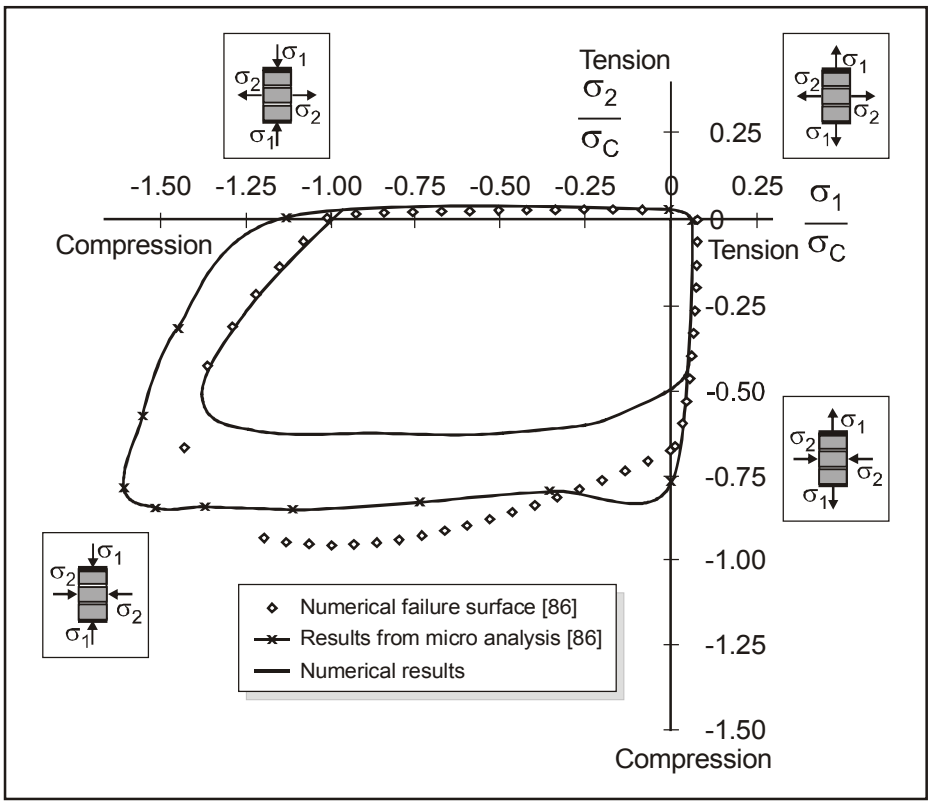

Figure 3.5: The failure surface for the four zones

In Figures 3.6(a),(b) the values of the shear force versus the horizontal displacement at the top of the wall for sinusoidal loading history are presented. In Figures 3.7(a),(b), in addition to the sinusoidal loading history, a constant vertical load is applied. The vertical load significantly influences the shear strength and the shear behaviour of the masonry wall. The behaviour of the wall when loaded with only the sinusoidal loading history is elasto-plastic, whereas, its behaviour for sinusoidal

loading history combined with a constant vertical load, is elasto-hardening.

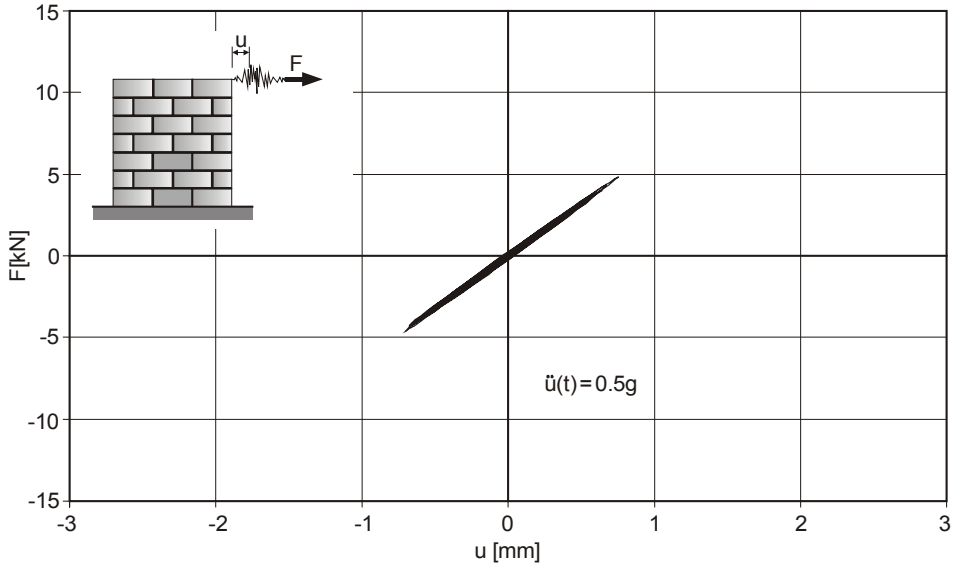

(a)

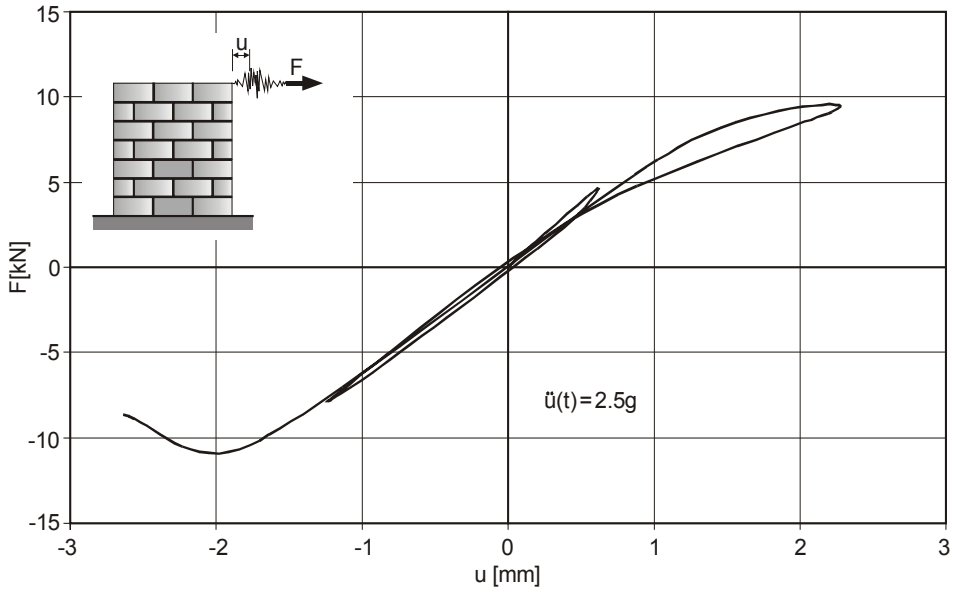

(b)

Figure 3.6: Shear force versus horizontal displacement at the wall-top for sinusoidal loading history: a) factor=0.5g; b) factor=2.5g

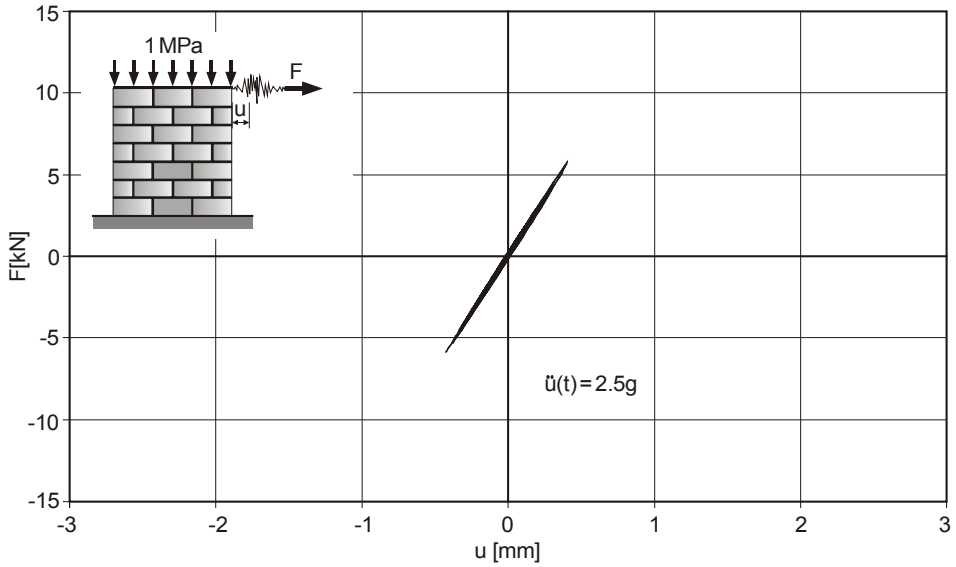

(a)

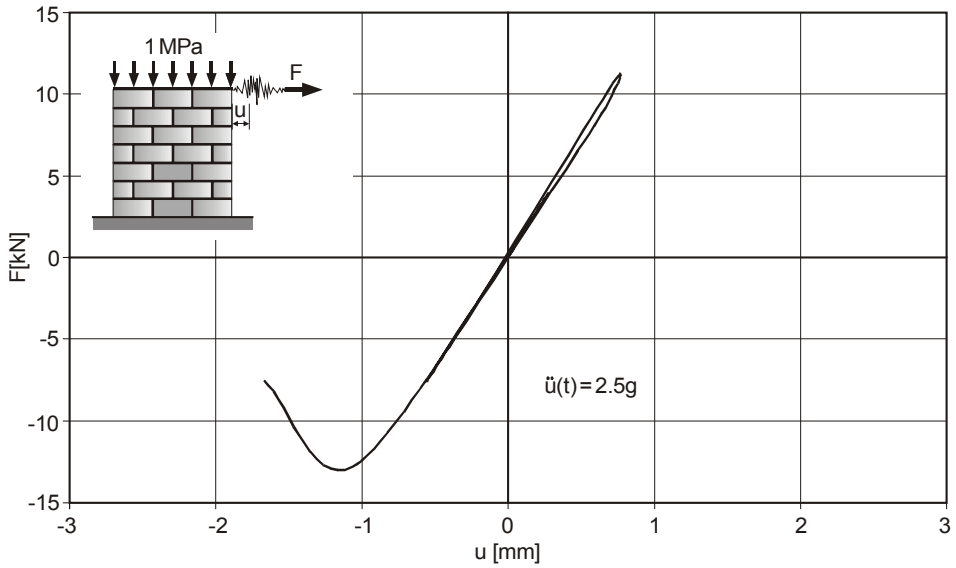

(b)

Figure 3.7: Shear force versus horizontal displacement at the wall-top for sinusoidal loading history and vertical load: a) factor=0.5g; b) factor=2.5g

The following is a calculation of an example from [216] with the constitutive law developed in this work.

- **Loading**

As loading, Friaul time-history in Buja (15.09.1976), is used. Its strong-quake-phase is relatively long. The magnitudes of the acceleration, velocity and displacement time-history are shown in Figure 3.8.

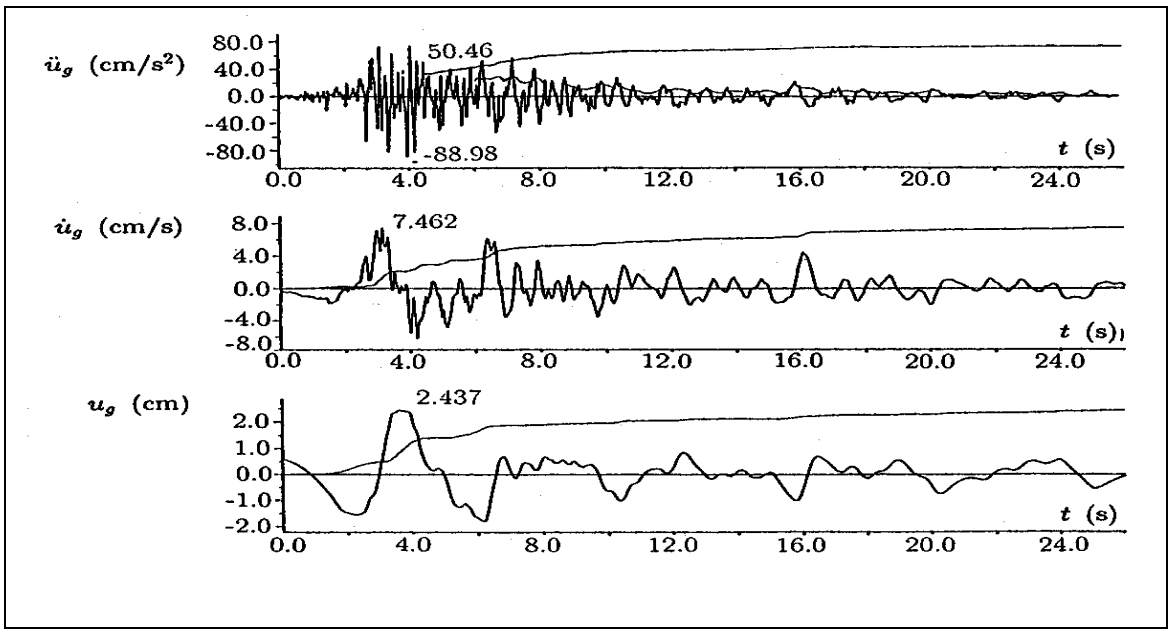

Figure 3.8: Acceleration, velocity and displacement of the Friaul-earthquake in Buja, (15.9.1976)

- **Input Data**

The dimensions and the mechanical properties of the wall with the constitutive law developed are the same as those used in [216] with a dimensions: $3.0 \times 3.0 \times 0.3\, m^3$, with upper and lower reinforced concrete beams for a good load distribution. The bottom beam is fixed, while the upper beam is free to move. The compression strength of the wall is $f_c = 10 MPa$, $E_0 = 1000 f_c$, $v = 0.2$, and $\rho = 0.0015\, MN.\sec^2/m^4$. On the top of the wall a concentrated mass is put to compensate the big mass of the upper floors ($m = 0.03 MN.\sec^2/m^4$). For the finite element-calculation, an 8-noded, solid element is used. For the reinforced concrete beams (upper and lower), a bilinear elastic-plastic constitutive law is used with $E_0 = 42700\, MPa$, $v = 0.2$, $\sigma_y = 26\, MPa$. Since the stresses in the layers of

the masonry wall are very small, the beams always deforme in the linear-elastic part.

- **Results Representation**

In Figures 3.9 and 3.10, the results of the force-displacement of the upper layer of the masonry wall, which are obtained from the

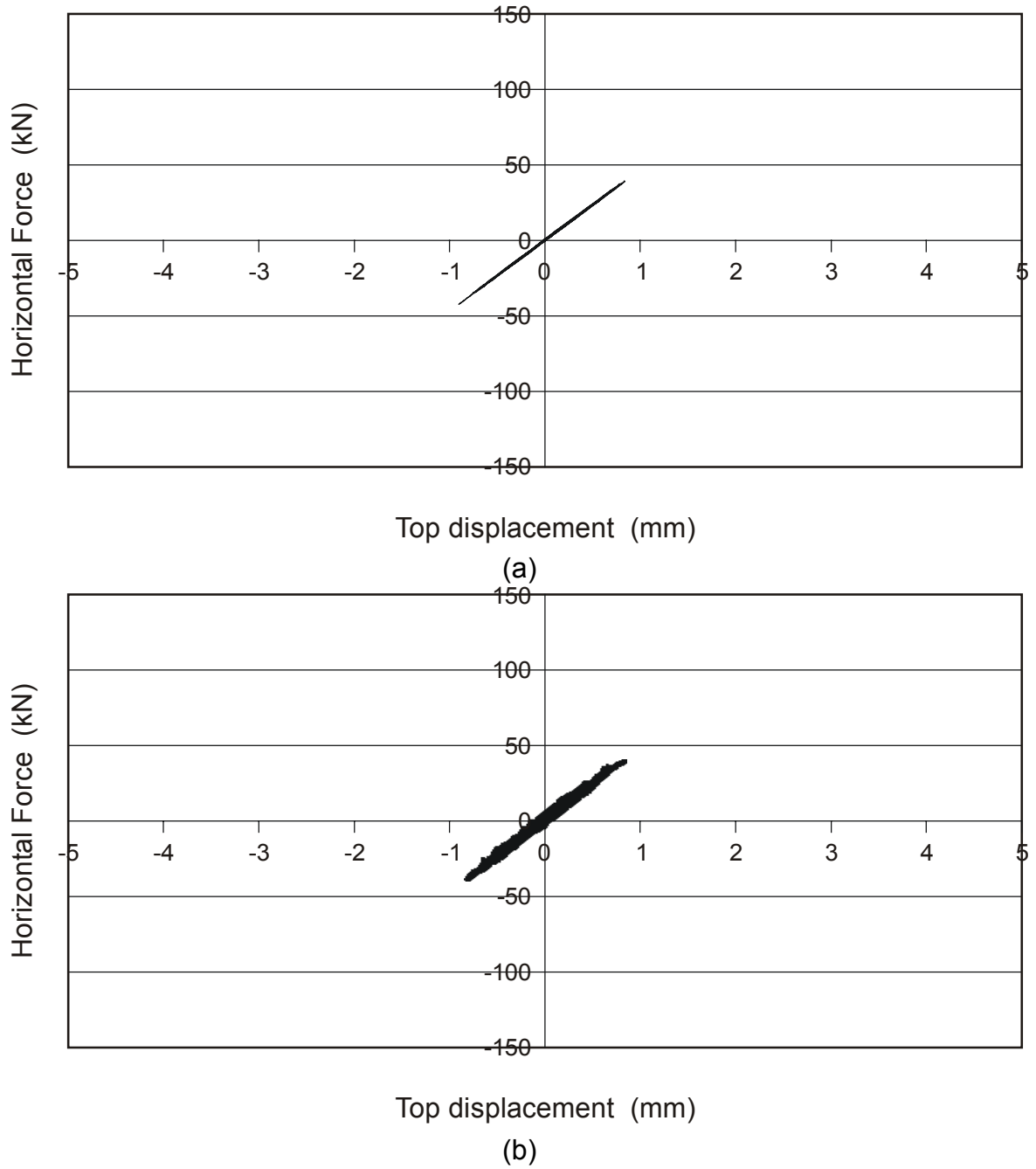

Figure 3.9: Comparison of numerical results (a) with [216]'s results (b) for $(\ddot{u})_{\max} = 0.1g$.

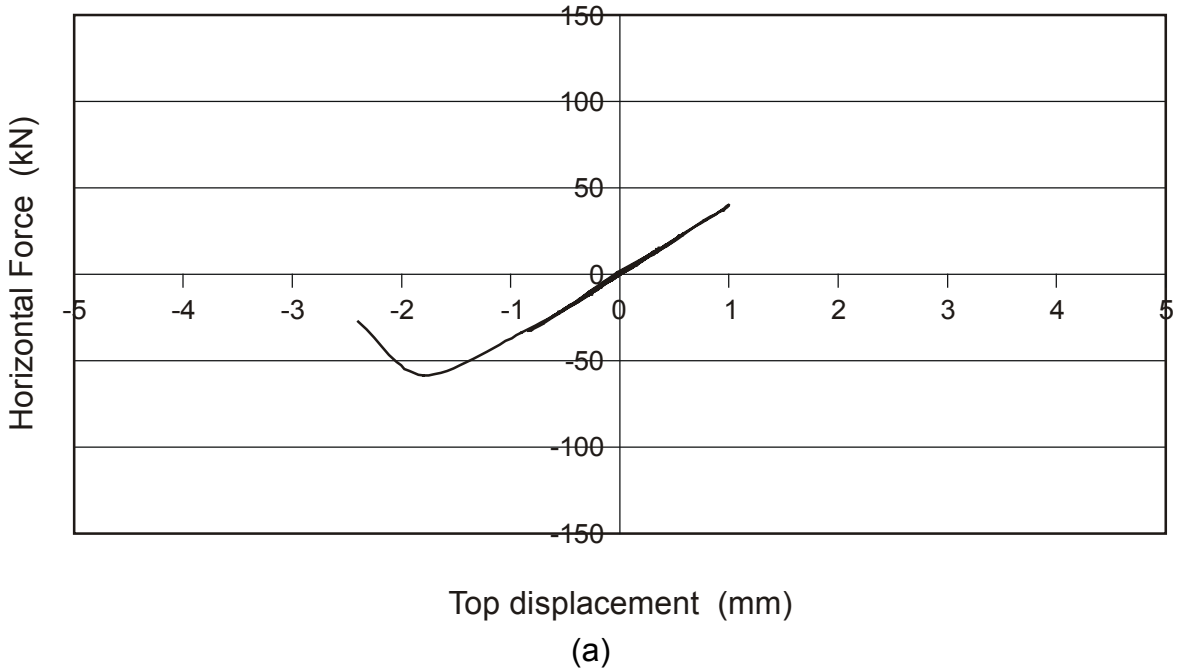

(a)

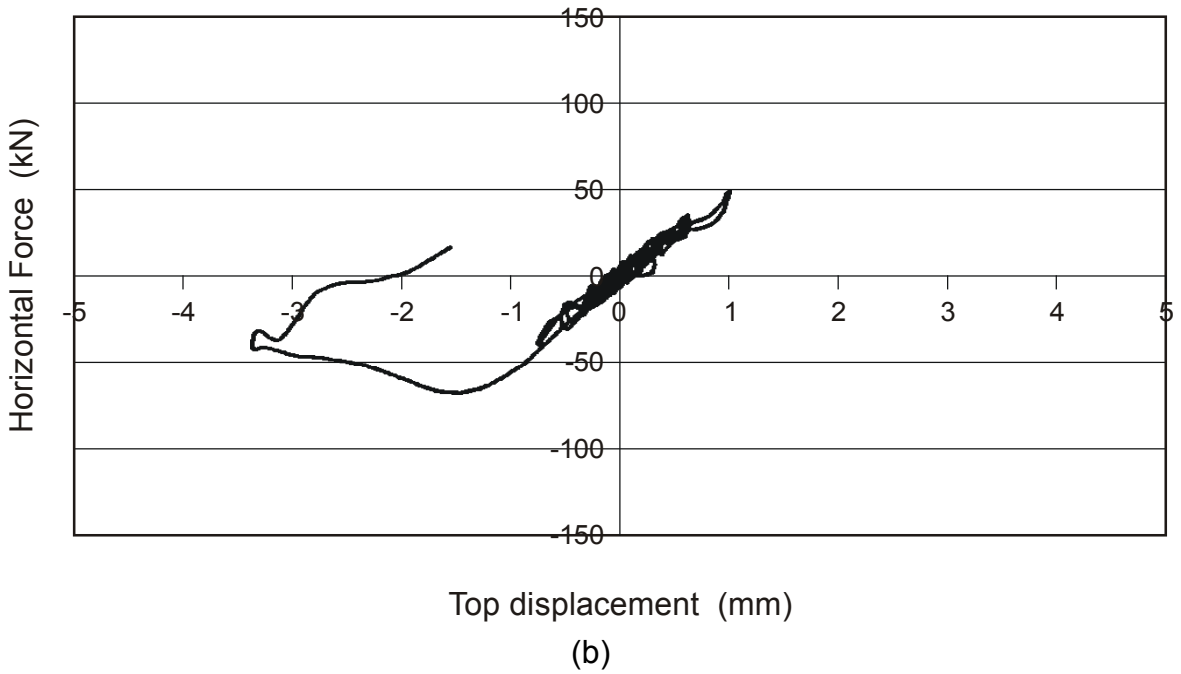

(b)

Figure 3.10: Comparison of numerical results (a) with [216]'s results (b) for $(\ddot{u})_{max} = 0.4\,g$ a).

programmed model for different values of the Friaul acceleration time-history, are presented. These Figures accurately show the behaviour of the masonry wall.

The comparison between these results and the results of [216] shows that the results obtained closely agree.

The experimental result presented in [12] for a masonry panel of $1.5m \times 3.0m \times 0.38m$ is calculated in the following numerically with the developed model. The mechanical parameters used in the numerical calculation are the same as those used in the experiment: $E = 3000\,MPa,\quad G = 900\,MPa,\quad \sigma_c = 7.61\,MPa$. The experimental set-up is shown in Figure 3.11, in which the panel is tested in a static testing frame with vertical load is applied by two hydraulic jacks and cyclic horizontal displacement history applied using a double-effect hydraulic jack. In the numerical analysis the wall is loaded at the top with constant static vertical load and horizontal cyclic load untill the damage is reached.

To show the validity of non-local concept of the continuum damage theory, the masonry wall, experimented on by Berto [12], will be studied to show that there is no effect for the size of the mesh. The wall is analysed with the developed continuum damage model using 80-element mesh and 320 element-mesh as shown in Figure 3.12. The results of both the analysis and experiment are shown in Figure 3.13. these results show that there is no mesh sensivity using the continuum damage concept for the analysis of masonry walls and compare well with the experiemental results.

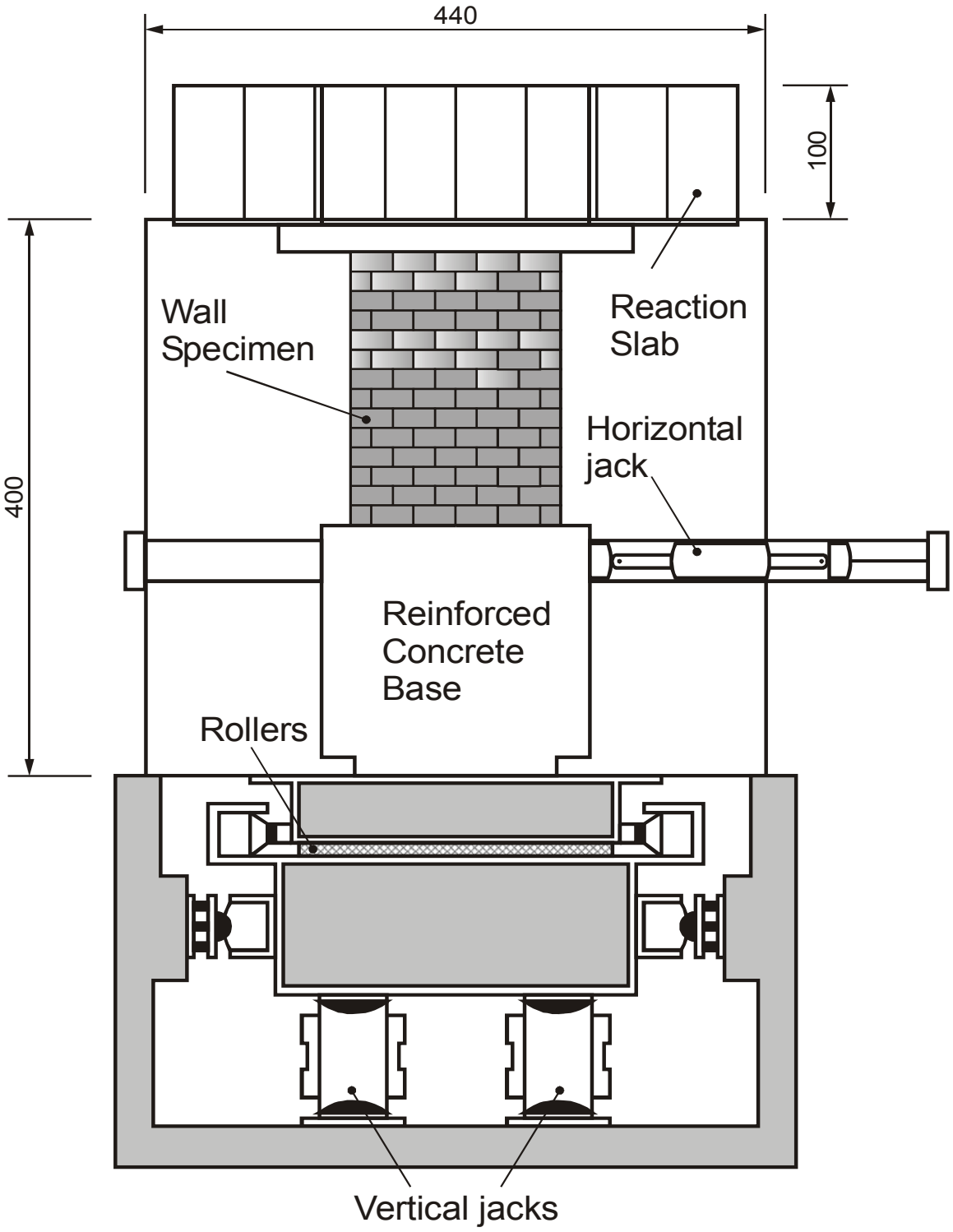

Figure 3.11: Experimental set-up [12]

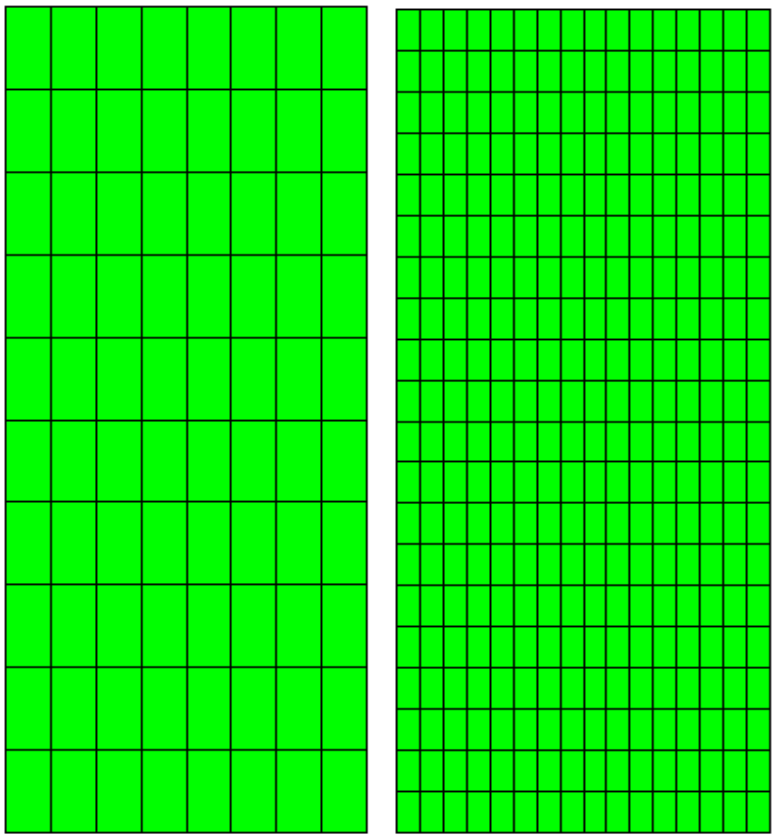

(a) (b)

Figure 3.12: Finite element meshes used: (a) Mesh of 80 elements and (b) Mesh of 320 elements

The contour of the maximum principal stresses developed from the numerical analysis in the two directions is shown in Figure 3.14. It leads to the shape of failure modes of the experimental shear wall shown in Figures 2.9 and 2.12. As is shown here, the numerical results compare well with the experimental; there is no mesh effect and the failure mode is well captured. This testifies for the effectiveness of the developed damage model in describing the masonry behaviour.

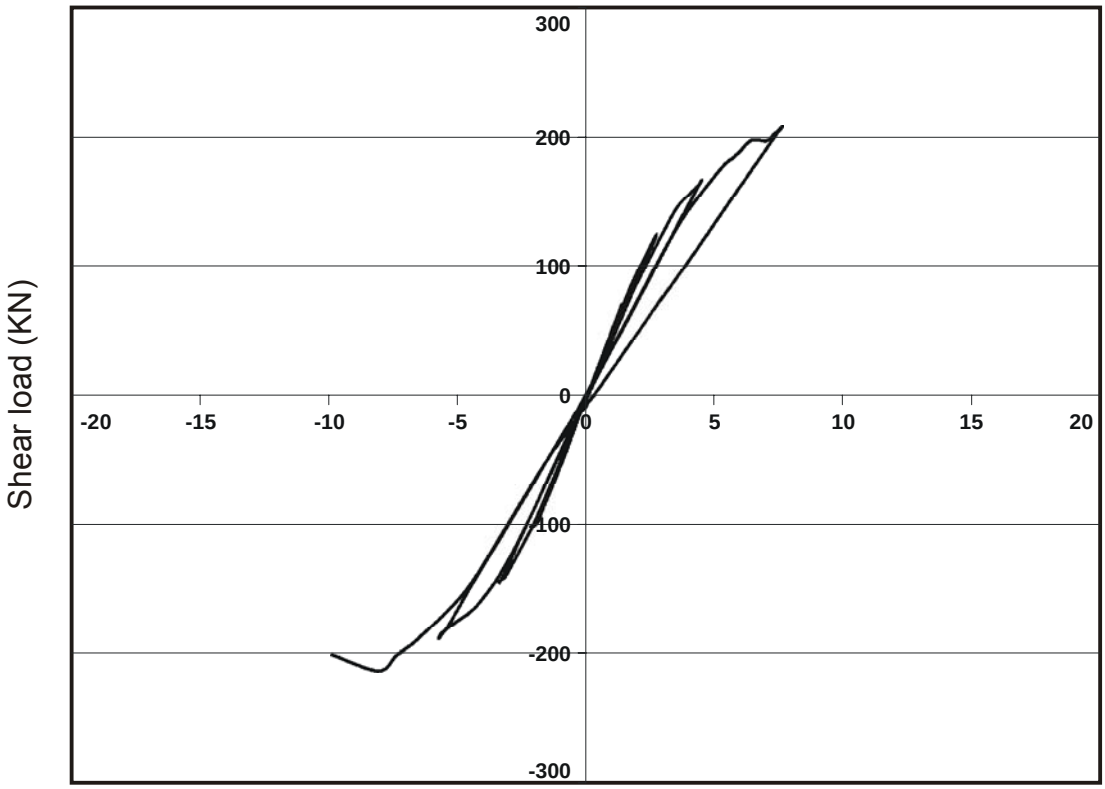
Shear load (KN)
300
200
100
0
-100
-200
-300
-20
-15
-10
-5
0
5
10
15
20
Horizontal Displacement (mm)

(a)

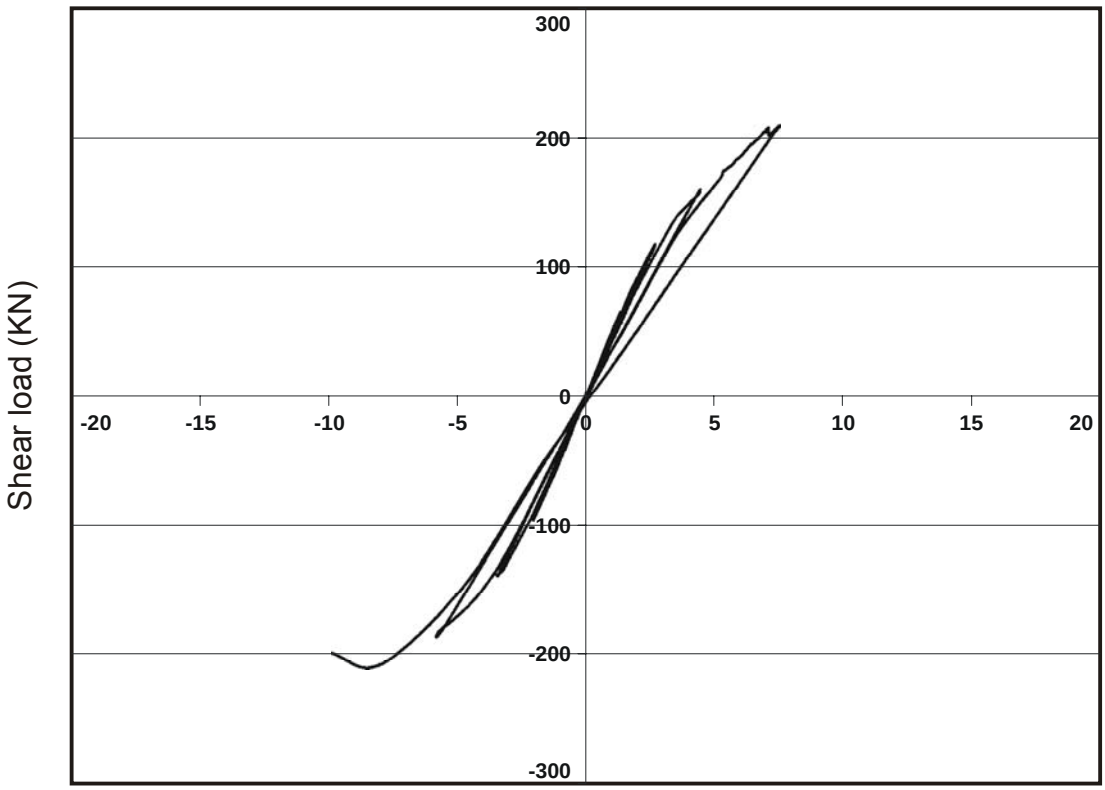
Shear load (KN)
300
200
100
0
-100
-200
-300
-20
-15
-10
-5
0
5
10
15
20
Horizontal Displacement (mm)

(b)

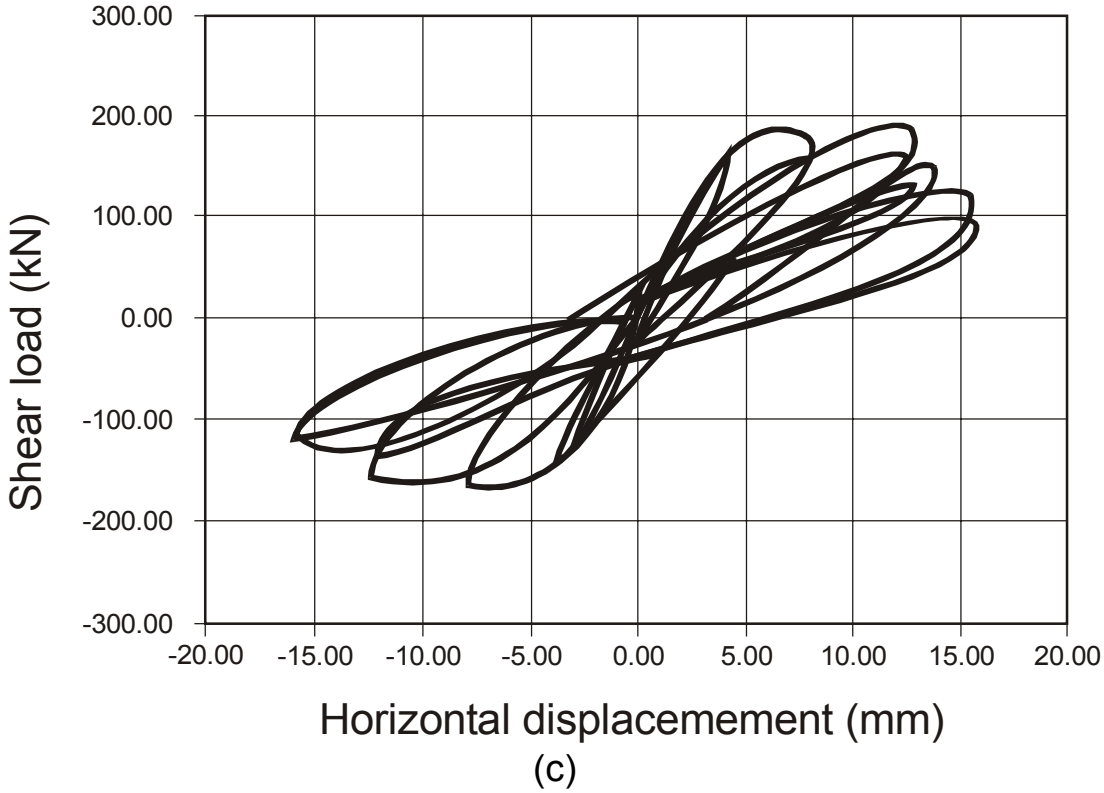

Figure 3.13: Load-displacement of panel obtained with meshes shown in Figure 3.12 (a) 80-elements; (b) 320-elements and (c) experimental results [12]

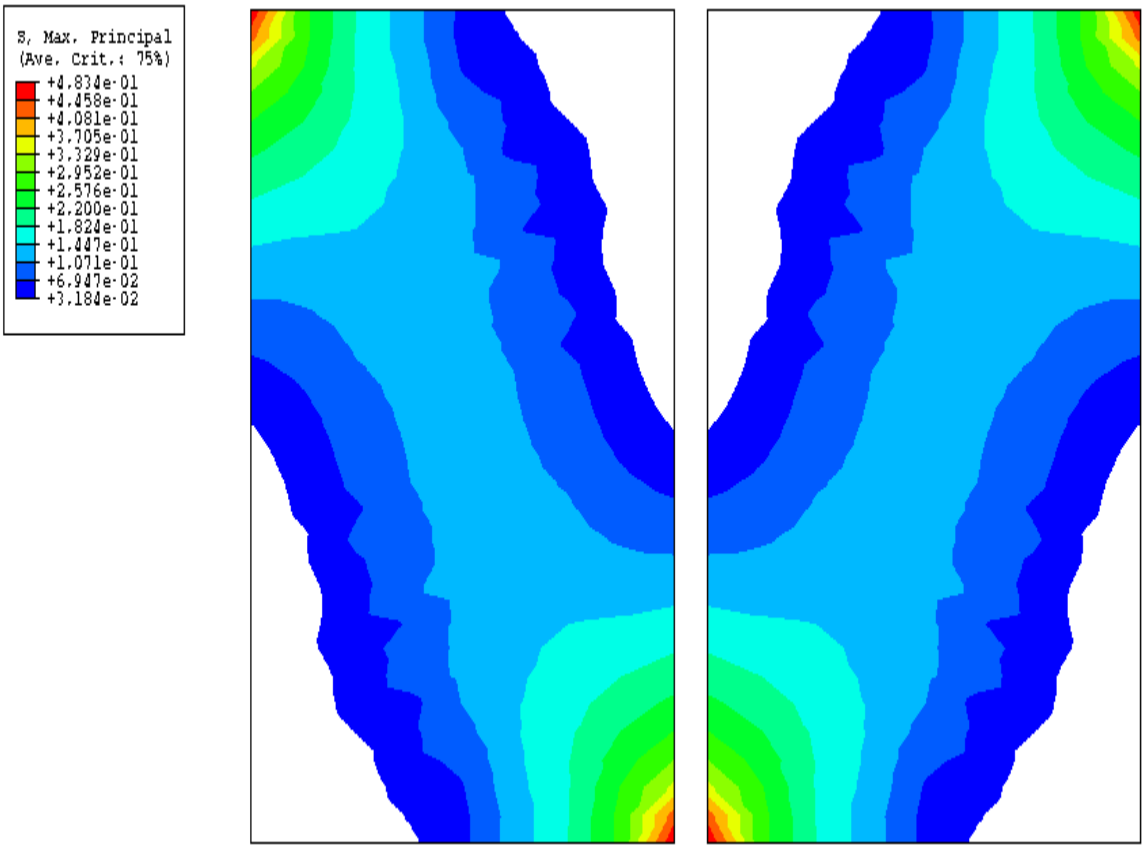

Figure 3.14: Principal maximum stresses in the two directions

3.3 Experimental Results of a Wall made from Autoclaved Aerated Concrete (AAC) Blocks

Pseudo-dynamic experiments were conducted in the laboratory of the the Institute of Reinforced Concrete Structures, at the University of Karlsruhe on a virgin wall made from autoclaved aerated concrete (AAC) blocks with the dimensions: $2.50m \times 2.50m \times 0.24m$. The wall is loaded with a constant static vertical load of $0.132\,MN/m$, which is equivalent to the load from the upper stories on a wall in the lowermost-floor. As a dynamic earthquake loading, the 1990-Bucharest acceleration time-history, north-south values are chosen with different scale factors until cracking of the wall occured. The material properties are shown in Table 3.1. The experimental set-up is shown in Figure 3.15.

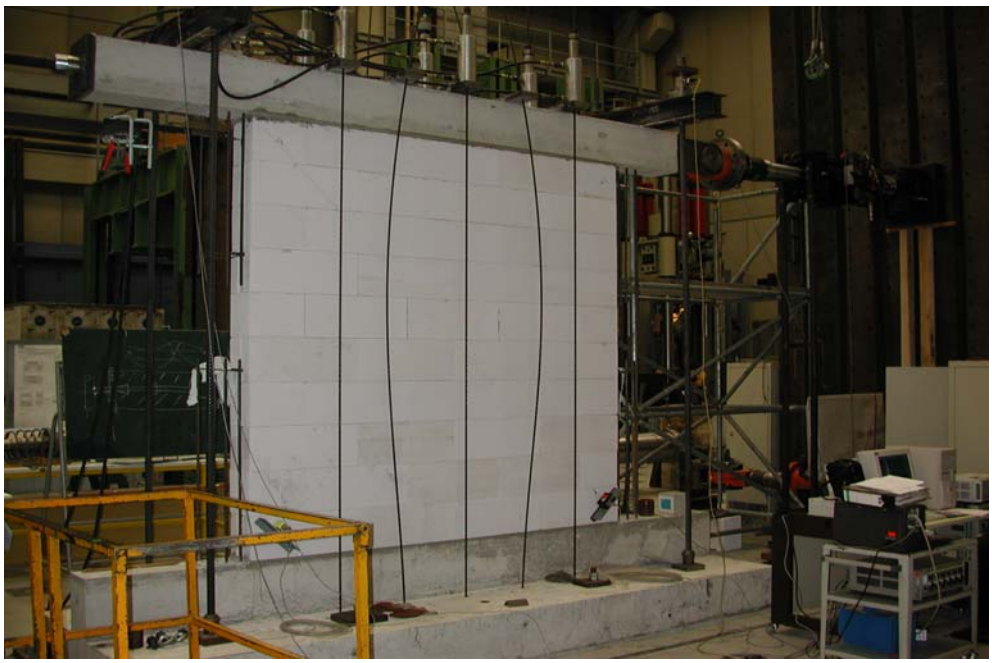

Figure 3.15: Experiment-Set-up of the wall

In the experiments with a scale of 0.5 for the acceleration time-history, i.e., with $38.5\,cm/s^2$ as peak ground acceleration (PGA), the behaviour of the wall is nearly elastic (see Figure 3.16). The maximum force in this experiment is approximately $62\,KN$ with a maximum displacement of approximately $1.1\,mm$.

Material properties of the autoclaved aerated concrete-blocks	
Identification	PPW4-0.5
Dimensions l / b / h	624 / 249 / 240 mm
Cube compression Stress	4.39 N/mm^2
Block compression stress	5.00 N/mm^2
Dry density $\rho_{105°}$	0.47 kg/dm^3

Table (3.1): The material properties of AAC Blocks

By using the original acceleration-time history values of the 1990-Bucharest earthquake with $76.6\ cm/s^2$ PGA, the first diagonal, thin cracks appeared having a crack width of $0.1mm$. This is due to the maximum tension capacity of the wall being reached.

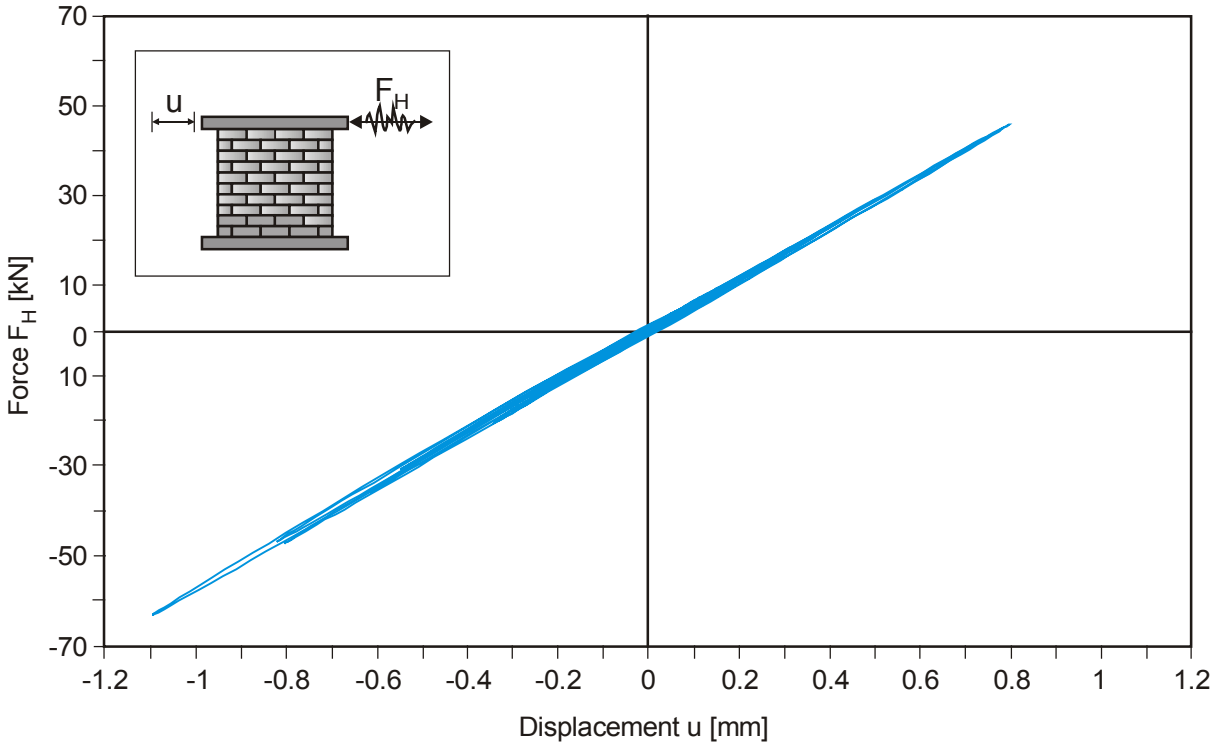

Figure 3.16: Force-displacement diagram of the autoclaved aerated concrete (AAC) blocks wall, PGA=38.3 cm/s^2

After loading the wall with 1.5 times of the acceleration-time history (PGA=$114.9\ cm/s^2$), the maximum loading capacity of the wall is reached. Figure 3.17 shows the force-displacement diagram for this case of with a maximum horizontal force of $153\,KN$ and a maximum displacement of $5\ mm$. A big number of cracks at the front and back of the wall were

clearly visible after this experiment. The wall cracked, because the maximum tension capacity of blocks was reached. In this experiment, the non-linear behaviour of the wall and a strong hysteretic behaviour with a high damping were clear comparing to the experiment with PGA= $38.5\ cm/s^2$ (see Figure 3.16).

In Figure 3.18, the nominal spectral acceleration, which is calculated by using the obtained acceleration from the aforementioned explained experiments, are presented. Figure 3.19 shows the increasing factor of the response-spectra, which can be obtained by dividing the nominal spectral acceleration of PGA=$114.9\ cm/s^2$ by that of PGA=$38.5\ cm/s^2$.
Here one can clearly see that, by increasing the loading, i.e., by increasing the PGA, the stiffness is decreased. While the eigen-period (T) equals $0.3s$ in the elastic experiment, the peak value of the nominal spectral acceleration moved into the range of the greater periods for PGA=$114.9\ cm/s^2$. In addition to this, the nominal spectral acceleration values in this range are greater than those for the elastic experiment.

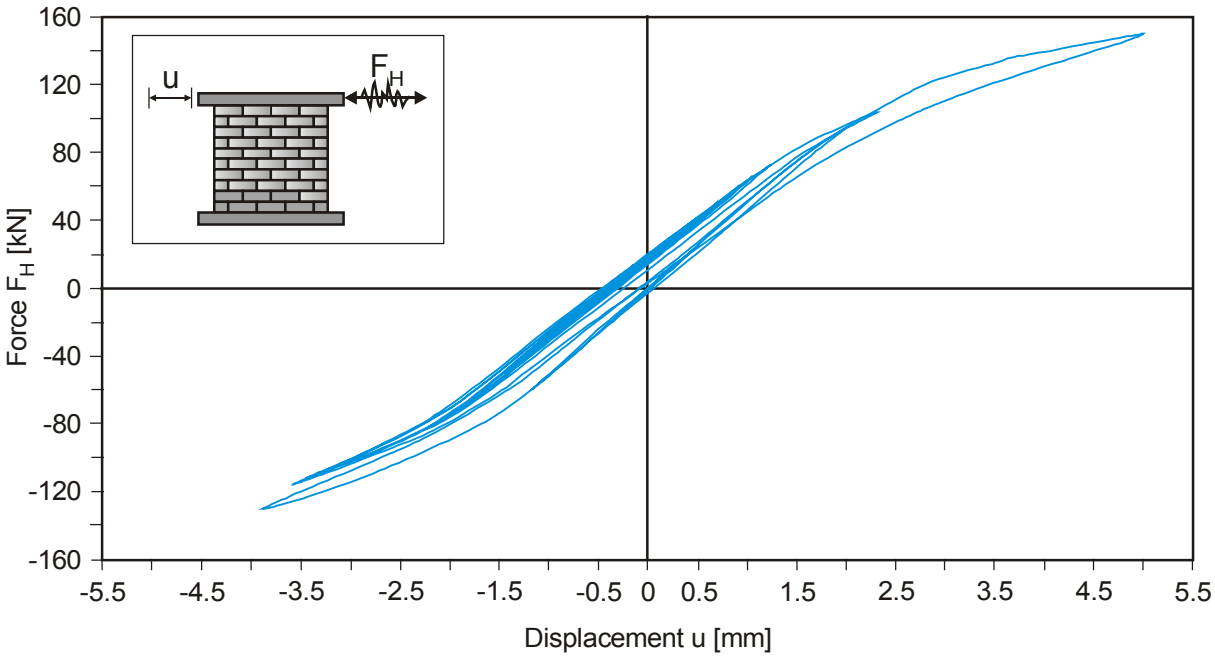

Figure 3.17: Force-displacement diagram of the autoclaved aerated concrete (AAC) blocks wall, PGA=114.9 cm/s^2

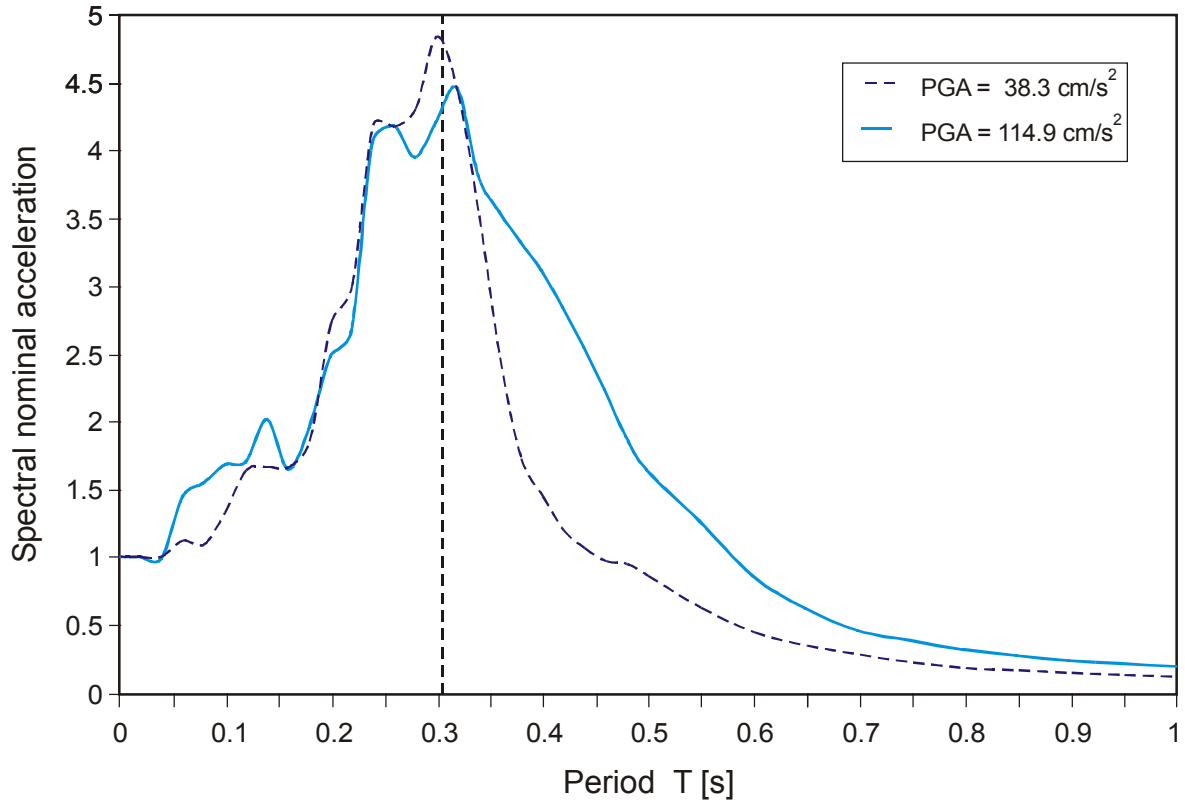

Figure 3.18: The nominal spectral acceleration from the experiments on the wall for PGA=38.3 cm/s^2 versus for PGA=114.9 cm/s^2

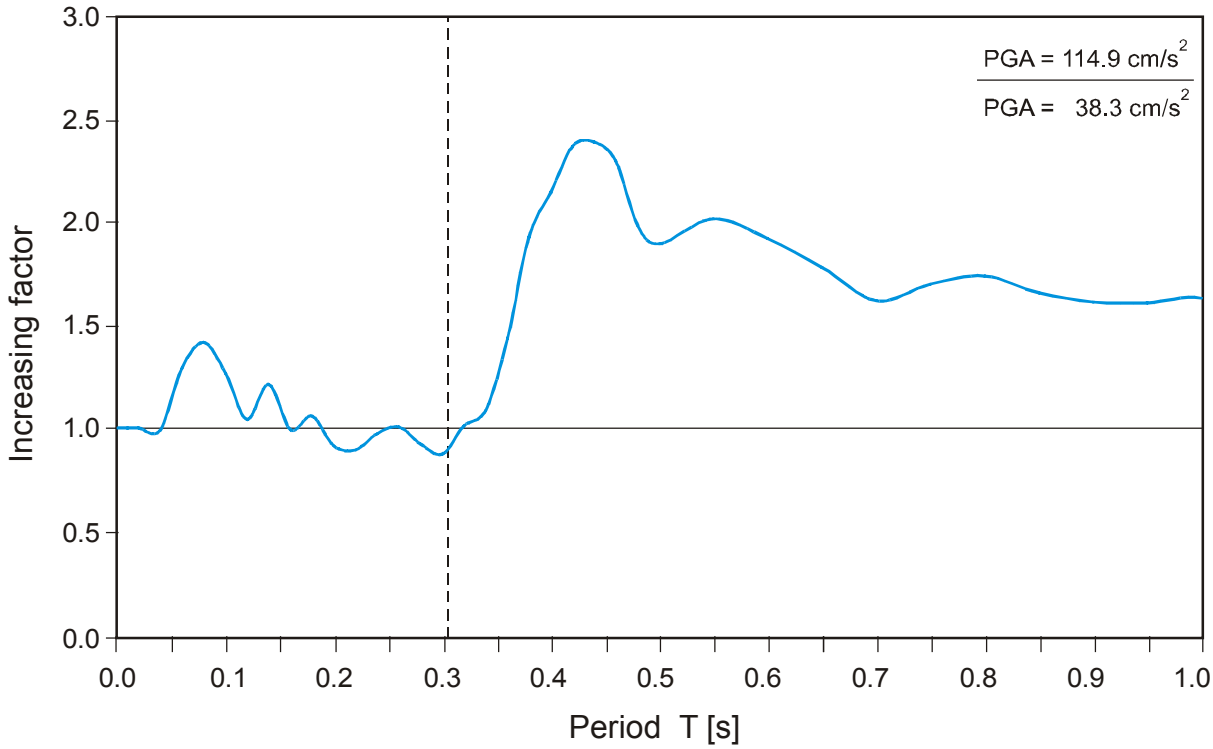

Figure 3.19: increasing-factors of the response spectra from the experiments on the wall, comparison between the cracked case, PGA=114.9 cm/s^2 and non-cracked case, PGA=38.3 cm/s^2

After the end of the dynamic experiments on the wall, a static displacement of $6\,mm$ in both directions is applied at the head of the wall, to have a definite initial condition for the subsequent experiments on this damaged wall when it is being retrofitted. For this static displacement, the maximum obtained horizontal load equals $152\,KN$ (see Figure 3.20 and further diagonal cracks untill $1.5\,mm$ width are developed in the blocks. The resulting crack-pattern in the wall at the end of all experiments is shown in Figure 3.21.

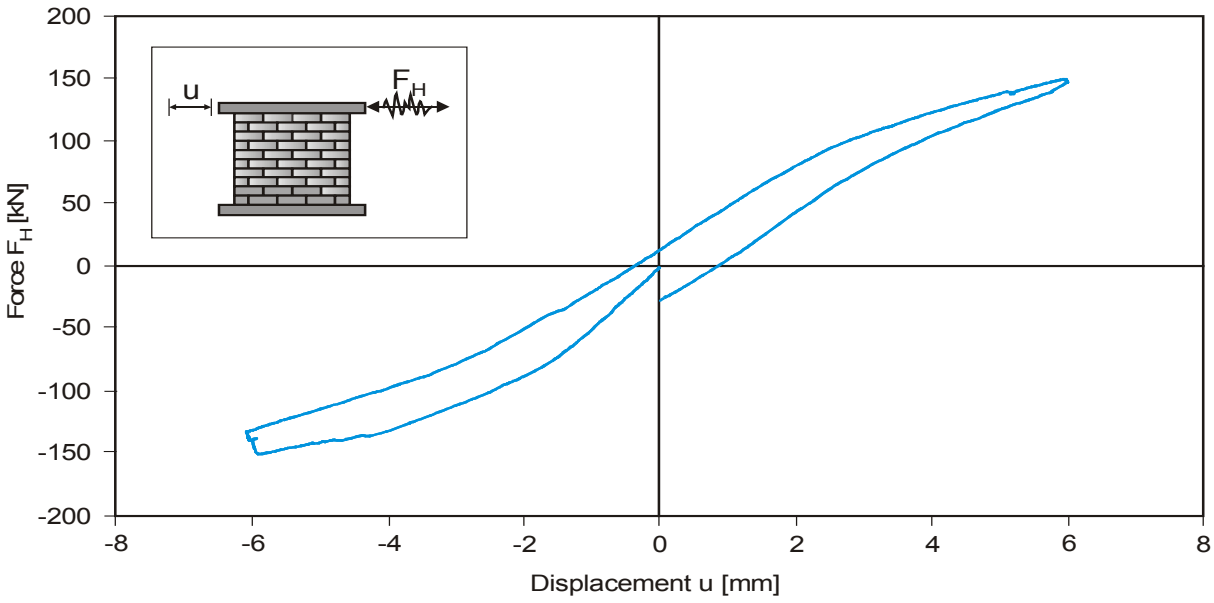

Figure 3.20: Load-displacement diagram of the static test

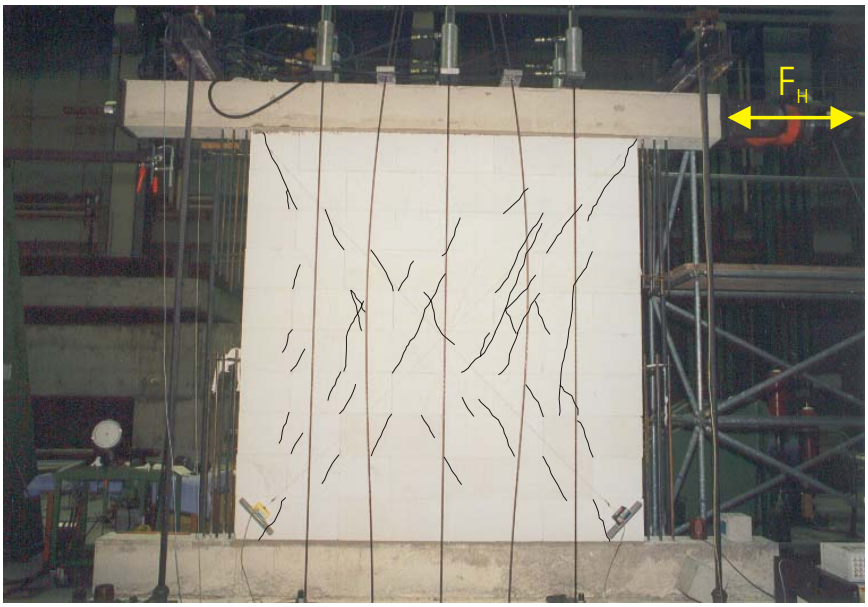

Figure 3.21: Crack-pattern in the wall at the end of all experiments

3.4 Comparison between the Experimental and Calculation Results of the wall made from Autoclaved Areated Concrete (AAC) Blocks

In the following, the autoclaved aerated concrete (AAC) blocks wall (see section 3.3) is calculated with the developed non-linear finite element program. The calculated results are compared with the corresponding experimental results.

- **Loading**

As loading, the time-history of 1990-Bucarest earthquake, north-south components are used with $0.5\sigma_0$ constant vertical load. The magnitudes of the acceleration time-history are shown in Figure 3.22. This acceleration time-history is scaled in the calculation with the same scaling factors used in the experimental programme untill the failure of the wall is reached. The wall is loaded with this acceleration time-history in its plane.

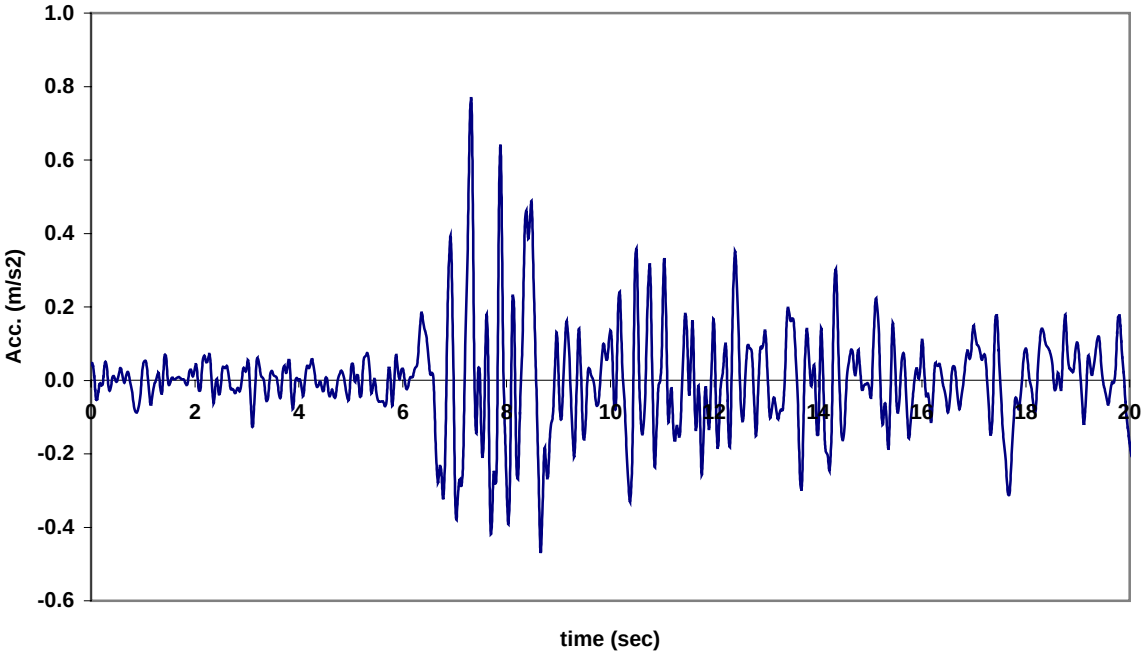

Figure 3.22: Bucharest-1990 Acceleration time-history

- **Input Data**

The dimensions and mechanical properties of the wall calculated with the developed model are the same as those used for the experimented wall. These are included in Table 3.1.

- **Results Representation**

Table 3.2 shows the results of the calculations versus the results of the experiment for PGA= $38.3\,cm/s^2$.

	Max. Force (KN)	Max. Disp. (mm)
Experimented wall	62.337	1.085
Calculated wall	61.61	1.072

Table 3.2: The results of the calculation versus those from the experiment of the wall for PGA=38.3 cm/s^2

Table 3.3 shows the values of the force and the displacement from the calculated and experimented wall for a PGA= $114.9\,cm/s^2$.

	Max. Force (KN)	Max. Disp. (mm)
Experimented wall	155.36	5.075
Calculated wall	152.815	4.992

Table 3.3: The results of the calculation versus those from the experiment of the wall for PGA=114.90 cm/s^2

Tables 3.2 and 3.3 show the agreement of the calculated and the experimental results in the elastic state and in the damage state, respectively.

Figure 2.23 shows the acceleration response spectra for both of the calculated and the experimented wall for PGA= $38.3\,cm/s^2$. This shows close agreement with the experimented results with a period of $0.3\,s$.

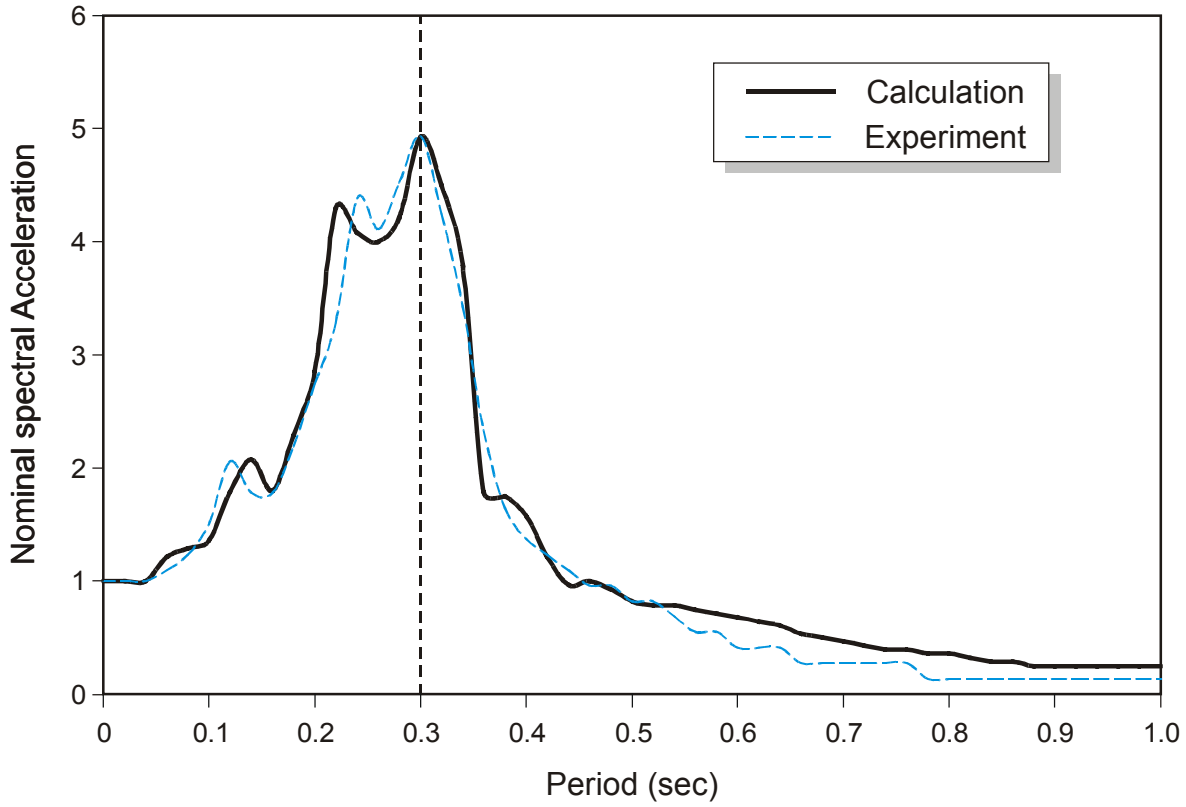

Figure 3.23: Comparison of the nominal spectral acceleration of the wall from the calculation and the experiment, PGA=38.3 cm/s^2

Figure 3.24 shows the acceleration response spectra from the calculation versus that from the experiment for PGA=114.9 cm/s^2, which are in close agreement, where the eigen-period moves due to the stiffness degradation in the direction of higher values and the wall becomes softer.

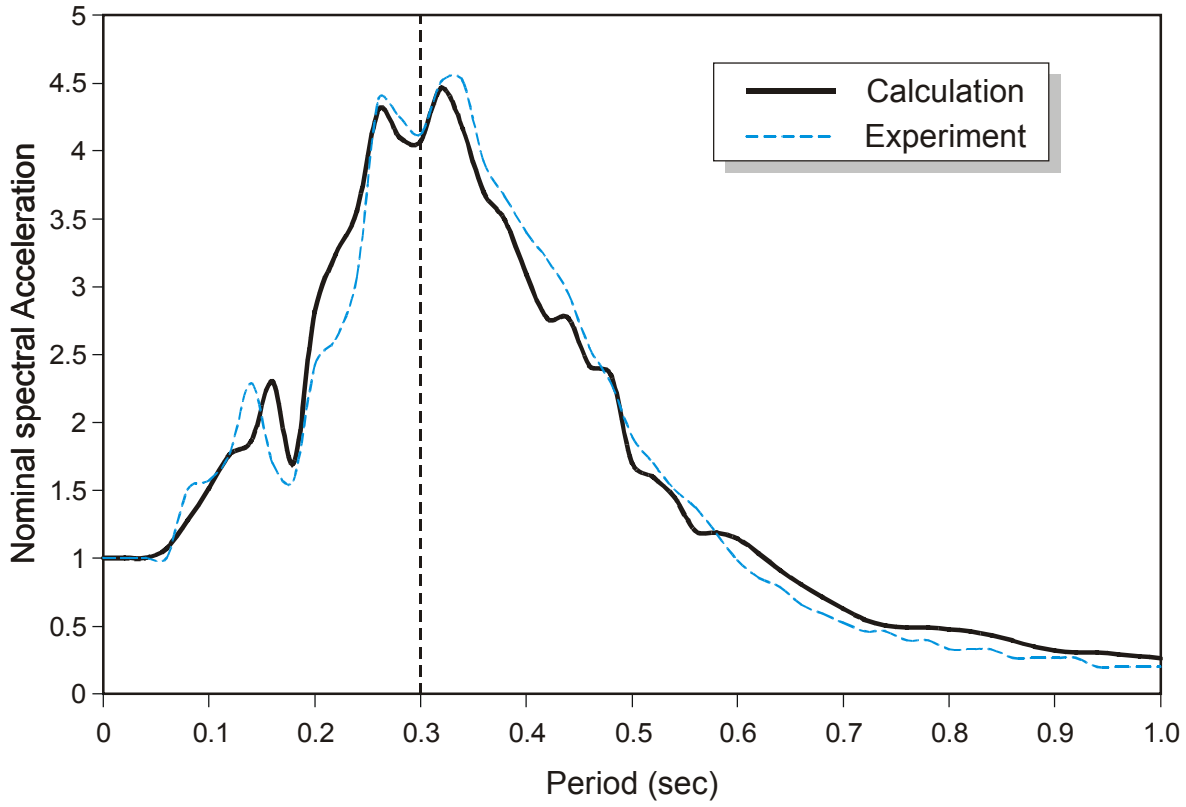

Figure 3.24: Comparison of the nominal spectral acceleration of the wall from the calculation and the experiment, PGA=114.9 cm/s^2

The wall experimented by Berto [12] (see Figure 3.11) is now studied numerically with the same dimensions and mechanical properties, but with a central opening of $50cm \times 100cm$.

Figures 3.25(a),(b) show the contours of the pressure distribution and the symbols of the principal stresses, respectively, which lead to the failure mechanism as that of [112] (see Figure 2.13).

The horizontal displacement versus the horizontal load of the upper layer of the wall is shown in Figure 3.26. The comparison of the results of this case with that of the wall without an opening, showed that there is a reduction in the shear stiffness of the wall as a result of the opening.

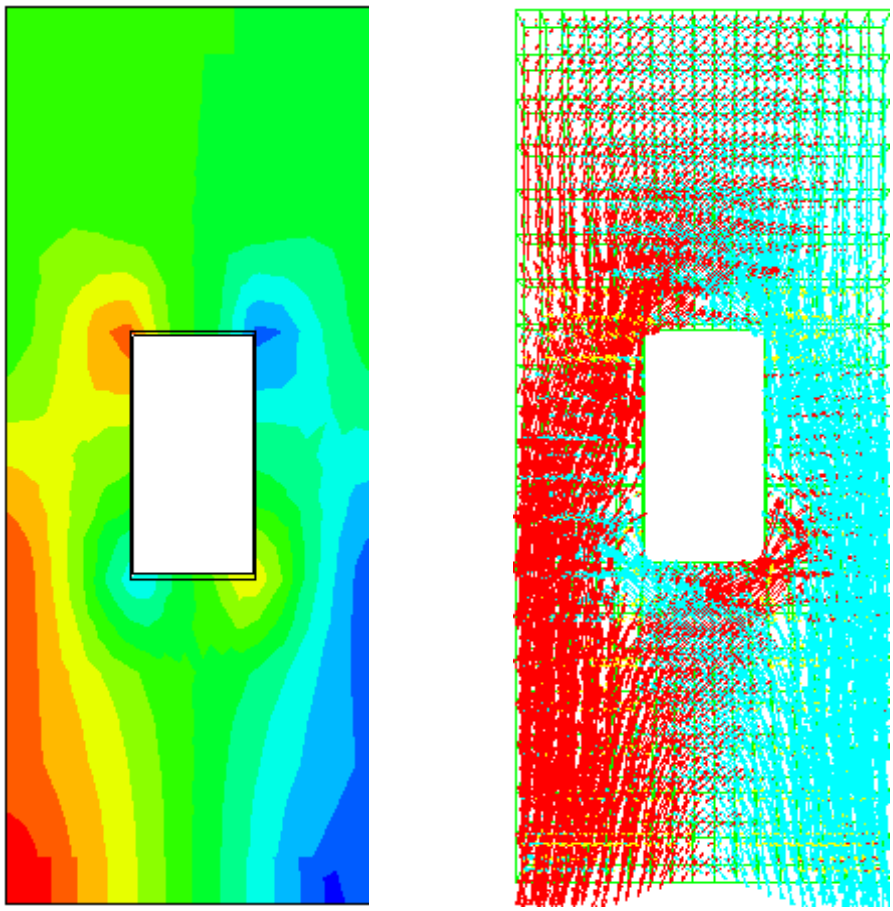

(a) (b)

Figure 3.25: Pressure contour (a) and principal stress symbols (b) of the wall with opening

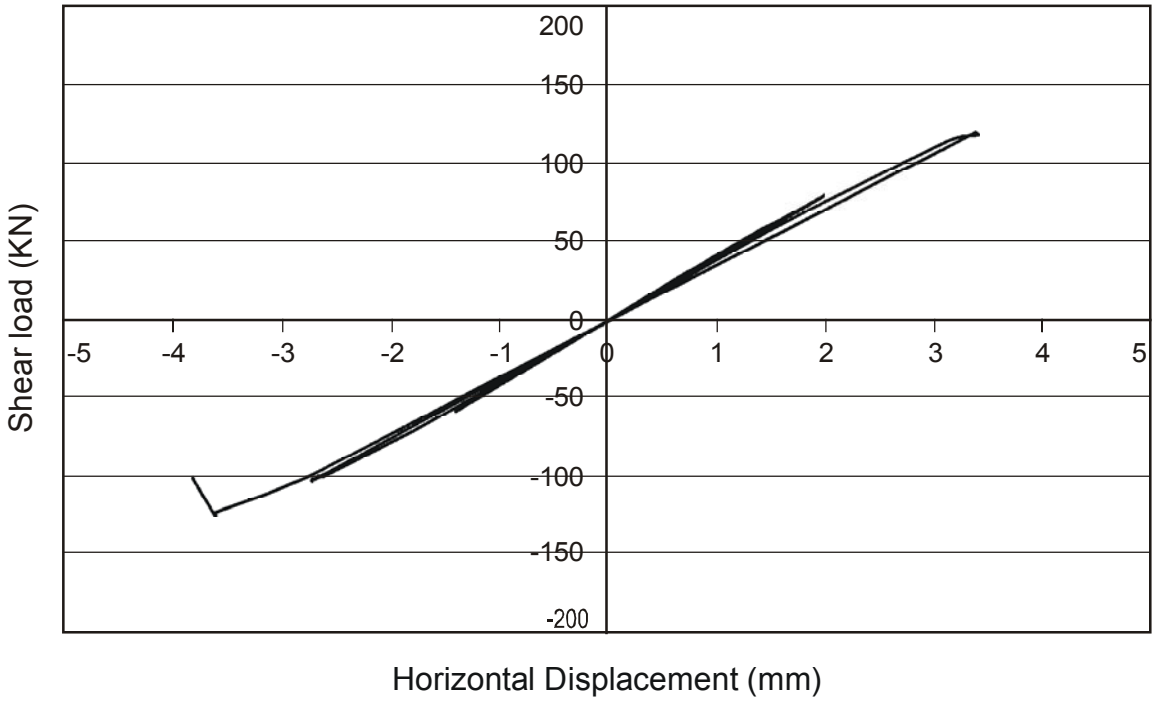

Figure 3.26: Horizontal load versus horizontal displacement for the wall with opening

4 Anchorage Strength Model for Fibre Reinforced Polymers (FRP) bonded to Masonry

4.1 Fibre Reinforced Polymers (FRP) Properties

The use of advanced composite materials in construction is an exciting, newly emerging technology. The composite materials are lightweight, non-corrosive, durable and allow for a high degree of design flexibility. These field-proven materials exhibit low creep and elongation. The composite materials are lighter, thinner and have 10 times the tensile strength capacity when compared to steel. In addition to these advantages, the composite system is also faster and easier to install than the conventional strengthening techniques.

Since the 1960s, external bonding of steel plates has been used in the retrofitting and strengthening of different structural elements. In recent years, fibre-reinforced polymers (FRP) has been increasingly replacing the steel plates due to their superior properties.
The most important factor in the design of an effective retrofitting solution using externally bonded plates and/or sheets is the end anchorage strength.

First, a review of the theory of the composites and the properties of the different materials used in the construction of the laminate is introduced. Then, a review of the current anchorage strength models for both FRP-to-concrete blocks and steel-to-concrete blocks bonded joints under shear are presented. An assessment for these models with the experimental data collected from the relevant literature, reveals the deficiencies of all existing models. Then, the new, simple and rational model [89], based on an existing fracture mechanics analysis and experimental observations is presented. This new model not only matches experimental observations of bond strength closely, but also correctly predicts the effective bond length. This new model is, thus, suitable for practical application in the design of FRP-to-concrete as well as steel-to-concrete bonded joints.

Based on this new model [89] and the experimental data gained at the Institute of Reinforced Concrete structures, at the University of Karlsruhe, for the GFRP-sheets bonded to AAC-blocks and concrete strengthened with CFRP sheets, a new model is developed.

Several techniques for strengthening masonry exist. These methods include, application of a thin layer of reinforced shot crete, surface treatment by means of steel wire mesh and high performance bonding material, the introduction of new concrete elements such as columns and pilasters and the application of steel bracing system. Among the previous methods, external bonding of FRP-laminates on masonry is seen to be one of the most effective ways of increasing the shear capacity and ductility of such structures.

4.1.1 Basic Properties of the Composite Materials

In its most basic form, a composite material is one, which is composed of at least two elements working together to produce material properties that are different to the properties of those elements on their own (see Figure 4.1). In practice, most composites consist of a bulk material (the 'matrix'), and a reinforcement of some kind, added primarily to increase the strength and stiffness of the matrix. It is made to be extremely thin, yet very strong. This reinforcement is usually in fibre form. The reinforcement provides the oriented strength and the polymer matrix holds the reinforcement in proper orientation in order to provide optimum properties. Today, the most common man-made composites are the polymer matrix composites (PMC's). Also known as FRP - Fibre Reinforced Polymers (or Plastics). These materials use a polymer-based resin as the matrix, and a variety of fibres such as glass, carbon and aramid as reinforcement.

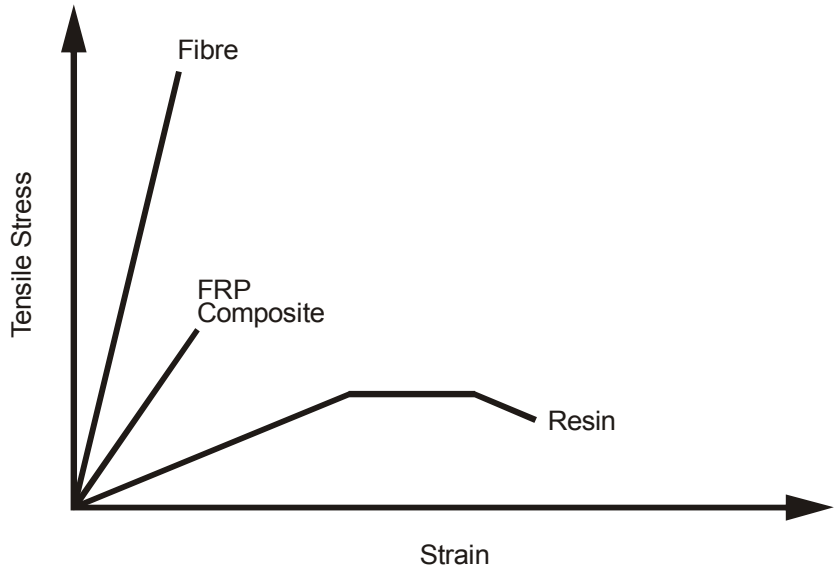

Figure 4.1: Stress-Strain relationship of the composite

Advanced fibre reinforcement materials for construction are primarily:

- E-Glass, (GFRP)
- Carbon fibre (CFRP)
- Aramid, (AFRP)

The inherent advantages of the composite materials when compared to conventional materials include:

- Corrosion resistance
- Light weight
- High strength
- Design flexibility
- Low maintenance
- Durability

The structural benefits of a composite system include an increase in strength, stiffness and toughness. Moreover, this high performance technology saves 25% to 50 % in labour costs due to the ease of its installation.

4.1.2 Resin Systems

Any resin system for use in a composite material requires the following properties:

1. Good mechanical properties
2. Good adhesive properties
3. Good toughness properties
4. Good resistance to environmental degradation

It should also be noted that when a composite is loaded in tension, for the full mechanical properties of the fibre component to be achieved, the resin must be able to deform to at least the same extent as the fibre.

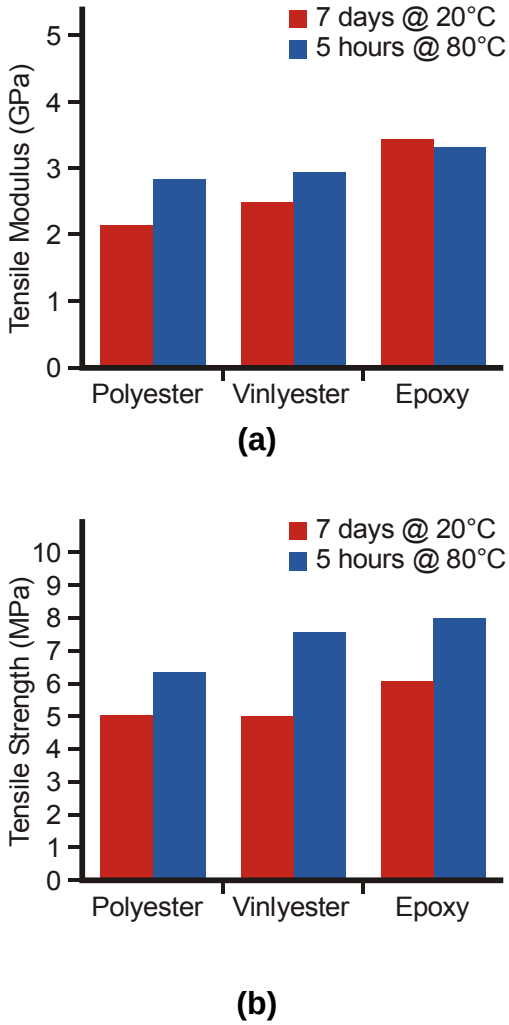

Figure 4.2: Mechanical properties of the different resin systems: Tensile Modulus (a); Tensile Strength (b)

- **Mechanical Properties of the Different Resin Systems**

Two important mechanical properties of any resin system are its tensile strength and stiffness. Figures 4.2(a),(b) show results for tests carried

out on commercially available polyester, vinyl ester and epoxy resin systems cured at 20°C and 80°C.
After a cure period of seven days at room temperature it can be seen that a typical epoxy will have higher properties than a typical polyester or vinyl ester for both strength and stiffness. The beneficial effect of a post cure at 80°C for five hours can also be seen.
Also of importance to the composite designer and builder is the amount of shrinkage that occurs in a resin during and following its cure period. Shrinkage occurs due to the resin molecules rearranging and re-orientating themselves in the liquid and semi-gelled phase. Polyester and vinylesters require considerable molecular rearrangement to reach their cured state and can show shrinkage of up to 8%. The different nature of the epoxy reaction, however, leads to very little rearrangement and with no volatile by-products being evolved, typical shrinkage of an epoxy is reduced to around 2%. The absence of shrinkage is, in part, responsible for the improved mechanical properties of epoxies over polyester, as shrinkage is associated with built-in stresses that can weaken the material. Furthermore, shrinkage through the thickness of a laminate leads to 'print-through' of the pattern of the reinforcing fibres, a cosmetic defect that is difficult and expensive to eliminate.

The polyesters, vinylesters and epoxies discussed here account for some 90% of all thermosetting resin systems used in structural composites.

The comparison between the different types of resin is as follows:

- **Polyesters**

The advantages of the polyester resin are that it is easy to use and costs the least of all resins available.
The disadvantages are: its moderate mechanical properties, high styrene emissions in open moulds, high cure shrinkage and limited range of working times.

- **Vinylesters**

Vinylesters advantages are: their high chemical/environmental resistance and their higher mechanical properties than polyesters.
Its disadvantages are: post cure is generally required for high properties, they have high styrene content, higher cost than polyesters and high cure shrinkage.

- **Epoxies**

Epoxy resins are two part polymers, which, during the cure form strong molecular chains.
They can be customized to produce and possible combinations of properties such as high tensile strength, which tends to be brittle with low adhesive strength, or lower tensile strength resins with very high adhesion. For most strengthening needs, high adhesion is the most important factor since the fibres have such high strength themselves.
Epoxies are easy to mix and to apply and have little or no odour. They have no VOCs (volatile organic compounds) and are not flammable.
Cured epoxy is inert, making disposal easy. In addition, epoxies have advantages such as: high mechanical and thermal properties, high water resistance, long working times available, temperature resistance can be up to 140°C wet / 220°C dry and low cure shrinkage.
Overall, epoxies are the most environmentally friendly resins available.
Its disadvantages are: its cost above that of vinylesters and its critical mixing.

4.1.3 Properties of Fibres and other Engineering Materials

The Basic Properties of fibres and other engineering materials are shown in Table 4.1.

Material type	Tensile Str. (Mpa)	Tensile Modulus (Gpa)	Typical Density (g/cc)	Specific Modulus
Carbon Hs	3500	160-270	1.8	90-150
Carbon IM	5300	270-325	1.8	150-180
Carbon HM	3500	325-440	1.8	180-240
Carbon UHM	2000	440+	2.0	200+
Aramid LM	3600	60	1.45	40
Aramid HM	3100	120	1.45	80
Aramid UHM	3400	180	1.47	120
Glass-E glass	2400	69	2.5	27
Glass-S2 glass	3450	86	2.5	34
Glass-quartz	3700	69	2.2	31
Aluminium-Alloy (7020)	400	1069	2.7	26
Titanium	950	110	4.5	24
Mild Steel (55- Grade)	450	205	7.8	26
Stainless Steel- (A5-80)	800	196	7.8	25
HS Steel (17/4 H900)	1241	197	7.8	25

Table 4.1: Basic Properties of fibres and other engineering materials

4.1.4 Fibre Laminates Types

The different kinds of fibre laminates are:

- **E-Glass Fibres**

E-Glass is produced by melting a form of glass (Borosilicate) in a large vat. The molten glass is drawn through tiny platinum holes and cooled

until it forms thin fibres. The fibres are then cleaned and a chemical is applied to the surface to protect the fibre and promote adhesion to the resin. Once it has cooled it is gathered into bundles, which can then be woven into a fabric. E-Glass is cheaper than carbon fibre.

- **Carbon Fibres**

Carbonising a pre-cursor fibre produces carbon fibres. The pre-cursor is usually PAN (Poly-acrylonitrile) which is very similar to rayon.
The pre-cursor is drawn through an oven at high temperature in an inert atmosphere and tensioned. The amount of tensioning and temperature determines the strength and stiffness of the fibres.
Once all the impurities have been burned off, the fibre is pure carbon. This is then cleaned and a chemical is applied to the surfacein a similar manner to E-Glass. Once bundled, the fibres can then be woven into a fabric.
Carbon fibres are very small, usually about 7 microns in diameter or approximately 5 million fibres per square inch.
The dry carbon fibres have about 10 times the strength of steel, 4500 MPa. Once mixed with the resin, this drops to approximately 1000 to 1400 MPa, still significantly stronger than steel.

- **Aramid Fibres**

Aramid fibres are extremely tough; a high strength fibre made from an aromatic polyamide, Dupont’s KEVLAR, is an example, and is often used in bullet resistant jackets.
Although strong, aramid fibres have some specific characteristics make it less desirable for strengthening. The fibres are hydroscopic, meaning that they tend to soak up water, and should only be used when they are completely protected from the environment. The fibres themselves are quite abrasive, and under repeated loading, they can abrade against each other, weaking the laminate.
Aramid fibres are extremely difficult to cut, usually requiring specialized tools such as ceramic shears. aramids excel, however, when they are incorporated into blast mitigation upgrade.

4.1.5 Laminate Mechanical Properties

The properties of the fibres only show part of the picture. The properties of the composite derives from those of the fibre, but also the way it interacts with the resin system used, the resin properties itself, the volume of fibre in the composite and its orientation. Figure 4.3 shows a basic comparison of the main fibre types when used in a typical high-performance unidirectional epoxy prepreg, at the fibre volume fractions.

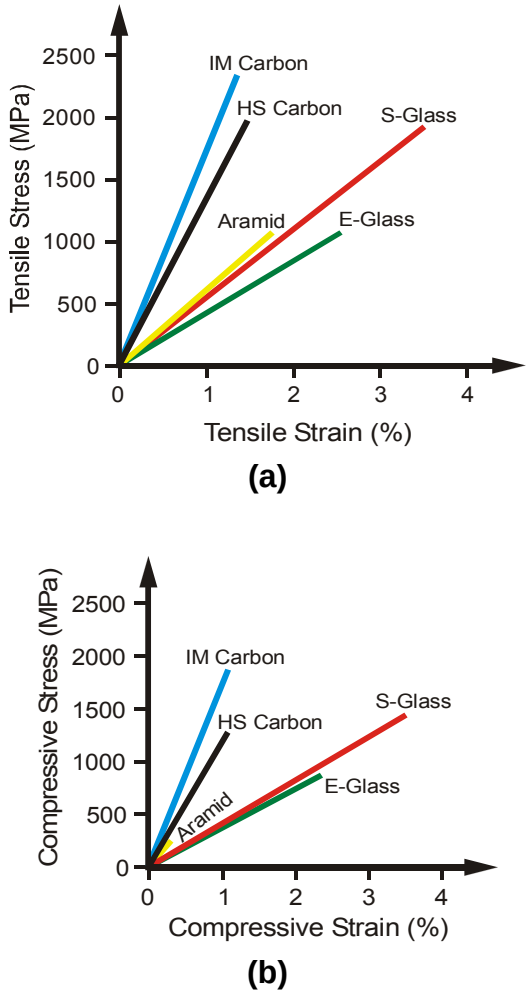

Figure 4.3: Laminate mechanical properties: Tensile Stress (a); Compressive Stress (b)

Figure 4.3 shows also the strengths and maximum strains of the different composites at failure. The gradient of each graph also indicates the stiffness (modulus) of the composite; the steeper the gradient, the higher its stiffness. The graphs also show how some fibres, such as aramid,

display very different properties when loaded in compression, compared with loading in tension.
When looking for advantages and disadvantage of the above different strengthening materials, one finds that the E-Glass is the most suitable material for repair and/or strengthening of the masonry. It is also used for this purpose in this work.

4.2 Anchorage Strength Models for FRP and Steel Plates bonded to Concrete Blocks

The most common failure mode with anchorage is due to crack propagation parallel to the bonded plate in the blocks a few millimetres beneath the block/adhesive interface due to exceeding the lateral tension strength of the blocks, starting from the critically stressed position toward the anchored end of the plate. Interfacial failure between the adhesive and the blocks or between the adhesive and the GFRP-sheets is not found. This is a consequence of the availability of strong adhesives that bond well to GFRP and blocks. For the same reason, adhesive failure is rare.

Several techniques for the strengthening of masonry structures using advanced composite have been proposed but, recently, two kinds of reinforcement have emerged: The embedding of rods into grooves to the surface (near-surface mounted FRP rods) and bonding of composite laminates to the surface of the masonry.

Experimental tests on masonry elements have been carried out to evaluate the effectiveness of both strengthening techniques [116], [209], [41], [210], [65], and [39].
Creazza [39] analysed the mechanical behaviour of some masonry structures reinforced by FRP numerically by using a two-parameter, scalar, isotropic, damage model to represent the masonry, considered as an homogeneous material, and an elastic constitutive law for the FRP material.
Luciano [116] proposed a simple homogenisation technique, which allows for computing the strain in the mortar, block and FRP.

Experiments have been carried out using several set-ups, including single shear tests [29]; [16], [17]; [204], double shear tests [213], [203]; [96]; [66]; [23];[68], [118]; [148] (as shown in Figure 4.4) and modified beam tests [213]; [226].
Theoretical work has included both fracture mechanics analysis [211]; [82]; [204]; [220; [221] and the development of models based on experimental data and/ or simplistic assumptions [213]; [28]; [92].

4.2.1 Failure Modes

In theory, for an FRP or steel plate bonded to concrete, for single or double shear tests there are six possible distinct failure modes. These are listed below in the order of their likeliness, based on existing test data collected in Table 4.2

- Concrete failure
- Plate tensile failure including FRP rupture or steel yielding
- Adhesive failure
- FRP delaminating for FRP-to-concrete joints
- Concrete-to-adhesive interfacial failure
- Plate-to-adhesive interfacial failure

The data in Table 4.2 show that most experimental joints failed in the concrete a few millimetres beneath the concrete/adhesive interface [213]; [118]. Interfacial failure, between either the adhesive and the concrete or the adhesive and the plate, is not found in Table 4.2. This is a consequence of the availability of strong adhesives that bond well to steel, FRP and concrete. For the same reason, adhesive failure is rare. A small number of specimens failed by FRP rupture and an equal number of specimens failed by FRP delaminating. This work is primarily concerned with concrete failure beneath the plate-to-concrete interface.
Neubauer and Rostasy [148] showed that the same energy release rate model is applicable to both the concrete fracture failure mode and the FRP delaminating failure mode. This is because, even in the FRP delaminating failure mode, concrete failure usually occurs in the first 20-50% of the bond length. This is the key failure process and predominates the fracture energy realse rate. Cracking then extends into the FRP

matrix, leading to FRP delamination. Therefore, the developed model in this work is applicable to the masonry/concrete failure beneath the GFRP/CFRP-sheet-to-masonry/concrete interface and GFRP/CFRP delaminating failures, where the other failure modes are rare.

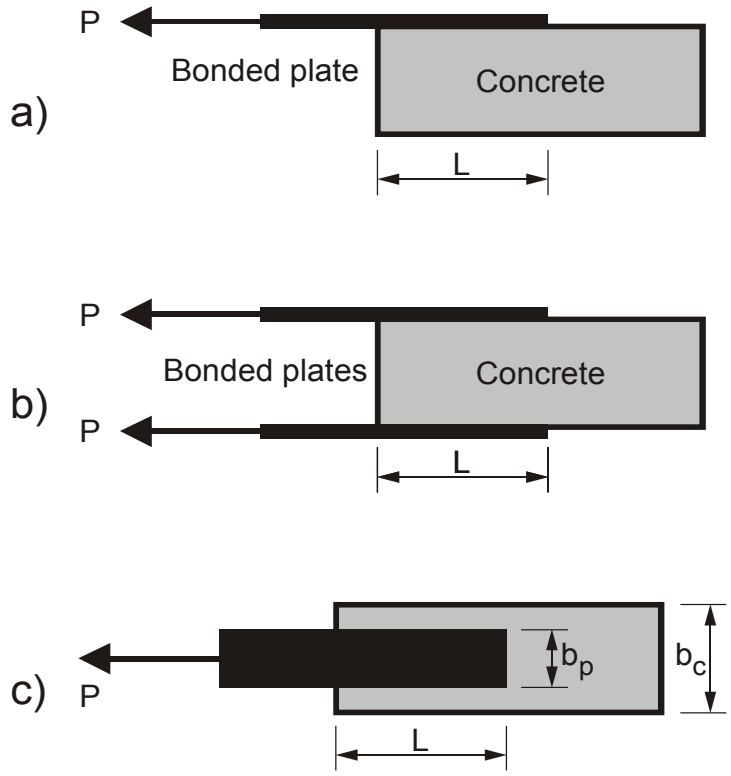

Figure 4.4: Shear tests,
(a) Single shear test; (b) Double shear test; (c) Plan

Van Gemert [213] examined the stresses in a steel plate bonded to a rectangular concrete plain concrete prism in a double shear test. The tensile force in the steel plate was found to decay exponentially toward the anchored end of the plate. At higher loads, the distribution of the tensile force became more and more even in the initial bond zone. This means that practically no force was transferred from the plate to the concrete in this zone, because the cracking of the concrete near the applied load shifted the active bond zone to new areas farther away from the loading point. This phenomenon has been confirmed by many other studies on steel-to-concrete bonded joints [204] and FRP-to-concrete bonded joints [118]. The shift of the active bond zone means that at any one time, only part of the bond is effective. That is, as cracking in the concrete propagates, bond resistance is gradually lost in the zone near the load, but, in the meantime, it is activated farther away from the load.

The implication is, then, that the anchorage strength cannot always increase with an increase in the bond length, and that the ultimate tensile strength of a plate may never be reached, however long the bond length is.

		Concrete					Plate							
Specimen reference number	Adhesive E_a (MPa)	Width b_c (mm)	Thickness t_c (mm)	Compressive strength f'_c (MPa)	Young's modulus E_c (MPa)	Tensile strength f_{ct} (MPa)	Type	Thickness t_p (mm)	Width B_p (mm)	Bond length L (mm)	Young's modulus E_p (MPa)	Ultimate strength f_{up} (MPa)	Measured failure load P_u (N)	Failure mode
BN1	3,304	150	150	42.5	33,500	3.50	GFRP	1	25.4	180	29,200	472	11,410	FR
BN2	3,304	150	150	42.5	33,500	3.50	GFRP	2	25.4	320	29,200	472	21,400	FR
BN3	3,257	150	150	42.5	33,500	3.50	CFRP	0.33	25.4	160	75,700	1,014	8,500	FR
BN4	3,257	150	150	42.5	33,500	3.50	CFRP	0.66	25.4	320	75,700	1,014	15,100	FR
C1	5,172	228.6	152.4	36.1	—	—	GFRP	1.016	25.4	76.2	108,478	1,655	8,462	CF
C2	5,172	228.6	152.4	47.1	—	—	GFRP	1.016	25.4	76.2	108,478	1,655	9,931	CF
C3	5,172	228.6	152.4	47.1	—	—	GFRP	1.016	25.4	76.2	108,478	1,655	10,638	CF
C4	5,172	228.6	152.4	47.1	—	—	GFRP	1.016	25.4	76.2	108,478	1,655	10,638	CF
C5	2,207	228.6	152.4	43.6	—	—	GFRP	1.016	25.4	76.2	108,478	1,655	10,531	CF
C6	234	228.6	152.4	43.6	—	—	GFRP	1.016	25.4	76.2	108,478	1,655	8,956	AF
C7	234	228.6	152.4	43.6	—	—	GFRP	1.016	25.4	76.2	108,478	1,655	9,610	CF
C8	1,584	228.6	152.4	43.6	—	—	GFRP	1.016	25.4	76.2	108,478	1,655	10,518	CF
C9	1,584	228.6	152.4	43.6	—	—	GFRP	1.016	25.4	76.2	108,478	1,655	11,199	CF
C10	1,584	228.6	152.4	24.0	—	—	GFRP	1.016	25.4	76.2	108,478	1,655	9,869	CF
C11	1,584	228.6	152.4	28.9	—	—	GFRP	1.016	25.4	76.2	108,478	1,655	9,343	CF
C12	1,584	228.6	152.4	43.7	—	—	GFRP	1.016	25.4	76.2	108,478	1,655	11,204	CF
C13	1,584	228.6	152.4	36.4	—	—	GFRP	1.016	25.4	50.8	108,478	1,655	8,094	CF
C14	1,584	228.6	152.4	36.4	—	—	GFRP	1.016	25.4	101.6	108,478	1,655	12,811	CF
C15	1,584	152.4	152.4	36.4	—	—	GFRP	1.016	25.4	152.4	108,478	1,655	11,917	CF
C16	1,584	152.4	152.4	36.4	—	—	GFRP	1.016	25.4	203.2	108,478	1,655	11,570	CF
M1	5,000	100	100	40.8	—	—	CFS	0.11	50	75	230,000	3,500	5,800	FD
M2	5,000	100	100	40.8	—	—	CFS	0.11	50	150	230,000	3,500	9,200	FD
M3	5,000	100	100	43.3	—	—	CFS	0.11	50	300	230,000	3,500	11,950	FD
M4	5,000	100	100	42.4	—	—	CFS	0.165	50	75	380,000	3,000	10,000	CF
M5	5,000	100	100	42.4	—	—	CFS	0.165	50	150	380,000	3,000	7,300	FR
M6	5,000	100	100	42.7	—	—	CFS	0.22	50	65	230,000	3,500	9,550	CF
M7	5,000	100	100	42.7	—	—	CFS	0.22	50	150	230,000	3,500	16,250	FD
M8	5,000	100	100	44.7	—	—	CFS	0.11	50	700	230,000	3,500	10,000	FD
C100 50A	6,700	200	200	—	35,000	3.90	CFRP	1.25	50	100	170,000	2,497	17,300	CF
C200 50A	6,700	200	200	—	35,000	4.10	CFRP	1.25	50	200	170,000	2,497	27,500	CF
C300 50A	6,700	200	200	—	35,000	4.30	CFRP	1.25	50	300	170,000	2,497	35,100	CF
C400 50A	6,700	200	200	—	35,000	4.30	CFRP	1.25	50	400	170,000	2,497	26,900	CF
S100 40A	6,700	200	200	—	35,000	4.20	Steel	2.9	40	100	205,000	399	21,100	CF
S200 40A	6,700	200	200	—	35,000	3.90	Steel	2.9	40	200	205,000	399	39,500	CF
S400 40A	6,700	200	200	—	35,000	4.30	Steel	2.9	40	400	205,000	399	41,100	CF
S50 60A	6,700	200	200	—	35,000	4.20	Steel	2.9	60	50	205,000	403	12,700	CF
S100 60A	6,700	200	200	—	35,000	4.10	Steel	2.9	60	100	205,000	399	20,000	CF
S150 60A	6,700	200	200	—	35,000	4.30	Steel	2.9	60	150	205,000	403	46,300	CF
S200 60B	6,700	200	200	—	35,000	4.10	Steel	2.9	60	200	205,000	399	48,800	CF
S400 60A	6,700	200	200	—	35,000	4.30	Steel	2.9	60	400	205,000	403	58,400	CF
S400 60B	6,700	200	200	—	35,000	4.10	Steel	2.9	60	400	205,000	399	53,000	CF
S100 80C	6,700	200	200	—	35,000	4.40	Steel	2.9	80	100	205,000	403	39,600	CF
S150 80A	6,700	200	200	—	35,000	3.90	Steel	2.9	80	150	205,000	403	50,900	CF
S200 80A	6,700	200	200	—	35,000	4.30	Steel	2.9	80	200	205,000	403	67,300	CF
S300 80C	6,700	200	200	—	35,000	4.10	Steel	2.9	80	300	205,000	403	68,000	CF
S500 80C	6,700	200	200	—	35,000	4.40	Steel	2.9	80	500	205,000	399	67,300	CF
S600 80B	6,700	200	200	—	35,000	4.10	Steel	2.9	80	600	205,000	403	71,400	CF
S800 80A	6,700	200	200	—	35,000	4.10	Steel	2.9	80	800	205,000	403	61,600	CF
S1	430–2,000	60	60	19.8	—	—	Steel	3	60	150	200,000	365–400	19,530	CF
S2	430–2,000	60	60	35.5	—	—	Steel	3	60	150	200,000	365–400	22,680	CF
S3	430–2,000	60	60	47.6	—	—	Steel	3	60	150	200,000	365–400	24,930	CF
S4	430–2,000	60	60	56.3	—	—	Steel	3	60	150	200,000	365–400	29,970	CF
S5	430–2,000	60	60	35.6	—	—	Steel	3	60	150	200,000	365–400	21,780	CF
S6	430–2,000	60	60	35.6	—	—	Steel	3	60	150	200,000	365–400	21,420	CF
S7	430–2,000	60	60	35.6	—	—	Steel	3	60	150	200,000	365–400	25,470	CF

Specimens:
BN1-BN4 are from Bizindavyi and Neal (1999);
A1-A5 and B1-B5 are from Brosens and van Gemert (1997);
C1-C16 are from Chajes et al. (1996);
M1-M8 are from Maeda et al. (1997);
C100-C400 and S100-S800 are from Täljsten (1997);
S1-S7 are from Swamy et al. (1986);
Failure Mode: FR=FRP rupture; CF=Concrete fracture;
FD=FRP delimination; AF=Cohesive failure through the adhesive

Table 4.2: Literature review for the single and double shear test data

This leads to the important concept of effective bond length, beyond which any increase in the bond length cannot increase the anchorage strength, as confirmed by many experimental studies [29]; [118]; [204] and fracture mechanics analyses [82]; [221]; [220]. However, a longer

bond length may improve the ductility of the failure process. This phenomenon is believed to be the primary reason for the observed low stresses in bonded plate at anchorage failure (see Figure 4.5). The average ultimate in FRP at failure is 28% of the ultimate tensile strength and, for steel-to-concrete, is 71%.

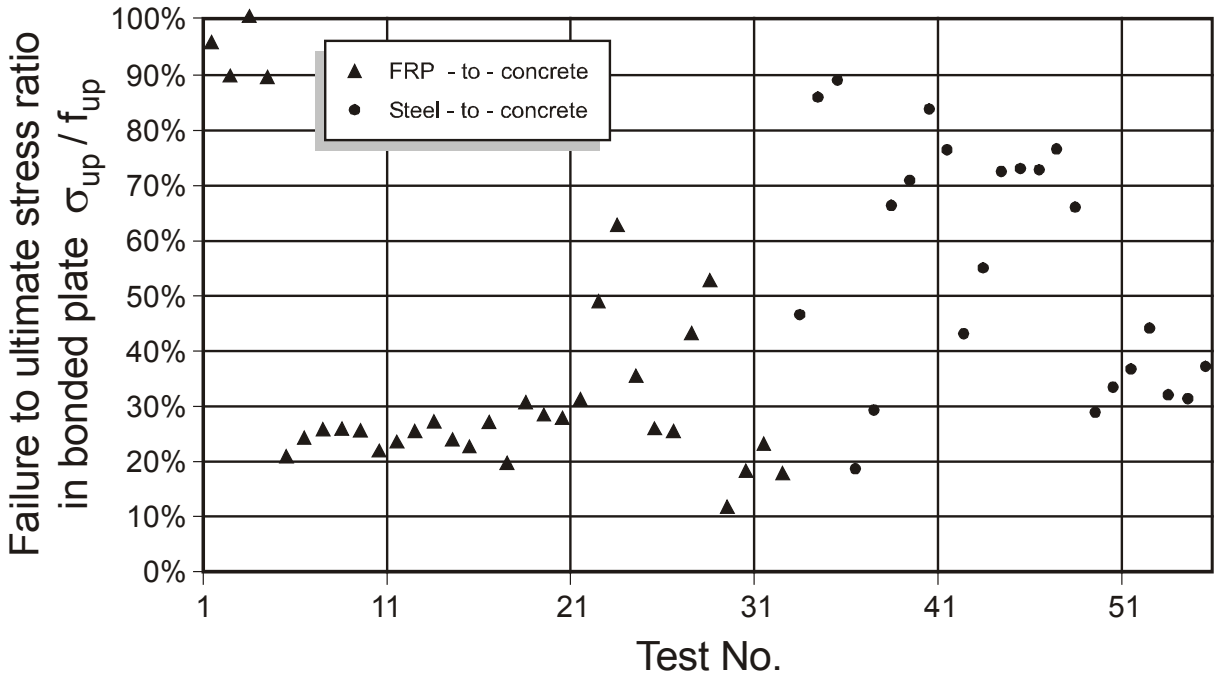

Figure 4.5: Maximum plate stress at bond failure

4.2.2 Existing Shear Anchorage Strength Models

A review of the models, which have been developed in the last few years, is presented below. These models may be classified into three categories: empirical models based on the test data, fracture mechanics models, and design proposals that generally make use of some simple assumptions.

4.2.3 Empirical Models

A set of double shear experiments on carbon fibre sheets (CFS) strengthened RC members are made by Hiroyuki and Wu [81], they derived the following empirical relationship between the bond length, L (cm) and the average bond shear stress at failure, τ_u

$$\tau_u = 5.88L^{-0.669} \quad (MPa) \tag{4.1}$$

Tanaka [206] presented another simple expression [186] as

$$\tau_u = 6.13 - \ln L \quad (MPa) \tag{4.2}$$

where L is measured in millimetres. The ultimate bond load of the joint P_u is given by multiplying τ_u by the width b_p and the length L of the bond area in the above two models.
Maeda et al. [118] developed a more robust model that considers the effective bond length as

$$\tau_u = 110.2 \times 10^{-6} E_p t_p \quad (MPa) \tag{4.3}$$

where $t_p(mm)$ and $E_p(MPa)$, are the thickness and Young's modulus of the bonded plate, respectively.

The ultimate bond load P_u is obtained by multiplying τ_u by the width b_p and the effective bond length L_e. Here, the effective bond length is given by

$$L_e = e^{6.13 - 0.580 \ln E_p t_p} \tag{4.4}$$

Note that E_p is in gigapascals and t_p is in millimetres in (4.4). This model is obviously invalid if $L \langle L_e$.

4.2.4 Fracture Mechanics-Based Models

The bond strength between a steel plate and concrete is investigated by using the non-linear fracture mechanics (NLFM) of Holzenkämpfer [82]. Niedermeier [152] and Blaschko et al. [18] developed a modified form, which calculates the bond strength by using

$$P_u = \begin{cases} 0.78 b_p \sqrt{2 G_f E_p t_p} & \text{if } L \geq L_e \\ 0.78 b_b \sqrt{2 G_f E_p t_p}\, \dfrac{L}{L_e}\left(2 - \dfrac{L}{L_e}\right) & \text{if } L \langle L_e \end{cases} \tag{4.5}$$

where the fracture energy G_f and the effective bond length L_e are given by

$$G_f = c_f k_p^2 f_{ctm} \quad (N.mm/mm^2); L_e = \sqrt{\frac{E_p t_p}{4 f_{ctm}}} \quad mm \tag{4.6}$$

where $f_{ctm}(MPa)$ is average surface tensile strength of the concrete determined in a pull-off test according to DIN1048 [42], c_f is a constant determined in a linear regression analysis using the results of double shear or similar tests; and k_p is geometrical factor related to the width of the bonded plate b_p and the width of the concrete member b_c

$$k_p = \sqrt{1.125 \frac{2 - b_p / b_c}{1 + b_p / 400}} \tag{4.7}$$

Täljsten [205] also developed a similar model using an NLFM analysis

$$P_u = \sqrt{\frac{2 E_p t_p G_f}{1 + \alpha_T}}\, b_p \tag{4.8}$$

where

$$\alpha_T = \frac{E_p t_p}{E_c t_c} \tag{4.9}$$

Yuan and Wu [221] and Yuan et al. [220] studied the bond strength between FRPs and concrete using linear elastic fracture mechanics (LEFM) and (NLFM). Their LEFM investigation resulted in the same equation as (4.8), but included the effect of widths of the plate and concrete member, i.e., α_T in (4.8) is replaced by

$$\alpha_Y = \frac{b_p E_p t_p}{b_c E_c t_c} \tag{4.10}$$

The non-linear equations for five different shear stress-slip relationships (see Figure 4.6) are also solved by them. The linearly-ascending and then descending relationship (see Figure.4.6(d)) may be closest to reality. The maximum load carrying capacity for this is [220].

$$P_u = \frac{\tau_f b_p}{\lambda_2}\frac{\delta_f}{\delta_f - \delta_1}\sin(\lambda_2 a) \tag{4.11}$$

where a is obtained by solving

$$\tanh[\lambda_1(L-a)] = \frac{\lambda_2}{\lambda_1}\tan(\lambda_2 a) \tag{4.12}$$

where τ_f is the maximum stress on the shear-slip curve of the bond; δ_1 its corresponding slip; δ_f is the maximum slip; and λ_1 and λ_2 are given by

$$\lambda_1^2 = \frac{\tau_f}{\delta_1 E_p t_p}(1+\alpha_Y) \text{ and } \lambda_2^2 = \frac{\tau_f}{(\delta_f - \delta_1)E_p t_p}(1+\alpha_Y) \tag{4.13}$$

Yuan et al. [220] define the effective bond length, as the value corresponding to 97% of the load carrying capacity if L is infinite. This gives

$$L_e = a_0 + \frac{1}{2\lambda_1}\ln\frac{\lambda_1 + \lambda_2\tan(\lambda_2 a_0)}{\lambda_1 - \lambda_2\tan(\lambda_2 a_0)} \tag{4.14}$$

where

$$a_0 = \frac{1}{\lambda_2}\sin^{-1}\left(0.97\sqrt{\frac{\delta_f - \delta_1}{\delta_f}}\right) \tag{4.15}$$

Nuebauer and Rostasy [148] made a series of double shear tests on carbon fibre reinforced polymer (CFRP)-to-concrete bonded joints. They concluded that, for both concrete fractures failure and FRP delaminating failure, the shear-slip relationship may be represented by a triangular, model as shown in Figure 4.6(d)). The fracture energy could be calculated by

$$G_f = c_f f_{ctm} \tag{4.16}$$

where f_{ctm} is the tensile strength of concrete. They reported an average value of 0.204 mm with a standard deviation of 0.053 for c_f for 51 specimens. They presented a modified form of Holzenkämpfer's [82] model, which can be applied to both CFRP and steel plates.

$$P_u = \begin{cases} 0.64 k_p b_p \sqrt{E_p t_p f_{ctm}} & \text{if } L \geq L_e \\ 0.64 k_p b_b \sqrt{E_p t_p f_{ctm}} \dfrac{L}{L_e}\left(2 - \dfrac{L}{L_e}\right) & \text{if } L < L_e \end{cases} \tag{4.17}$$

$$L_e = \sqrt{\frac{E_p t_p}{2 f_{ctm}}} \tag{4.18}$$

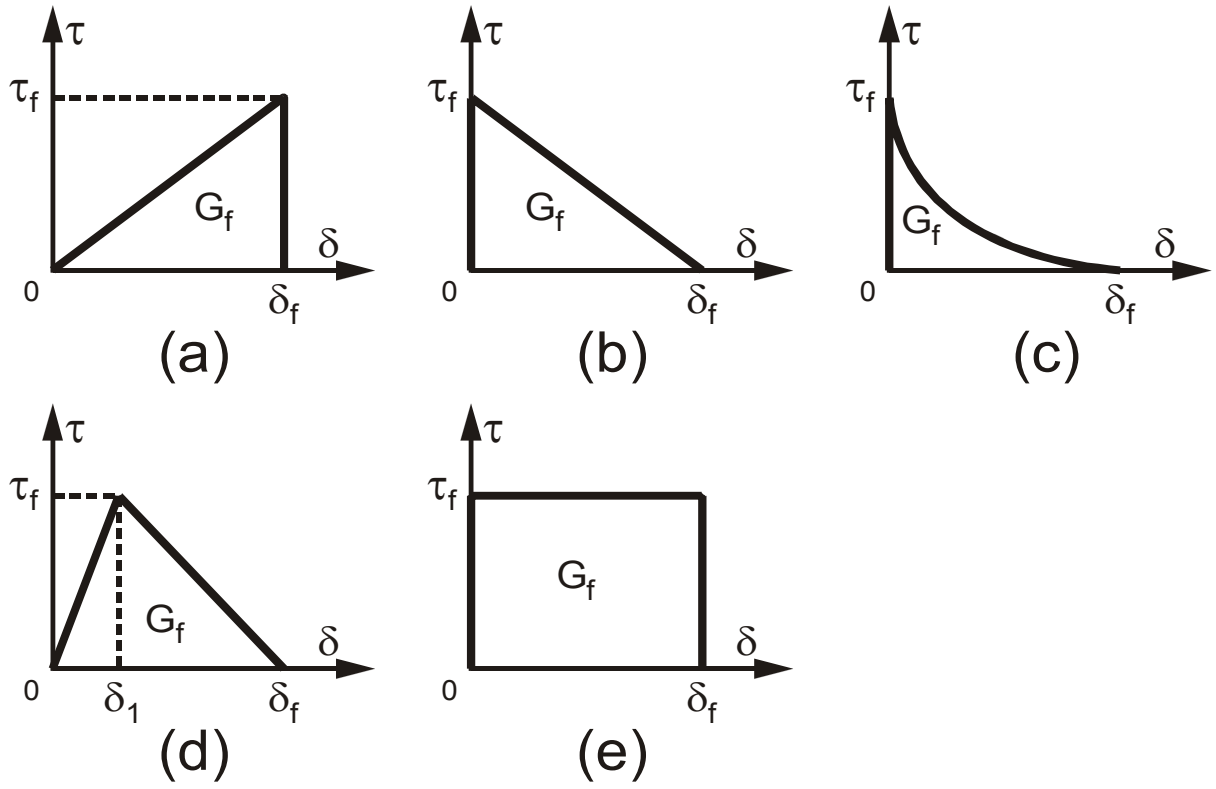

Figure 4.6: Shear-slip models for plates to concrete bonded joints [221]

4.2.5 Design Proposals

Van Gemert [213] proposed a design rule [23] by assuming a triangular shear stress distribution (see Figure 4.6(d)) as

$$P_u = 0.5 b_p L f_{ctm} \tag{4.19}$$

In (4.19) the only material parameter is the concrete surface tensile strength f_{ctm}.(4.19) does not take into account the strength reserve after

first cracking, where it gives the load at the cracking of the concrete in the initial force transfer zone. This interpretation is invalid, because the limit of the effective bond length is not included in (4.19). The equation implies that the full tensile strength of the bonded plate can be reached by using a sufficiently long bonded joint. This, conceptually, is misleading, as it contradicts the well-established fact that any additional bond length beyond the effective bond length cannot increase the anchorage strength.

Based on studies by Roberts [182] and Varastehpour and Hamelin [214], Chaallal et al.[28] proposed a design model, in which the bond behaves as a Mohr-Coulomb material. They assumed that the maximum shear stress is twice the average stress τ_{avg} and the maximum shear stress does not exceed the Mohr-Coulomb strength equation given by Varastehpour and Hamelin [214]. This leads to

$$\tau_{avg} = \frac{\tau_{\max}^{debonding}}{2} = \frac{2.7}{1 + k_1 \tan 33^0} \tag{4.20}$$

where

$$k_1 = t_p \sqrt[4]{\frac{k_a}{4E_p I_p}} \text{ and } k_a = E_a \frac{b_a}{t_a} \tag{4.21}$$

where b_a, t_a, and E_a are the width, thickness and Young's modulus of the adhesive, respectively; and I_p is the moment of inertia of the FRP plate.

As (4.21) was based on limited experimental data and does not relate to the strength of concrete, its applicability is seriously limited. Another disadvantage of this model is that the effective bond length is not considered.

Khalifa et al. [92] proposed a modification of Maeda et al.'s [118] model, (4.3) and included the effect of concrete strength, so that it can be used for design. They used the relationship that the bond strength between the FRP sheet and the concrete surface is a function of $(f_c)^{2/3}$ [83]. Because the concrete strength was 42 MPa in the experiments carried out by Maeda et al. [118], the modified equation is given by

$$\tau_u = \frac{110.2}{10^6}\left(\frac{f_c'}{42}\right)^{2/3} E_p t_p \qquad (4.22)$$

The effective bond length is calculated using (4.4).

Neubauer and Rostasy [148] proposed to use 75% of the ultimate bond strength for design, to reduce the factor 0.64 in (4.17) to 0.5.

Source	FRP-to-concrete			Steel-to-concrete			Both FRP and steel-to-concrete		
	Average	SD	COV	Average	SD	COV	Average	SD	COV
Hiroyuki and Wu [83] (4.1)	2.87	0.95	33%	3.85	1.18	31%	3.24	1.09	34%
Tanaka [206] (4.2)	2.92	1.65	56%	5.51	5.30	96%	4.02	3.96	99%
Van Gemert [213] (4.19)	2.19	1.12	51%	1.64	0.57	35%	1.91	0.96	50%
Chaallal et al. [28] (4.20)	1.81	0.89	49%	1.68	0.70	42%	1.71	0.79	46%
Khalifa et al. [92] (4.22)	1.07	0.24	23%	0.76	0.26	34%	0.93	0.29	31%
Neubauer and Rostasy [148] (4.17)	0.82	0.15	18%	0.65	0.09	13%	0.74	0.15	20%
(4.27)	1.05	0.18	17%	0.94	0.11	12%	1.0	0.16	16%
Note: SD=standard deviation; COV= coefficient of variation									

Table 4.3: Experimented to predicted bond strength ratios

4.3 Comparison with Experimental

Table 4.3 compares the performance of some of the above models in predicting the experimental bond strengths given in Table 4.2 (20 FRP and 23 steel bond tests) after excluding those failing by FRP rupture. The models, based on the pure fracture mechanics, are excluded in this comparison due to the unavailability of the fracture energy and the shear-slip parameters. The first four models in Table 4.3 clearly do not fit with the experimental data statistically. They hugely underestimate the

bond strength and lead to very large scatter. The main reason for the poor performance of these models is that the effective bond length is not considered. A reasonable performance shown in the models of Khalifa et. al [92] and Neubauer and Rostasy [148]. Khalifa et al.'s [92] proposal based on the model proposed by Maeda et al. [118] from the regression of test data of FRP-to-concrete joints. As a result, it agrees reasonably well with experimental data for FRP-to-concrete joints, but not so well for steel-to-concrete joints. The main disadvantage of this model is that it greatly overestimates the shear stress at failure and underestimates the effective bond length. For example, (4.22) predicts an average shear stress at failure of about $60\,MPa$ and (4.4) predicts an effective bond length of about $11mm$ for the set of steel –to-concrete joints reported by Täljsten [204], compared with an observed effective bond length of about 300mm. Thus, it cannot be used safely in practical design.

In their models, Holzenkämpfer [82] and Neubauer and Rostasy [148] used the concrete surface tensile strength f_{ctm}. As this strength is not readily available, the splitting tensile strength f_{ct} can be used instead. it is estimated from f_c' (MPa) [117] as

$$f_{ct} = 0.53\sqrt{f_c'} \tag{4.23}$$

From Table 4.3, Neubauer and Rostasy's model [148] had the experimental results 0.82 of those predicted on average for FRPs. This means that the calculations are (1-0.82)/0.82=22% greater than the experiments, on average. For steel plates, on average, the ratio of the experiments to the calculated results is 0.65, i.e., the calculated results are 55% higher than the experiments. For both the FRP and steel experiments, in Neubauer and Rostasy's model, the calculated results are 35% higher than experiments on average. In this model, the use of surface tensile strength is disadvantage, because this strength is not available and requires special tests. The compressive strength is available in most cases.

4.4 New Model by J.F. Chen

As the above-described models showed many disadvantages and deficiency, it is necessary to develop a new model, which is capable of capturing the features of the bond behaviour and of predicting the bond length and the bond strength with good accuracy.
Yuan and Wu [221] developed this new model using the $\tau - \delta$ behaviour, which is shown in Figure 4.6(d), based on NLFM solution

$$P_u = \begin{cases} \dfrac{\tau_f b_p}{\lambda} & \text{if } L \geq L_e \\ \dfrac{\tau_f b_p}{\lambda} \sin(\lambda L) & \text{if } L < L_e \end{cases} \tag{4.24}$$

where

$$L_e = \frac{\pi}{2\lambda} \text{ and } \lambda^2 = \frac{\tau_f}{\delta_f E_p t_p}(1+\alpha_Y) \tag{4.25}$$

(4.6), (4.16), (4.19), and (4.22) are related to the concrete surface tensile strength. However, various experiments [29] showed that the ultimate bond strength is proportional to $\sqrt{f_c'}$ similar to the bond of internal steel [22] and FRP reinforcement [60]. This is also approved by the regression analysis of the experimental results in Table 4.2.
The regression of the tests data of Table 4.2, which is presented in Figure 4.7, shows that the ultimate bond strength is linear to β_p, where

$$\beta_p = \sqrt{\frac{2 - b_p / b_c}{1 + b_p / b_c}} \tag{4.26}$$

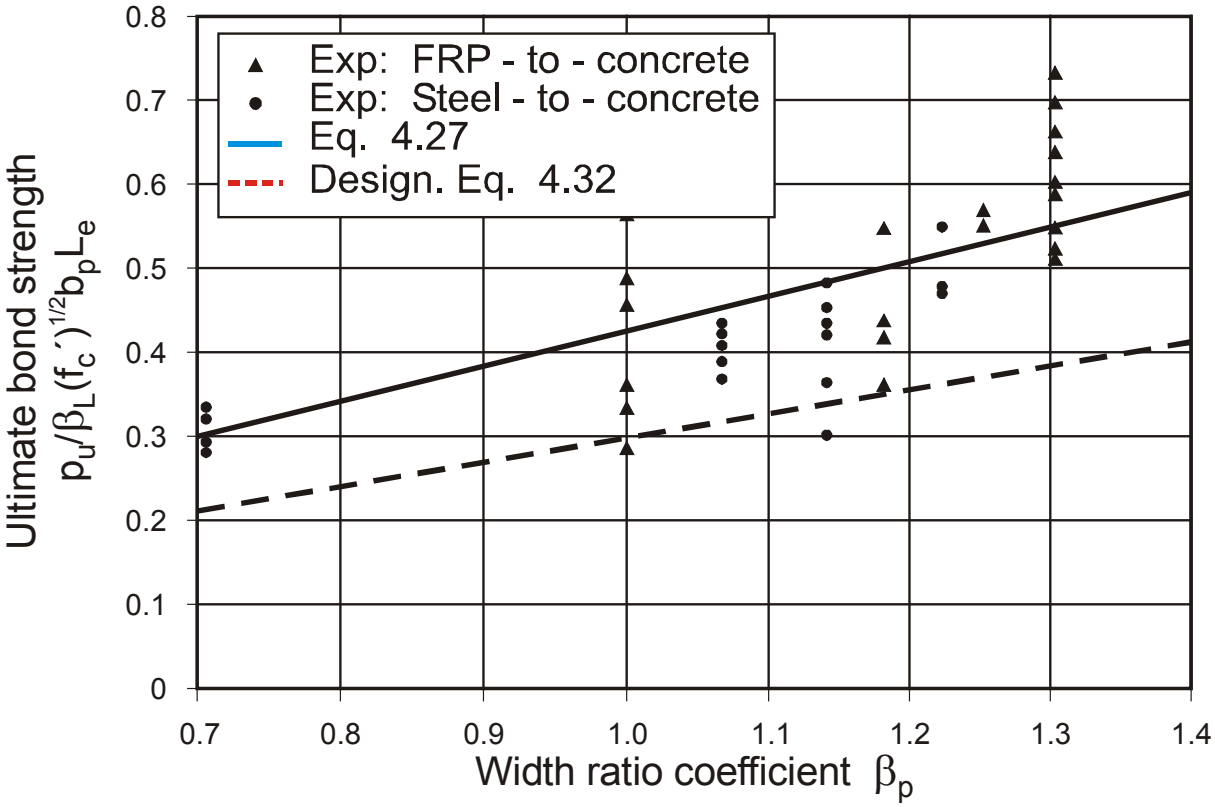

Figure 4.7: Bonded plate to concrete width ratio effect on the ultimate bond strength

Based on (4.24), the regression test data in Table 4.2 and taken into consideration the above considerations, a simple ultimate bond strength model may be proposed

$$P_u = 0.427\beta_p\beta_L\sqrt{f_c'}\,b_pL_e \tag{4.27}$$

where

$$L_e = \sqrt{\frac{E_p t_p}{\sqrt{f_c'}}} \tag{4.28}$$

$$\beta_L = \begin{cases} 1 & \text{if } L \geq L_e \\ \sin\dfrac{\pi L}{2Le} & \text{if } L < L_e \end{cases} \tag{4.29}$$

In (4.27) the units are megapascals and millimetres.

This new model uses the cylinder concrete compressive strength f_c', which is available in most cases. Thus, this model is more suitable for practical applications. To have a comparison of this model with the experimental tests in Table 4.2, it is necessary to convert the concrete

split tensile strength f_{ct} for the experimental results of Täjsten [204]. This is achieved by first calculating f_c' from f_{ct} by using (4.23) and then scaling the results by multiplying all of the f_c' values obtained from f_{ct} by a single factor. This is done so that the average Young's modulus E_c found by using the American concrete Institute [5] relationship $E_c = 5730\sqrt{f_c'}$ is $3.5 GPa$, as given by Täljsten [204].

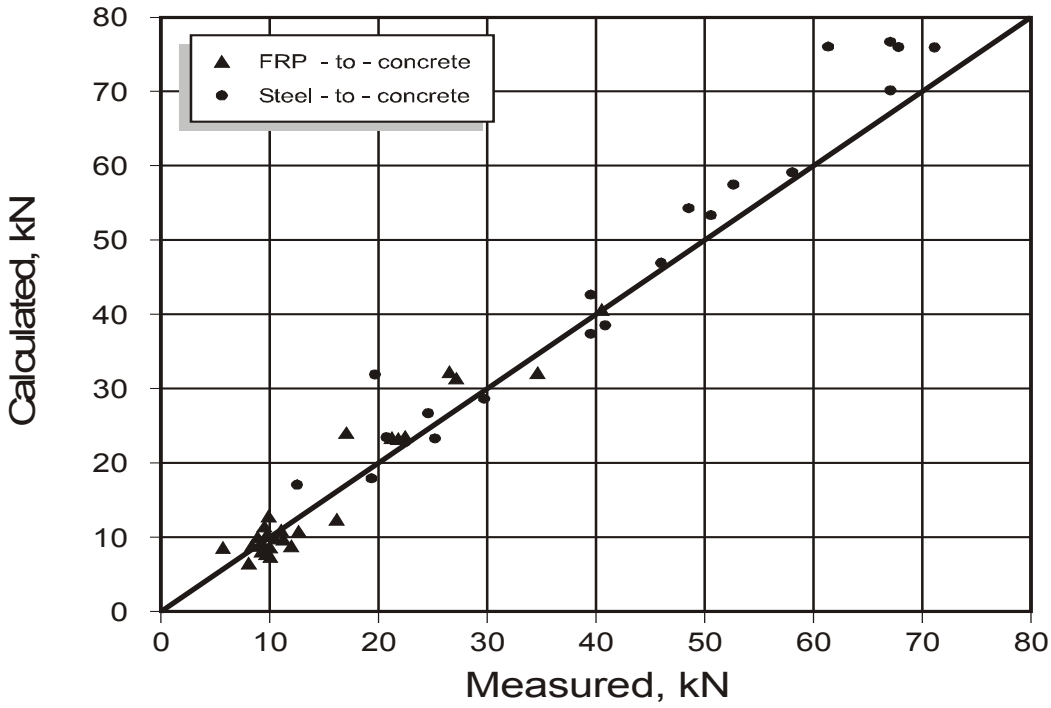

Figure 4.8: Experimental versus Calculated values

In Table 4.3 it is shown that (4.27) agrees well with the test data for both FRP-to-concrete and steel-to-concrete bonded joints. The ratio of the experimental results to the calculated for the two types of joints has an overall average value of 1.0 and a corresponding standard deviation of 0.159 (see Figure 4.8).

L_e Increases linearly with $\sqrt{E_p t_p}$ as shown in (4.28).

The values calculated for the effective bond length for this model are in close agreement with the experimental results (see Table 4.4). The comparison in Figure 4.9 shows that the empirical model proposed by Maeda et al. [118] predicted the wrong trend on the effect of $E_p t_p$ on the effective bond length.

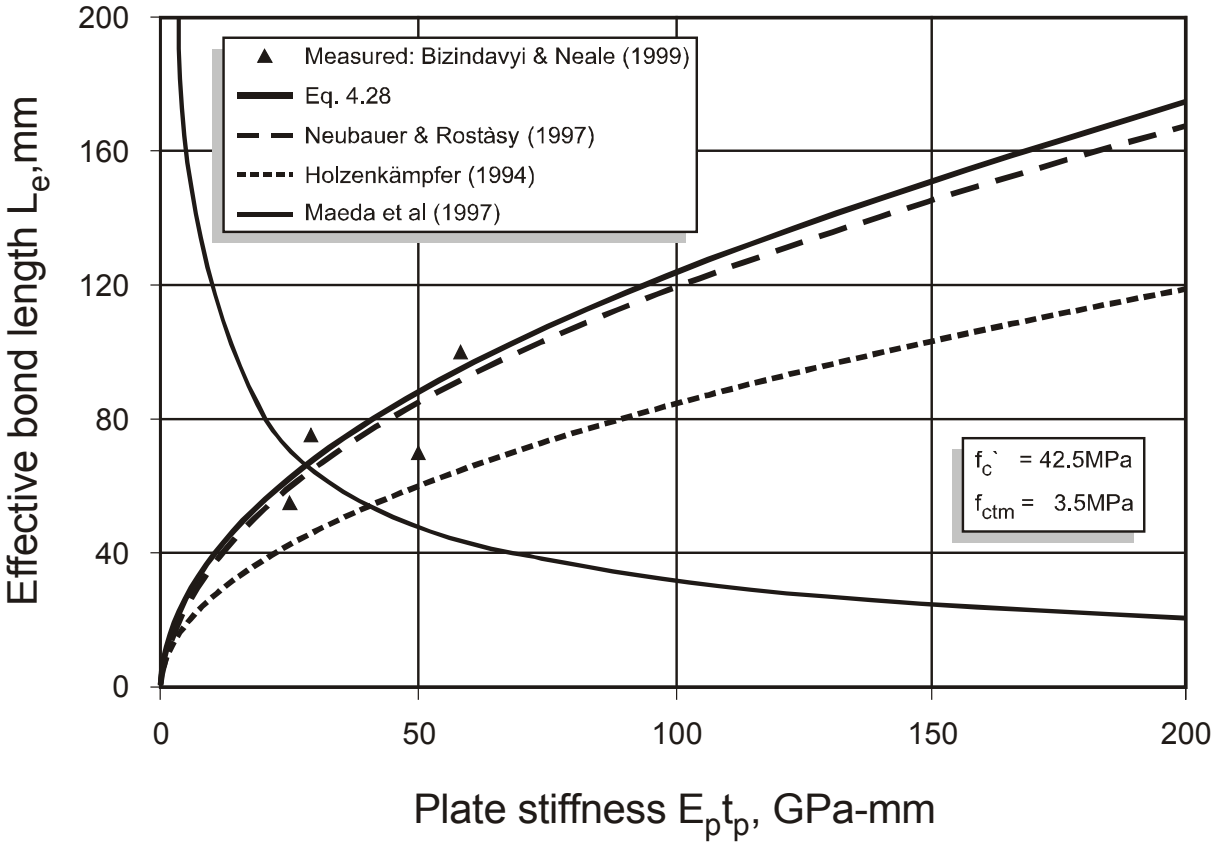

Figure 4.9: Bonded plate stiffness on the effective bond length

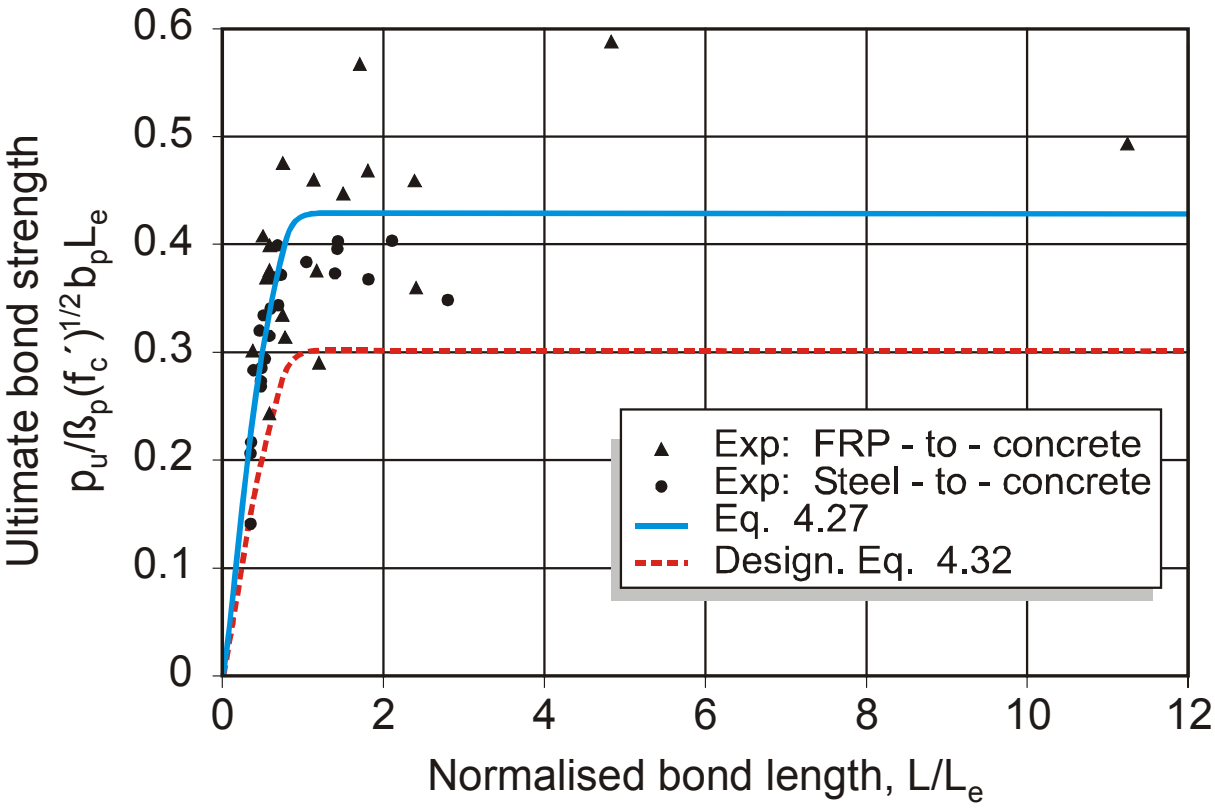

Figure 4.10: Bonded length effect on the ultimate bond strength

Data source	Test specimen (Table 2.3)	Experimented	Prediction			Chen (2001)/ experimented
			Kalifa et al. (1998)	Neubauer and Rostasy (1997)	Chen (2001)	
Bizindavyi and Neale (1999)	BN1 (GFRP)	75	65.1	64.4	66.9	0.89
Bizindavyi and Neale (1999)	BN2 (GFRP)	100	43.6	91.3	94.6	0.95
Bizindavyi and Neale (1999)	BN3 (GFRP)	55	71.3	59.7	61.9	1.13
Bizindavyi and Neale (1999)	BN4 (CFRP)	70	47.7	84.5	87.5	1.25
Täljsten (1997)	S100-40A to S800-80A (steel)	~300	11.3	260-280	275-293	0.94

Table 4.4: Effective bond length L_e (mm)

The effect of the bond length on the ultimate bond strength is shown in Figure 4.10. The experimental data are closely scattered around the curve predicted by (4.27), which shows the importance of the concept of the effective bond length.

4.4.1 Stress in Bonded Plate

To have the stress in the bonded plate, substitute (4.28) and $\sigma_p = P_u / b_p t_p$ into (4.27) which leads to

$$\sigma_p = 0.427\beta_p\beta_L\sqrt{\frac{E_p\sqrt{f_c'}}{t_p}} \tag{4.30}$$

As is shown in (4.30), to have high bond stress in the bonded plate, one can use plates with high Young's modulus and small thickness (where the concrete strength can hardly be changed in the strengthening works). The ratio of the stress in the plate at bond failure to the plate tensile strength can be

$$\frac{\sigma_p}{f_p} = \frac{0.427\beta_p\beta_L}{E_p\varepsilon_p}\sqrt{\frac{E_p\sqrt{f_c'}}{t_p}} = \frac{0.427\beta_p\beta_L}{\varepsilon_p}\sqrt{\frac{\sqrt{f_c'}}{E_p t_p}} \tag{4.31}$$

where ε_p is the ultimate strain of FRPs or yield strain of steel plates.

It is clear that, if two materials have similar ultimate strains (such as GFRP and CFRP), a thin plate made of the material with lower elastic modulus should be used in order to best utilize the full tensile strength of the material.

The coefficient in (4.30) can be reduced to the 95th percentile characteristic value of $0.427\times(1-1.64\times 0.159) = 0.315$ to be used for the ultimate strength design, thus

$$\sigma_p = 0.315\beta_p\beta_L\sqrt{\frac{E_p\sqrt{f_c'}}{t_p}} \tag{4.32}$$

Swamy [203] showed that the cracking Strength at the loaded end is about 60% of the ultimate strength. Therefore, the coefficient in (4.32) may be further reduced to $0.315\times 0.6 \approx 0.2$, thus

$$\sigma_p = 0.2\beta_p\beta_L\sqrt{\frac{E_p\sqrt{f_c'}}{t_p}} \tag{4.33}$$

4.5 Constitutive Model for the Analysis of Retrofitting of Masonry

4.5.1 Introduction

The use of the GFRP-laminate on URM-walls enhances the in-plane seismic behaviour of these walls when subjected to cyclic loading.
The GFRP laminates create an engineering wall with stable post peak behaviour as well as providing containment of the hazardous URM damage, preventing catastrophic failure as well as its out-of-plane spalling.
The GFRP prevent both shear and tension cracking by supplying the required tensile strength.
This stability allows the wall to withstand more loads and prevents a sudden drop in the load carrying capacity.

The retrofitting technique helps to repair and strengthen masonry and eliminates the anisotropic behaviour of masonry by eliminating the effects of the shear-compression interaction in the mortar joints [62]. This transforms the anisotropic masonry wall into an orthotropic wall, which simplifies the analytical modelling process. The masonry wall behaves in an orthotropic manner in two principal directions; parallel and perpendicular to the bed joints.
The retrofitting technique using the GFRP, forces the whole wall to act as one unit and allows for the redistribution of forces. Also allows for unstressed areas to pick up load from the overstressed areas, eliminating the diagonal failure mode and reducing the sudden draft associated with such failure. The diagonal crack is resisted by GFRP-laminates.

The object of the retrofitting part of the work is to investigate the bonding of GFRP laminates to URM-walls as a seismic retrofitting scheme, in order to improve the seismic performance of these widely used building systems, by developing the suitable bond strength model.
Using the GFRP-laminates on URM-walls has a great influence on strength, post peak behaviour as well as failure modes. An increase of

90% for compressive strength was achieved using the GFRP-laminates and shear strength increased by fourteen folds [62].

Investigations have shown that for walls subjected to in-plane loads, the shear capacity was notably enhanced when strengthened with FRP-laminates. In addition, the strengthened walls exhibited amore ductile behaviour ([101],[191]).

4.5.2 Anchorage Strength Model for Glass Fiber Reinforced Polymers (GFRP) bonded to Masonry

Based on the thorough study of the shear anchorage behaviour and strength of FRP and steel plates bonded to concrete blocks represented, in the above sections and the experimental results at the Institute of Reinforced Concrete Structures, at the University of Karlsruhe, a bond model for the retrofitted masonry walls can now be presented.

For concrete the main failure mode is in the concrete itself, when it is strengthened with a FRP or steel plate. For the AAC-blocks, the failure also lies in the blocks themselves, at few millimetres beneath concrete/adhesive failure, as shown in Figure 4.11(a) for AAC-blocks strengthened with GFRP-sheets and in Figure 4.11(b) for concrete blocks strengthened with CFRP-sheets, assuming that the bond strength depends strongly on the block strength, in addition to the sheet-to-block member width ratio. The above discussion proved the necessity of the effective bond length in modelling the bond model. Thus, it is necessary, in the bond model for masonry, that the concept of the effective bond length be taken into consideration.

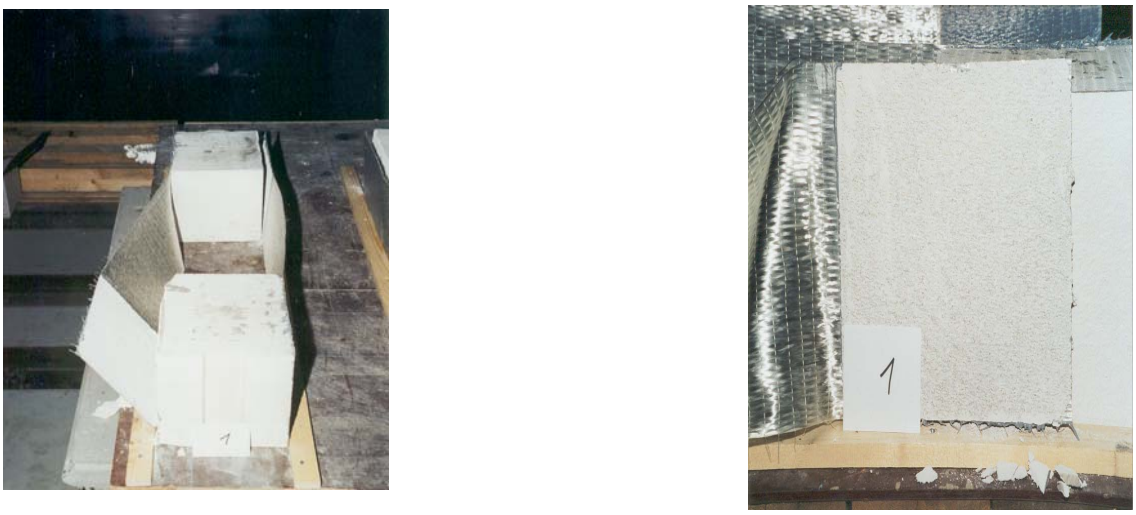

(a)

(b)

Figure 4.11: Failure shape: AAC-blocks strengthened with GFRP-sheet (a); Concrete-blocks strengthened with CFRP-sheet failure shape (b).

Since the deficiencies and disadvantages of the other models are treated by the new model proposed by Chen, J. F. (see section 4.4), then this new model is chosen for the case of retrofitted and repair of masonry using a damage factor (D). The $\tau - \delta$ relationship is taken a triangular. Where, τ is increased linearly until the shearing capacity of GFRP is reached. Then, a descending damage relationship with a damage factor is taken into account. The new anchorage bond model for masonry can correctly predict strength and effective bond length.

The shear wall can be considered as a strut with the effective area, generally ranging between 10-30% of the wall height multiplied by the wall thickness [62]. This was given by

$$A_{strut} = \frac{(1-\alpha_c)\alpha_c h_w t_w}{\cos\theta}; \quad \theta = \tan^{-1}\frac{h_w}{L_w} \tag{4.34}$$

where

h_w = the wall-height

L_w = the wall-length

The parameter α_c represents the ratio between the wall height and the width of the strut in the directions of wall-height and wall-length, whereas

$$\alpha_c h_w \le 0.4 h_w \tag{4.35}$$

A more conservative value of $\alpha_c = 0.28$ is used in this work. Thus, for the retrofitted wall, where $h_w = 2.50\,m$ the diagonal width of the strut is of $1.0\,m$, i.e., twice the width of used GFRP-laminate.

The following are examples, which demonstrate the suitability of the proposed model for the case of masonry. An experiment of FRP bonded to concrete (C9 of Täljsten) from Table4.2 is calculated. For this case, the calculations refer to equations presented in section 4.4 are as follows

L_e=129.2mm

as $L \rangle L_e$ then $\beta_L = 1$

β_p=1.30

σ_p=467.47 (MPa) and $(\sigma_p)_{\exp}$=433.962 (MPa)

$$\frac{\sigma_p}{(\sigma_p)_{\exp}} = 1.077$$

Thus, the results calculated by the new model of J.F.Chen closely agree with the experimental results.

In the case of masonry experiment (PGA=$214.5\,cm/s^2$) conducted at the Institute of Reinforced Concrete structures, at the University of Karlsruhe, the calculations are as follows

$\beta_p = \beta_L = 1.0$

$\sigma_p = 132.20 \quad (MPa)$ When σ_p compared with the experimental result ($(\sigma_p)_{\exp} = 125.5 \quad (MPa)$), then $(\sigma_p)_{\exp} = 1.05\sigma_p$. This shows the validity of this model to be applied to the case of masonry walls retrofitted with GFRP-sheets.

The stress-strain relationship is taken a triangular, with a damage function, where

$$\sigma = (1 - D) E_0 \varepsilon \tag{4.36}$$

with non-linear damage function, D is given by

$$D = -4088.3\left(\tilde{\varepsilon}\right)^2 + 143.79\left(\tilde{\varepsilon}\right) - 0.2104 \tag{4.37}$$

This model is programmed and implemented in the finite element program, Abaqus6.4 [1].

4.6 Experiments to determine the Performance of the Glass Fibre Reinforced Polymers (GFRP) on the Autoclaved Aerated Concrete (AAC) Blocks

Before executing the experiments on the retrofitted wall, experiments on small test samples were carried out to determine the surface bonding-strength of GFRP on the autoclaved aerated concrete blocks and to determine a suitable retrofitting way for the wall. Due to the problem of corrosion and the expensive manufacture-cost of the steel-lamellae, since some years, the steel is replaced with another material with better properties. One of these materials is the GFRP, which is used mainly for the retrofitting of masonry walls in shape of sheets, with a matrix of epoxy-resin as a bonding-agent. The application of these materials is simple and effective.

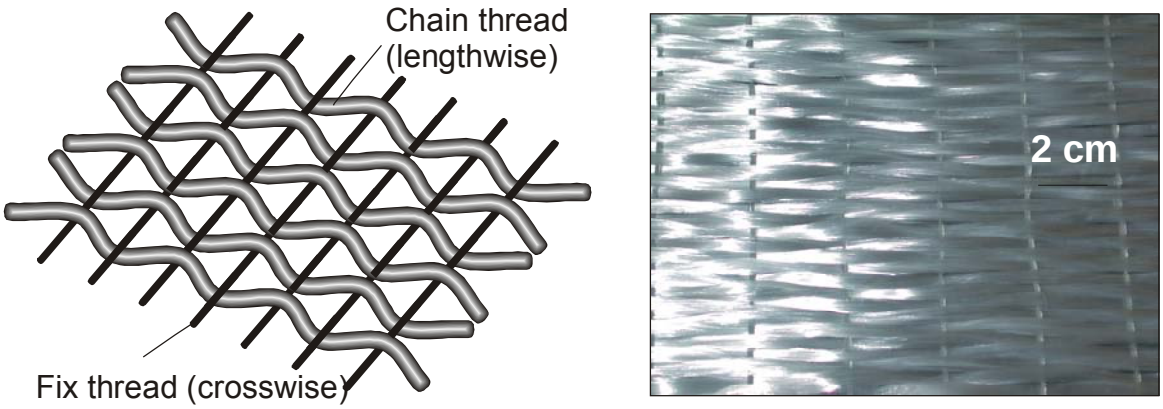

Figure 4.12: Structure of glass fibre reinforced polymer (GFRP)-sheet

The advantage of GFRP-sheets is not only its corrosion resistance but, also is its high-tension strength and its lightweight. It is proven by the experiments of Schwegler [191], that these materials have a ductile behaviour, which is required for earthquake loading.

For the experiments on the retrofitted wall, the system of the firma Sika is used (Sika Wrap Hex-230 C sheet with epoxy resin matrix). The properties of these (GFRP)-sheets, which are used in the experiments are shown in Table 4.5 (see also the Sika technical bulletin 1.99 [195]). The experiment-set-up is shown in Figure 4.13.

Fibre-type	Glass fibre
Fibre-direction	0° (unidirectional)
Weight	430 g/m²
Thickness	0,17 mm
Width	610 mm
Length / Roll	≥ 45,7 m
Tension strength Of the fibres	2250 N/mm²
E-Modulus	70000 N/mm²
Failure strain	3,1 %

Table 4.5: Material properties of the used GFRP-sheets

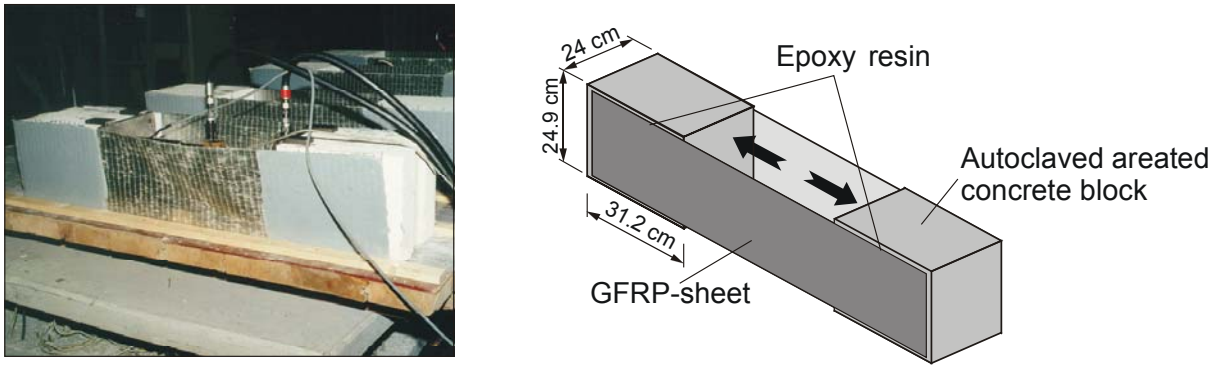

Figure 4.13: Experiment-set-up for the small-test samples

Four small test samples are tested, where two of them, approximately 24 hours before the application of the GFRP-sheets, are pre-treated with Sikafloor 156. The GFRP-sheets are glued on the blocks using the epoxy resin matrix. Two compression forces in opposite directions are applied on the test samples via a hydraulic cylinder. The values measured are; the displacement and the force. The results are shown in Figure 4.14. These experiments showed that the joints failed in the blocks a few millimetres beneath the block/adhesive interface due to the lateral tension strength of the blocks being exceeded. Interfacial failure between the adhesive and the blocks or between the adhesive and the GFRP-sheets is not found. This is a consequence of the availability of strong adhesives that bond well to GFRP and blocks. For this reason, adhesive failure is rare. The adhesive strength, which can be obtained by dividing the measured force by the bond area in each test, equals 0.227 MN/m^2 and 0.18 MN/m^2 for the pre-treated and non-pre-treated samples, respectively.

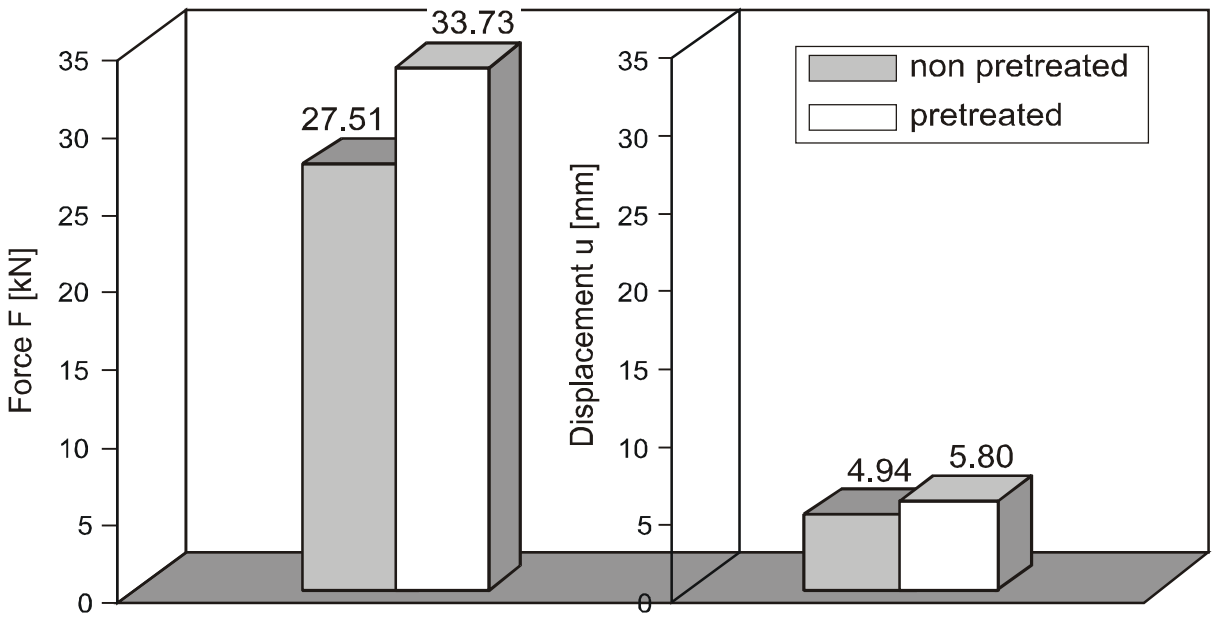

Figure 4.14: Measured force and displacement from the experiments on the small test samples

4.7 Experimental Results of Pre-Damaged-Retrofitted Wall of Section (3.3) with the Glass Fibre Reinforced Polymers (GFRP)-Sheets

The pre-damaged wall from the experiments in section 3.3 is now retrofitted with uni-directional GFRP-sheets crosswise in both sides. The structure of this GFRP-sheet is shown in Figure 4.12.

Based on the informations from the experiments on the small-test samples (see section 4.6), the pre-damaged, pre-treated wall is retrofitted on both sides crosswise, with the GFRP-sheets. The epoxy resin matrix sikadur 330 is used as a bonding agent.
Figure 4.15 shows the retrofitted wall. The loading is increased successively with different factors multiplied by the acceleration-time-history of 1990-Bucharest earthquake.
By comparing the force-displacement diagram in Figure 4.16 with that of Figure 3.16, it is found that, by retrofitting, the wall can be loaded with the same load, in the case of a virgin wall and that the wall is restored to its initial state. This, Then shows the efficiency of using GFRP-sheets as a retrofitting material.

Figure 4.17 shows the force-displacement diagram with PGA=$214.5\,cm/s^2$, where, by this PGA, the maximum load-carrying capacity of the wall is reached.
The behaviour of the retrofitted wall with these GFRP-sheets is ductile-behaviour with greater displacement (untill $13\,mm$) and high load-carrying capacity (untill $250\,KN$).

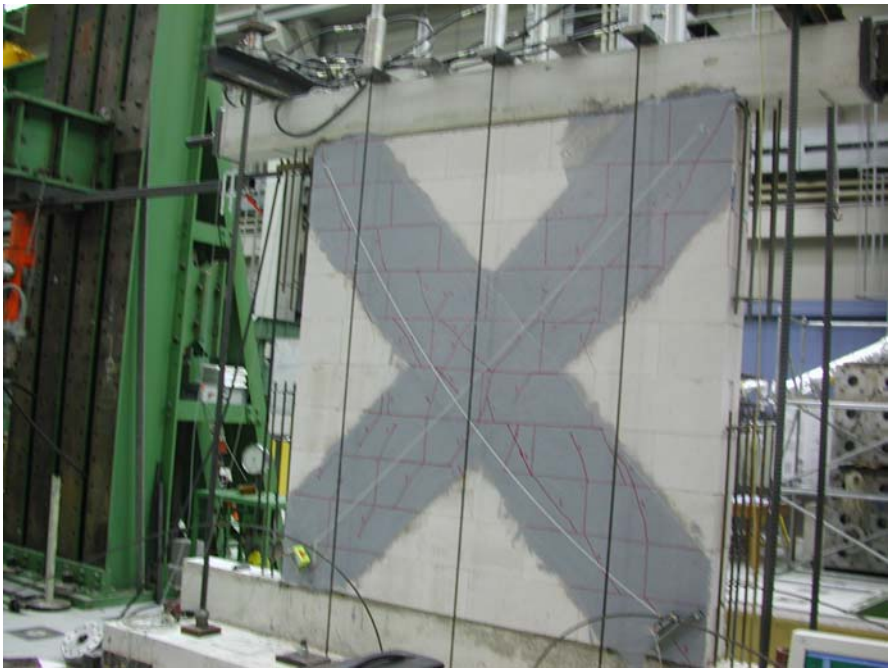

Figure 4.15: Retrofitted wall with GFRP-sheets crosswise in both directions

Compared to the non-retrofitted wall (see Figure 3.17), the hysteretic-loops are clearly definitive and more stable.
From the comparison with the non-retrofitted wall, where its maximum force is $155\,KN$ with a maximum displacement of $5\,mm$, it is found that by retrofitting the ductility and the load carrying capacity of the wall is increased untill 60%.

Figure 4.18 shows the nominal response spectra for the pre-mentioned experiments. Figure 4.19 shows the increasing factor of the response spectra, which is obtained by dividing the nominal spectral acceleration (PGA=$214.5\,cm/s^2$) by that of PGA=$38.3\,cm/s^2$.

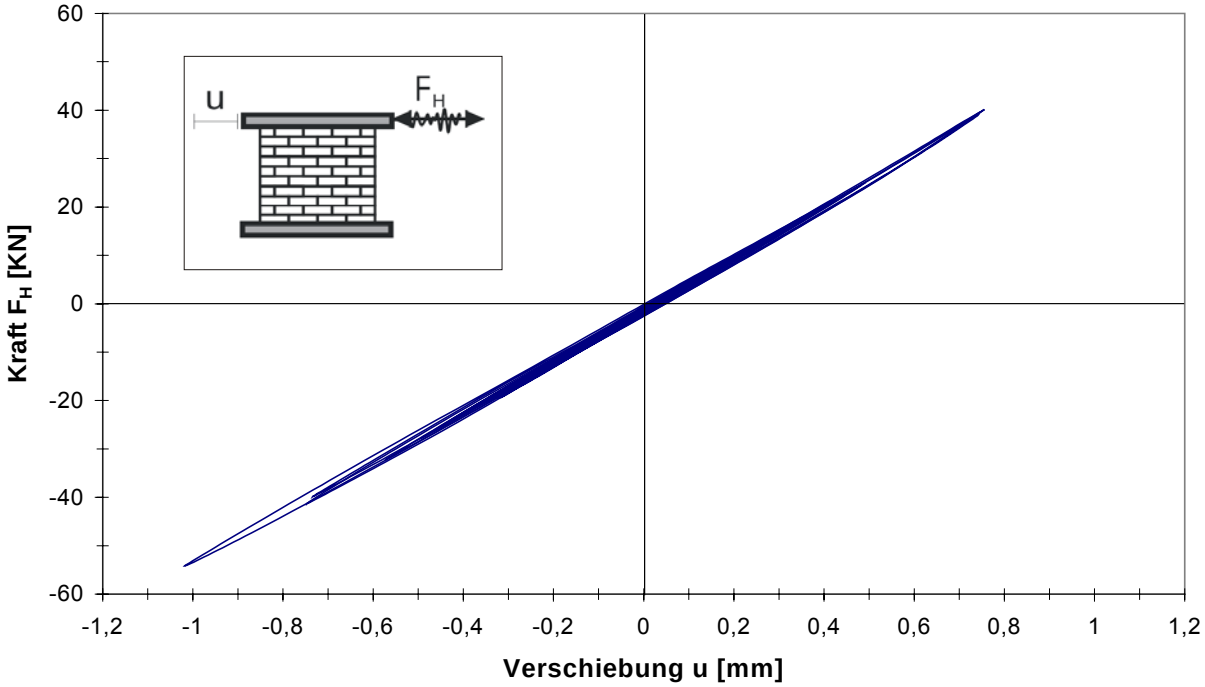

Figure 4.16: Force-displacement diagram for the retrofitted wall, PGA=38.3 cm/s^2

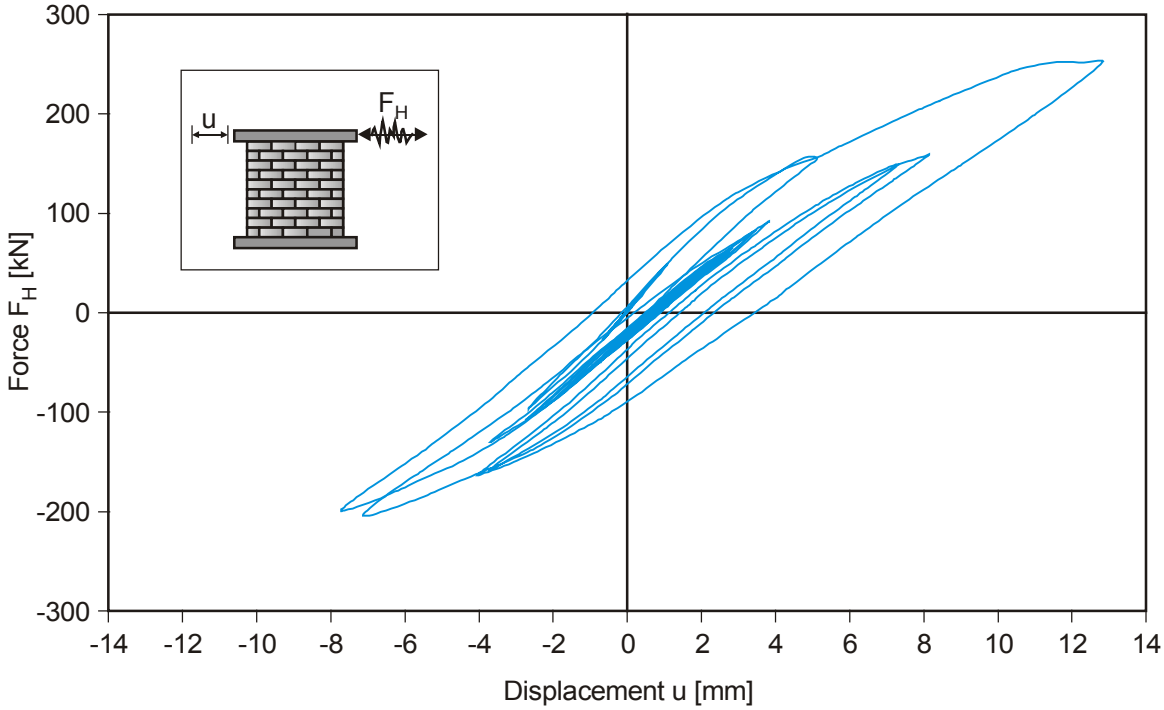

Figure 4.17: Force-displacement diagram for the retrofitted wall, PGA=214.5 cm/s^2

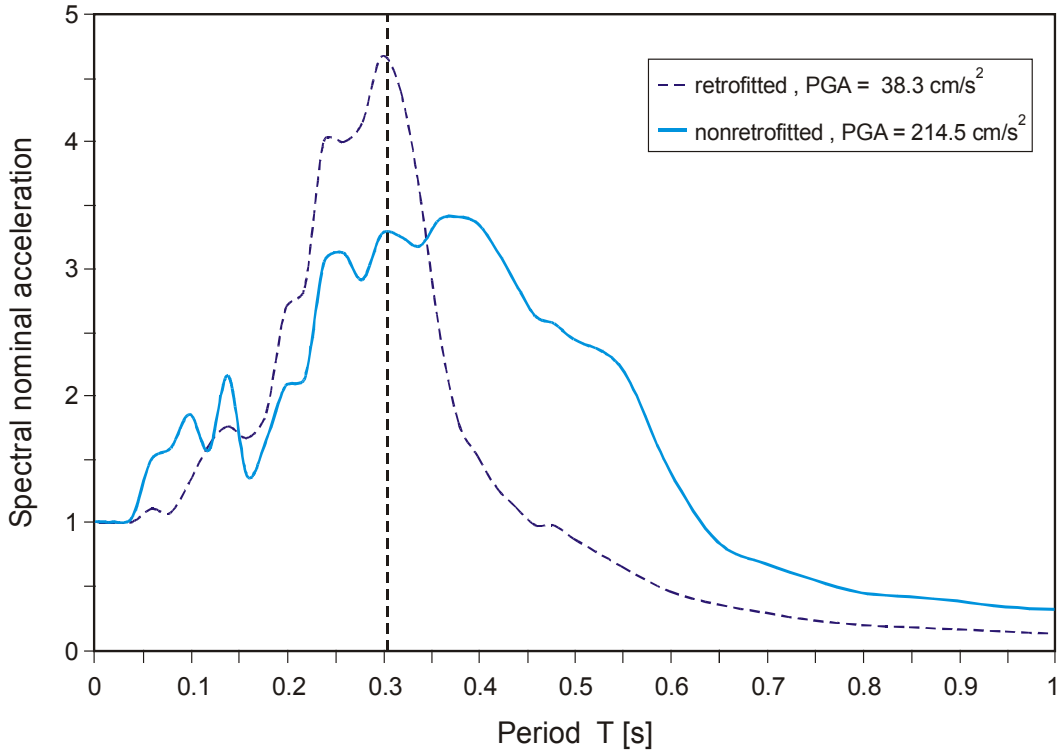

Figure 4.18: The nominal spectral acceleration from the experiments on the retrofitted wall for PGA=38.3 cm/s^2 versus for PGA=214.5 cm/s^2

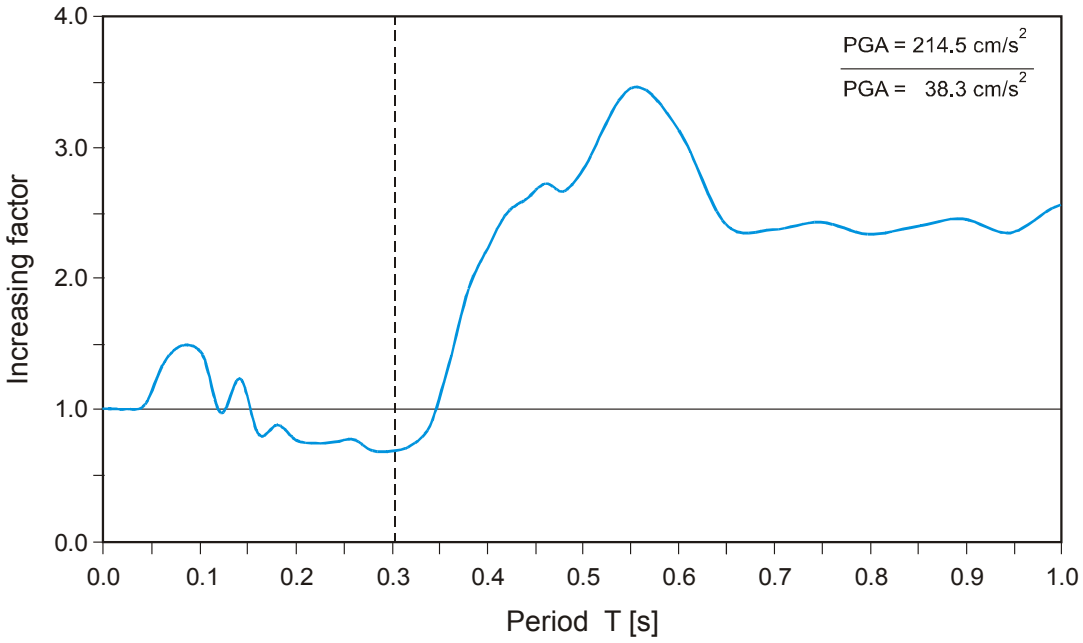

Figure 4.19: Comparison of the increasing-factors of the response spectra from the experiments on the retrofitted wall, PGA=114.9 cm/s^2 and PGA=38.3 cm/s^2

The retrofitted wall has an eigen-period of $0.3s$ in the elastic range as, does the non-retrofitted wall. By increasing the scale factor, the system is softer and the eigen-period moves in the direction of higher periods.

It is evident from the experiments that the loss of shear stiffness in the pre-damaged wall is to large extent, well adjusted by the retrofitting procedure using GFRP-sheets. This is also clear from the response spectra, where the period for the retrofitted wall concentrated again around $0.3s$ (see Figure 4.20). This is also clear from Figure 4.21, where there is no difference between response spectra. This means that by using this retrofitting technique the wall returns to its original loading capacity.

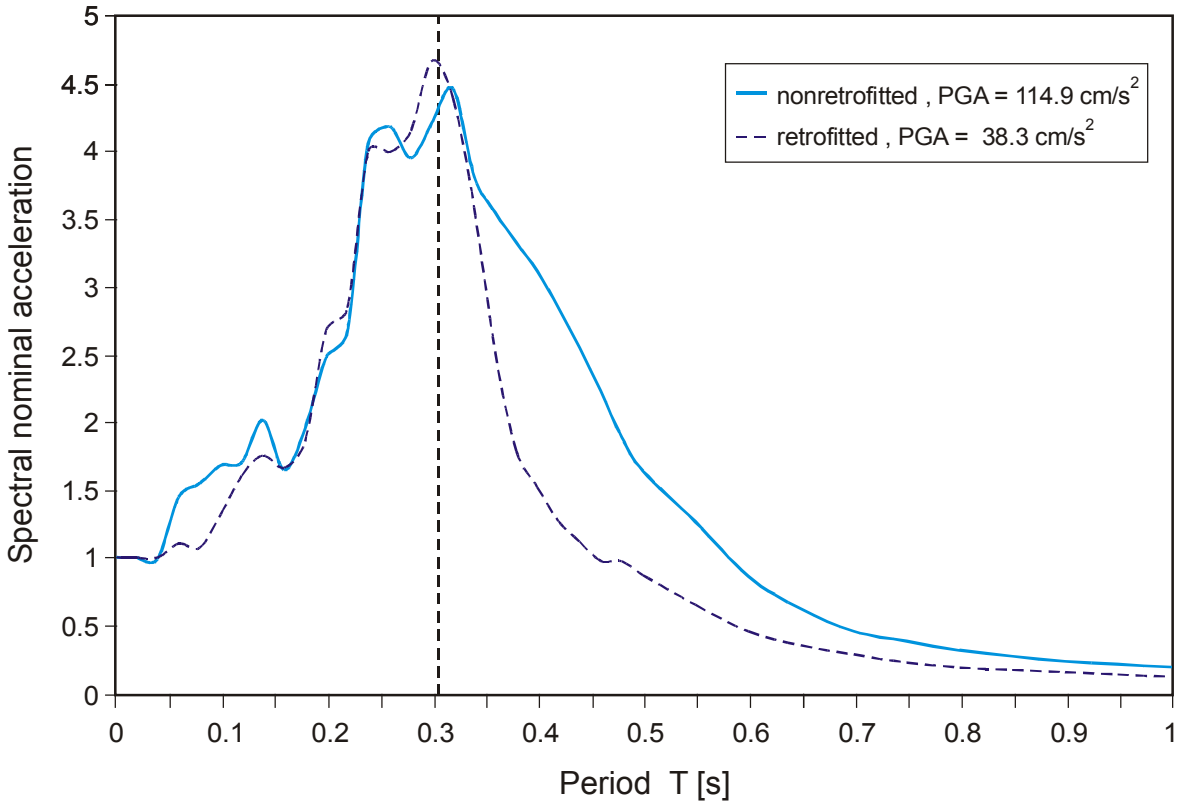

Figure 4.20: The nominal spectral acceleration of the retrofitted wall, PGA=38.3 cm/s^2 versus that for nonretrofitted wall, PGA=114.9 cm/s^2

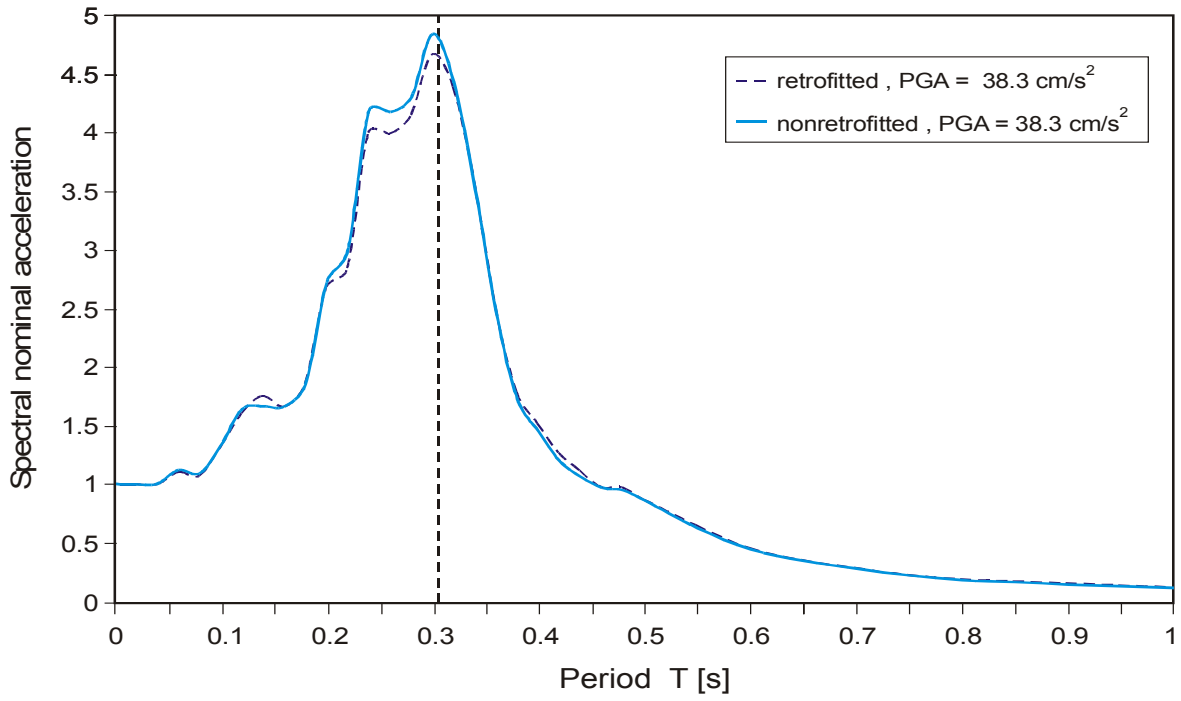

Figure 4.21: The nominal spectral acceleration of the retrofitted wall, PGA=38.3 cm/s^2 versus that for nonretrofitted wall, PGA=38.3 cm/s^2

4.7.1 Numerical Results

In the following, the retrofitted experimented wall is calculated using the new developed non-linear finite element program.
The retrofitted wall with GFRP-sheets applied crosswise was shown in Figure 4.15.

In the calculation, successive increasing factors for the acceleration-time-history for loading the retrofitted pre-damaged wall are adopted.
This acceleration-time-history is scaled in the calculation with the same scale, as in the experimental programme, untill the failure of the wall is reached.

For the PGA=$38.3\,cm/s^2$, the results from the experiment and the calculation are shown in Table 4.6. The nominal spectral acceleration is shown in Figure 4.22.

	Max-Force (KN)	Max.Disp. (mm)
Experimental wall (see also chapter three)	54	1.0
Calculated wall	50	0.94

Table 4.6: The results of the calculation versus those from the experiment for the pre-damaged, retrofitted wall, PGA=38.3 cm/s^2

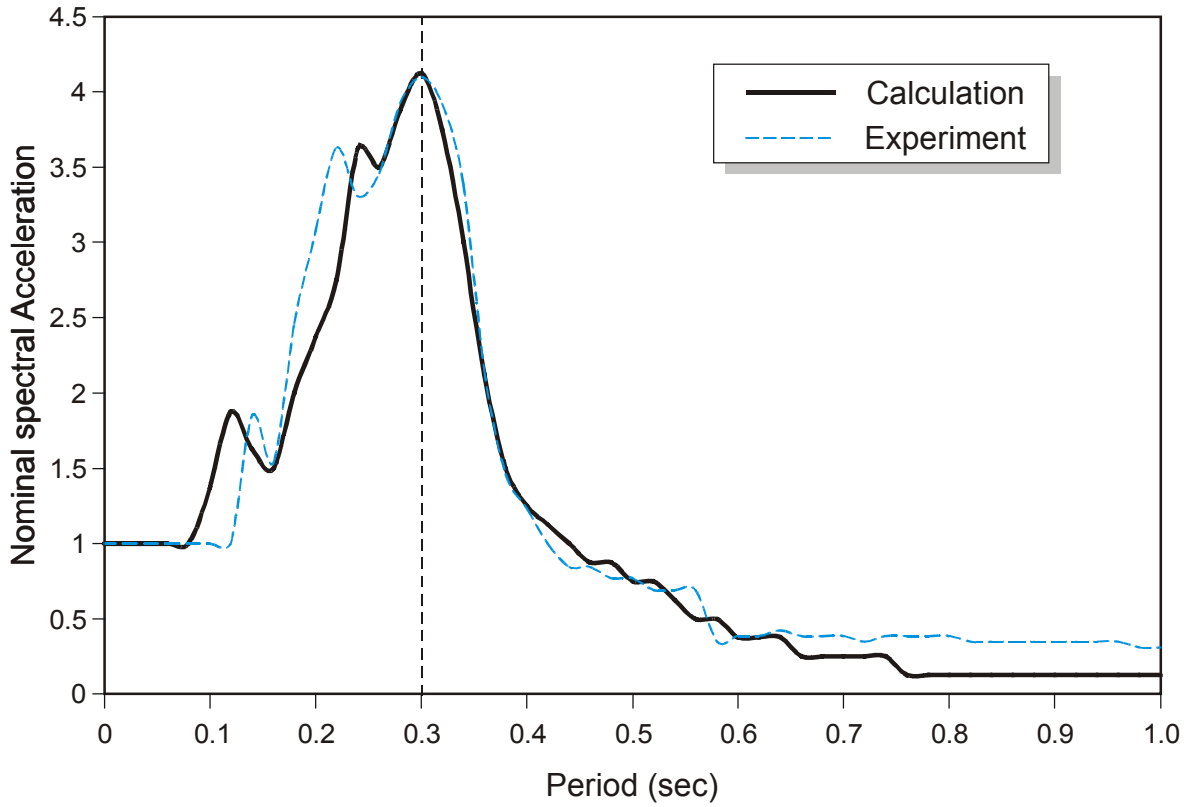

Figure 4.22: Comparison of the nominal spectral acceleration of the pre-damaged, retrofitted wall from the calculation and the experiment, PGA=38.3 cm/s^2

The retrofitted wall in the elastic experiment has an eigen-period of Teig=$0.3s$, like the virgin wall. By increasing the scale factors, the system becomes softer and the eigen- period moves in to the range of higher periods. Table 4.6 and Figure 4.22 show that the calculations closely agree with the experiments.

When the properties of the retrofitted wall are compared to those of the non-retrofitted wall, it can be seen that by retrofitting the wall, the loss in

the shear stiffness to a large extent is well adjusted. The response spectra of the repaired wall, again, concentrates around the eigen-period of Teig=$0.3s$. Thus, with the repair system, the original stiffness of the wall is retained.

For the PGA=$214.5 cm/s^2$, the results from the experiment and the calculation are shown in Table 4.7. The nominal spectral acceleration is shown in Figure 4.23.

	Max-Force (KN)	Max.Disp. (mm)
Experimental wall (see also chapter three)	251	12.87
Calculated wall	257	13.18

Table 4.7: The results of the calculation versus those from the experiment for the pre-damaged-retrofitted wall, PGA=214.5 cm/s^2

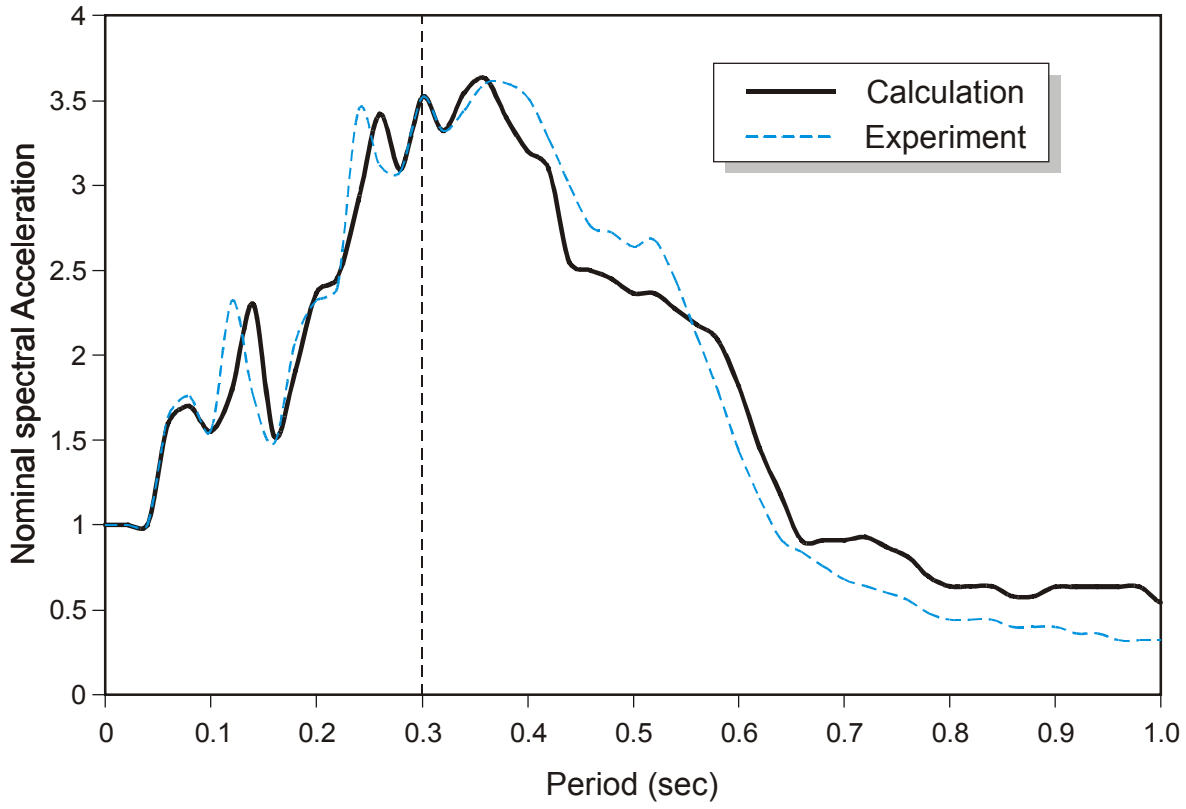

Figure 4.23: The nominal spectral acceleration of pre-damaged repaired wall from the calculation and the experiment, PGA=214.5 cm/s^2

Table 4.7 and Figure 4.23 show also that the calculations closely agree with the experiments for the PGA= $214.5\,cm/s^2$.
The repaired wall has a highly ductile behaviour with large displacement (untill $13\,mm$) and a large loading capacity (untill $0.25\,MN$). The wall failed by the exceeding of the maximum tension principal stress in the cross-sectional direction in the corner extent. The adhesion stress and/or the detachment of GFRP-sheets are not reached.

From the above presented comparisons, it is concluded that by retrofitting the pre-damaged wall with GFRP-sheets, the initial shear stiffness was restored again, the ductility raised and the carrying capacity increased about 60%. These results show that this kind of retrofitting is a reliable method for retrofitting masonry walls.

Figure 4.24 shows the response spectra curves for masonry wall made from AAC-blocks, retrofitted with the GFRP-sheets crosswise on the two sides for different values of $\frac{h_w}{l_w}$ with $PGA = 214.5\,cm/s^2$. The decreasing of the stiffness is seen clearly here by moving the eigen-period in the range of higher periods, i.e., in the direction of the decreasing branch of the response spectrum. This also leads to decreasing the resulted forces. It is clear from Figure 4.24, that as the value of $\frac{h_w}{l_w}$ increased, the bending deformation, as a part of the total deformation, increased. The wall behaviour is clearly ductile.

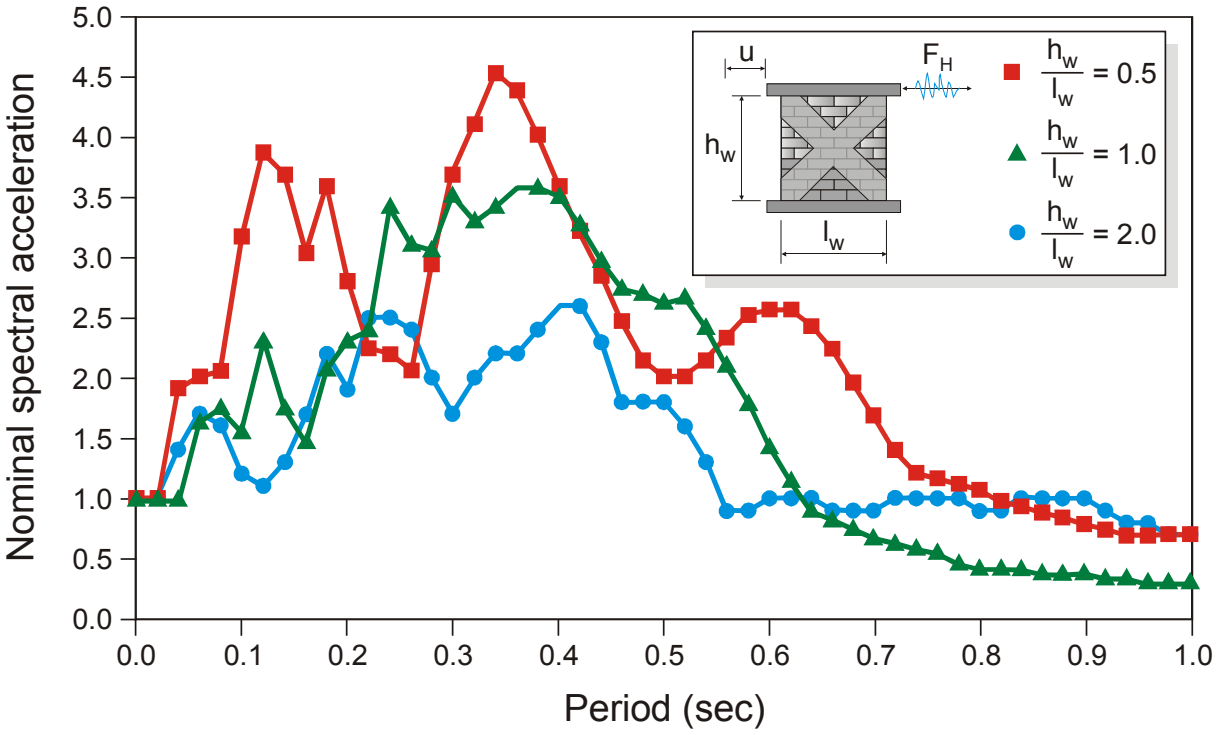

Figure 4.24: The nominal spectral acceleration of pre-damaged-retrofitted AAC-blocks wall for different $\frac{h_w}{l_w}$, PGA=214.5 cm/s^2

The wall experimented on by Berto [12], with a disposition of an central opening (see Figure 3.25(a)), is retrofitted and then studied using the developed constitutive law. As the symbols of the principal stresses takes the shape presented in Figure 3.25(b), the retrofitted shape with FRP takes the shape shown in Figure 4.25. The force displacement diagram is shown in Figure 4.26 for the retrofitted wall with the central opening. In comparison with the non-retrofitted wall, the increase in the ductility and shear stiffness is clear.

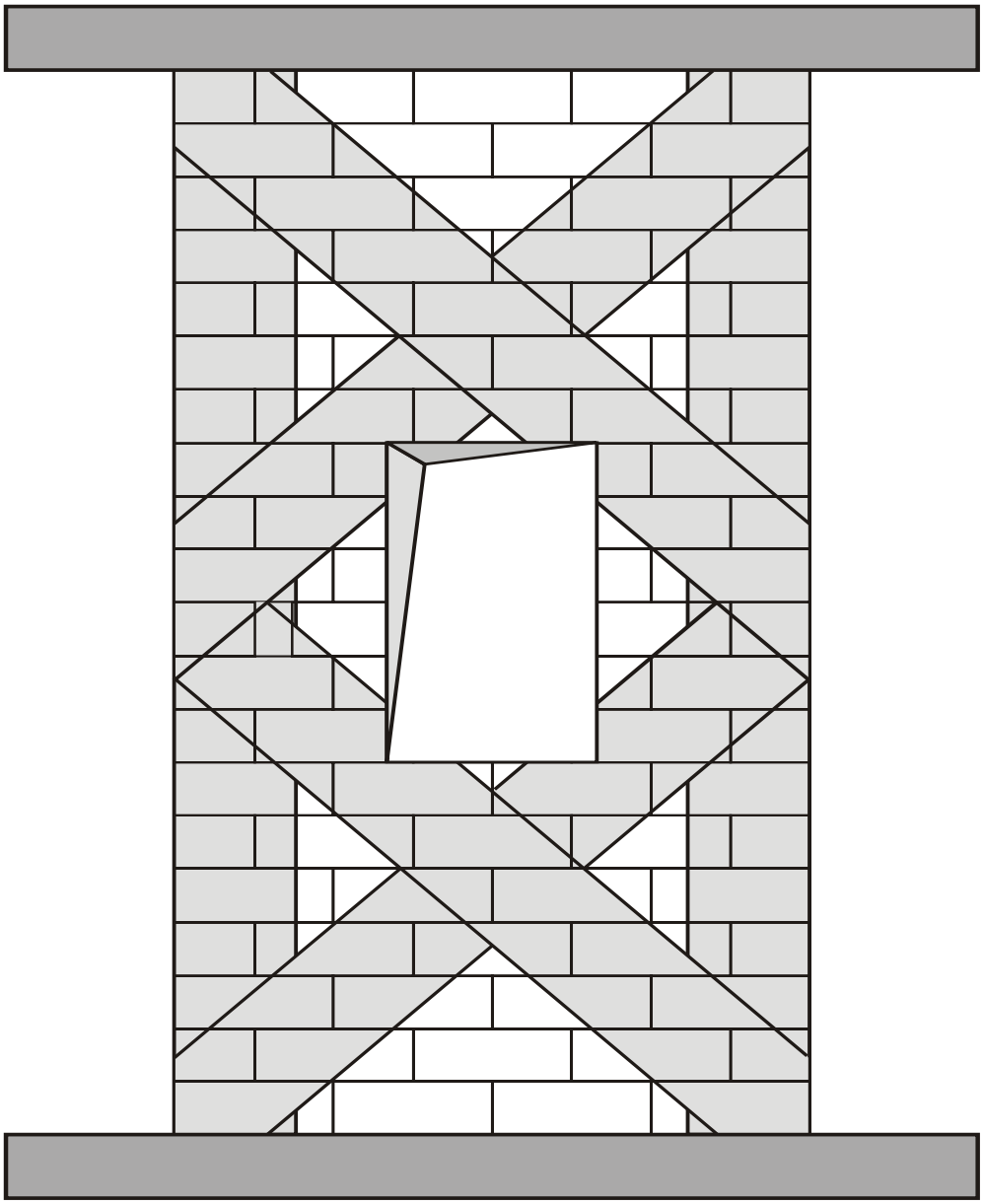

Figure 4.25: Retrofitting shape for the wall with opening with GFRP-sheets

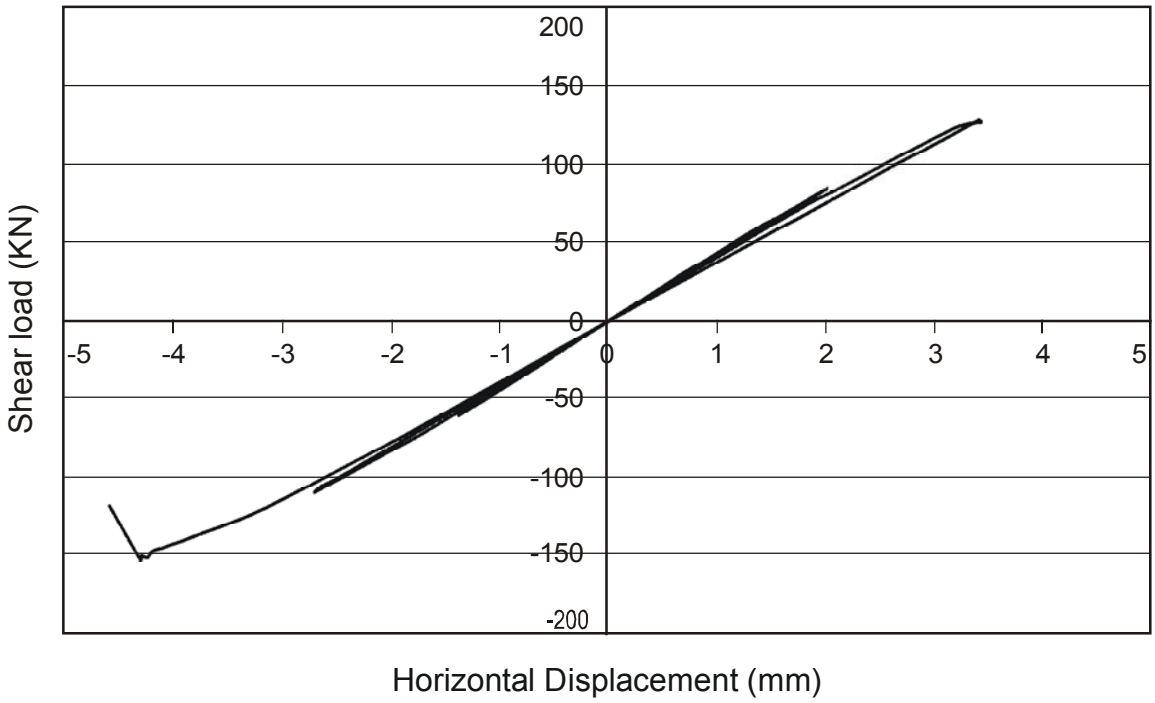

Figure 4.26: Horizontal load versus Horizontal displacement for the retrofitted wall with opening

5 Summary, Conclusions and Recommendations

Masonry is still primarily used for cladding. Its use as a structural material is secondary. However, in recent years the application of masonry as a major load bearing material has increased rapidly due to the recognition of problems associated with concrete structures and to its higher aesthetic appeal.

The masonry walls have a dramatic effect in changing the dynamic characteristics of the building and its response to seismic loads, creating a major source of hazard during seismic events.

The recent earthquake in different countries of the world, such as those in Vrancea (1997), Turkey (1999), India (2001), Algeria (2003) and Iran (2003) have shown, that masonry walls were particularly damaged. Therefore, it is necessary to find practical solutions to analyse and/or to retrofit these masonry walls.

After studying the behaviour of masonry under monotonic and/or cyclic loading, using the developed damage model, the main objectives of repairing of masonry walls were:

1. To use practical and effective retrofitting technique by the application of externally bonded GFRP-sheets. GFRP-sheets were chosen due to their superior properties over the other retrofitting techniques.
2. To restore the initial shear stiffness of the masonry wall.
3. To improve the seismic behaviour of an un-reinforced masonry wall by raising its carrying capacity, ductility and energy dissipation.
4. To develop a bond model to study the retrofitting of masonry walls.

A summary, conclusions of the work, and recommendations for future research are now introduced.

5.1 Summary

The present study had two stages; The first stage aimed to study the behaviour of masonry walls by developing a suitable constitutive model; While the second stage was concerned with the investigating of the strengthening and/or repairing of the masonry walls structures using glass fibre reinforced laminates (GFRP) that are epoxy-bonded to the exterior faces of the walls. The numerical investigation was accomplished by developing anchorage strength bond model to study the effect of such GFRP material on masonry.

An experimental program has been conducted at the Institute of Reinforced Concrete Structures, at the University of Karlsruhe, Germany to analyse the behaviour of masonry walls without and with retrofitting using the pseudo-dynamic experimental set-up that was designed at the Institute.

To study masonry walls numerically, a three-dimensional non-linear finite element model, based on two-parameter damage coefficients has been developed. The developed model, which was based on the continuum damage theory, takes into account for different behaviours in tension and compression. Such an approach, revealed to be valuable in understanding the global behaviour of masonry structures. The numerical results are in close agreement with experimental data.
The masonry was treated as a homogenized material, for which the material properties were obtained by a homogenisation technique. The damage theory proved to be a good choice to exploit in this area of structural mechanics due especially to its efficiency combined with simplicity.

Another constitutive model was also developed to study the effect of retrofitting numerically.

Both of the constitutive models were programmed and incorporated into a three-dimensional finite element code: Abaqus 6.4 [1]. It has been verified and validated with experimental results.

The comparisons between the numerical and experiment results have shown close agreement.

These results have shown that this kind of retrofitting will be a reliable method.

5.2 Conclusions

The following conclusions can be drawn from the present study:

1. A three-dimensional damage model, based on the continuum damage theory, has been developed for the analysis of masonry walls under vertical load and/or cyclic shear. It has been programmed and implemented in the finite element programme Abaqus 6.4 [1].
2. For this analysis, an 8-noded, solid element, together with orthotropic material properties, derived from the strain energy of the composite material, was used throughout.
3. The model was based on the introduction of two damage variables, which describe the behaviour of material subjected to cyclic loads and takes into account for the different behaviour in tension and compression. It has been validated with reference to available experimental data.
4. The numerical results have shown that the shear strength and the shear behaviour of the wall was much influenced when loading the wall with vertical load in addition to the shear force.
5. The numerical implementations performed gave a good description of the failure process, as well as an accurate prediction of the behaviour of masonry structures.
6. An opening made in the shear wall leads to a decrease in the shear stiffness and cracks concentration around the opening.
7. As the experiments on the small test samples of blocks and on the masonry wall retrofitted with GFRP-sheets have shown that joints failed in the blocks a few millimetres beneath the block/adhesive interface, the developed bond model was based on the masonry failure.

8. By retrofitting the pre-damaged wall with GFRP-laminates, the initial shear stiffness can be restored, the ductility raised and carrying capacity increased by 60%.
9. The GFRP-retrofitted masonry walls are more energy dissipation in cyclic loading, stronger, and fail gradually.
10. The GFRP-laminate will serve as an external reinforcement for un-reinforced or under-reinforced walls, thus providing a quick and cost-effective solution.
11. The GFRP-laminates help in confining the masonry wall, thus, allowing it to carry higher loads.
12. These results have shown that this kind of retrofitting is a reliable method.

5.3 Recommendations for Future Work

1. Further investigation of the confining effect of reinforced concrete or steel frames on the behaviour of masonry walls without and with retrofitting.
2. Using the developed model to study the out-of-plane behaviour of the masonry walls.
3. Studying the behaviour of masonry walls containing different openings configurations without and with retrofitting.
4. Investigating the use of different composite fabrics to retrofit the masonry walls.
5. Provide guidelines for the design the FRPs-retrofitted masonry walls to optimise the composite materials selection to retrofit URM-walls.

Kurzfassung

Mauerwerk ist ein traditioneller Baustoff, der in der ganzen Welt eine weite Verbindung in der Bauindustrie findet.
Seit den Anfängen der Geschichte ist die weit verbreitete Geographische Verfügbarkeit seiner Rohstoffe der grösste Vorteil des Mauerwerks. Dieser Umstand ist auch heute noch gültig, da viele Entwicklungsländer Mauerwerk als wirtschaftlichstes Baumaterial ansehen. In den letzen Jahren ist die Verwendung von Mauerwerk als vorwiegend lastabtragendes Baumaterial stark gestiegen, möglicherweise wegen Problemen, die mit Betonbauteilen in Zusammenhang gebracht werden, oder seines ästhetischeren Aussehens.

Das Verhalten von Mauerwerk unter zyklischer Belastung zeigt einen deutlichen Abfall der Steifigkeit und möglicherweise auch der Druckfestigkeit (softening).

Herkömmliche Verstärkungstechniken können als Schadensreparatur oder Ertüchtigung des Bauwerks eingeteilt werden.
Die Verstärkungsmethoden haben sich zumeist als unbrauchbar erwiesen, sie erhöhen beträchtlich die Masse, sind arbeitsaufwendig und verursachen hohe Kosten.
Um die soeben genannten Probleme zu vermeiden, wird die Verwendung von Faserbewehrten Polymeren (FRP's) als neuer Trend im Bereich von Reparatur und Verstärkung von Mauerwerksbauteilen vorgeschlagen.

Die jüngsten Erdbeben in verschiedenen Ländern der Welt-wie in Iran (2003), Algerien (2003), Indien (2001), Türkei (1999) und Vrancea (1997) haben gezeigt, dass besonders Bauwerke aus Mauerwerk beschädigt

wurden. Daher ist es notwendig, praktische Lösungen zu finden, um das Verhalten dieser Wänden ohne/oder mit Verstärkung auf experimentellen und numerischen Weg unter monotoner und/oder zyklischer Erdbebenlast zu studieren.

Für eine solche Studie wurden am Institut für Massivbau und Baustofftechnologie, Universität Karlsruhe, Germany, ein experimentelles Programm durchgeführt, in dem das Verhalten von Mauerwerkswänden mit und ohne Verstärkung mit Hilfe des Pseudo-dynamischen Versuchsstandes, der im Institut entwickelt worden war, analysiert wurde.

Die vorliegende Arbeit umfasst zwei Ebenen. Zu der ersten Ebene sollte das verhalten von Mauerwerkswänden durch die Entwicklung passendes Werkstoffgesetz studiert werden, während sich die zweite Ebene mit der Untersuchung einer Verstärkung und/oder Zustandsetzung der vorgeschädigten Mauerwerkwände unter Verwendung von Glasfaserbewehrten Laminaten (GFRP), die mit Epoxide-harzen auf die Aussenseiten der Wände geklebt werden, befasst die numerischen Untersuchung wurde begleitet durch die Entwicklung eines Verbundmodells um den Einfluss der GFRP-Laminate auf Mauerwerk zu untersuchen.

Zur numerischen Erforschung des Verhaltens von Mauerwerkswänden wurde ein dreidimensionales Finite-Elemente-Modell auf der Grundlage von zwei-Parametrigen Schadenskoeffizienten entwickelt. Das Modell, dass auf der Kontinuum-Schaden-Theorie fusst, berücksichtigt für Zug und Druck ein unterschiedliches Verhalten. Ein solche Ansatz führt zu einem guten Verständnis des globalen Verhaltens von Mauerwerk; die numerisch Rechenwerte sind in guter Überstimmung mit den

experimentellen Messwerten. Das Mauerwerk wurde als homogenisiertes Material behandelt. Die Schadens-Theorie zeigte sich als gute Wahl auf diesem Gebiet Bereich der Baumechanik, besonders wegen ihrer Wirksamkeit und Einfachheit.

Das entwickelte Materialgesetz wurde programmiert und in eine dreidimensionale Finite-Elemente-Berechnung eingearbeitet
(Abaqus 6.4).
Die Ergebnisse, die mit diesen Programm ermittelt wurden, stimmten mit den experimentellen Ergebnissen gut überein.
Die numerischen Ausführungen ergaben ebenso eine gute Beschreibung des Versagensprozesses und eine genaue Vorhersagung des Mauerwerksverhaltens.
Die Rechnungen zeigten, dass eine lotrechte Belastung der Wand, die zusätzlich zur Schubbelastung erfolgt, die Schubfestigkeit und Schubverhalten stark beeinflusst.

Zur numerischen Untersuchung einer verstärkten Mauerwerkswand wurden ein weiteres Verbund-Modell entwickelt, programmiert und in (Abaqus6.4) eingebaut.
Die numerischen Ergebnissen lagen im allgemeine in guter Übereinstimmung mit den experimentellen Werten.

Nach der Verstärkung der vorgeschädigte Wand mit GFRP-Laminaten konnte die ursprüngliche Schubfestigkeit wieder erreicht werden, die Tragfähigkeit erhöht sich und die Duktilität erhöht sich um 60%.
Die Ergebnisse zeigte, dass diese Art der Verstärkung geeignet ist, die Schubkapazität und Tragfähigkeit von Mauerwerkswänden wieder herzustellen. Es ist ein verlässliches Verfahren, und erhöht die Wirksamkeit unbewehrter Mauerwerksbauten.

Die Arbeit besteht aus fünf Kapitalen. Das erste Kapitel beinhaltet allgemeine Bemerkungen der Problemstellung und die Ziele der Arbeit.

Der seismologische Hintergrund wird im zweiten Kapitel aufgezeigt. Dieses Kapitel enthält auch verschiedenen Normen und Richtlinien zur Anwendung von Mauerwerk in Erdbebebgebieten. Weiterhin sind in diesem Kapitel das Verhalten von Mauerwerk unter Zug-, Druck- und Belastung in Wandebene sowie die Bruchkriterien und Aussagen über Schadenstheorienangeben.

Kapitel drei zeigt das selbst entwickelte Schadensmodell zur Beschreibung des Verhaltens von Mauerwerksbauteilen auf der Grundlage der Kontinuum-Schadens-Theorie. Es werden Rechenbeispiele angegeben, die das entwickelte Schadensmodell für Mauerwerk benutzen. Ein Vergleich zwischen Berechnung und experimentellen Versuchen, die am Institut für Massivbau und Baustofftechnologie, Universität Karlsruhe an Mauerwerks aus Porenbeton durchgeführt wurde, ist ebenfalls im Kapitel drei enthalten.

Kapitel vier beinhaltet eine Übersicht über die Theorie von verbundwerstoffen und die Eigenschaften verschiedener Materialien, die als Laminte verwendet werden. Weiterhin werden Modelle für die Tragfähigkeit von FRP-Verankerungen, die mit Mauerwerk und/oder Beton verbunden sind, aufgezeigt.
Das weiterentwickelte Verbundmodell für FRP’s, welches das Verhalten von Mauerwerk beschreibt, das mit FRP’s verstärkt worden ist, wird ebenso in Kapitel vier angegeben wie ein Vergleich zwischen numerischen Ergebnissen nach dem Verbund Modell und den experimentellen Ergebnissen an Porenbeton-Mauerwerkswänden, die

mit GFRP-Gewebe verstärkt im Institut für Massivbau und Baustofftechnologie, Universität Karlsruhe, geprüft worden waren.

Kapitel fünf fasst die Ergebnisse der Vorgelegten Arbeit zusammen und gibt Empfehlungen für zukünftige Forschungsarbeiten auf dem Gebiet der Berechnung von Mauerwerk und der Verstärkung von Mauerwerk mit FRP-Materialen.

List of References

[1] Abaqus Version 6.4, User Manual Hibbit, Karlsson & Sorensen, Inc., USA, 2004.

[2] Abrams, D. R.: *Masonry Carries the Load*. The Institute of Civil Engineers, United Kingdom, February 1993, pp.66-67.

[3] Ali, S., Page, A.W.: *The Use of Discrete Cracking Modelling in the Finite Element Analysis of Concentrated Loads on Masonry*. In: 10th Australasian Conf. On the Mechanics of Structures and Materials, Univ. of Adelaide, 1986, pp.193-198.

[4] Ali, S.S. and Page, A.W.: *Finite Element Model for Masonry subjected to concentrated loads*. In: Journal of Structural Engineering, ASCE, 114(1988), No. 8, pp. 1761-1784.

[5] American Concrete Institute (ACI): *Building Code Requirements for Reinforced Concrete*. In: ACI 318-89, 1989

[6] Atkinson, R.H., Noland, J.L.and Abrams, D.P.: *A deformation Failure Theory for Stack-Bond Brick Masonry Prisms in Compression.* In: 7th procc. Int. Brick Masonry Conf., Melbourne, Australia, 1985, pp.577.592.

[7] Bath, K.J.: *Finite Element Procedures in Engineering Analysis*. Prentice-Hall, 1982.

[8] Bath, K.J.: *Finite Elemente-Methoden*. Springer-Verlage, 1986.

[9] Bazant, Z.P., Bittnar, Z., Jirasek, M. and Mazars, J.: *Fracture and Damage in Quasi-Brittle Structures:* Experiment, Modelling and Computer Analysis. E& FN SPON, London, 1994.

[10] Bazant,P.: *Why Continuum Damage is Nonlocal: Micro-Mechanics Argument*. In: Journal of Mechanics, 5(117),May 1991, pp.1070-1087.

[11] Bernardini A., Modena C., and Vesconi U.: *An anisotropic biaxial failure criterion for hollow clay brick masonry*. In: the International Journal of Masonry Construction, 2 (1982), Nr.4.

[12] Berto, L., Saetta, A., Scotta, R. and Vitaliani: *An Orthotropic Model for Masonry Structures.* In: Int. J. Numer. Meth. Engng., 55(2002), pp. 127-157.

[13] Berto, L., Scotta, R. and Vitaliani, V.: *An Orthotropic Damage Model for Non Linear Masonry Walls: Irreversible Strain and Friction Effects.* In: Historical Constructions, Lourenco, P.B. and Roca, P. (eds.), 2001.

[14] Biggs, J.M.: *Introduction to Structural Dynamics*. McGraw-Hill Book Company, 1964

[15] Binda, L., Fontana, A., and Frigerio, G.: *Mechanical Behaviour of Brick Masonries derived from Unit and Mortar Characteristics*. In: International Brick and Block Masonry Conference, Calgary, Canada, 1994, pp.205-216.

[16] Bizindavyi, L.; and Neale, K. W.: *Experimental and Theoretical Investigation of Transfer Lengths for Composite Laminates Bonded to Concrete.* . In: Proc., Annu.Conf. Of Can. Soc. For Civ.Engrg.: Telecommunication Towers. Vol. 6, Canada: Sherbrooke, 1997, S.51-60.

[17] Bizindavyi, L.; and Neale, K. W.: *Transfer Lengths and Bonded Strengths for Composites Bonded to Concrete*. In: J. Compos. for Constr., ASCE. 3 (1999), Nr.4, S. 153-160.

[18] Blaschko, M., Niedermeier, R., and Zilch, K.: *Bond Failure Modes of Flexural Members Strengthened with FRP*. In: fibre Compos. In Infrastruct., Proc., 2nd Int. Conf. on Compos. in Infrastruct., H. Saadatmanesh and M. R. Ehsani, eds., 1996, S. 315-327.

[19] Bosiljkov, V., Kralj, B., Zarnic, R. and Pande, G.N.: *Finite Element Analysis of Model Shear Tests*. In: Procc. Computer Methods in Structural Masonry-4, 3-5 September, Italy, 1997, pp.153-160.

[20] Brain, H. and Humerto, R.: *Shear behaviour of mortar joints in Brickwork subjected to non-uniform compressive stress*. In: Proc. of the 8th International Brick/Block Masonry Conference, Dublin, Sep. 1988.

[21] Bricoli Bati, S., Ranocchiai, G., and Rovero, L.: *Numerical Validation of a Close-Form Approach to Localization in Linear Elastic Homogenisation of Masonry.* In: Proc. Computer Methods in Structural Masonry-4, (Pande, G.N., eds), 3-5 September, Italy, 1997, pp.27-34.

[22] British Standards Institution (BSI), BSI 8110: *Structural Use of Concrete*, Part 1, Code of Practise For Design and Construction, London, 1985.

[23] Brosens, K., and van Gemert, D.: *Anchoring Stresses between Concrete and Carbon Fibre Reinforced Laminates.* In: Non-Metallic (FRP) Reinforcement for Concrete Struct., Proc., 3rd Int. Symp. Vol.1, Japan: Concrete Institute,

1997, S. 271-278.

[24] Carlo, I., Rizzi, E., Willam, K.: *Current Issue in Elastic Degradation and Damage. In: Engineering Mechanics*, Proc. of the 10th Conference, USA, 1 (1995), pp.521-524.

[25] Carlo, I., Rizzi, E., Willam, K.: *On the Formulation of Isotropic and Anisotropic Damage. In: Proc. of the Euro-C, Conference on Computational Modelling of Concrete Structures*, 1998, pp. 183-192.

[26] Carlo, I., Rizzi, E., Willam, K.: Spurious Energy Dissipation /Generation in Modelling of Stiffness Recovery for Elastic degradation and Damage. In: Int.J.Solids and Structure, 33(1996), Nr.20-22, pp.2939-2957.

[27] Carol I., Rizzi, E., William, K.: A Unified theory of Elastic Degradation and Damage based on a Loading Surface. In: Int. J. Solids Structures, 31 (1994), pp.2835-2865.

[28] Chaallal, O., Nollet, M. J., and Peraton, D.: *Strengthening of Reinforced Concrete Beams with Externally Bonded Fibre-Reinforced-Plastic Plates*. In: Can. J.Civ. Engrg.,: Design Guidelines for Shear and Flexure. 25 (1998), Nr. 4, S. 692-704.

[29] Chajes, M. J., Finch, W. W. Jr., Januszka, T.F., and Thomson, T. A. Jr.: *Bond and Force Transfer of Composite Material Plates Bonded to Concrete*. In: ACI Struct. J., 93 (1996), Nr.2, S. 295-303.

[30] Chajes, M. J., Januszka, T.F., Jr Merta, D.R., Thomson, T. A. Jr, and Finch, W. W. Jr Merta, D.R.: *Shear Strengthening of Reinforced Concrete Beams using Externally applied Composite Fabrics*. In: : ACI Struct. J., 92 (1995), Nr.3, S. 295-303.

[31] Chen, Wai-Fah, Atef F. Saleeb: *Constitutive Equations for Engineering Materials.* London: Elsevier, 1994.

[32] Chopra, A. K.: *Dynamics of Structures, Theory and Applications to Earthquake Engineering*. Prentice Hall, 1995.

[33] Clough, R.W, Penzien J.: *Dynamics of Structures*. McGraw-Hill Book Company, 1986.

[34] Coleman, B.D., Gurtin, M.E.: *Thermodynamics with Internal State Variables*. In: J. Chemical Physics, 47 (1967), pp. 597-613.

[35] Collatz, L.: *The Numerical Treatment of Differential Equations*. New York: Springer Verlag, 1966.

[36] Conseil International du Batiment (CIB), International Recommendations for Design and Errection of Un-Reinforced and Reinforced Masonry Structures with an Appendix on Recommendations for Seismic Design of Un-reinforced, Confined and Reinforced Masonry Structures, 1987.

[37] Crandall, S.H.: *Engineering Analysis*. New York: McGraw-Hill Book Company, 1956.

[38] Creazza, G., Saetta, A., Scotta, R., Vitaliani, R., and Onate, E.: (1995). '' *Mathematical Simulation of Structural Damage in Historical Buildings*. '' In: STREMA 95, Structural studies of historical buildings, Crete, Greece, May 22-24, 1995, Architectural studies, Materials, Comp. Mech. (Analysis, Brebbia and leftheris, eds.), Vol.1 (1995), pp. 111-118.

[39] Creazza, G., Saetta, V. A., Matteazzi, R. and Vitaliani, V.R.: *Analysis of masonry Structures reinforced by FRP*. In: Historical Constructions, Lourenco, P.B. and Roca, P. (eds.), 2001.

[40] D'Ayala, D.F.: *Numerical Modelling of Masonry Structures Reinforced or Repaired*. In: Proc., Computer Methods in Structural Masonry-4, 3-5 September, Italy, 1997, pp.161-168.

[41] De Lorenzis, L, Tinazzi, D. and Nanni, A.: *Near Surface Mounted FRP Rods for Masonry strengthening: Bond and Flexural Testing.* In: Symposium, '' Meccanica delle Strutture in Muratura Rinforzate con FRP Materials'', Venezia, Itality, Dec. 7-8, 2000.

[42] Deutsches Institut für Normung, e.V.: *DIN 1048, Ausgabe 6.91, Teil 2: Prüfverfahren für Beton, Festbeton in Bauwerken und Bauteilen*. Berlin: Beuth, 1991.

[43] Dhanasekar, M., Page, A.W. and Kleeman, P.: *The Failure of Brick Masonry under Biaxial Stress.* In: Procc. Of the Institution of Civil Engineers, Part 2, 79(1986), pp.295-313.

[44] Dhansekar, M., Kleeman, P.W., Page, A.W.: *Biaxial Stress-Strain Relations for Brick Masonry.* In: J. Struct. Of Engng., 111(1985), No. 5, pp.1085-1100.

[45] Dialer, C.: *Bruch and Verformungsverhalten von Schubbeanspruchten Mauerwerksscheiben.* In: Mauerwerk-Kalender 1992, Verlag Ernst&Sohn, Berlin, 1992.

[46] DIN 1053-1(1996-1-1): Mauerwerk: Teil 1: Berechnung und Ausführung, November, 1996.

[47] DIN V ENV 1996-1-1, (1996-12): Eurocode 6: Bemessung und Konstruktion von Mauerwerksbauten-Teil 1-1: Allgemeine Regeln; Regeln für bewehrtes und unbewehrtes Mauerwerk, Deutsche Fassung ENV 1996-1-2:1995.

[48] DIN V ENV 1996-1-3, (1999-08): Eurocode 6: Bemessung und Konstruktion von Mauerwerksbauten-Teil 1-1: Allgemeine Regeln-Detaillierte Regeln bei horizontaler Belastung; Deutsche Fassung ENV 1996-1-3: 1998.

[49] DIN V ENV 1996-3, (2000-10): Eurocode 6: Berechnung und Ausführung von Mauerwerksbauten-Teil 3: Vereinfachte Berechnungsmethoden und einfache Regeln für Mauerwerk; Deutsche Fassung ENV 1996-3:1999.

[50] DIN V ENV 1998-1-1, (1997-06): Eurocode 8, Auslegung von Bauwerken gegen Erdbeben-Teil 1-1: Grundlagen; Erdbebeneinwirkungen und allgemeine Anforderung an Bauwerke, Deutsche Fassung ENV 1998-1-1:1994.

[51] DIN V ENV 1998-1-2, (1997-06): Eurocode 8, Auslegung von Bauwerken gegen Erdbeben-Teil 1-2: Grundlagen; Allgemeine Regeln für Hochbauten, Deutsche Fassung ENV 1998-1-2:1994.

[52] DIN V ENV 1998-1-3, (1997-06): Eurocode 8, Auslegung von Bauwerken gegen Erdbeben-Teil 1-3: Grundlagen; Baustoffspezifische Regeln für Hochbauten, Deutsche Fassung ENV 1998-1-3:1995.

[53] Djaalali, F., Afra, H. and Beerai, M.K.: *Seismic damage assessment for masonry structures*. In: 11th European Conference on Earthquake Engineering, Rotterdam, 1998.

[54] Dougill, J.W.: *On Stable progressively Fracturing Solids*. In: Zeitschrift fuer Angewendete Mathematik und Physik, 17 (1976), pp.423-437.

[55] Dougill, J.W.: *Some Remarks on Path Independence in the Small in Plasticity*. In: Quarterly of Applied Mechanics, 5 (1975), pp. 233-243.

[56] Dragon, A., Mroz, Z.: *A Continuum Model for Plastic-Brittle Behaviour of Rock*

and Concrete. In: International Journal Engineering Science, 17 (1979), pp.137.

[57] E DIN 4149: Bauten in deutschen Erdbebengebieten: Auslegung von Hochbauten gegen Erdbeben. Entwurf, Oktober 2002.

[58] Earthquake Resistant Regulations: A World-List-2002.

[59] EDGE: *A Guide for Composite Strengthening*. In. WWW.EDGEFRP.COM.

[60] Ehsani, M. R., Saadatmanesh, H., and Tao, S.*: Design Recommendations for Bond of GFRP Rebars to Concrete*. In: J. Struct. Engrg., ASCE, 122 (1996), Nr. 3, S. 247-254.

[61] Eibl J., Henseleit, O., Schlüter, F.H.: *Baudynamik*. In: Beton-Kalender, Teil 2, Berlin, 1988.

[62] El Dakhakhni.W.W.: *Experimental and Analytical Seismic Evaluation of Concrete Masonry-Infilled Steel Frames Retrofitted using GFRP Laminates.* Drexel University, Dissertation, 2002.

[63] ENV 1996, *Euro code 6-Design of Masonry Structures*, English Version, draft, 1996.

[64] Euro code 8-Design of Structures for Earthquake Resistance –part 1: General Rules, seismic actions and rules for buildings. Entwurf. Mai 2000.

[65] Faccio, P. and Foraboschi, P: *Experimental and Theoretical Analysis of Masonry Vaults with FRP Reinforcement*. In: 3rd Int. Conference on advanced Composite Materials in Bridges and Structures, Ottawa, Canada, 2000.

[66] FORCA two Sheets Technical Notes. Autocon Composites Inc., New York, 1994.

[67] Frantziskonis, G., Desai, C.S.: *Analysis of Strain-Softening Constitutive Model*. In: International Solids and Structures, 23 (1987), Nr. 6, pp. 751-767.

[68] Fukuzawa, K., Numao, T., Wu, Z., Yoshizawa, H., and Mitsui, M.: *Critical Strain Energy Release Rate of Interface Debonding between Carbon Fibre Sheet and Mortar.* In: Non-Metallic (FRP) Reinforcement for Concrete Struct., Proc., 3rd Int. Symp. Vol. 1, Japan: Concrete Institute, 1997, S. 295-303

[69] Ganz, H.R. and Thürlimann, B.: *Design of Masonry Walls under Normal force and Shear*. In: Proc. Of the 8th International Brick and Block Masonry Conference, Dublin, 1988, pp.1457-1447.

[70] Ganz, H.R. and Thurlimann, B.: *Tests on Masonry Bricks under Normal and Shear Forces.* Zurich: Swiss Federal Technical University: Institute for Structural Statics and Construction, 1984.

[71] Ganz, H.R. and Thurlimann, B.: *Tests on the Strength of Masonry Walls under Biaxial loads.* Zurich: Swiss Federal Technical University: Institute for Structural Statics and Construction. Report Y/OLS-93/7, 1982

[72] Ganz, H.R., Thurlimann B.: *Design of masonry walls under normal force and shear*. In Proceedings of the Eighth international Brick and Block masonry conference, 19-21 September, 1988, Trinity College, Dublin, V3.

[73] Ganz, H.R., Thurlimann B.: *Shear Design of masonry walls*. In Proceedings of ASCE structures congress, 85,hicago, September, 1985

[74] Ganz, H.R.: *Masonry Walls Subjected to Normal and Shear Forces* (in German), Report No. 109, Institute of Structural Engineering, ETH Zurich, Sept. 1985.

[75] Hampe, E, Mußtow, L.: *Einführung in den Entwurf erdbebenresistenter Bauwerke.* In: Wissenschaftlicher Zeitschrift der Hochschule für Architektur und Bauwesen, Heft 4, Weimar, 1984.

[76] Hampe, E.: *Bauwerke unter der seismischen Einwirkung*. Institut für Aus-und Weiterbildung im Bauwesen, Germany.

[77] Hendry, A.W.: *Reinforced and Pre-stressed Masonry.* Longman, 1991.

[78] Hendry, A.W.: *Structural Brickwork*. The McMillan Press Ltd., 1981.

[79] Hilsdorf, H., K., Reinhardt, H.W.: *Beton Kalender*, Vol. 1, Berlin, Germany, 1997, Ernst&Sohn, pp. 1-150.

[80] Hilsdorf, H.K.: *Investigation into Failure Mechanism of Brick Masonry Loaded in Axial Compression.* In: Procc. of Int. Conf. on Masonry Structural Systems, Gulf Pub. Col., Houston, Texas, 1969, pp.34-41.

[81] Hiroyuki, Y., and Wu, Z.: *Analysis of Debonding Fracture Properties of CFS Strengthened Member Subjected to Tension.* In*:* Non-Metallic (FRP)

Reinforcement for Concrete Struct., Proc., 3rd Int. Symp. Vol. 1, Japan: Concrete Institute, 1997, S. 287-294.

[82] Holzenkämfer, O.: *Ingenieurmodelle des Verbundes geklebter Bewehrung für Betonbauteile.* TU Braunschweig, Germany, Dissertation, 1994.

[83] Horiguchi, T., and Saeki, N.: *Effect of Test Methods and Quality of Concrete on Bond Strength of CFRP Sheet*. In: Non-Metallic (FRP) Reinforcement for Concrete Struct., Proc., 3rd Int. Symp. Vol. 1, Japan: Concrete Institute, 1997, S. 475-480.

[84] Houbolt, J.C.: *A Recurrence Matrix Solution for the Dynamic Response of Elastic Aircraft*. In: Journal of Aeronautical Science, 17 (1950), pp. 540-550.

[85] Hudson, D.E.: *Reading and Interpreting Strong Motion Accelerograms*. In: Earthquake Engineering Research Institute, Berkeley, 1979, pp.22-70 and 95-97.

[86] Hughes, T.G. and Baker, M.J.: *A Finite Element Model of Arch Ring Behaviour* . In: Proc., Computer Methods in Structural Masonry-4, 3-5 September, Italy, 1997, pp.200-207.

[87] International Association for Earthquake Engineering (IAEE), Basic concepts of Seismic Codes, Tokyo, 1980.

[88] International Association for Earthquake Engineering (IAEE), Guidelines for Earthquake Resistant Non-Engineered Construction, Tokyo, Oct., 1986.

[89] J.F. Chen, J.G. Teng: Anchorage Strength Models For FRP and Steel Plates Bonded to Concrete. In: J. Struct. Engrg., 127 (2001), Nr. 7, S. 784-791.

[90] Jankluvski, E. and Parsanejad, S.: *Hysteresis Behaviour of Plain Brick Masonry Walls: An Experimental Investigation*. In: Proceedings of Australasian Structural Engineering Conference, Sydney, 1994, pp. 679-683.

[91] Kachanov, L. M.: Time to the Rupture Process under Creep Conditions. In: Izv.Akad.Nauk USSR Otd. Techn. Nauk, 8 (1958), pp.26-31.

[92] Khalifa, A., Gold, W. J., Nanni, A., and Aziz, A: *Contribution of Externally Bonded FRP to Shear Capacity of RC Flexural Members*. In: J. Compos. For Constr., ASCE, 2 (1998), Nr. 4, S. 195-203.

[93] Kirtschig, K. and Kasten, D.: *Evaluation of Experiment Results.* Institut für Baustoffkunde und Material- Prüfung der Universität Hannover, 43(1979.

[94] Kirtschig, K. and Meyer, J.: *On the Load-Bearing Capacity of Constructed with Light Masonry Mortar.* In: Mauerwerk-Kalender, 1987, pp.471-87.

[95] Kloop, G. M. and Griffith, M.C.: *Earthquake Simulator Tests of Un-reinforced Brick Panels.* In: Australasian Conference on Mechanics of Structures and Materials, Wollongong, 1993, pp. 469-476.

[96] Kobatake, Y., Kimura, K., and ktsumata, H.: *A Retrofitting Method for Reinforced Concrete Structures using Carbon Fibre*/ A. Nanni (eds.). In: Fibre Reinforced-Plastic (FRP) Reinforcement for Concrete. Amsterdam: Elsevier Science, 1993 (Properties and application), S. 435-440.

[97] Krajcinovic, D., Fonseka, G. U.: *The Continuum Damage Theory of Brittle Materials, Part I and Part II. In: Journal of Applied Mechanics*, ASME, 48 (1981), pp. 809-824.

[98] Krajcinovic, D., Lemaitre, J.: *Continuum Damage Mechanics, Theory and Applications*. Springer, 1987.

[99] Krajcinovic, D.: *Damage Mechanics*, NY: Elsevier, 1996.

[100] Lacy, T. E, McDowell D.L., Willice, P.A. and Talreja R.: *On Representation of Damage Evolution in Continuum Damage Mechanics.* In: Int. J. of Damage Mechanics, 6(1997), pp.62-95.

[101] Laursen P.T., Seible, F., Hegmeir, G. A., and Innamrato, D.: *Seismic Retrofit and Repair of Masonry Walls with Carbon Overlays.* In: Non-Metallic (FRP) Reinforcement for Concrete Structures. (Taerwe, L.eds.), RILEM, 1995, pp.616-627.

[102] Lee, J.S., Pande, G.N. and Kralj, B.: *A comparative study on the approximate analysis of masonry structures*. In: Material and Structures Journal, 31(1998), pp.473-479.

[103] Lee, J.S., Pande, G.N., Liang, J.X., Kralj, B. and Middleton, J. '' *Analysis of Tensile Strength of Masonry.* In: *Proc. 10th Int. Brick/Block* Masonry Conf., Calgary, Canada, 1994, pp.21-29.

[104] Lemaître, J. : *A Course on Damage Mechanics*. Springer, 1990.

[105] Lemaître, J. and Chaboche, J.L.: *Mécanique des martiaux solides*, Dunod, Paris, 1985.

[106] Lemaître, J., Mazars, J.: *Application de la Theorie de L'endommagementau Comportment non-Lineaire et a la Rupture du Beton de Structure.* Am. Inst. Tech. Batim. Trav. Publics 401(1982), pp.115-138.

[107] Lemaître, J.: *A Course on Damage Mechanics*. Springer-Verlage, Berlin, 1992.

[108] Liang, J.X.: *''A Finite Element Equivalent Material Model for Structural Masonry'', PhD thesis, University of Wales Swansea, 1993.*

[109] Lourenco, P., Rots, J. and Blaawendraad, J.: *Two Approaches for the Analysis of Masonry Structures; micro and macro modelling*. Heron, 40(1995), No.4, pp.313-340.

[110] Lourenco, P.B. and Rots, J.G.: *On the Use of Homogenisation Techniques for the Analysis of Masonry Structures*, Delft, 3(1997).

[111] Lourenco, P.B., De Borst, R., and Rots, J.G., (1997).'' *A Plane Stress Softening Plasticity Model for Orthotropic Materials.* ''In: Int. J. Numer. Methods Eng., 40 (1997), pp. 4033-4057.''

[112] Lourenco, P.B.: *Computational Strategies for Masonry Structures*. Ph.D. Thesis, Delft University Press, Holland, February 1996.

[113] Lourenco, P.B.: *Computational Strategies for Masonry Structures*. Delft UP, 1995.

[114] Lourenco, P.B.: *Computational Strategy for Masonry Structures,* Delft University Press, and the Netherlands, 1996.

[115] Luciano, R. Sacco, E.: *A damage for Masonry Structures*. In: European Journal of Mechanics, A Solids, 17(1998), pp. 285-303.

[116] Luciano, R. Sacco, E.: *A damage of masonry panels reinforced by FRP sheets.* In: Int. J. of Solids and Struct., 35 (1998), No. 15, pp.1723-41.

[117] MacGregor, J. G.: *Reinforced Concrete: Mechanics and Design*/ Englewood Cliffs, N.J., Prentice-Hall, 1988.

[118] Maeda, T., Asano, Y., Sato, Y., Ueda, T., and Kakuta, Y.: *A Study on Bond*

Mechanism of Carbon Fibre Sheet. In Non-Metallic (FRP) Reinforcement for Concrete Struct., Proc., 3rd Int. Symp. Vol. 1, Japan: Concrete Institute, 1997, S. 279-.285.

[119] Maier, G. and Papa, E. and Nappi, A.: *On Damage and Failure of Brick Masonry*: In: Experimental and Numerical Methods in Earthquake Engineering, Donea, J. and Jones, M. (eds.), Netherlands, 1991, pp. 223-245.

[120] Malek, A. M., Saadamanesh, H., and Ehsani, M. R.: *Prediction of Failure Load of R/C Beams Strengthened with FRP Plate due to Stress Concentration at the Plate End.* IN: ACI Struct. J., 95 (1998), Nr. 1, S. 142-152.

[121] Mann, W. and Müller, H.: *Cracking Characteristics of Transversely Loaded Brick Masonry in Theory and Practice.* In: procc. 5th IBMaC Washington, 1979, page 239.

[122] Mann, W. and Müller, H.: *Failure of Shear Stressed Masonry-An Enlarged Theory, Tests and Application to Shear Walls*. In: Procc. Of the British Ceramic Society, No.30, 1982.

[123] Mann, W. and Müller, H.: *Schubtragfähigkeit von gemauerten Wänden und Voraussetzungen für das Entfallen des Windnachweises.* Mauerwerk-Kalender, Ernst&Sohn, Berlin, 1978, Seite 95.

[124] Mann, W. and Müller, H.: *Schubtragfähigkeit von Mauerwerk. In*: Mauerwerk-Kalender, Ernst&Sohn, Berlin, 1978, Seite 35.

[125] Mann, W., König, G. and Ötes, A.: *Tests of Masonry Walls Subjected to Seismic Forces.* In: procc. 8th International Brick and Block Masonry Conference, Ireland, 1988.

[126] Mann, W.: *Compressive Strength of Masonry, a Static Evaluation of Experimental Results in Closed Representation* Using Exponential Functions. In: Mauerwerk-Kalender, 1983, pp. 687-99.

[127] Marigo, J.J.: *Modelling of Brittle and Fatigue Damage for Elastic Material by Growth of Micro-voids*. In: Eng. Fract. Mech., 24(1985), No. 4, pp.861-874.

[128] Marsden, J.E. and Hughes T.J.R.; *Mathematical Foundations of Elasticity.* Prentice-Hall, Inc., Englewood Cliffs, 1983.

[129] Marzahn, G.A.: *Extended Investigation of Mechanical Properties of Masonry Units.* König and Heunisch Consulting Engineers, Leipzig, 04109, Germany, Lacer No. 7, 2002.

[130] Masiani, R., Rizzi, N and Trovalusci, P.: *Masonry as Structured Continuum*. In: Meccanica, 30 (1995), pp.673-83.

[131] Mazars, J. and Pijandier-Cabot, G.: *Continuum Damage Theory: Application to Concrete.* In: J.Eng. Mech., ASCE, 115(1989), pp.345-365.

[132] Mazars, J. : *Application de la mécanique de l'endommagement au comportement non linéaire et a la rupture du béton de structure.* ''Thèse de Doctorat d'Etat, L.M.T., Université Paris, France, 1984.

[133] Mazars, J., Pijaudier G.: *Continuum Damage Theory-Application to Concrete.* In: J. of Engrg. Mech., 115 (1989), Nr. 2, pp. 345-365.

[134] Mazars, J.: *A description of Micro- and Macro Scale Damage of Concrete Structures.* In: Eng. Fract. Mech., 25(1986), No. 5/6, pp. 729-737.

[135] Mazars, J.: *A Description of Micro-and-Macro-Scale Damage of Concrete Structure.* In: Engineering Fracture Mechanics, 25 (1986), Nr. 5/6, pp. 729-737.

[136] Mazars, J.: *A Model of Unilateral Elastic Damageable material and its application to Concrete*. In: Proceedings of the International Conference on Fracture Mechanics of Concrete, Lausanne, Switzerland, 1986.

[137] Mehlmann, M. and Oppermann, B.: *The Role of Masonry and Rendering Mortar in Modern Masonry Construction.* In: International Brick and Block Masonry Conference, Calgary, Canada, 1994, pp.139-149.

[138] Meskouris, K.: *Structural Dynamics, Models, Methods, Examples*. Germany: Ernst&Sohn, 2000.

[139] Mirabella Roberti, G., Binda, L. and Cardani, G.: *Numerical Modelling of Shear Bond Tests on Small Brick-Masonry Assemblages.* In: Compt.Meths in Struct. Masonry-4, UK., 1998.

[140] Mohamed, A., Stempniewski, L.: Damage Model for Masonry based on the Continuum Damage Theory. In: Earthquake Loss Estimation and Risk Reduction Conference, Bucharest, Romaina, 2002.

[141] Mojsilvoic, N. and Marti, P.: *Strength of Masonry Subjected to Combined Actions*. In: ACI Structural Journal, 94 [1997], No. 6, pp.633-642.

[142] Mojsilvoic, N.: *On the Response of Masonry Subjected to Combined Actions* (in German), Report No. 216, Institute of Structural Engineering, ETH Zurich, Dec. 1995.

[143] Müller, F. P, Keintzel, E.: *Erdbebensicherung von Hochbauten.* Berlin: Ernst&Sohn, 1978.

[144] Müller, F. P.: *Baudynamik*. In: Beton-Kalender II, Berlin: Ernst&Sohn, 1978.

[145] Müller, F. P.: *Erdbebensicherung von Bauwerken*: In: Deutsche Bauzeitung 11/80:

[146] Nationales Anwendungsdokument (NAD), Richtlinie zur Anwendung von DIN 1996-1-1, Eurocode 6, Bemessung und Konstruktion von Mauerwerksbauten-Teil 1-1: Allgemeine Regeln; Regeln für bewehrtes und unbewehrtes Mauerwerk, 1997.

[147] Nationales Anwendungsdokument (NAD), Richtlinie zur Anwendung von DIN V ENV 1996-1-1, Eurocode 6, Bemessung und Konstruktion von Mauerwerksbauten, Teil 1-1: Regeln für bewehrtes und unbewehrtes Mauerwerk, 1997.

[148] Neubauer, U., and Rostasy, F.S: *Design Aspects of Concrete Structures Strengthened with Externally Bonded CFRP Plates*. In: Proc., 7th Int. Conf. on Struct. Vol. 2, Scotland: ECS Publications, 1997, S. 109-118.

[149] Newmark, N.M: A Method of Computation for Structural Dynamics. In: ASCE, Journal of Engineering Mechanics Division, 85 (1959), pp. 67-94.

[150] Nichols, J.M. and Totoev, Y.Z.: *Criteria for Establishing a dynamic Test Loading Pattern for Masonry.* In: Australasian Structural Engineering Conference, Auckland, Sept 30-Oct 2, 1998.

[151] Nichols, J.M.: *A Study of the Progressive degradation of masonry shear walls subjected to Harmonic loading*. Ph.D. Thesis, University of Newcastle, 2000.

[152] Niedermeier, R.: *Stellungnahme zur Richtlinie für das Verkleben von Betonbauteilen durch Ankleben von Stahllaschen.* Technischen Universität München, Munich, Germany, Schreiben 1390 vom 30.10.1996 des Lehrstuhls für Massivbau, 1996.

[153] Oritz, M.: *A Constitutive Theory for the Inelastic Behaviour of Concrete*. In: Mechanics of Materials, 4 (1985), pp.67-93.

[154] Ötes, A.: *Vergleichende Untersuchungen zum Nachweis der Erdbebensicherung von repräsentativen Mauerwerksbauten in deutschen Erdbebengebieten nach DIN 4149 und Eurocode 8*. Forschungsbericht, Frankfurt am Main, 1992.

[155] Page, A. W.: *Finite Element model for Masonry*. In: Journal of the Structural Division, 104 (ST8, 1978), pp.1267-1285.

[156] Page, A.W. and Marshall R.: *The Influence of Brick and Brick Work Prism Aspect Ratio on the Evaluation of Compressive Strength.* In: Proc. Of the 7th International Brick Masonry Conference, Vol. I, Melbourne, Feb. 1985.

[157] Page, A.W., Kleeman, R.W. and Dhanasekar, M.: *An In-Plane Finite Element model for Brick Masonry*. In: New Analysis Techniques for Structural Masonry, Proceedings, ASCE Structures Congress, Chicago, (Anand, S.C., eds.), 1985, pp.1-18.

[158] Page, A.W., Samarasingle, W. And Hendry, A.W.: *The Failure of Masonry Shear Walls.* In: The International Journal of Masonry Construction, 1(1980), No. 2.

[159] Page, A.W., Samarasingle, W. And Hendry, A.W.: *The In-Plane Failure of Masonry-* A Review. In: Proc. of the 7th International Symposium on Load-Bearing Brickwork, London, Nov.1980.

[160] Page, A.W., Samarasinhe, W. and Hendry, A.W.: *The Failure of masonry Shear Walls*. In: International Journal of Masonry Construction, 1(1980), No.2, pp.52-57.

[161] Page, A.W.: *A biaxial Failure Criterion for Brick Masonry in the Tension-Tension* Range. In: International Journal of Masonry Construction, 1(1980), No.2, pp.26-29.

[162] Page, A.W.: *An Experimental Investigation of the Biaxial Strength of Brick Masonry.* In: Proc. of the 6th International Brick Masonry Conference, Rome, May 1982.

[163] Page, A.W.: *Influence of Material Properties on the Behaviour of Brick Masonry Shear Walls.* In: Proc. of the 8th International Brick/Block Masonry Conference, Dublin, Sep. 1988.

[164] Page, A.W.: *Masonry-Literature Review*. Newcastle: University of Newcastle, Australia, 1973.

[165] Page, A.W.: *The biaxial Compression Strength of Brick Masonry*. In: Proc. Instn. Civ. Engrs., Part 2, 71(1981), pp. 893-906.

[166] Page, A.W.: *The In-Plane Deformation and Failure of brickwork*., Diss., UN., 636, 1979.

[167] Page, A.W.: *The Strength of Brick Masonry under Biaxial Tension-Compression.* In: The International Journal of Masonry Construction, 3(1983), No. 1.

[168] Page, A.W: *Un-reinforced Masonry Structures-An Australian Overview.* Research Paper 15, Published in PDF (Acrobat) Format in May 2002.

[169] Pande, G.N., Liang, J. X. and Middleton, J.: *Analysis of the compressive strength of masonry given by the equation* $f_k = k\left(f_b{}'\right)^{\alpha}(f_m)^{\beta}$. In: Struct. Engnr. 71 (1994), pp. 7-12.

[170] Pande, G.N., Liang, J. X. and Middleton, J.: Equivalent *elastic modules for brick masonry.* In: Comput. Geotech. 8 (1989), pp. 243-265.

[171] Pande, G.N., Liang, J.X. and Middleton, J.: *Analysis of the Compressive Strength of Masonry given by the EC6 Equation.* In: The Structural Engineer, 71(1994), No. 1, pp. 7-12.

[172] Pande, G.N., Liang, J.X. and Middleton, J.: *Equivalent Elastic Modulus for Brick Masonry*. In Computers and Geotechnics, Elsevier Science Publishers, England, 1990, pp. 243-265.

[173] Pande, G.N., Middleton, J., Lee, J.S. and Kralj, B.: *Numerical Simulation of Cracking and Collapse of Masonry. In: International Brick and Block Masonry* Conference, Calgary, Canada, 1994.

[174] Papa; E. A.: *A uni-lateral damage model for masonry based on a homogenisation procedure.* In: mechanics of Cohesive-Frictional Materials, 1 (1996), pp. 349-366.

[175] Powell, B. and Hodgkinson, H.R.: *The Determination of Stress/Strain Relationship of Brickwork.* In: Masonry Conference, Brugge, Apr. 1976.

[176] Powell, G.H.: *Seismic damage prediction by deterministic method: Concepts and procedures.* In: Earthquake Engineering and Structural Dynamics, 16(1988), pp.719-734.

[177] PrEN 1998-1 draft: Euro code 8: Design of Structures for Earthquake Resistance, Part 1: general Rules, Seismic Actions and Rules for Buildings, May, 2002.

[178] Priestley, M.J.N.: *Seismic Behaviour of Un-reinforced Masonry Walls*. In: Bulletin of New Zealand Society for Earthquake Engineering, 18(1985), No. 2, pp.191-205.

[179] Referatensammlung: Eurocode 8/DIN 4149, neue Regeln bei der Auslegung von Bauwerken gegen Erdbeben, 1998.

[180] Resende, L. and Martin, J.B.: *A progressive Damage Continuum model for Granular Materials*. In: Comp. Meth. Appl. Mech. Eng., 42(1984), pp. 1-18.

[181] Resende, L.: *A Damage Mechanics Constitutive Theory for the Inelastic Behaviour of Concrete.* In: Comp. Meth. Appl. Mech. Eng., 60(1987), pp. 57-93.

[182] Roberts, T. M.: *Approximation Analysis of Shear and Normal Stress Concentrations in The Adhesive Layer of Plated RC Beams.* In: The Struct. Engr. , 67 (1989), Nr. 12/20, S. 229-233.

[183] Rosman R.: *Erdbebenwiderstandfähiges Bauen*. Berlin: Ernst&Sohn, 1983.

[184] Saetta, A., Scotta, R. and Vitaliani R.: *An Orthotropic Fourth-Rank Damage Model for Masonry Structures.* In: European Congress on Computational Methods in Applied Sciences and Engineering, Eccomas, Barcelona, 11-14 Sept., 2000.

[185] Saetta, A., Scotta, R., and Vitaliani, R.: *An Orthotropic Second-Rank Damage Model for Masonry*. In: Proc. Eccomas, Barcelona, Spain, September 11-14, 2000.

[186] Sato, Y., Ueda, T., Kakuta, Y., and Tanaka, T.: *Shear Reinforcing Effect of Carbon Fibre Sheet Attached to Side of Reinforced Concrete Beams*. El-Badry (eds.) In Proc., 2nd Int. Conf. on Advanced Compos. Mat. In Bridges and Struct. Montreal: Canadian Society for Civil Engineering, 1996, S. 621-627.

[187] Schneider, R: R., Dickes, W.L.: *Reinforced Masonry Design*. Prentice-Hall, Inc.: Newjersy, 1980.

[188] Schubert, P.: *Compressive and Tensile Strength of Masonry*. In: procc. 8th International Brick and Block Masonry Conference, Ireland, 1988, pp. 406-419.

[189] Schwegler G.: *Masonry Construction Strengthened with Fibre Composites in Seismically Endangered Zones*. In: Proc. of the Tenth European Conference on Earthquake Engineering, Rotterdam, 1995, pp. 2299-2303.

[190] Schwegler, G. and Kelterborn, P.: *Earthquake Resistance of Masonry Structures Strengthened with Fibre Composites*. In: Eleventh World Conference on Earthquake Engineering, Acapilco, Mexico, June 23-28, 1996.

[191] Schwegler, G.: *Verstärken von Mauerwerk mit Faserverbundwerkstoffen in seismisch gefährdeten Zonen.* Bericht Nr. 229, Eidgenössische Material-prüfungs-und Forschungsanstalt, EMPA, Zürich, 1994.

[192] Sedlacek, G.: *Erdbebenberechnung von Bauwerke im internationalen Vergleich.* In: Deutsche Bauzeitung 11/80.

[193] Shing, P.B., Nakashima, M., Bursi, O.S*.: Application of Pseudodynamic test Method to Structural Research.* In: Earthquake Spectra, 12(1996), Nr.1.

[194] Shiono, K.: *Interpretation of Published data of the 1976 Tangshan, China Earthquake for the determination of a fatability rate function*. Japan Society of Civil Engineers, Structural Engineering, Earthquake Engineering, 11(1995) No. 4, pp.1555-1635

[195] Sika Technisches Merkblatt 1.99: *Technisches Merkblatt zum Kohlenstofffaser-Gewebe-Verstärkungssystem SikaWarp Hex-230C/Sikadur-330.*

[196] Simo, J.C., Ju, J.W.: *Strain-and Stress-Based Continuum Damage Models-I Formulation.* In: J.Solids Structures, 23(1987), pp.821-840.

[197] Simo, J.C., JU, J.W.: *Strain-and stress-based continuum damage models-I. Formulation-II. Computational aspects*. In Int. J.Solids Structures, 23 (1987), pp.821-869.

[198] Simo, J.C., Taylor, R.L.: *Quasi-Incompressible Finite Elasticity in Principal Stretches: Continuum Basis and Numerical Algorithms*. In: Appl.Mech. Engrg., 85(1991), pp.273-310.

[199] Simo, J.C.: *On a Fully Three-Dimensional Finite-Strain Visco-Elastic Damage Model: Formulation and Computational Aspects.* In: Comput. Meths. Appl. Mech. Engrg., 60(1987), pp.153-157.

[200] Sinha, B.P. and Pedreschi, R.: *Compressive Strength and some Elastic Properties of Brickwork.* In: The International Journal of Masonry Construction, 3(1983), No. 1.

[201] Smith, S. T., Teng, J. G., and Chen, J. F.: *Debonding in FRP Plated RC Beams induced by Intermediate Cracking.* In: Proc. , ACUN-3 Int. Conf. : Technol. Convergence in Compos. Applications. Australia, 2001, S. 67-72.

[202] Stempniewski, L.: *Schadensprognose-Methoden zur nachträglichen Ertüchtigung bestehender evtl. vorgeschädigter Bauwerke*. Teilprojekt C2 Bericht, Universität Karlsruhe, 2001.

[203] Swamy, R. N., Jones, R., and Charif, A.: *Shear Adhesion Properties of Epoxy Resin Adhesives. In: Proc., Int. Symp. on Adhesion between Polymers and Concrete.* Chapman and Hall, London, 1986, S. 741-755.

[204] Täljsten, B.: *Defining Anchor Lengths of Steel and CFRP Plates Bonded to Concrete.* In: Int. J. Adhesion and Adhesive, 17 (1997), Nr. 4, S. 319-327.

[205] Täljsten, B.: *Plate Bonding: Strengthening of Existing Concrete Structures with Epoxy Bonded Plates of Steel or Fibre Reinforced Plastics*. Lulea University, Sweden, Diss., 1994.

[206] Tanaka, T.: Shear resisting Mechanism of Reinforced Concrete Beams with CFS as Shear Reinforcement. Hokkaido University, Japan, Diss., 1996.

[207] Teng, J. G., Chen, J.F., Smith, S. T., and Lam, L.: *RC Structures Strengthened with FRP Composites.* The Hong Kong Polytechnic University, Hong Kong, China, 2000.

[208] Tercelj, S., Sheppard, P. and Turnsek, V.: *The influence of Frequency on the Shear Strength and Ductility of Masonry Walls in Dynamic Loading Tests.* In: Procc. of the Fifth International Conference on Earthquake Engineering, 3(1969), pp. 2292-9.

[209] Third Inter. Conf. on Advanced Composite Materials in Bridges and Structures, Ottawa, Canada, Humar, J. and Razaqpur (eds.), 15-18 Aug. 2000.

[210] Tinazzi, D., Modena, C. and Nanni, A.: *Strengthening of Masonry Assemblages with FRP Rods and Laminates.* In: Procc. Advancing with Composites, Italy, May 9-11, 2000, pp.411-418.

[211] Triantafillou, T. C., and Plevris, N.: *Strengthening of RC Beams with Epoxy-Bonded Fibre-Composites Materials.* In: Mat. And Struct., 25 (1992), S. 201-211.

[212] Tumialan, G., Myers, J.J. and Nanni, A.: *Field Evaluation of Un-reinforced Masonry Walls Strengthened with FRP Composites Subjected to Out-of-Plane Loading.* In: ASCE Structures Congress, Philadelphia, (M.Elgaaly, eds.), May 8-10,2000.

[213] Van Gemert, D.: *Force Transfer in Epoxy-Bonded Steel-Concrete Joints. In: Int. J. Adhesion and Adhesives*, 1 (1980), S. 67-72.

[214] Varastehpour, H., and Hamelin, P.: *Analysis and Study of Failure Mechanism of RC Beams Strengthened with FRP Plate*. El-Badry (eds.) In Proc., 2nd Int. Conf. on Advanced Compos. Mat. In Bridges and Struct. Montreal: Canadian Society for Civil Engineering, 1996, S. 527-537.

[215] Volnyy, V. A., and Pantelides, C. P.: *Bond Length of CFRP Composites attached to precast Concrete Walls.* In: J. Compos. For Constr., ASCE, 3 (1999), Nr. 4, S. 168-176.

[216] Vratsanou, V.: *Das nichtlineare Verhalten unbewehrter Mauerwerkscheiben unter Erdbebenbeanspruchung- Hilfsmittel zur Bestimmung der q-Faktoren*. Universität Karlsruhe, Germany, Diss., 1992.

[217] Wakabayashi, M.: *Design of Earthquake-Resistant Buildings*. McGraw Hill Book Company, 1986.

[218] Wilson, E.L., Farhoomand, Bath, K.J.: Non-linear Dynamic Analysis of Complex Structures. In: International Journal of Earthquake Engineering and Structural Dynamics, 1 (1973), pp. 241-252

[219] Wood, P.E.: *Load Distribution of Masonry Walls Subject to Concentrated Loads over Openings*. Ph.D. Thesis, University of Pittsburgh, 1998.

[220] Yuan, H., and Wu, Z. S., and Yoshizawa, H.: *Theoretical Solutions on*

Interfacial Stress Transfer of Externally Bonded Steel/Composite Laminates. In: J. Struct. Mech. And Earthquake Engrg., Tokyo, 2001.

[221] Yuan, H., and Wu, Z. S: *Interfacial Fracture Theory in Structures Strengthened with Composites of Continuous Fibre. In: Proc., Symp. of China and Japan: Sci. and Technol. of 21 Century*, Tokyo, Sept., 1999, S. 142-155.

[222] Zhang, S., Raoof, M., and Wood, L.A.: *Prediction of Peeling Failure of Reinforced Concrete Beams with Externally Bonded Plates*. In: Proc., Inst. of Civ. Engrs., Struct. and Build., Vol. 122. London, 1997, S. 493-496.

[223] Zhao, Y.H. and Weig, G.J.: *Effective Elastic Moduli of Ribbon-Reinforced Composites*. In: J. Appl. Mech., 57(1990), pp.158-167.

[224] Zhuge, Y., Thambiratnam, D. and Corderoy, J.: *Experimental Testing of Masonry Walls under In-Plane Cyclic Loads.* In: Proceedings, 10th IBMAC, Calgary, July 1994, pp. 313-323.

[225] Zienkiewicz, O.C.: *The Finite Element Method*. New York: McGraw-Hill Company, 3rd Ed., 1977.

[226] Ziraba, Y. N., Baluch, M. H., Basunbul, A. M., Azad, A. K., Al-Sulaimani, G.J., and Sharif, I. A.: *Combined Experimental-Numerical Approach to Characterization of Steel-Glue-Concrete Interface*. In: Mat. And Struct. Vol.28, Paris, 1995, S. 518-525.

Appendices

Appendix A: Orthotropic Material Properties of Masonry

Derivations of the equivalent orthotropic material properties of the masonry, which includes brick and bed as well as perpend mortar joint, are based on the strain energy criterion. Referring to Figure 3.2, the volume fraction of brick and bed joint can be described as

$$\mu_b = \frac{h_b}{h_b + t_{bj}}; \mu_{bj} = \frac{t_{bj}}{h_b + t_{bj}} \tag{A.1}$$

where subscripts b and b_j represents the brick and bed joints, respectively. Assuming homogenous, isotropic properties of constituent materials and defining the following coefficients

$$\alpha = \frac{\mu_b E_b (1-u_{bj}^2) + \mu_{bj} E_{bj} (1-u_b^2)}{(1-u_b^2)(1-u_{bj}^2)}$$

$$\zeta = \frac{\mu_b u_b E_b (1-u_b^2) + \mu_{bj} u_{bj} E_{bj} (1-u_{bj}^2)}{(1-u_b^2)(1-u_{bj}^2)}$$

$$X_b = \frac{\mu_b u_b}{(1-u_b)}$$

$$X_{bj} = \frac{\mu_{bj} u_{bj}}{(1-u_{bj})} \tag{A.2}$$

$$X = X_b + X_{bj}$$

The following orthotropic material properties for the layer homogenized with brick and bed joint are obtained as

$$
\begin{aligned}
&E_x^{/} = \alpha - \zeta \upsilon_{xz}^{/} \\
&\frac{1}{E_y^{/}} = \frac{\mu_b}{E_b} + \frac{\mu_{bj}}{E_{bj}} + 2\chi_b\left(\frac{\upsilon_{zy}^{/}}{E_z^{/}} - \frac{\upsilon_b}{E_b}\right) + 2\chi_{bj}\left(\frac{\upsilon_{zy}^{/}}{E_z^{/}} - \frac{\upsilon_{bj}}{E_{bj}}\right) \\
&E_z^{/} = \alpha - \zeta \upsilon_{xz}^{/} = E_x^{/} \\
&\frac{1}{G_{xy}^{/}} = \frac{\mu_b}{G_b} + \frac{\mu_{bj}}{G_{bj}} \\
&\frac{1}{G_{yz}^{/}} = \frac{\mu_b}{G_b} + \frac{\mu_{bj}}{G_{bj}} \\
&G_{xz}^{/} = \mu_b G_b + \mu_{bj} G_{bj} \\
&\upsilon_{xz}^{/} = \frac{\zeta}{\alpha} \\
&\upsilon_{xy}^{/} = \chi(1 - \upsilon_{xz}^{/}) \\
&\upsilon_{zx}^{/} = \upsilon_{xz}^{/} \\
&\upsilon_{zy}^{/} = \chi(1 - \upsilon_{zx}^{/})
\end{aligned}
\tag{A.3}
$$

and the relationship below also is established

$$
\upsilon_{yx}^{/} = \upsilon_{xy}^{/} \frac{E_y^{/}}{E_x^{/}} \tag{A.4}
$$

For the system of masonry walls, the homogenisation is applied to the layered material and perpend joint , respectively, based on the assumption of continuous perpend joint. Now, volume fractions of the constituent materials are

$$
\mu_{eq} = \frac{l_b}{l_b + t_{hj}};\ \mu_{hj} = \frac{t_{hj}}{l_b + t_{hj}}, \tag{A.5}
$$

where, subscript eq and h_j represent layered material and perpend joint, respectively. Defining the following coefficients

$$
\begin{aligned}
\overline{\alpha} &= \frac{\mu_{eq} E_y^{/}}{(1-\upsilon_{yz}^{/}\upsilon_{zy}^{/})} + \frac{\mu_{hj} E_{hj}}{(1-\upsilon_{hj}^{2})} \\
\overline{\beta} &= \frac{\mu_{eq} E_z^{/}}{(1-\upsilon_{yz}^{/}\upsilon_{zy}^{/})} + \frac{\mu_{hj} E_{hj}}{(1-\upsilon_{hj}^{2})} \\
\overline{\zeta} &= \frac{\mu_{eq} \upsilon_{yz}^{/} E_z^{/}}{(1-\upsilon_{yz}^{/}\upsilon_{zy}^{/})} + \frac{\mu_{hj} \upsilon_{hj}^{/} E_{hj}}{(1-\upsilon_{hj}^{2})} \\
\overline{X}_{eq} &= \frac{\mu_{eq}(\upsilon_{zx}^{/} + \upsilon_{yx}^{/}\upsilon_{zy}^{/})}{(1-\upsilon_{yz}^{/}\upsilon_{zy}^{/})} \\
\overline{X}_{hj} &= \frac{\mu_{hj}\upsilon_{hj}}{(1-\upsilon_{hj})} \\
\overline{X} &= \overline{X}_{eq} + \overline{X}_{hj} \\
\overline{\lambda}_{eq} &= \frac{\mu_{eq}(\upsilon_{yx}^{/} + \upsilon_{yz}^{/}\upsilon_{zx}^{/})}{(1-\upsilon_{yz}^{/}\upsilon_{zy}^{/})} \\
\overline{\lambda}_{hj} &= \frac{\mu_{hj}\upsilon_{hj}}{(1-\upsilon_{hj})} \\
\overline{\lambda}_{eq} &= \overline{\lambda}_{eq} + \overline{\lambda}_{hj}
\end{aligned}
\qquad \text{(A.6)}
$$

The orthotropic material properties of the masonry panel are derived as

$$\frac{1}{\overline{E}_x} = \frac{\mu_{eq}}{E_x^{/}} + \frac{\mu_{hj}}{E_{hj}} + \overline{\lambda}_{eq}\left(\frac{\overline{\upsilon}_{yx}}{\overline{E}_y} - \frac{\upsilon_{xy}^{/}}{E_x^{/}}\right) + \overline{\lambda}_{hj}\left(\frac{\overline{\upsilon}_{yx}}{\overline{E}_y} - \frac{\upsilon_{hj}^{/}}{E_{hj}}\right)$$
$$+ \overline{\chi}_{eq}\left(\frac{\overline{\upsilon}_{zx}}{\overline{E}_z} - \frac{\upsilon_{xz}^{/}}{E_x^{/}}\right) + \overline{\chi}_{hj}\left(\frac{\overline{\upsilon}_{zx}}{\overline{E}_z} - \frac{\upsilon_{hj}^{/}}{E_{hj}}\right)$$

$$\overline{E}_y = \frac{\overline{\alpha}\,\overline{\beta} - \overline{\zeta}^2}{\overline{\beta}}$$

$$\overline{E}_z = \frac{\overline{\alpha}\,\overline{\beta} - \overline{\zeta}^2}{\overline{\alpha}}$$

$$\frac{1}{\overline{G}_{xy}} = \frac{\mu_{eq}}{G_{xy}^{/}} + \frac{\mu_{hj}}{G_{hj}}$$

$$\overline{G}_{yz} = \mu_{eq} G_{yz}^{/} + \mu_{hj} G_{hj}$$

$$\frac{1}{\overline{G}_{xz}} = \frac{\mu_{eq}}{G_{xz}^{/}} + \frac{\mu_{hj}}{G_{hj}}$$

$$\overline{\upsilon}_{yx} = \overline{\lambda} - \frac{\overline{\zeta}\,\overline{\chi}}{\overline{\beta}}$$

$$\overline{\upsilon}_{yz} = \frac{\overline{\zeta}}{\overline{\beta}} \qquad \text{(A.7)}$$

$$\overline{\upsilon}_{zx} = \overline{\chi} - \frac{\overline{\zeta}\,\overline{\lambda}}{\overline{\alpha}}$$

$$\overline{\upsilon}_{zy} = \frac{\overline{\zeta}}{\overline{\alpha}}$$

Appendix B: Structural Relationship of Masonry Constituent Materials

A general form of structural matrix S can be written as

$$[S]=\begin{pmatrix} S_{11} & S_{12} & S_{13} & 0 & 0 & 0 \\ S_{21} & S_{22} & S_{22} & 0 & 0 & 0 \\ S_{31} & S_{32} & S_{33} & 0 & 0 & 0 \\ 0 & 0 & 0 & S_{44} & 0 & 0 \\ 0 & 0 & 0 & 0 & S_{55} & 0 \\ 0 & 0 & 0 & 0 & 0 & S_{66} \end{pmatrix} \tag{B.1}$$

and the non-zero components of structural matrix between perpend joint and equivalent material $\left[S_{hj}\right]$ are

$$\begin{aligned} &S_{hj,11}=1.0 \quad S_{hj,44}=1.0 \quad S_{hj,66}=1.0 \\ &S_{hj,21}=\frac{u_{hj}}{1-u_{hj}}-C_{hj}\left(\frac{\bar{u}_{yx}}{\bar{E}_y}+\frac{\bar{u}_{zx}u_{hj}}{\bar{E}_z}\right) \\ &S_{hj,22}=C_{hj}\left(\frac{1}{\bar{E}_y}-\frac{\bar{u}_{zy}u_{hj}}{\bar{E}_z}\right) \\ &S_{hj,23}=C_{hj}\left(\frac{u_{hj}}{\bar{E}_z}-\frac{\bar{u}_{yz}}{\bar{E}_y}\right) \\ &S_{hj,31}=\frac{u_{hj}}{1-u_{hj}}-C_{hj}\left(\frac{\bar{u}_{zx}}{\bar{E}_z}+\frac{\bar{u}_{yx}u_{hj}}{\bar{E}_y}\right) \\ &S_{hj,32}=C_{hj}\left(\frac{u_{hj}}{\bar{E}_y}-\frac{\bar{u}_{zy}}{\bar{E}_z}\right) \\ &S_{hj,22}=C_{hj}\left(\frac{1}{\bar{E}_z}-\frac{\bar{u}_{yz}u_{hj}}{\bar{E}_y}\right) \\ &S_{hj,55}=\frac{G_{hj}}{\bar{G}_{yz}} \end{aligned} \tag{B.2}$$

where

$$C_{hj}=\frac{E_{hj}}{1-u_{hj}^2} \tag{B.3}$$

To derive structural matrices of brick and bed joint, the structural relationship for layered system $\left[S^{\prime}\right]$ is established first. That is

$$
\begin{aligned}
&S_{11}^{\prime}=1.0 \quad S_{44}^{\prime}=1.0 \quad S_{66}^{\prime}=1.0 \\
&S_{21}^{\prime}=C^{\prime}\left\{(u_{yx}^{\prime}+u_{yz}^{\prime}u_{zx}^{\prime})-\frac{\bar{u}_{yx}E_{y}^{\prime}}{\bar{E}_{y}}-\frac{\bar{u}_{zx}u_{yz}^{\prime}E_{z}^{\prime}}{\bar{E}_{z}}\right\} \\
&S_{22}^{\prime}=C^{\prime}\left\{\frac{E_{y}^{\prime}}{\bar{E}_{y}}-\frac{\bar{u}_{zy}u_{yz}^{\prime}E_{z}^{\prime}}{\bar{E}_{z}}\right\} \\
&S_{23}^{\prime}=C^{\prime}\left\{\frac{u_{yz}^{\prime}E_{z}^{\prime}}{\bar{E}_{z}}-\frac{\bar{u}_{yz}E_{y}^{\prime}}{\bar{E}_{y}}\right\} \\
&S_{31}^{\prime}=C^{\prime}\left\{(u_{zx}^{\prime}+u_{zy}^{\prime}u_{yx}^{\prime})-\frac{\bar{u}_{zx}E_{z}^{\prime}}{\bar{E}_{z}}-\frac{\bar{u}_{yx}u_{zy}^{\prime}E_{y}^{\prime}}{\bar{E}_{y}}\right\} \\
&S_{32}^{\prime}=C^{\prime}\left\{\frac{u_{zy}^{\prime}E_{y}^{\prime}}{\bar{E}_{y}}-\frac{\bar{u}_{zy}E_{y}^{\prime}}{\bar{E}_{z}}\right\} \\
&S_{33}^{\prime}=C^{\prime}\left\{\frac{E_{z}^{\prime}}{\bar{E}_{z}}-\frac{\bar{u}_{yz}u_{zy}^{\prime}E_{z}^{\prime}}{\bar{E}_{y}}\right\} \\
&S_{55}^{\prime}=\frac{G_{yz}^{\prime}}{\bar{G}_{yz}}
\end{aligned}
\tag{B.4}
$$

where

$$
C^{\prime}=\frac{1}{1-u_{yz}^{\prime}u_{zy}^{\prime}} \tag{B.5}
$$

Finally, structural matrices of brick and bed joints $[S_b]$ and $\left[S_{bj}\right]$ are derived from the following relationships

$$
\begin{aligned}
\sigma_{b}&=[S_{b}]\sigma^{\prime} \\
\sigma_{bj}&=\left[S_{bj}\right]\sigma^{\prime}
\end{aligned}
\tag{B.6}
$$

where the general form of $[P]$ has the same form as in (B.1) and, for brick

$$
\begin{aligned}
&P_{b,22} = 1.0 \quad P_{b,44} = 1.0 \quad P_{b,55} = 1.0 \\
&P_{b,11} = C_b \left(\frac{E_b}{E_x^{/}} - \frac{u_{zx}^{/} u_b E_b}{E_z^{/}} \right) \\
&P_{b,12} = C_b \left\{ u_v (1 + u_b) - \left(\frac{u_{xy}^{/} E_b}{E_x^{/}} - \frac{u_{zy}^{/} u_b E_b}{E_z^{/}} \right) \right\} \\
&P_{b,13} = C_b \left(\frac{u_b E_b}{E_z^{/}} - \frac{u_{zx}^{/} E_b}{E_x^{/}} \right) \\
&P_{b,31} = C_b \left(\frac{u_b E_b}{E_x^{/}} - \frac{u_{zx}^{/} E_b}{E_z^{/}} \right) \\
&P_{b,32} = C_b \left\{ u_v (1 + u_b) - \left(\frac{u_{xy}^{/} E_b}{E_z^{/}} - \frac{u_{xy}^{/} u_b E_b}{E_x^{/}} \right) \right\} \\
&P_{b,33} = C_b \left(\frac{E_b}{E_z^{/}} - \frac{u_{xz}^{/} u_b E_b}{E_x^{/}} \right) \\
&P_{b,66} = \frac{G_b}{G_{xz}^{/}}
\end{aligned}
\tag{B.7}
$$

where

$$
C_b = \frac{1}{1 - u_b^2} \tag{B.8}
$$

also for the bed joints

$$
\begin{aligned}
&P_{bj,22} = 1.0 \quad P_{bj,44} = 1.0 \quad P_{bj,55} = 1.0 \\
&P_{bj,11} = C_{bj}\left(\frac{E_{bj}}{E_x^{/}} - \frac{u_{zx}^{/} u_{bj} E_{bj}}{E_z^{/}}\right) \\
&P_{bj,12} = C_{bj}\left\{u_{bj}(1+u_{bj}) - \left(\frac{u_{xy}^{/} E_{bj}}{E_x^{/}} + \frac{u_{zy}^{/} u_{bj} E_{bj}}{E_z^{/}}\right)\right\} \\
&P_{bj,13} = C_{bj}\left(\frac{u_{bj} E_{bj}}{E_z^{/}} - \frac{u_{xz}^{/} E_{bj}}{E_x^{/}}\right) \\
&P_{bj,31} = C_{bj}\left(\frac{u_{bj} E_{bj}}{E_x^{/}} - \frac{u_{zx}^{/} E_{bj}}{E_z^{/}}\right) \\
&P_{bj,32} = C_{bj}\left\{u_{bj}(1+u_{bj}) - \left(\frac{u_{zy}^{/} E_{bj}}{E_z^{/}} + \frac{u_{xy}^{/} u_{bj} E_{bj}}{E_x^{/}}\right)\right\} \\
&P_{bj,33} = C_{bj}\left(\frac{E_{bj}}{E_z^{/}} - \frac{u_{xz}^{/} u_{bj} E_{bj}}{E_x^{/}}\right) \\
&P_{bj,66} = \frac{G_{bj}}{G_{xz}^{/}}
\end{aligned}
\tag{B.9}
$$

where

$$
C_{bj} = \frac{1}{1-u_{bj}^2} \tag{B.10}
$$

From (B.5) and (B.6)

$$
\begin{aligned}
&\sigma_b = [P_b]\left[S^{/}\right]\sigma^{/} = [S_b]\sigma^{/} \\
&\sigma_{bj} = \left[P_{bj}\right]\left[S^{/}\right]\sigma^{/} = \left[S_{bj}\right]\sigma^{/}
\end{aligned}
\tag{B.11}
$$

where

$$
\begin{aligned}
&S_b = [P_b]\left[S^{/}\right] \\
&S_{bj} = \left[P_{bj}\right]\left[S^{/}\right]
\end{aligned}
\tag{B.12}
$$

Schriftenreihe des
Instituts für Massivbau und Baustofftechnologie

Herausgeber:
Prof. Dr.-Ing. Harald S. Müller und Prof. Dr.-Ing. Lothar Stempniewski
ISSN 0933-0461

Heft 1 Manfred Curbach: *Festigkeitssteigerung von Beton bei hohen Belastungsgeschwindigkeiten*. 1987

Heft 2 Franz-Hermann Schlüter: *Dicke Stahlbetonplatten unter stoßartiger Belastung - Flugzeugabsturz*. 1987

Heft 3 Marlies Schieferstein: *Der Zugflansch von Stahlbetonplattenbalken unter Längsschub und Querbiegung bei kritischer Druckbeanspruchung von Beton*. 1988

Heft 4 Thomas Bier: *Karbonatisierung und Realkalisierung von Zementstein und Beton*. 1988

Heft 5 Wolfgang Brameshuber: *Bruchmechanische Eigenschaften von jungem Beton*. 1988

Heft 6 Bericht DFG-Forschungsschwerpunkt: *Durability of Non-Metallic Inanorganic Building Materials*. 1988

Heft 7 Manfred Feyerabend: *Der harte Querstoß auf Stützen aus Stahl und Stahlbeton*. 1988

Heft 8 Klaus F. Schönlin: *Permeabilität als Kennwert der Dauerhaftigkeit von Beton*. 1989

Heft 9 Lothar Stempniewski: *Flüssigkeitsgefüllte Stahlbetonbehälter unter Erdbebeneinwirkung*. 1990

Heft 10 Jörg Weidner: *Vergleich von Stoffgesetzen granularer Schüttgüter zur Silodruckermittlung*. 1990

Heft 11 Pingli Yi: *Explosionseinwirkungen auf Stahlbetonplatten*. 1991

Heft 12 Rainer Kunterding: *Beanspruchung der Oberfläche von Stahlbetonsilos durch Schüttgüter*. 1991

Heft 13 Peter Haardt: *Zementgebundene und kunststoffvergütete Beschichtungen auf Beton*. 1991

Heft 14 Günter Rombach: *Schüttguteinwirkungen auf Silozellen - Exzentrische Entleerung*. 1991

Heft 15 Harald Garrecht: *Porenstrukturmodelle für den Feuchtehaushalt von Baustoffen mit und ohne Salzbefrachtung und rechnerische Anwendung auf Mauerwerk*. 1992

Heft 16 Violandi Vratsanou: *Das nichtlineare Verhalten unbewehrter Mauerwerksscheiben unter Erdbebenbeanspruchung - Hilfsmittel zur Bestimmung der q-Faktoren*. 1992

Heft 17 Carlos Rebelo: *Stochastische Modellierung menschenerzeugter Schwingungen*. 1992

Heft 18 Seminar 29./30. März 1993: *Erdbebenauslegung von Massivbauten unter Berücksichtigung des Eurocode 8*. 1993

Heft 19 Hubert Bachmann: *Die Massenträgheit in einem Pseudo-Stoffgesetz für Beton bei schneller Zugbeanspruchung*. 1993

Heft 20 DBV/AiF-Forschungsbericht: H. Emrich: *Zum Tragverhalten von Stahlbetonbauteilen unter Querkraft- und Längszugbeanspruchung.* 1993

Heft 21 Robert Stolze: *Zum Tragverhalten von Stahlbetonplatten mit von den Bruchlinien abweichender Bewehrungsrichtung - Bruchlinien-Rotationskapazität*. 1993

Heft 22 Jie Huang: *Extern vorgespannte Segmentbrücken unter kombinierter Beanspruchung aus Biegung, Querkraft und Torsion*. 1994

Heft 23 Rolf Wörner: *Verstärkung von Stahlbetonbauteilen mit Spritzbeton*. 1994

Heft 24 Ioannis Retzepis: *Schiefe Betonplatten im gerissenen Zustand*. 1995

Heft 25 Frank Dahlhaus: *Stochastische Untersuchungen von Silobeanspruchungen.* 1995

Heft 26 Cornelius Ruckenbrod: *Statische und dynamische Phänomene bei der Entleerung von Silozellen.* 1995

Heft 27 Shishan Zheng: *Beton bei variierender Dehngeschwindigkeit, untersucht mit einer neuen modifizierten Split-Hopkinson-Bar-Technik.* 1996

Heft 28 Yong-zhi Lin: *Tragverhalten von Stahlfaserbeton.* 1996

Heft 29 DFG: *Korrosion nichtmetallischer anorganischer Werkstoffe im Bauwesen.* 1996

Heft 30 Jürgen Ockert: *Ein Stoffgesetz für die Schockwellenausbreitung in Beton.* 1997

Heft 31 Andreas Braun: *Schüttgutbeanspruchungen von Silozellen unter Erdbebeneinwirkung.* 1997

Heft 32 Martin Günter: *Beanspruchung und Beanspruchbarkeit des Verbundes zwischen Polymerbeschichtungen und Beton.* 1997

Heft 33 Gerhard Lohrmann: *Faserbeton unter hoher Dehngeschwindigkeit.* 1998

Heft 34 Klaus Idda: *Verbundverhalten von Betonrippenstäben bei Querzug.* 1999

Heft 35 Stephan Kranz: *Lokale Schwind- und Temperaturgradienten in bewehrten, oberflächennahen Zonen von Betonstrukturen.* 1999

Heft 36 Gunther Herold: *Korrosion zementgebundener Werkstoffe in mineralsauren Wässern.* 1999

Heft 37 Mostafa Mehrafza: *Entleerungsdrücke in Massefluss-Silos - Einflüsse der Geometrie und Randbedingungen.* 2000

Heft 38 Tarek Nasr: *Druckentlastung bei Staubexplosionen in Siloanlagen.* 2000

Heft 39 Jan Akkermann: *Rotationsverhalten von Stahlbeton-Rahmen-ecken.* 2000

Heft 40 Viktor Mechtcherine: *Bruchmechanische und fraktologische Untersuchungen zur Rißausbreitung in Beton.* 2001

Heft 41 Ulrich Häußler-Combe: *Elementfreie Galerkin-Verfahren – Grundlagen und Einsatzmöglichkeiten zur Berechnung von Stahlbetontragwerken.* 2001

Heft 42 Björn Schmidt-Hurtienne: *Ein dreiaxiales Schädigungsmodell für Beton unter Einschluß des Dehnrateneffekts bei Hochgeschwindigkeitsbelastung.* 2001

Heft 43 Nazir Abdou: *Ein stochastisches nichtlineares Berechnungsverfahren für Stahlbeton mit finiten Elementen.* 2002

Heft 44 Andreas Plotzitza: *Ein Verfahren zur numerischen Simulation von Betonstrukturen beim Abbruch durch Sprengen.* 2002

Heft 45 Timon Rabczuk: N*umerische Untersuchungen zum Fragmentierungsverhalten von Beton mit Hilfe einer netzfreien Lagrangemethode.* 2002

Heft 46 Norbert J. Krutzik: *Zu Anwendungsgrenzen von FE-Modellen bei der Simulation von Erschütterungen in Kernkraft-bauwerken bei Stoßbelastungen.* 2002

Heft 47 Thorsten Timm: *Beschuß von Flüssigkeitsgefüllten Stahl-Behälter.* 2002

Heft 48 Slobodan Kasic:. *Tragverhalten von Segmentbauteilen mit interner und externer Vorspannung ohne Verbund.* 2002

Heft 49 Christoph Kessler-Kramer: *Zugtragverhalten von Beton unter Ermüdungsbeanspruchun* . 2002

Heft 50 Nico Herrman:. *Experimentelle Erfassung des Betonverhaltens unter Schockwellen.* 2003

Heft 51 Michael Baur: *Elastomerlager und nichtlineare Standorteffekte bei Erdbeben.* 2003

Heft 52 Seminar 02.Juli 2004: *DIN 1045-1 Aus der Praxis für die Praxis.* 2004

Heft 53 Abdelkhalek Saber Omar Mohamed: *Behaviour of Retrofitted Masonry Shear Walls Subjected to Cyclic* Loading 2004

Frühere Berichte des
Instituts für Massivbau und Baustofftechnologie

Ulrich Häußler: *Geschwindigkeits- und Spannungsfelder beim Entleeren von Silozellen*. 1984

Wilfried Gladen: *Numerische Untersuchungen der Lasten in Silozellen beim exzentrischen Entleeren*. 1985

Bezug der Hefte: Institut für Massivbau und Baustofftechnologie
Universität Karlsruhe
Postfach 6980, **D - 76128 Karlsruhe**
Tel. 0721/608-2263; Fax 0721/608-2265

Druckkostenzuschuss incl. Porto: je Heft 18 €

Außerdem noch erhältlich:

Festschrift
Prof. Dr.-Ing. Dr.-Ing. E.h. Dr.techn. h.c. Josef Eibl

Aus dem Massivbau und seinem Umfeld

788 Seiten, Preis incl. Versand: 25 €